Chapter 6: Carbon and Other Biogeochemical Cycles

Coordinating Lead Authors: Philippe Ciais (France), Christopher Sabine (USA)

Lead Authors: Govindsamy Bala (India), Laurent Bopp (France), Victor Brovkin (Germany), Josep Canadell (Australia), Abha Chhabra (India), Ruth DeFries (USA), James Galloway (USA), Martin Heimann (Germany), Christopher Jones (UK), Corinne Le Quéré (UK), Ranga Myneni (USA), Shilong Piao (China), Peter Thornton (USA)

Contributing Authors: Ayako Abe-Ouchi (Japan), Anders Ahlström (Sweden), Oliver Andrews (UK), David Archer (USA), Vivek Arora (Canada), Gordon Bonan (USA), Alberto Borges (Belgium), Philippe Bousquet (France), Lori Bruhwiler (USA), Kenneth Caldeira (USA), Long Cao (China), Jerôme Chappellaz (France), F. Chevallier (France), Cory Cleveland (USA), Peter Cox (UK), Frank J. Dentener (Italy), Scott Doney (USA), Jan Willem Erisman (The Netherlands), Eugenie Euskirchen (USA), Pierre Friedlingstein (UK), S. Gourdji (USA), Nicolas Gruber (Switzerland), Guido van der Werf (Netherlands), K. Gurney (USA), Paul Hanson (USA), Elizabeth Holland (USA), Richard A. Houghton (USA), Jo House (UK), Sander Houweling (TN), Stephen Hunter (UK), George Hurtt (US), A. Jacobson (USA), Atul Jain (USA), Fortunat Joos (Switzerland), Johann Jungclaus (Germany), Jed Kaplan (Switzerland), Etsushi Kato (Japan), Ralph Keeling (USA), Samar Khatiwala (USA), Stefanie Kirschke (France), Kees Klein Goldewijk (Netherlands), Silvia Kloster (Germany), Charlie Koven (USA), Carolien Kroeze (Netherlands), Jean-François Lamarque (USA), Keith Lassey (New Zealand), R. Law (Australia), Andrew Lenton (Australia), Spencer Liddicoat (UK), Mark R. Lomas (UK), Yiqi Luo (USA), Takashi Maki (Japan), Gregg Marland (USA), Damon Matthews (Canada), David McGuire (USA), Joe Melton (Switzerland), Nicolas Metzl (France), Vaishali Naik (USA), Y. Niwa (Japan), Richard Norby (USA), James Orr (France), Geun-Ha Park (USA), Prabir Patra (Japan), W. Peters (The Netherlands), Philippe Peylin (France), Stephen Piper (USA), Julia Pongratz (USA), Ben Poulter (France), Peter A. Raymond (USA), P. Rayner (Australia), Andy Ridgwell (UK), Bruno Ringeval (France), C. Roedenbeck (Germany), Marielle Saunois (France), Andreas Schmittner (USA), Edward Schuur (USA), Elena Shevliakova (USA), Stephen Sitch (UK), Renato Spahni (Switzerland), Benjamin Stocker (Switzerland), Taro Takahashi (USA), Rona Thompson (France), Jerry Tjiputra (Norway), Detlef van Vuuren (Netherlands), Apostolos Voulgarakis (USA), Rita Wania (Canada), Soenke Zaehle (Germany), Ning Zeng (USA)

Review Editors: Christoph Heinze (Norway), Pieter Tans (USA), Timo Vesala (Finland)

Date of Draft: 5 October 2012

Notes: TSU Compiled Version

Table of Contents

Executive Summary

This chapter focuses of the biogeochemical cycles carbon dioxide, methane, and nitrous oxide, which are perturbed by human activities. The three most influential greenhouse gases are carbon dioxide (CO_2), methane (CH_4) and nitrous oxide (N_2O), since they altogether amount to 80% of the total radiative forcing from long-lived greenhouse gases. With a *very high level of confidence*, the concentration increase of these greenhouse gases in the atmosphere is caused by anthropogenic emissions, and modulated by natural biogeochemical processes [6.1].

During the past 800,000 years, atmospheric CO_2 varied by 50–100 ppm between glacial (cold) and interglacial (warm) periods. This is well established from multiple ice core measurements. There is a *high confidence* that those variations in atmospheric CO_2 were caused primarily by changes in ocean carbon storage. It is *very likely* that carbon storage in the ocean decreased from glacial to interglacial periods, resulting from increased ocean mixing, decreased marine biological productivity caused by changes in atmospheric iron deposition, and increased carbonate formation. In parallel, it is *very likely* that carbon storage on land increased from glacial to inter-glacial, in part compensating the effect of ocean carbon changes on atmospheric CO_2. Uncertainties in reconstructing glacial conditions and deficiencies in understanding the partitioning of carbon between surface and deep ocean waters prevent an unambiguous interpretation of the variations of CO_2 between glacial and interglacial periods [6.2; Figure 6.5].

During the present interglacial period, the Holocene (circa 7000 BP to year 1750), atmospheric CO_2 increased continuously by 20 ppm. Although the *confidence in underlying processes is medium*, **the contribution of CO_2 emissions from early anthropogenic land use is *unlikely* sufficient to explain the CO_2 increase during the Holocene.** Atmospheric CH_4 levels rose between 4 ka and year 1750 by about 100 ppb [Figure 6.6]. *About as likely as not*, early anthropogenic land use significantly contributed to this increase. Causes for variability of CO_2 during the last millennium, especially for the decrease by 5 to 8 ppm around year 1600, have not yet been firmly established. Climatic and anthropogenic forcing are proposed to explain variability in the atmospheric CH_4 during the last millennium, such as the decrease in the late 16th century by about 40 ppb, but the *confidence in these mechanisms is low* [6.2; Figure 6.7].

Changes in atmospheric CO_2 since the beginning of the Industrial Era (1750) have been dominated by anthropogenic influence. CO_2 emissions from fossil fuel combustion and cement production estimated from energy statistics have released 365 ± 30 PgC to the atmosphere, while human land use change activities (mainly deforestation) are estimated to have released 180 ± 80 PgC. Of these 545 ± 85 PgC, only 240 ± 10 PgC have accumulated in the atmosphere as CO_2. This historical increase of CO_2 from 278 ± 5 ppm in 1750 to 390 ppm in 2011, is known with very high accuracy from ice core and atmospheric station measurements. The remaining amount of carbon released by fossil fuel and land use change emissions since 1750 has been absorbed by the ocean and by terrestrial ecosystems. Ocean measurements and models consistently indicate that the ocean carbon reservoir has increased in storage with a *very high level of confidence* and this increased is estimated to be of 155 ± 30 PgC. Natural terrestrial ecosystems (those not affected by land use change) are estimated by difference from changes in other reservoirs to have accumulated 150 ± 90 PgC. The gain of carbon by natural terrestrial ecosystems is *likely* to take place mainly through the uptake of CO_2 by enhanced photosynthesis at higher CO_2 levels and N deposition and longer growing seasons in high latitudes, and the regrowth of temperate forests. These processes vary regionally [6.3; Table 6.1; Figure 6.8].

During the most recent decade (2002–2011), CO_2 emissions from fossil fuel combustion and cement production were 8.3 ± 0.7 PgC yr^{-1}, and reached 9.4 ± 0.8 PgC in 2012 – 53% above 1990 levels. The growth rate in these emissions was 2.9% yr^{-1} compared to 1.0% yr^{-1} during 1990–1999 as reported by the IPCC Fourth Assessment Report. CO_2 emissions from land use change were 0.9 ± 0.8 PgC yr^{-1} on average during 2002–2011. This estimate includes gross deforestation emissions of around 3 PgC yr^{-1} compensated by 2 PgC yr^{-1} of forest regrowth in some regions; mainly abandoned agricultural land. It is *more likely than not* that land use change emissions decreased since 2000 compared to the 1990s due to decreases in regional tropical deforestation rates. During 2002–2011, atmospheric CO_2 concentration increased at a rate of 2.0 ± 0.1 ppm yr^{-1} (equivalent to 4.3 ± 0.2 PgC yr^{-1}); the ocean and the natural terrestrial ecosystems also increased at a rate of 2.4 ± 0.7 PgC yr^{-1} and 2.5 ± 1.3 PgC yr^{-1}, respectively. It is *likely* that recent changes in temperature, surface winds and ocean circulation have affected the regional carbon uptake by the ocean in the past 20 years over the North Atlantic, Southern Ocean and equatorial Pacific, together these processes

reduce ocean uptake by 0.2 ± 0.2 PgC yr^{-1}, partly compensating the growth in global ocean uptake of 0.3 ± 0.1 PgC yr^{-1} that driven by the increase in atmospheric CO_2 alone [6.3; Table 6.1; Table 6.2; Figure 6.8; Figure 6.10]. It is *likely* that the global CO_2 sink in natural terrestrial ecosystems remained approximately the same between 2002 and 2011 (2.5 ± 1.3 PgC yr^{-1}) and the 1990s (–2.6 ± 1.2 PgC yr^{-1}) [6.3; Table 6.1]

Atmospheric CH_4 has been multiplied by a factor 2.5 since 1750, reaching 1794 ppb in 2010, mostly in response to of increasing anthropogenic emissions. The methane budget is 177–284 Tg(CH_4)yr^{-1} for natural wetlands emissions, 195–263 Tg(CH_4)yr^{-1} for agriculture (rice and animals), 85–116 Tg(CH_4)yr^{-1} for fossil related emissions, 46–185 Tg(CH_4)yr^{-1} for other natural emissions including geological emissions, and 16–20 Tg(CH_4)yr^{-1} for biomass burning. Uncertainties in estimates of major emission sources have been reduced since the AR4 although they remain significant. By including natural geological sources not accounted for in previous budgets, the fossil component of the total CH_4 emissions (both anthropogenic and natural) has been re-evaluated as up to 30% of the total CH_4 emissions. Natural wetlands and biomass burning emissions are confirmed to be the main drivers of global inter-annual variability of CH_4 emissions, and a more consistent quantification of the magnitude of inter-annual variability of the chemical sink compared to previous budgets has been established. However, the causes of the methane concentration stabilization in the early 2000s are still debated, as those of the observed recent increase of methane concentrations since 2007.

Global emissions of N_2O are difficult to estimate, but global and regional budgets are constrained by inverse modelling studies. **During the 2000s, food production is *likely* responsible for 80% of the increase in atmospheric N_2O**. The long atmospheric lifetime of N_2O implies that it will take decades before abundances stabilize even if global emissions are reduced. This is of concern not only because of its contribution to the global radiative forcing, but also because N_2O is currently the dominant ozone depleting substance.

The availability of nitrogen for plant growth will *likely* limit 21st century land carbon uptake resulting in higher atmospheric CO_2 concentration. A key update since AR4 is the introduction of nutrient dynamics in some land carbon models, in particular the limitations imposed by nitrogen availability. Models including the nitrogen cycle predict a that the future uptake of anthropogenic CO_2 by land ecosystems is *very likely* to be less than when no nitrogen limitation is modeled. These models also predict that this limitation effect is partly offset by nitrogen supplied by atmospheric deposition, and increased soil nitrogen availability due to warming. In all cases, the net effect is a smaller predicted land sink for a given trajectory of anthropogenic CO_2 emissions. CMIP5 models that neglect nitrogen cycle interactions project excessive land carbon uptake by 2100 by up to 400 PgC [6.4.6, Figure 6.36].

Projections of the global carbon cycle to 2100 using so called 'CMIP5 Earth System Models' that represent a wider range of complex interactions between the carbon cycle and the physical climate system, consistently estimate a positive feedback between climate and the carbon cycle, i.e., reduced natural sinks or increased natural CO_2 sources in response to future climate change, like in the previous AR4 coupled carbon climate simulation results. According to CMIP5 model results it is *very likely* that the global ocean will continue as a net carbon sink for all 4 RCP concentration scenarios. For scenarios with decreasing areas of anthropogenic land use (RCP4.5, 6.0), it is *very likely* global land will continue as a net carbon sink. For scenarios with increasing areas of land use (RCP2.6, 8.5), a net land sink remains *likely* but some models project a source by 2100. CMIP5 models predict that carbon sinks in tropical land ecosystems are *very likely* to decrease because of climate change. CMIP5 model projections of ocean carbon uptake show less spread in response to CO_2 and climate than the previous C4MIP generation of models, but there is still significant model spread (4–5 times greater than ocean carbon) in future land carbon storage. Future land use change, and the response of terrestrial ecosystems to it, is an important driver of future terrestrial carbon cycle and contributes significant additional spread to model estimates [6.4; Figure 6.19, Figure 6.20, Figure 6.21, Figure 6.22; Figure 6.24].

The combined effect of all processes on future ocean and land carbon uptake allows us to quantify the trajectory of fossil fuel emissions compatible with the RCP future CO_2 concentration pathway scenarios. For RCP2.6 all CMIP5 models project large reductions in emissions relative to present day levels. It is about as *likely as not* that sustained globally negative emissions will be required to achieve the reductions in atmospheric CO_2 in this scenario. CMIP5 models are generally consistent with RCP scenario emissions except for RCP8.5 where the CMIP5 Earth System models project lower natural carbon uptake

and lower compatible emissions than in this RCP scenario. This difference would be greater if nitrogen limitation on land carbon uptake was included in more of the CMIP5 models [6.4, Figure 6.25, Figure 6.26].

With a *very high level of confidence*, the increased storage of carbon by the ocean will increase acidification in the future, continuing the observed trends of the past decades. Ocean carbon cycle models consistently project continued ocean acidification worldwide at high latitudes to 2100 for all RCP pathways. The largest decrease in pH and surface carbonate ion (CO_3^{2-}) is projected to occur in the warmer low and mid-latitudes. However, it is the colder high-latitude oceans that are projected to first become undersaturated with respect to aragonite. Aragonite undersaturation in surface waters is *likely* to be reached by 2100 in the Southern Ocean as highlighted in AR4, but new studies project that undersaturation will even *likely* occur before 2100 in the Arctic [6.4; Box 6.5, Figure 6.28].

Regarding the ocean loss of dissolved oxygen (de-oxygenation), ocean carbon and oxygen models suggest that it is *likely* that large decreases in oceanic dissolved oxygen will occur during the 21st century, predominantly in the sub-surface mid-latitude oceans, due to enhanced stratification and warming. There is however no consensus on the future development of the volume of hypoxic and suboxic waters because of large uncertainties in potential biogeochemical effects and in the evolution of tropical ocean dynamics.

With a *very high level of confidence*, ocean and land ecosystems will continue to respond to climate change and atmospheric CO_2 increases created during the 21st century, even for centuries after any stabilization of CO_2 and climate. Ocean acidification will continue in the future as long as atmospheric CO_2 concentrations remain higher than average ocean CO_2 partial pressure. The so called *committed* land ecosystem carbon cycle changes, i.e., induced changes in CO_2 sources and sinks, will manifest themselves further beyond the end of the 21st century. In addition, there is *medium confidence* that large areas of permafrost will experience thawing, but uncertainty over the magnitude of frozen carbon losses through CO_2 or CH_4 emissions to the atmosphere are large, although most of AR5 model results produce significantly increased CO_2 emissions by the end of the 21st century. Future methane emissions from natural sources are *very likely* to be affected by climate change, but there is limited confidence in quantitative projections of these changes. Models and ecosystem warming experiments show agreement that per unit area of wetland CH_4 emissions will increase in a warmer climate, but wetland areal extent may increase or decrease depending on regional climate-induced changes in wetland hydrology. Estimates of the future release of CH_4 from gas hydrates in response to seafloor warming are poorly understood, and might possibly lead to significant release from the sea floor by the end of the 21st century but subsequent emissions to the atmosphere are likely to remain low due to oxidation of hydrate emitted CH_4 in the water column and slow propagation of warming to the seafloor.

This chapter was termed to assess the scientific consequences for so called human induced 'Carbon Dioxide Removal (CDR)' that have been proposed to accelerate / augment the removal of CO_2 from the atmosphere to reduce climate change. These methods are based on human induced changes in natural carbon cycle processes. [6.5, list in Table 6.15, FAQ 7.3 Figure 1] and were analysed only here for their potential effects on the global carbon cycle. Scientific considerations for evaluating CDR methods include storage capacity, the permanence of the storage, potential adverse side effects, and the so called 'rebound effect': when carbon is removed from the atmosphere, the subsequent rate of removal of CO_2 from the atmosphere by natural carbon cycle processes on land and oceans will be reduced.

CDR schemes may not present a viable option to rapidly affect climate on decadal and centennial time scales because of the long time required by relevant natural carbon cycle processes to remove atmospheric CO_2. Currently, the maximum physical potential of atmospheric CO_2 removal by any single CDR scheme that rely on natural carbon cycle processes is at most about 1 PgC yr^{-1}. However, CDR based on land use options may not be achievable in the real world because of other constraints, such as competing demands for land. The level of scientific knowledge on the effectiveness of CDR methods, their side effects on climate, and their potential effects on carbon and other biogeochemical cycles, including ocean acidification and de-oxygenation, is low and uncertainties are very large [6.5, Figure 6.40, Figure 6.41, Table 6.16].

So called 'Solar Radiation Manipulation (SRM)' are addressed in Chapter 7, and were only analysed in this Chapter for their potential effects on carbon cycling. SRM methods are *likely* to impact the carbon cycle through their climate effects, SRM proposals might counter the global-average radiative effects of CO_2 but they will leave the direct 'fertilization' effects of CO_2 on natural ecosystems on land (e.g., enhanced plant productivity and reduced plant transpiration) and in oceans including ocean acidification.

6.1 Introduction

The radiative properties of the atmosphere are strongly influenced not only by the natural water vapour, but also by the abundance of long-lived greenhouse gases, including carbon dioxide (CO_2), methane (CH_4) and nitrous oxide (N_2O). The concentrations of these gases have substantially increased over the last 200 years caused primarily by anthropogenic emissions (see Chapter 2). Long-lived greenhouse gases represent the atmospheric phase of the natural global biogeochemical cycles, which describe the flows and transformations of the major elements between the different components of the Earth System (atmosphere, ocean, land, lithosphere) by physical, chemical, biological and geological processes. Since these processes are themselves also dependent on the prevailing climate, feedbacks induced by climate changes can also modify the concentrations of CO_2, CH_4 and N_2O, e.g., during the glacial-interglacial cycles (see Chapter 5) but also in the next century (see Chapter 12).

This chapter summarizes the scientific understanding of budgets, variability and trends of the three major biogeochemical trace gases, CO_2, CH_4 and N_2O, their underlying major source and sink processes and their perturbations caused by past and present climate changes and direct human impacts. After the introduction (Section 6.1), Section 6.2 assesses the present understanding of the mechanisms responsible for the variations of CO_2, CH_4 and N_2O in the past emphasizing glacial-interglacial changes, variations during the Holocene since the last glaciation and their variability over the last millennium. Section 6.3 focuses on the fossil fuel era since 1750 addressing the major source and sink processes, and their variability in space and time. This information is then used to evaluate critically the simulation models of the biogeochemical cycles, including their sensitivity to changes in atmospheric composition and climate. Section 6.4 assesses future projections of carbon and other biogeochemical cycles computed with off-line and coupled climate-carbon cycle models. This includes a quantitative assessment of the direction and magnitude of the various feedback mechanisms as represented in current models, as well as additional processes that might become important in the future but which are not yet fully described in current biogeochemical models. Finally, Section 6.5 addresses the effects of deliberate carbon dioxide removal methods and solar radiation management on the carbon cycle.

6.1.1 Global Carbon Cycle Overview

6.1.1.1 CO_2 Cycle

Atmospheric CO_2 represents the atmospheric phase of the global carbon cycle. The global carbon cycle can be viewed as a series of reservoirs of carbon in the Earth System, which are connected by exchange fluxes of carbon. One can principally distinguish two domains in the global carbon cycle. (1) A fast domain with large exchange fluxes and relatively rapid reservoir turnovers, which consists of carbon in the atmosphere, the ocean and on land carbon in living vegetation, soils, and freshwaters. Reservoir turnover times, defined as reservoir mass of carbon divided by the exchange flux, range from a few years for the atmosphere, to decades-millennia for the major carbon reservoirs of the land vegetation and soil and the various domains in the ocean. (2) A second, slow domain consists of the huge carbon stores in rocks and sediments, which exchange carbon with the fast domain through volcanic emissions of CO_2, weathering, erosion and sediment formation on the sea floor (Sundquist, 1986). Geological turnover times of the reservoirs of the slow domain are 10,000 years or longer. On time scales of the anthropogenic interference with the global carbon cycle, the slow domain can be assumed to be at steady state. Natural exchange fluxes between the slow and the fast domain of the carbon cycle are relatively small (<0.3 PgC yr^{-1}) and can be assumed as approximately constant in time (volcanism, sedimentation), although erosion and river fluxes may have been modified by human induced changes in land use (Raymond and Cole, 2003).

During the Holocene prior to the Industrial Era (starting in 1750) the fast domain was close to steady state as witnessed by the relatively small variations of atmospheric CO_2 recorded in ice cores (see Section 6.2). By contrast, since the beginning of the Industrial Era, fossil fuel extraction from geological reservoirs, and their combustion has resulted in the transfer of significant amount of fossil carbon from the slow domain into the fast domain, thus causing an unprecedented and major human induced perturbation in the carbon cycle. A schematic of the global carbon cycle with focus on the fast domain is shown in Figure 6.1. The numbers represent the estimated current pool sizes in PgC (1 PgC = 10^{15} g C) and the magnitude of the different main exchange fluxes in PgC yr^{-1} averaged over the time period 2000–2009.

[INSERT FIGURE 6.1 HERE]

Figure 6.1: Simplified schematic of the global carbon cycle. Numbers represent reservoir sizes (in PgC), and carbon exchange fluxes (in PgC yr^{-1}). Dotted arrow lines denote carbon fluxes between the fast and the slow carbon cycle domain (see text). Darkblue numbers and arrows indicate reservoir sizes and natural exchange fluxes estimated for the time prior to the Industrial Era. Red arrows and numbers indicate fluxes averaged over 2000–2009 time period resulting from the emissions of CO_2 from fossil fuel combustion, cement production , and changes in land use, and their partitioning among atmosphere, ocean and terrestrial reservoirs (see Section 6.3). Red numbers in the reservoirs denote cumulative changes over the Industrial Period 1750–2011.

In the atmosphere, CO_2 is the dominant carbon bearing trace gas with a current concentration of approximately 390 ppm (January 2011), which corresponds to a mass of 828 PgC. Additional trace gases include methane (CH_4, current content mass ~3.8 Pg C) and carbon monoxide (CO, current content mass ~2 PgC), and still smaller amounts of hydrocarbons, black carbon aerosols, and organic compounds.

The terrestrial biosphere reservoir contains carbon in organic compounds in vegetation living biomass (450–650 PgC; Prentice et al., 2001) and in dead organic matter in litter and soils (1500–2400 PgC; Batjes, 1996), with an additional amount of old soil carbon in wetland soils (200–450 PgC) and in permafrost soils (~1670 PgC; Tarnocai et al., 2009). CO_2 is removed from the atmosphere by plant photosynthesis (123 ± 8 PgC yr^{-1}; Beer et al., 2010), and carbon is then cycled through plant tissues, litter and soil carbon and released back into the atmosphere by autotrophic (plant) and heterotrophic (soil microbial) respiration and additional disturbance processes (e.g., sporadic fires) on a very wide range of time scales (seconds to millennia). The imbalance of CO_2 uptake by photosynthesis during the growing season with the near year-round CO_2 release by respiration in the northern hemisphere causes the characteristic sawtooth seasonal cycle observed in atmospheric CO_2 measurements (see Figure 6.3). A small amount of terrestrial carbon is transported from soils to the coastal ocean via freshwaters and rivers (~0.8 PgC yr^{-1}), under the form of dissolved inorganic carbon, dissolved and particulate organic carbon.

The oceanic carbon reservoir (~38,000 PgC) contains predominantly Dissolved Inorganic Carbon (DIC): carbonic acid (dissolved CO_2 with water), bicarbonate (dominant form) and carbonate ions, which are tightly coupled via ocean chemistry. In addition, the ocean contains Dissolved Organic Carbon (DOC, ~662 PgC; Hansell et al., 2009), of which a major fraction is very rapidly recycled. Marine organisms, phytoplankton and other microorganisms, represent a small carbon pool (~3 PgC), which is turned over very rapidly in days to a few weeks. Photosynthesis by phytoplankton in the ocean surface layer removes dissolved CO_2, which is subsequently cycled through the marine food chain and finally respired back to DIC by microbes through heterotrophic respiration processes. After death of the organisms, some of the organic carbon that they contain sinks to deeper waters where it is remineralized to inorganic carbon. This process creates and maintains a natural negative concentration gradient of DIC between the surface ocean and the deeper waters. Deeper waters are therefore supersaturated with carbon and release this in the form of CO_2 back to the atmosphere where these deeper waters outcrop to the atmosphere in upwelling, whereas on annual average CO_2 is removed from the atmosphere elsewhere in surface waters by marine organisms photosynthesis. This natural branch of the ocean carbon cycle is termed the 'marine biological soft-tissue pump'. It is limited primarily by radiation and the prevailing nutrients (phosphate, nitrate and additional micronutrients e.g., iron and manganese). A second natural branch of the oceanic carbon cycle, the 'marine carbonate pump' is generated by the formation of calcareous shells of certain oceanic microorganisms in the surface ocean which, after sinking to depth are mostly dissolved and transformed back into DIC and calcium ions. Paradoxically, this marine carbonate pump operates counter to the marine biological pump: in the formation of calcareous shells, bicarbonate ions are split into carbonate ions and dissolved CO_2 with increases dissolved CO_2 in surface waters, while the reverse takes place during shell dissolution at depth. Only a small fraction (~0.2 PgC yr^{-1}) of the carbon exported by biological processes (both soft-tissue and carbonate pumps) from the surface reaches the sea floor and is stored in sediments for millennia and longer. A third natural branch of the oceanic carbon cycle exists due to higher solubility of CO_2 in colder waters. This 'solubility pump' pumps CO_2 from the atmosphere into the ocean in colder surface waters and releases CO_2 back to the atmosphere in warmer surface waters, and this process is coupled to the ocean general circulation.

6.1.1.2 CH_4 Cycle

Methane is a very important gas, because of the stronger radiative properties per molecule of CH_4 compared to CO_2 (Chapter 8), its interactions with photochemistry. The global biogeochemical cycle of atmospheric methane (CH_4) is a short 'sub-cycle' of the global carbon cycle, as methane turnover time is less than 10 years in the troposphere. The sources of CH_4 at the surface of the Earth can be thermogenic, including (1) natural emissions of fossil CH_4 from geological sources (marine and terrestrial seepages, geothermal vents and mud volcanoes), and (2) emissions caused by leakages from fossil fuel extraction and use (natural gas, coal and oil industry; Figure 6.2). A second category of CH_4 sources consists in pyrogenic sources including natural fires and incomplete burning of fossil fuels and biomass. A third category of CH_4 sources consists of biogenic sources including natural biogenic emissions from wetlands, by far the largest natural source, and by termites as well, with a small ocean source, and the anthropogenic biogenic emissions from rice paddy agriculture, ruminants, landfills, man-made lakes and wetlands and waste treatment. In general, biogenic CH_4 is produced from organic matter under low oxygen conditions by fermentation processes of methanogenic microbes (Conrad, 1996). As compared to the AR4 assessment report, a new and large CH_4 source from plants under aerobic conditions has been hypothesized (Keppler et al., 2006), which, however, has not been confirmed in subsequent studies (e.g., Dueck et al., 2007; Nisbet et al., 2009). CH_4 is primarily removed from the atmosphere by photochemistry, through atmospheric chemistry reactions with the OH radical to CO and subsequently to CO_2. Other smaller removal processes of atmospheric CH_4 take place in the stratosphere through reaction with chlorine and oxygen radicals, at the surface by oxidation in well aerated soils, and possibly by reaction with chlorine in the marine boundary layer (Allan et al., 2007).

[INSERT FIGURE 6.2 HERE]

Figure 6.2: Schematic of the global cycle of CH_4. Numbers represent fluxes in Tg(CH_4) yr^{-1} estimated for the time period 2000–2009 (see Section 6.3). Green arrows denote natural fluxes, red arrows anthropogenic fluxes, and orange arrow denotes a combined natural+anthropogenic flux.

A very large geological pool, (1500–7000 PgC; Archer, 2007; with low confidence) of CH_4 exists in the form of frozen hydrate deposits in permafrost soils, shallow Arctic ocean sediments and on the slopes of continental shelves. These CH_4 hydrates are stable under conditions of low temperature and high pressure. Warming or changes in pressure, e.g., due to lowering sea level could render some of these hydrates unstable with a potential release of CH_4 to the overlying ocean and/or atmosphere.

6.1.2 Industrial Era

6.1.2.1 CO_2 Cycle

Since the beginning of the Industrial Era defined as 1750 in this chapter, human activities have been producing energy by burning of fossil fuels (coal, oil and gas), a process which is releasing large amounts of carbon dioxide into the atmosphere (Boden et al., 2011; Rotty, 1983). The amount of fossil fuel CO_2 emitted to the atmosphere can be estimated with an accuracy of about 5% for recent decades from statistics of fossil fuel use (Andres et al., 2012). Estimates of fossil fuel CO_2 emissions for the period prior to 1950 are less certain (Rotty, 1983). Total cumulative emissions between 1750 and 2011 amount to 365 ± 30 PgC (see Section 6.3 and Table 6.1), including a contribution of 8 PgC from the production of cement.

The second major anthropogenic emission of CO_2 to the atmosphere is caused by changes in land use and land management, which cause a net reduction in land carbon storage. In particular deforestation for procurement of land for agricultural or pasture is associated with a loss of terrestrial carbon. Estimation of this CO_2 source to the atmosphere requires knowledge of changes in land area as well as estimates of the carbon stored per area before and after the land use change transition. In addition, longer term effects, such as the decomposition soil organic matter after land use change, have to be taken into account as well. Since 1750, anthropogenic land use changes have been important: currently an area of about 43 million km^2 is used for cropland and pasture, corresponding to about 35% of the total ice-free land area (Foley et al., 2007) in contrast to an estimated cropland and pasture area of 7.5–9 million km^2 in the 18th century (Goldewijk, 2001; Ramankutty and Foley, 1999). The net CO_2 emissions from land use changes between 1750 and 2011 are estimated at approximately 180 ± 80 PgC (see Section 6.3 and Table 6.1).

The almost exponentially increasing anthropogenic CO_2 emissions from fossil fuel burning and land use change are the cause of the observed increase in atmospheric CO_2. Several lines of evidence support this

conclusion beyond the fact that the rate of CO_2 emissions from fossil fuel burning and land use change is about twice the rate of atmospheric CO_2 increase:

- Since most of the fossil fuel CO_2 emissions take place in the industrialized countries north of the equator, on annual average, atmospheric CO_2 measurement stations in the Northern Hemisphere record slightly higher CO_2 concentrations than stations in the Southern Hemisphere, as witnessed by the observations from Mauna Loa, Hawaii, and the South Pole (Figure 6.3). The annually averaged concentration difference between the two stations follows extremely well the estimated difference in emissions between the hemispheres (Fan et al., 1999; Keeling et al., 1989; Tans et al., 1989).
- CO_2 from fossil fuels and from the land biosphere has a lower $^{13}C/^{12}C$ stable isotope ratio than the CO_2 in the atmosphere, which induces a decreasing temporal trend in the atmospheric $^{13}C/^{12}C$ ratio of the CO_2 concentration as well as, on annual average, slightly lower $^{13}C/^{12}C$ values in the Northern Hemisphere (Figure 6.3).
- Because fossil fuel CO_2 is devoid of radiocarbon (^{14}C), reconstructions of the $^{14}C/C$ isotopic ratio of atmospheric CO_2 from tree rings show a declining trend (Levin et al., 2010; Stuiver and Quay, 1981) prior to the massive addition of 14C in the atmosphere by nuclear weapon tests which has been offseting that declining trend signal.
- An additional indication of the anthropogenic influence on atmospheric CO_2 is provided by the observed decrease in atmospheric O_2 content over the past two decades (see Figure 6.3 and Section 6.1.3.2).

[INSERT FIGURE 6.3 HERE]

Figure 6.3: Atmospheric concentration of CO_2, oxygen, $^{13}C/^{12}C$ stable isotope ratio in CO_2, CH_4 and N_2O recorded over the last decades at representative stations in the northern (solid lines) and the southern (dashed lines) hemisphere. (**a:** CO_2 from Mauna Loa and South Pole atmospheric stations (Keeling et al., 2005), O_2 from Alert and Cape Grim stations (http://scrippso2.ucsd.edu/ right axes), **b:** $^{13}C/^{12}C$: Mauna Loa, South Pole (Keeling et al., 2005), **c:** CH_4 from Mauna Loa and South Pole stations (Dlugokencky et al., 2010), **d:** N_2O from Adrigole and Cape Grim stations (Prinn et al., 2000).

6.1.2.2 CH_4 Cycle

Throughout the Holocene before the Industrial Era, atmospheric CH_4 levels varied only moderately (up to 50 ppb) around 700 ppb, indicating a long term balance between natural emissions and sinks of atmospheric CH_4 (see Section 6.2.3.2; MacFarling-Meure et al., 2006). After 1750, atmospheric CH_4 levels rose almost exponentially, reaching 1650 ppb by the mid 1980s. Between the mid 1980s and the mid 2000s the atmospheric growth of CH_4 has been declining to nearly zero. However, during the last few years atmospheric CH_4 has been observed to increase again, although it is not clear if this recent trend reflects a new imbalance between emissions and sinks or a short term variability episode (Dlugokencky et al., 2009).

There is very high level of confidence that the atmospheric CH_4 increase during the Industrial Era is being caused by anthropogenic activities. The massive expansion of the number ruminants, the emissions from fossil fuel extraction and use, emissions from landfills and waste, as well as the expansion of rice paddy agriculture are the dominant anthropogenic CH_4 sources. Total anthropogenic sources contribute at present between 45 and 65% of the total CH_4 sources. The fraction of fossil CH_4 to the total emission, fossil being the sum of both natural geological fossil emissions and anthropogenic fossil fuel emissions, has since AR4 been revised upwards to be 30% based on measurements of ^{14}C in atmospheric CH_4 and on detailed surveys of geological sources (Etiope et al., 2008; Lassey et al., 2007; Wahlen et al., 1989). The history of fossil fuel CH_4 emissions has also been constrained indirectly from ice core measurements of ethane (C_2H_6), which is co-emitted with fossil fuel CH_4 (Aydin et al., 2011). The dominance of anthropogenic CH_4 emissions in the Northern Hemisphere is evidenced furthermore by the observed north-south gradient in CH_4 concentrations (Figure 6.3), although this atmospheric signal contains also a contribution from the natural wetland emissions located in the Northern Hemisphere. Satellite based CH_4 concentration measurements averaged over the entire atmospheric column also indicate higher concentrations of CH_4 above and downwind of densely populated and intensive agriculture areas where anthropogenic emissions occur REF.

6.1.3 Connections Between Carbon and Other Biogeochemical Cycles

6.1.3.1 Global Nitrogen Cycle including N_2O

The biogeochemical cycles of nitrogen and carbon are tightly coupled with each other due to metabolic needs of organisms. Changes in the availability of one element will influence not only biological productivity but also influence the availability of the other element (Gruber and Galloway, 2008) and in the longer term, the structure and function of ecosystems as well.

Before the Industrial Era, creation of reactive nitrogen Nr (all nitrogen species other than N_2) from non-reactive atmospheric N_2 occurred primarily through two processes, lightning and biological nitrogen fixation (BNF). This input of Nr to the land and ocean biosphere was in balance at steady state with the loss of Nr though the denitrification process, returning N_2 back to the atmosphere (Ayres et al., 1994). This is no longer the case. Nr is produced by human activities and delivered to ecosystems at local, regional, and global scales. During the last decades, production of Nr by humans has been much greater than the natural production (Galloway et al., 1995). There are three main anthropogenic sources of Nr: (1) the widespread cultivation of legumes, and other crops that convert N_2 to Nr in organic compounds through BNF; (2) the combustion of fossil fuels, which converts atmospheric N_2 and fossil fuel N to nitrogen oxides (NO_x); and (3) the Haber-Bosch industrial process, employed massively to produce NH_3 from N_2 for N-fertilizers and for NH_3 as a feedstock for some industrial activities. In addition, mobilization of sequestered nitrogen from soils due to disturbance is also a potential source (Morford et al., 2011).

Anthropogenic sources of Nr over land exceed the magnitude of natural sources by at least of factor of two (Figure 6.4; Galloway et al., 2008) and perhaps more (Vitousek et al., subm.). The amount of anthropogenic Nr that is converted back to non-reactive N_2 is uncertain, with current estimates being of about 30–50% of the total source (Canfield et al., 2010; Galloway et al., 2004). The emission of Nr to the atmosphere by NH_3 and NO_x emissions is driven by agriculture and fossil fuel combustion, respectively. There is a net transfer of N_r from the continental atmosphere into the marine atmosphere by large-scale atmospheric transport, resulting in subsequent Nr deposition over the ocean. This Nr atmospheric deposition flux is greater than the Nr flux from riverine discharge to the coastal ocean (Galloway et al., 2004). The connection between the nitrogen and carbon cycles are discussed in Box 6.1.

[INSERT FIGURE 6.4 HERE]

Figure 6.4: Global nitrogen cycle. The upper panel (A) shows natural and anthropogenic process that create reactive nitrogen Nr. The middle panel (B) shows the flows of reactive Nitrogen species. The bottom panel (C) shows a schematic of the global cycle of N_2O. Blue arrows are natural, red arrows anthropogenic fluxes, and yellow arrows represent fluxes with an anthropogenic and natural component. Units: TgN yr^{-1}.

[START BOX 6.1 HERE]

Box 6.1: Nitrogen Cycle and Nitrogen Carbon Cycle Feedbacks

In the period preceding human agriculture, the total amount of Nr that was cycling naturally among various compartments of the atmosphere and the biosphere was quite small. The biodiversity and intricate webs of relationships found in nature are thought to have evolved as a result of intensive competition among many different life forms, many of them evolving under N-limited conditions (Vitousek et al., subm.). Following the discovery of N as an element, of microbial processes that transform Nr from one species to another biological nitrogen fixation, nitrification, denitrification), and of the importance of Nr as a nutrient for sustaining plant productivity, the discovery of the Haber-Bosch process (synthesis of NH_3 from N_2) marked the onset of large scale human interference with the nitrogen cycle. Currently, human creation of Nr (Haber-Bosch process, fossil fuel combustion, agricultural biological nitrogen fixation) is dominating Nr creation relative to biological nitrogen fixation in natural ecosystems on a global basis. This dominance has profound impacts on human health, ecosystem health and the radiation balance of the Earth.

The time-course of Nr production from 1850 to 2005 shows both the rate and magnitude of this change (Box 6.1, Figure 1). After mid-1970s, human production of Nr became more important than natural production. Currently food production (mineral fertilizers, legumes) accounts for three-quarters of Nr created by humans, with fossil fuel combustion and industrial uses accounting equally for the remainder.

[INSERT BOX 6.1, FIGURE 1 HERE]

Box 6.1, Figure 1: Reactive nitrogen (Nr) creation fluxes (in TgN yr^{-1}) from fossil fuel burning (green line), cultivation-induced BNF, C-BNF (red line), Haber-Bosch process (blue line), and total creation (purple line). Source: Galloway et al. (2003), Galloway et al. (2008).

Of all the questions that could be asked about this, the three most relevant questions regarding anthropogenic perturbation of the N cycle with respect to global change are: 1) What is the fate of anthropogenic Nr? 2) What are the impacts of the excess of Nr on humans and ecosystems? 3) What are the direct and indirect effects of increased Nr on climate change?

With respect to its fate, Nr is released to the environment on various time scales: immediately for fuel combustion, within about a year for human made N-fertilizers, and from immediately to years for industrial sources depending on the use. Once released, Nr is transported, and transformed or stored. Large amounts of Nr are injected into the atmosphere and to coastal systems (Figure 6.4). A portion of this flux (30–50%) is converted back to N_2 but this amount is uncertain and is one of the most critical issues concerning the human influence on the nitrogen cycle today.

The impacts of anthropogenic Nr production on climate and biogeochemistry can be both positive and negative. Nr derived from the Haber-Bosch process is necessary to sustain global crop production. However, most of the Nr created today by humans also enters non-agricultural environments, and impact tropospheric ozone, tropospheric aerosol content, contributes to the acidification of the atmosphere, soils and fresh waters, lead to fertilisation of productivity in forests, grasslands, coastal waters and open ocean and could lead to reduction in biodiversity in terrestrial and aquatic ecosystems. Although outside the scope of this chapter, it is worth noting that Nr induced increases in nitrogen oxides, aerosols, ozone, and nitrates in drinking water have negative impacts on human health (Davidson, 2012; Galloway et al., 2008). A single Nr molecule can contribute to several of these impacts as it cycles in sequence between atmospheric, terrestrial and hydrologic systems. Returning Nr to the atmosphere as N_2 is critical to halt this 'Nitrogen Cascade' essentially once a molecule of N_2 is split and the nitrogen atoms become reactive (e.g., NH_3, NO_x), any given nitrogen atom can contribute to all of the impacts noted above in sequence (Box 6.1, Figure 2). Because of the Nitrogen Cascade, the creation of any molecule of Nr from N_2, at any location, has the potential to affect climate, either directly or indirectly, as explained below. This potential exists until the Nr is converted back to N_2.

[INSERT BOX 6.1, FIGURE 2 HERE]

Box 6.1, Figure 2: Illustration of the nitrogen cascade showing the sequential effects that a single atom of N can have in various reservoirs after it has been converted from nonreactive N_2 to a reactive form (yellow arrows). Abbreviations: NH_3, ammonia; NH_x, ammonia plus ammonium; NO_3^-, nitrate; NO_x, nitrogen oxides; NO_y, NO_x and other combinations of N and O (except N O); N_2O, nitrous oxide (after Galloway et al.; 2003).

The most important processes causing direct links between anthropogenic Nr and climate change include: (1) N_2O emissions by soils and environments (e.g., groundwater) where Nr can accumulate, (2) formation of tropospheric O_3 from anthropogenic NO_x, and (3) formation of nitrate aerosols. The first two processes have warming effects; the third one can have a warming or a cooling effect. The most important processes causing an indirect link between anthropogenic Nr and climate change include: (1) nitrogen dependent changes in soil organic matter decomposition affecting heterotrophic respiration, (2) changes in marine and terrestrial primary productivity, generally an increase, in response to Nr deposition, (3) changes in wetland CH_4 production and consumption due to Nr deposition, (4) changes in CH_4 emission by ruminants given more feed produced by nitrogen fertilizers, (5) a reduction of terrestrial productivity in response to ozone formation caused by Nr from NO_x, and (6) changes in the removal rate of CH_4 from the atmosphere by atmospheric OH radical caused by O_3 and NO_x mediated anthropogenic Nr (Erisman et al., 2011).

[END BOX 6.1 HERE]

6.1.3.2 Oxygen Cycle

The cycle of atmospheric oxygen is tightly coupled with the global carbon cycle. The burning of fossil fuels uses oxygen from the atmosphere in a tightly defined stoichiometric ratio depending on fuel carbon content. As a consequence of the burning of fossil fuels, atmospheric O_2 levels have been observed to decrease steadily over the last 20 years (Keeling and Shertz, 1992; Manning and Keeling, 2006). Compared to the

atmospheric oxygen content of 21% this decrease is very small, however, but it provides independent evidence that the rise in CO_2 must be due to an oxidation process, i.e., fossil fuel combustion, and is not caused by volcanic emissions or by outgassing of ocean dissolved O_2. The atmospheric oxygen measurements furthermore also show the north-south concentration O_2 gradient (higher in the south in mirror to the CO_2 north-south gradient) as expected from the stronger fossil fuel consumption in the Northern Hemisphere (Keeling et al., 1996).

On land, during photosynthesis and respiration, O_2 and CO_2 are exchanged in rather tightly defined stoichiometric ratios. However, with respect to exchanges with the ocean, O_2 behaves quite differently from CO_2, since compared to the atmosphere only a small amount of O_2 is dissolved in the ocean whereas by contrast the oceanic CO_2 content is much larger due to the carbonate chemistry. This different behaviour of the two gases with respect to ocean exchange provides a powerful method to assess independently the partitioning of the uptake of CO_2 by land and ocean (Manning and Keeling, 2006).

6.2 Variations in Carbon and Other Biogeochemical Cycles before the Fossil Fuel Era

Numerous mechanisms that were responsible for past changes in atmospheric CO_2, CH_4, N_2O related to changes in carbon and other biogeochemical cycles changes will likely operate in the future climate as well. Past archives of GHG and climate changes therefore provide useful knowledge, including constraints for biogeochemical models applied for future projections in Section 6.4.

6.2.1 Glacial-Interglacial GHG Changes

6.2.1.1 Key Processes Contributing to the Low Glacial GHG Concentrations

6.2.1.1.1 Main glacial-interglacial CO_2 drivers

Ice cores recovered from the Antarctic ice cap reveal that the concentration of atmospheric CO_2 at the height of the Last Glacial Maximum (LGM) around 20 thousand years ago (20 ka) was about one third lower than during the subsequent interglacial (Holocene) period started around 11 ka ago (Delmas et al., 1980; Monnin et al., 2001; Neftel et al., 1982). Longer (to 800 ka) records exhibit similar features, with CO_2 values of ~180–200 ppm during glacial intervals (Petit et al., 1999). Prior to around 400 ka, interglacial CO_2 values were 240–260 ppm rather than 270–290 ppm after that date (Luthi et al., 2008).

A variety of proxy reconstructions as well as diverse models of different complexity from conceptual to complex Earth System Models (ESM) have been used to test hypotheses for the cause of lower LGM atmospheric CO_2 concentrations. The ways in which the global carbon cycle operated at the LGM and its relative implications for CO_2 can be broken down by individual drivers (Figure 6.5). It should be recognized however that this breaking down is potentially misleading, as many of the component drivers shown in Figure 6.5 may combine non-linearly (Bouttes et al., 2011). Only well-established individual drivers are quantified (Figure 6.5), and discussed below.

Reduced terrestrial carbon storage. The $\delta^{13}C$ record of ocean waters as preserved in benthic foraminiferal shells has been used to infer that terrestrial carbon storage was reduced in glacial times, thus playing against recorded changes in atmospheric CO_2. Estimates of LGM land carbon storage deficit relative to pre-industrial range from a few hundreds to 1000 PgC (e.g., Bird et al., 1996; Ciais et al., 2012). Dynamic vegetation model simulations tend to favor values at the higher end (~800 PgC) (Kaplan et al., 2002; Otto et al., 2002) and indicate a larger role for the physiological effects of low CO_2 on photosynthesis at the LGM than that of climate-induced biome shifts (Prentice and Harrison, 2009).

Lower ocean temperatures. Reconstructions of sea-surface temperatures during the LGM suggest that the global surface ocean was on average 3–5°C cooler compared to the Holocene. Because the solubility of CO_2 increases at colder temperature (Zeebe and Wolf-Gladrow, 2001), a colder glacial ocean will hold more carbon. However, uncertainty in reconstructing the pattern of ocean temperature change, particularly in the tropics (Archer et al., 2000; Waelbroeck et al., 2009), together with problems in transforming this pattern to the resolution of (particularly box) models in light of the non-linear nature of the CO_2-temperature relationship (Ridgwell, 2001), creates a ~24 ppm spread in estimates of changes in CO_2, although it can be noted that most 3-D ocean GCM projections cluster more tightly.

Lower global sea level, increased ocean salinity and alkalinity. Changes in ocean volume also induces a well understood effect on CO_2 solubility, given the fact that LGM sea level was about ~120 m lower than today. This driver impacts the LGM ocean carbon cycle in three distinct ways. First, the resulting higher LGM ocean surface salinity induces an increase in atmospheric CO_2 (Bopp et al., 2003). Second, total dissolved inorganic carbon and alkalinity become more concentrated in equal proportions, which has the effect of driving atmospheric CO_2 higher. Finally, decreasing the ambient hydrostatic pressure at the ocean floor with a lowered sea level enhances the preservation of $CaCO_3$ in sediments and hence on the longer-term (~2–8 kyr; Archer et al., 2000; Ridgwell and Hargreaves, 2007) reduces alkalinity and acts to increase atmospheric CO_2 during LGM.

Ocean circulation. Potential re-organization in global circulation during glacial periods that promoted the retention of dissolved inorganic carbon in the deep ocean during the LGM has increasingly become the focus of recent research on the glacial-interglacial CO_2 problem. That ocean circulation likely plays a key role in low glacial period atmospheric CO_2 concentration is exemplified by the tight coupling observed between reconstructed deep ocean temperatures and atmospheric CO_2 (Shackleton, 2000). Evidence from bore hole sites (Adkins et al., 2002) and from surface ocean paleo-environmental data in polar regions (Jaccard et al., 2005) show that the glacial ocean was highly stratified compared to interglacial conditions and may thus have held a larger store of carbon during glacial times. Radiocarbon records from deep-sea corals (Burke and Robinson, 2012), as well as $\delta^{13}C$ ice core records (Schmitt et al., 2012) demonstrate the role of a deep and stratified Southern Ocean in LGM carbon storage. However, conflicting hypotheses exist on the drivers of increasing ocean stratification, e.g., northward shift and weakening of Southern Hemisphere westerly winds (Toggweiler et al., 2006), reduced air-sea buoyancy fluxes (Watson and Garabato, 2006), or massive brine rejections during sea ice formation (Bouttes et al., 2011). Ocean carbon cycle models have simulated a circulation-induced effect on LGM CO_2 that can explain lower values than during interglacial by 3 ppm (Bopp et al., 2003) to 57 ppm (Toggweiler, 1999).

Aeolian iron fertilisation. Both marine and terrestrial sediment records indicate higher rates of deposition of dust and hence iron (Fe) supply at the LGM (Mahowald et al., 2006), implying a potential link between Fe fertilisation of marine productivity and lower glacial CO_2 (Martin, 1990). However, despite the fact that models generally employ similar reconstructions of glacial dust fluxes (i.e., Mahowald et al., 1999; Mahowald et al., 2006), there is considerable disagreement among the ocean carbon cycle models in the associated CO_2 change. Ocean General Circulation Models-based Fe cycle models tend to cluster at the lower end of simulated CO_2 changes between glacial and interglacial (e.g., Archer at al., 2000; Bopp et al., 2003), whereas box models (e.g., Watson et al., 2000) or intermediate complexity models (EMICs) (e.g., Brovkin et al., 2007) tend to produce CO_2 changes which are at the higher end (Parekh et al., 2008). An alternative view comes from inferences drawn from the timing and magnitude of changes in dust and CO_2 in ice cores (Rothlisberger et al., 2004), assigning a 20 ppm limit for the lowering of CO_2 during the LGM in response to a Southern Ocean Fe fertilisation effect, and a 8 ppm limit for the same effect in the North Pacific.

Increased sea ice extent. A long-standing hypothesis is of increased LGM sea ice cover acting as a barrier to air-sea gas exchange and hence reducing the 'leakage' of CO_2 during winter months from the ocean to the atmosphere during glacial periods (Broecker and Peng, 1986). However, concurrent changes in ocean circulation and biological productivity complicate the estimation of the atmospheric CO_2 impact of increased sea ice extent (Kurahashi-Nakamura et al., 2007). Excepting for the results of an idealized box model (Stephens and Keeling, 2000), models are relatively consistent in projecting a small effect on maintaining atmospheric CO_2 lower during LGM, due to increased sea ice extent.

Other glacial CO_2 drivers. A number of further aspects of altered climate and biogeochemistry at the LGM are also likely to have affected atmospheric CO_2. Reduced bacterial metabolic rates/remineralization depth of organic matter (Matsumoto, 2007; Menviel et al., subm.), increased glacial supply of dissolved Si (required by diatoms to form frustules) (Harrison, 2000), 'silica leakage' (Brzezinski et al., 2002; Matsumoto et al., 2002), changes in net global weathering rates (Berner, 1992), reduction in coral reef growth and other forms of shallow water $CaCO_3$ accumulation (Berger, 1982), carbonate compensation (Ridgwell and Zeebe, 2005), and changes to the $CaCO_3$ to organic matter 'rain ratio' to the sediments (Archer and Maierreimer, 1994), will act to amplify or diminish the CO_2 effect of many of the above drivers.

Summary. All of the major drivers of the glacial-to-interglacial atmospheric CO_2 changes (Figure 6.5) are likely to have already been identified. However, significant uncertainties exist in reconstructing glacial boundary conditions and deficiencies in fully understanding some of the primary controls on carbon storage in the ocean and in the land. This uncertainty prevents an unambiguous interpretation and attribution to individual mechanisms of the causes of low glacial CO_2. Assessment of the balance of mechanisms before deglacial transitions or glacial inceptions will likely provide additional insights into the drivers of low glacial CO_2. Several of these identified drivers (e.g., organic matter remineralization, ocean stratification) are likely to be sensitive to climate change in general, improved understanding drawn from the glacial-interglacial cycles will help constrain the magnitude of future ocean feedbacks on atmospheric CO_2. Other drivers (e.g., iron fertilization) are involved in geoengineering methods, improved understanding could also help constrain the potential of these methods (see Section 6.5.2)

[INSERT FIGURE 6.5 HERE]

Figure 6.5: Carbon dioxide concentrations changes from LGM to late Holocene (top) and from early/mid Holocene (7 ka) to late Holocene (bottom). Filled black circles represent individual model-based estimates for individual ocean, land, geological or human drivers. Solid color bars represent expert judgment (to the nearest 5 ppm) rather than a formal statistical average. References for the different model assessment used for the glacial drivers are as per Kohfeld and Ridgwell (2009) with excluded model projections in grey. References for the different model assessment used for the Holocene drivers are Joos et al. (2004), Brovkin et al. (2008), Kleinen et al. (2010), Broecker et al. (1999), Ridgwell et al. (2003), Brovkin et al. (2002), Schurgers et al. (2006), Yu (2011), Kleinen et al. (2011), Ruddiman (2003, 2007), Strassmann et al. (2008), Olofsson and Hickler (2008), Pongratz et al. (2009), Kaplan et al. (2011), Lemmen (2009), Stocker et al. (2011) and Roth and Joos (2012).

6.2.1.1.2 Glacial CH_4 and N_2O

Polar ice core analyses show that atmospheric CH_4 and N_2O were much lower under glacial conditions compared to interglacial ones. Their reconstructed history encompasses the last 800 kyr (Loulergue et al., 2008; Schilt et al., 2010a). Glacial CH_4 mixing ratios are in the 350–400 ppbv range during the eight glacial maxima covered by the ice core record. This is about half the levels observed during interglacial conditions. The N_2O concentration amounts to 202 ± 8 ppbv, compared to the Early Holocene levels of about 270 ppbv (Fluckiger et al., 1999).

CH_4 and N_2O isotopic ratio measurements in polar ice provide additional constraints on the mechanisms responsible for their temporal changes. N_2O isotopes suggest a similar increase in marine and terrestrial N_2O emissions for the last deglaciation (Sowers et al., 2003), whereas marine sediment proxies of ocean oxygenation suggests that most of the observed N_2O deglacial rise was of marine origin (Jaccard and Galbraith, 2011). δD and ^{14}C isotopic composition measurements of CH_4 have shown that catastrophic methane hydrate degassing events are unlikely to have caused the last deglaciation CH_4 increase (Bock et al., 2010; Petrenko et al., 2009; Sowers, 2006). $\delta^{13}C$ and δD measurements of CH_4 combined with interpolar gradient changes suggest that most of the methane increase observed during the last deglaciation was caused by increased source from boreal and tropical wetlands and an increase in CH_4 residence time due to a reduced oxidative capacity of the atmosphere (Fischer et al., 2008). The biomass burning source apparently changed little on the same time scale, whereas this CH_4 source experienced large fluctuations over the last millennium (Mischler et al., 2009; Wang et al., 2010b).

Several modelling studies (Kaplan et al., 2006; Valdes et al., 2005) addressed the mechanisms behind methane variations on glacial-interglacial time-scales. Changes in atmospheric oxidising capacity of the atmosphere are probably negligible (Levine et al., 2011) and tropical temperature influencing tropical wetlands and global vegetation were found to be the dominant controls for global CH_4 atmospheric concentrations changes on glacial-interglacial time-scales (Konijnendijk et al., 2011).

6.2.1.2 Processes Controlling Changes in CO_2, CH_4 and N_2O During Abrupt Glacial Events

Greenhouse gases (CO_2, CH_4 and N_2O) reveal sharp millennial-scale changes in the course of glaciations, associated with the so-called Dansgaard/Oeschger (DO) climatic events (see Chapter 5, Section 5.6.1), but their amplitude, shape and timing differ. During these millennial scale climate events, atmospheric CO_2 concentrations varied by about 20 ppm, in phase with Antarctic temperatures, but not with Greenland ones. CO_2 increased during cold (stadial) events in Greenland, attaining a maximum at around the time of the rapid

warming in Greenland, which lasted about 1000 years and decreased afterward (Ahn and Brook, 2008). Methane and N_2O showed rapid transitions trending with Greenland temperatures with little or no lag. CH_4 changes are in the 50–200 ppbv range (Fluckiger et al., 2004) and are in phase with Greenland warmings at a decadal time scale (Huber et al., 2006). N_2O fluctuations can reach glacial-interglacial amplitudes, and for the warmest and longest DO events N_2O starts to increase several centuries before Greenland temperature and CH_4 (Schilt et al., 2010b).

However, conflicting hypotheses exist on the drivers of these sharp millennial-scale changes. Some model simulations suggest that both CO_2 and N_2O fluctuations can be explained by changes in the Atlantic meridional overturning ocean circulation (Schmittner and Galbraith, 2008), CO_2 variations being mainly explained by changes in the efficiency of the biological pump which affects deep ocean carbon storage (Bouttes et al., 2011), whereas N_2O variations could be due to changes in productivity and oxygen concentrations in the subsurface ocean (Schmittner and Galbraith, 2008). Other studies, however, suggest that the millennial-scale CO_2 fluctuations can be explained by changes in the land carbon storage (Bozbiyik et al., 2011; Menviel et al., 2008), and that terrestrial processes can explain most of the N_2O changes (Goldstein et al., 2003).

6.2.2 GHG Changes over the Holocene (last 11,000 Years)

6.2.2.1 Understanding Processes Underlying Holocene CO_2 Changes

The evolution of the atmospheric CO_2, CH_4, and N_2O concentrations during the Holocene, the interglacial period which began 11.7 ka ago, is known with high certainty from ice core analyses (Figure 6.6). A decrease in atmospheric CO_2 of about 7 ppm from 11 to 8 ka was followed by a 20 ppm CO_2 increase until the onset of the Industrial Era (Elsig et al., 2009; Indermuhle et al., 1999; Monnin et al., 2004). These variations in atmospheric CO_2 over the past 11,000 years preceding industrialization are more than five times smaller than the observed CO_2 increase during the Industrial Era. Despite the small scale of atmospheric CO_2 variations prior to the Industrial Era, these changes are nevertheless essential for understanding the role of natural forcing in carbon and other biogeochemical cycles during interglacial climate conditions.

[INSERT FIGURE 6.6 HERE]

Figure 6.6: Variations of CO_2, CH_4, and N_2O concentrations during the Holocene. The data are for Antarctic ice cores: EPICA Dome C (Fluckiger et al., 2002; Monnin et al., 2004), triangles; Law Dome (MacFarling-Meure et al., 2006), circles, and for Greenland ice core GRIP (Blunier et al., 1995), squares. Lines are for spline fits.

Since the IPCC AR4, mechanisms underlying the observed 20 ppm CO_2 increase during the Holocene between 7 ka and the Industrial Era have been a matter of intensive debate. During three separate interglacial periods prior to the Holocene, CO_2 did not increase, and this led to a hypothesis that pre-industrial anthropogenic CO_2 emissions associated with early land use change were a main driver of the Holocene CO_2 changes (Ruddiman, 2003, 2007). However, ice core CO_2 data (Siegenthaler et al., 2005b) indicate that during Marine Isotope Stage 11 (Chapter 5), an interglacial period that lasted from 400 to 420 ka, CO_2 was increasing similarly to the Holocene period. Drivers of atmospheric CO_2 changes during the Holocene can be divided into oceanic and terrestrial processes (Figure 6.5) and their role is examined below.

6.2.2.1.1 Oceanic processes

Very likely, the change in oceanic carbonate chemistry state explains the slow CO_2 increase during the Holocene since 7 ka. Proposed mechanisms include: (1) a shift of oceanic carbonate sedimentation from deep sea to the shallow waters due to sea level rise onto continental shelves and excessive accumulation of $CaCO_3$ on shelves including coral reef growth (Kleinen et al., 2010; Ridgwell et al., 2003), (2) a 'carbonate compensation' to release of carbon from the deep ocean during deglaciation and build-up of terrestrial biosphere in the early Holocene (Broecker et al., 1999; Elsig et al., 2009; Joos et al., 2004; Menviel and Joos, 2012). The proxies for the carbonate ion concentration in the deep sea (Yu et al., 2010) and increased dissolution of carbonate sediments in the deep tropical Pacific (Anderson et al., 2008) support the hypothesis of the ocean being a source of CO_2 to the atmosphere during the Holocene. Changes in sea surface temperatures (SST) over the last 7 ka (Kim et al., 2004) could led to slightly lower (Brovkin et al., 2008) or higher (Menviel and Joos, 2012) atmospheric CO_2 concentration but, very likely, SST-driven CO_2 change represents only a minor contribution to the observed CO_2 increase during the Holocene after 7 ka.

6.2.2.1.2 Terrestrial processes: ice core isotope evidence

$\delta^{13}C$ of atmospheric CO_2 trapped in ice cores is a proxy for changes in terrestrial biospheric carbon pools. Calculations based on inferred $\delta^{13}C$ of atmospheric CO_2 during the Holocene suggest an increase in terrestrial carbon stocks of about 300 PgC between 11 and 5 ka and small overall terrestrial changes in the period thereafter (Elsig et al., 2009).

6.2.2.1.3 Natural terrestrial processes

After 7 ka, increasing atmospheric CO_2 concentrations stimulated gross primary productivity of terrestrial vegetation resulting in increases in carbon storage. Modelling studies suggest that this CO_2 fertilisation process contributed a substantial land additional storage of carbon (>100 PgC) on Holocene timescales (Joos et al., 2004; Kaplan et al., 2002; Kleinen et al., 2010). Orbitally forced climate variability, including the intensification and decline of the Afro-Asian monsoon and the mid-Holocene warming of the high-latitudes of the Northern Hemisphere are estimated in models to have resulted in additional changes in vegetation distribution and terrestrial carbon storage. These climate-induced carbon storage changes are estimated using models to have been smaller than changes due to the CO_2 fertilisation (Brovkin et al., 2002; Schurgers et al., 2006). The Holocene evolution of carbon in peatlands has been reconstructed globally, suggesting a land carbon additional storage of several hundred PgC between the early Holocene and the Industrial Era, although uncertainties remain on this estimate (Kleinen et al., 2011; Tarnocai et al., 2009; Yu, 2011). Volcanic CO_2 emissions to the atmosphere between 12 and 7 ka were inferred to be two to six times higher than during the last millennium, of about 0.1 PgCyr (Huybers and Langmuir, 2009; Roth and Joos, 2012) but the confidence in changes of volcanic CO_2 emissions is low.

6.2.2.1.4 Land use

Global syntheses of the observational, paleoecological and archaeological records for Holocene land use change are not currently available (Gaillard et al., 2010). Available global reconstructions of anthropogenic land use and land cover change (LULCC) prior to the last millennium hence currently extrapolate using models and assumptions the relationship of the land cover change and population density from a single region and specific time period to the entire globe and Holocene (Kaplan et al., 2011) or extrapolate the changes of per-capita land requirements occurring with agro-technological progress over time from single regions to changes in all regions of the world (Goldewijk et al., 2011). Because of regional differences in land use systems and uncertainty in historical population estimates, the confidence in spatially explicit LULCC reconstructions is low.

Some recent studies focused on reconstructing LULCC while making very simple assumptions regarding the effect of land use on carbon, and therefore patterns of terrestrial carbon storage (Lemmen, 2009; Olofsson and Hickler, 2008), while other studies relied on more sophisticated terrestrial biosphere models to simulate carbon storage and loss in response to pre-industrial LULCC during the late Holocene period (Pongratz et al., 2009; Stocker et al., 2011; Strassmann et al., 2008). The conclusion of the above studies was that cumulative Holocene carbon emissions as a result of pre-industrial LULCC were not large enough (~50–150 Pg before 1850) to have had a significant influence on late Holocene CO_2 concentrations. However, a recent modelling study by Kaplan et al. (2011) suggested that these attempts represented significant underestimates and that more than 350 PgC could have been released as a result of LULCC between 8 ka and year 1850.

6.2.2.1.5 Human impacts on holocene biomass burning

In addition to clearing of forests for crop and pasture, biomass burning by humans before the Industrial Era has been hypothesized as a source of both CO_2 and CH_4 over the Holocene. Studies that synthesized charcoal records from lake and bog sediments initially indicate that there could be large-scale correlations between burning activity and atmospheric CO_2 (Carcaillet et al., 2002), but this human induced biomass burning hypothesis is opposed by two later global syntheses that used similar methods and concluded that fire activity followed climate variability, rather than human activities (Marlon et al., 2008; Power et al., 2008). In contrast, regional syntheses of charcoal and other paleo-evidence of biomass burning suggest fire is closely related to the dynamics of human societies (Archibald et al., 2012; McWethy et al., 2009; Nevle and Bird, 2008; Nevle et al., 2011).

6.2.2.2 Holocene CH_4 and N_2O Drivers

The Holocene atmospheric CH_4 levels were lowest at around 5 ka, and increased between 4 ka and year 1850 by about 100 ppb (Figure 6.6). Major Holocene agricultural developments, in particular rice paddy cultivation and widespread domestication of ruminants, have been proposed as an explanation for the Late Holocene CH_4 rise (Ruddiman, 2007). The most recent syntheses of archaeological data point to an increasing anthropogenic CH_4 source from domesticated ruminants after 5 ka and from rice cultivation after 4 ka (Fuller et al., 2011; Ruddiman, 2007). The modelling support for either natural or anthropogenic explanations of the Late Holocene increase in the atmospheric CH_4 concentration is equivocal. A study by Kaplan et al. (2006) suggested that a part of the Late-Holocene CH_4 rise could be explained by anthropogenic sources. Natural wetland CH_4 models driven by simulated climate changes are able (Singarayer et al., 2011) or unable (Konijnendijk et al., 2011) to simulate Late Holocene increase in the CH_4 concentration. No new studies are known about mechanisms of Holocene N_2O changes.

6.2.3 GHG Changes over the Last Millennium

6.2.3.1 A Decrease of CO_2 around Year 1600 and Possible Explanations for this Event

High resolution records of the atmospheric composition from ice cores reveals that atmospheric CO_2 during the last millennium varied with a drop in atmospheric CO_2 concentration by about 7–10 ppm around year 1600 followed by a CO_2 increase during the 17th century (Ahn et al., 2012; Siegenthaler et al., 2005a; Trudinger et al., 2002) as shown in Figure 6.7. The CO_2 decrease during the 17th century was used to evaluate the response of atmospheric CO_2 concentration to changes in global temperature (Cox and Jones, 2008; Frank et al., 2010; Scheffer et al., 2006) which was found to be dependent on the choice of global temperature reconstructions used in the model.

[INSERT FIGURE 6.7 HERE]

Figure 6.7: Variations of CO_2, CH_4, and N_2O during 900–1900 AD from ice cores. The data are for Antarctic ice cores: Law Dome (Etheridge et al., 1996; MacFarling-Meure et al., 2006), circles; West Antarctic Ice Sheet (Ahn et al., 2012; Mitchell et al., 2011), triangles; Dronning Maud Land (Siegenthaler et al., 2005a), squares. Lines are spline fits to individual measurements.

One of the possible explanations for the drop in atmospheric CO_2 around year 1600 is enhanced land and/or ocean carbon uptake in response to the cooling caused by reduced solar irradiance during the Maunder Minimum (Chapter 5). However, simulations using EMIC models (Brovkin et al., 2004; Gerber et al., 2003) and by complex ESM models (Jungclaus et al., 2010) suggest that solar irradiance forcing alone is not sufficient to explain the magnitude of the CO_2 decrease. The drop in atmospheric CO_2 around year 1600 could also be caused by a cooling in response to increased volcanic eruptions (Brovkin et al., 2010; Jones and Cox, 2001). Another hypothesis calls for a link between CO_2 and epidemics and wars and associated forest growth over abandoned lands, especially in Central America. Here, results are model- and scenario dependent. Simulations by (Pongratz et al., 2011) do not reproduce a decrease in CO_2, while simulations by Kaplan et al. (2011) suggest a considerable increase in land carbon storage during late 16th to early 17th century. The temporal resolution of Central American charcoal and pollen records is insufficient to support or falsify these model results (e.g., Nevle and Bird, 2008).

Ensemble simulations over the last 1200 years have been conducted using an ESM including a fully-interactive carbon cycle (Jungclaus et al., 2010). For two ensemble simulations using a lower and higher end estimate for the multi-centennial solar irradiance forcing variation, the sensitivity of atmospheric CO_2 concentration to Northern Hemisphere temperature changes was modelled to be of 2.7 and 4.4 ppm K^{-1}, respectively. This sensitivity falls within the range of 1.7–21.4 ppm K^{-1} of a recent reconstruction based on tree-ring Northern Hemisphere temperature reconstructions (Frank et al., 2010), though at its lower end.

6.2.3.2 Mechanisms Controlling CH_4 and N_2O during the Last Millenium

Recent high-resolution ice core records confirm a CH_4 decrease in the late 16th century by about 40 ppb (MacFarling-Meure et al., 2006; Mitchell et al., 2011). Correlations between this variation in CH_4 and temperature in the 15th and 16th centuries suggest that climate change affected CH_4 emissions by wetlands during this period. Additionally to changes in the wetland CH_4 source, long-term trends in biomass burning have been invoked to explain the Last Millenium CH_4 record (Ferretti et al., 2005; Marlon et al., 2008).

Changes in anthropogenic CH_4 emissions during times of war and plague hypothetically contribute to variability in atmospheric CH_4 concentration, although they cannot explain all variability (Mitchell et al., 2011). No studies are known about mechanisms of N_2O changes for the last millennium.

6.3 Evolution of Biogeochemical Cycles since the Industrial Revolution

6.3.1 CO_2 Emissions and their Fate Since 1750

Prior to the Industrial Era, that began in 1750, the concentration of atmospheric CO_2 fluctuated between 180 ppm and 290 ppm for at least 2.1 million years (Honisch et al., 2009; Luthi et al., 2008; Petit et al., 1999; see Section 6.2). Between 1750 and 2011, the combustion of fossil fuels (coal, gas, oil, and gas flaring) and the production of cement have released 365 ± 30 PgC to the atmosphere (Boden et al., 2011), with an additional 190 ± 80 PgC due to land use change, mainly deforestation (Table 6.1**;** see Section 6.3.2 for data sources). This carbon is called anthropogenic carbon.

Table 6.1: Global anthropogenic CO_2 budget, accumulated since the Industrial Revolution (onset in 1750) and averaged over the 1980s, 1990s, 2000s, and the last ten years until 2011. Note that, by convention, a negative ocean or land to atmosphere CO_2 flux is equivalent to a gain of carbon by the ocean or land reservoirs. The budget for the 1850–2005 time period is also provided for comparison with coupled carbon-climate models historical simulations and future projections (see Section 6.4.3). The uncertainty range of 90% confidence interval presented here differs from how uncertainties were reported in AR4 (68%).

	1750–2011 Cumulative PgC	1850–2005 Cumulative PgC	1980–1989 PgC yr^{-1}	1990–1999 PgC yr^{-1}	2000–2009 PgC yr^{-1}	2002–2011 PgC yr^{-1}
Atmospheric increase[a]:	240 ± 10[f]	200 ± 10[f]	3.4 ± 0.2	3.1 ± 0.2	4.0 ± 0.2	4.3 ± 0.2
Fossil fuel combustion and cement production[b]:	365 ± 30[f]	320 ± 25[f]	5.5 ± 0.4	6.4 ± 0.5	7.7 ± 0.6	8.3 ± 0.7
Ocean-to-atmosphere flux[c]:	–155 ± 30[f]	–125 ± 25[f]	–2.0 ± 0.7	–2.2 ± 0.7	–2.3 ± 0.7	–2.4 ± 0.7
Land-to-atmosphere flux: *partitioned as follows*	30 ± 45	5 ± 40	–0.1 ± 0.8	–1.1 ± 0.9	–1.4 ± 0.9	–1.6 ± 1.0
Net land use change[d]	180 ± 80[f]	150 ± 80[f]	1.4 ± 0.8	1.5 ± 0.8	1.1 ± 0.8	0.9 ± 0.8
Residual terrestrial sink[e]:	–150 ± 90[f]	–145 ± 90[f]	–1.5 ± 1.1	–2.6 ± 1.2	–2.5 ± 1.2	–2.5 ± 1.3

Notes:
(a) Data from Charles .D. Keeling, (http://scrippsco2.ucsd.edu/data/data.html), Thomas Conway and Pieter Tans, NOAA/ESRL (www.esrl.noaa.gov/gmd/ccgg/trends/) using a conversion factor of 2.123 PgC per ppm.
(b) CO_2 emissions are estimated by the Carbon Dioxide Information Analysis Center (CDIAC) based on UN energy statistics for fossil fuel combustion and US Geological Survey for cement production (Boden et al., 2011).
(c) Averaged from existing global estimates (see 6.3.2.5 and 6.3.2.6 for the mean values and Table 6.5 for the decadal trends). This flux does not include the natural river flux of carbon and the associated natural outgas of CO_2 to the atmosphere (see Figure 6.1).
(d) Based on the bookkeeping land use change flux accounting method of Houghton et al. (2012) (see text and Table 6.2).
(e) Sum of the Land-to-atmosphere flux minus Net Land Use Change, assuming the errors on each term are independent and added quadratically.(f) The 1750–2011 and 1850–2005 estimates and their uncertainties were rounded to the nearest 5 PgC.

Of the 545 ± 85 PgC of anthropogenic carbon emitted to the atmosphere from fossil fuel and cement and land use change, less than half have accumulated in the atmosphere (240 ± 10 PgC), resulting in an average atmospheric CO_2 concentration of 390.4 ppm in 2011 (Conway and Tans, 2011). The remaining anthropogenic carbon has been absorbed by the ocean and in terrestrial ecosystems: the carbon 'sinks' (Figure 6.8). The ocean stored 155 ± 30 PgC of anthropogenic carbon since 1750 (see Section 6.3.2.4.3). This ocean sink will continue to remove atmospheric CO_2 until the entire ocean has re-equilibrated with the higher atmospheric CO_2 (see Box 6.2).

[INSERT FIGURE 6.8 HERE]

Figure 6.8: Sources and sinks fluxes (PgC yr^{-1}) for the component of the global anthropogenic CO_2 budget from 1750 to 2010. (Top) Fossil fuel and cement CO_2 emissions by category, estimated by the Carbon Dioxide Information Analysis Center (CDIAC) based on UN energy statistics for fossil fuel combustion and US Geological Survey for cement production (Boden et al., 2011). (Bottom) Fossil fuel and cement CO_2 emissions as above. CO_2 emissions from net land use change, mainly deforestation for 1750–1850 are from the average of estimates (Pongratz et al., 2009; Shevliakova et al., 2009b; vanMinnen et al., 2009; Zaehle et al., 2011) and from Houghton et al. (2012) after 1850. The atmospheric CO_2 growth rate prior to 1960 is based on a spline fit to ice core observations (Etheridge et al., 1996; Friedli et al., 1986; Neftel et al., 1982) and a synthesis of atmospheric observations from 1960 (Conway and Tans, 2011). The fit to ice core observations does not capture the large interannual variability in atmospheric CO_2 and is represented with a dashed line on the figure. The ocean CO_2 sink prior to 1960 is from Khatiwala et al. (2009) and from a combination of model and observations from 1960 updated from (LeQuere et al., 2009). The residual land sink is computed from the residual of the other terms. The sources and sinks only include the fluxes that have changed since 1750, and not the natural CO_2 fluxes (e.g., atmospheric CO_2 uptake from weathering, natural river transport of carbon from land to ocean, and compensatory CO_2 outgassing by the ocean) between the atmosphere, and ocean reservoirs that existed before that date and still exist today. The uncertainties in the various terms are discussed in the text and reported in Table 6.1.

Terrestrial ecosystems not affected by land use change have accumulated 150 ± 90 PgC of anthropogenic carbon since 1750 (Table 6.1), thus not fully compensating the CO_2 losses from terrestrial ecosystems to the atmosphere from land use change during the same period estimated to 180 ± 80 PgC (Table 6.1). This increased storage in terrestrial ecosystems not affected by land use is thought to have been caused by enhanced photosynthesis at higher CO_2 levels and N deposition, changes in climate favoring carbon sinks such as longer growing seasons in mid-to-high latitudes, the expansion and increased biomass density of forests in temperate and boreal regions. This increased terrestrial carbon storage is called residual terrestrial sink in Table 6.1 because it is deduced by mass balance as the difference between fossil and land use change emissions and measured atmospheric and oceanic storage increase (Table 6.1).

[START BOX 6.2 HERE]

Box 6.2: CO_2 Residence Time

On average, CO_2 molecules are exchanged between the atmosphere and the Earth surface every few years. This fast CO_2 cycling through the atmosphere is linked to a much slower cycling of carbon through land vegetation, litter and soils, and the upper ocean (decades to centuries), deeper soils and the deep sea (centuries to millennia), and geological reservoirs, such as deep-sea carbonate sediments and the upper mantle (up to millions of years) as explained in Section 6.1. The amount of carbon involved into this chain of natural processes with increasing time scale, is very large compared to the atmospheric CO_2 storage. Emissions of anthropogenic carbon is now rapidly increasing atmospheric CO_2 content, but redistribution of this perturbation through slower reservoirs will take up to hundreds of thousand years. This extremely long relaxation timescale, of a large emission pulse of CO_2, is supported by geological evidence from Paleocene-Eocene thermal maximum event ca. 55 million years ago (McInerney and Wing, 2011).

The main chemical reactions that remove anthropogenic CO_2 and their typical timescales are:

Reaction	*Relevant timescale (years)*
Photosynthesis (land uptake): $6CO_2 + 6H2O + photons \rightarrow C6H12O6 + 6O2$	10–102
Seawater buffer (ocean invasion): $CO2 + CO32- + H2O \rightleftharpoons 2\ HCO3-$	10–103
Reaction with calcium carbonate: $CO2 + CaCO3 + H2O \rightarrow Ca2+ + 2\ HCO3-$	103–104
Silicate weathering (reaction with igneous rocks): $CO_2 + CaSiO_3 \rightarrow CaCO_3 + SiO_2$	10^4–10^6

These reactions are active on all time scales, but the relative importance of their role in the CO_2 removal is changing with time. Accordingly, the response times of atmospheric CO_2 toanthropogenic carbon emissions can be divided into three phases associated with increasingly longer typical timescales.

Phase 1.Within a few years of CO_2 emissions, about a half of the anthropogenic C stays in the atmosphere, while the rest is absorbed in the land and ocean most active pools (Figure 1, top). Within a few centuries, most of the released anthropogenic CO_2 will end up in the form of additional dissolved inorganic carbon in

the ocean, decreasing ocean pH (the ocean invasion phase). Within a thousand years, the airborne fraction of the CO_2 emissions (see Section 6.3.2.4) is expected to be between 15 and 40%, depending on the amount of carbon released (Archer et al., 2009b). If emissions are large enough, the carbonate buffer system of the ocean becomes depleted, so the larger the cumulative emissions, the higher the airborne fraction (Eby et al., 2009).

Phase 2. In the second stage, the pH of the ocean will be restored by the $CaCO_3$ cycle, partly replenishing the buffer capacity of the ocean and further drawing down atmospheric CO_2 as a new balance is re-established between $CaCO_3$ sedimentation in the ocean and terrestrial weathering (Figure 1, bottom). This stage has a time scale of 3–7 kyr, and pulls the cumulative airborne fraction (the fraction of an initial pulse of CO_2 that stays in the atmosphere) down to 10–25% of the original CO_2 pulse after about 10 kyr (Archer and Brovkin, 2008; Lenton and Britton, 2006; Montenegro et al., 2007; Ridgwell and Hargreaves, 2007; Tyrrell et al., 2007).

Phase 3. During the third phase, the rest of the anthropogenic CO_2 will be removed from the atmosphere by silicate weathering, a very slow process of CO_2 reaction with CaO and other minerals of igneous rocks. This geological process takes up to several hundred thousand years (e.g., Sundquist, 1990; Walker and Kasting, 1992).

Involvement of extremely long processes into the removal of anthropogenic CO_2 complicates comparison with the cycling of the other greenhouse gases. This is why the concept of a single, characteristic atmospheric lifetime is not applicable to CO_2 (Chapter 8).

[INSERT BOX 6.2, FIGURE 1 HERE]

Box 6.2, Figure 1: A fraction of a given amount of CO_2 emitted to the atmosphere remaining in the atmosphere in response to an idealized instantaneous CO_2 pulse in year 0 as calculated by a range of coupled climate-carbon cycle models. (Top) Multi-model mean (black line) and the uncertainty interval (±2 standard deviations, grey shading) simulated during 1,000 years following the instantaneous pulse of 100 PgC (Joos et al., submitted). (Bottom) A mean of models with oceanic and terrestrial carbon components (solid lines) and a maximum range of these models (grey shading) for instantaneous CO_2 pulse in year 0 of 100 PgC (black), 1,000 PgC (brown) and 5,000 PgC (red line) on a time interval up to ten thousand years (Archer et al., 2009b). (Blue boxes) the dominant processes that remove the excess of CO_2 emitted in the atmosphere on the sucessive timescales. Note that higher pulse of CO_2 emissions leads to higher airborne CO_2 fraction (Section 6.3.2.4) due to reduced carbonate buffer capacity of the ocean and positive climate-carbon cycle feedback (Section 6.3.2.6.6).

[END BOX 6.2 HERE]

6.3.2 Global CO_2 Budget

Since the AR4 (Denman et al., 2007), a number of new advancements on data availability and data-model synthesis have allowed the establishment of a more constrained anthropogenic CO_2 budget and a better attribution to its flux components. The advancements are: (1) revised data on the rates of land use change conversion from country statistics processed by the Food and Agriculture Organization (FAO, 2010) now providing an arguably more robust estimate of the land use change flux (Houghton et al., 2012; Section 6.3.2.2), (2) new global compilation of forest inventory data, based upon thousands of individual forest measurements in the northern forests, providing an independent estimate of the amount of carbon that has been gained by forests over the past two decades, albeit with very scarce measurements for tropical forest (Pan et al., 2011), (3) over 2 million new observations of the partial pressure of CO_2 at the ocean surface (pCO_2) have been taken, added to global databases (Pfeil et al., subm.; Takahashi et al., 2009), and used to quantify ocean CO_2 sink variability and trends (Section 6.3.2.5.4) and to evaluate and constrain models (Schuster et al., subm.; Wanninkhof et al., subm.), and (4) for both ocean and land regions, the use of multiple constraints with atmospheric inversions and combined atmosphere-ocean inversions (so called top down approaches) and the up-scaling of reservoir-based observations using models (so called bottom up approaches) providing coarse scale consistency checks on CO_2 flux estimates for a number of large regions of the globe (Ciais et al., 2010; McGuire et al., 2009; Piao et al., 2009a). The global anthropogenic CO_2 budget estimated from a range of observations and methods accounts for most of the trends in the CO_2 sinks, and a large part of the observed variability (Le Quere et al., 2009; Sitch et al., 2008). The causes of the year-to-year variability observed in the annual atmospheric CO_2 accumulation shown in Figure 6.8 are estimated

with a medium to high confidence to be largely driven by terrestrial processes occurring in tropical latitudes as inferred from atmospheric CO_2 inversions and supported by ocean data and models (Figure 6.9; Section 6.3.2.5.1).

[INSERT FIGURE 6.9 HERE]

Figure 6.9: The interannual variability of surface CO_2 fluxes from inversions of the TRANSCOM project for the period of 1981–2010. The ensemble of inversion results contains up to 17 atmospheric inversion models. The orange bars at the bottom panel indicates the number of available inversion models for each time period. The ensemble mean is bounded by the 1 sigma inter-model spread in ocean-atmosphere (blue) and land-atmosphere (green) CO_2 fluxes (PgC yr^{-1}) grouped into large latitude bands, and the global. For each flux and each region, the CO_2 flux anomalies were obtained by subtracting the long term mean flux from each inversion and removing the seasonal signal. Grey shaded regions indicate El Niño episodes, and the back bars indicate the cooling period following the Mt. Pinatubo eruption. A positive flux means a larger than normal source of CO_2 to the atmosphere (or a smaller CO_2 sink).

6.3.2.1 CO_2 Emissions from Fossil Fuel Combustion and Cement Production

Global CO_2 emissions from the combustion of fossil fuels used for this chapter are determined from national energy consumption statistics and converted to emissions by fuel type (Marland and Rotty, 1984). Estimated uncertainty for the annual global emissions are on the order of ± 8% (converted from ± 10% uncertainty for 95% confidence intervals in Andres et al. (2012) to the 90% confidence intervals used here). The uncertainty has been increasing in recent decades because a larger fraction of the global emissions originate from emerging economies where energy statistics and emission factors per fuel type are more uncertain (Gregg et al., 2008). CO_2 emissions from cement production were 4% of the total emissions during 2000–2009, compared to 3% in the 1990s. Additional emissions from gas flaring represent <1% of the global emissions.

Global CO_2 emissions from fossil fuel combustion and cement production were 7.7 ± 0.6 PgC yr^{-1} on average in the decade 2000–2009, 6.4 ± 0.5 PgC yr^{-1} during 1990–1999, and 5.5 ± 0.4 PgC yr^{-1} during 1980–1989 (Table 6.1; Figure 6.9). Global fossil fuel CO_2 emissions increased by 2.9% yr^{-1} on average during the decade 2000–2009 compared to 1.0% yr^{-1} in the 1990s and 1.9% yr^{-1} in the 1980s. The global financial crisis in 2008–2009 induced only a short-lived drop in global emissions in 2009 (1.3%; Peters et al., 2012), with the return to high annual growth rates of 5.9% and 3.2% in 2010 and 2011, respectively, and fossil fuel CO_2 emissions of 9.4 ± 0.8 PgC in 2011.

6.3.2.2 CO_2 Fluxes from Deforestation and other Land Use Change

CO_2 is emitted to the atmosphere by land use and land use change processes, in particular deforestation, and taken up from the atmosphere by other land use change processes such as afforestation and regrowth on abandoned lands. A critical distinction in estimating land use change is the difference between gross and net emissions. Gross emissions include all the emissions to the atmosphere from carbon loss in above ground vegetation (instantaneous) and soils (longer-term), while net emissions include in addition carbon uptake by forest regrowth and soil sequestration on abandoned agricultural lands, afforestation and long-term change of storage in wood products. Here we report net emissions, one of the drivers of the atmospheric CO_2 increase in the global budget assessment of Table 6.1. Land use change CO_2 emissions occur on different time scales including instantaneous release of carbon to the atmosphere, e.g., through combustion, and longer-term decomposition of dead plant material and soil organic matter. Logging and other forms of biomass removal emit CO_2 to the atmosphere when slash left on the ground burns or decomposes and when wood products (e.g., paper, timber) reach the end of their lifetime (e.g., through combustion or decaying in landfills).

Approaches to estimate net CO_2 fluxes from land use fall into three categories: (1) a 'bookkeeping' method that tracks carbon in living vegetation, dead plant material, wood products and soils with cultivation, harvesting and reforestation using country-level reports on changes in forest area and biome-averaged biomass values (Houghton, 2003); (2) process-based terrestrial ecosystem models that simulate on a grid the carbon stocks (biomass, soils) and exchange fluxes between vegetation, soil, and atmosphere using as input spatially-explicit time varying maps of the area of each biome (see references in Table 6.2), and (3) detailed regional (primarily tropical forests) analyses based on satellite data that estimate changes in forest area with high spatial resolution (Achard et al., 2004; DeFries et al., 2002) combined with the above-mentioned type of bookkeeping model (Achard et al., 2004; DeFries et al., 2002), and more recently combined with satellite derived maps of tropical forest biomass (Harris et al., 2012; Baccini et al., 2012). Satellite-derived estimates

of CO_2 emissions to the atmosphere from so-called deforestation fires (van der Werf et al., 2010) provide additional constraints on the spatial attribution and variability of land use change gross emissions. Most global estimates ignore emissions from peat burning or decomposition after a land use change, which are estimated at 0.30 PgC yr^{-1} over 1997–2006 (van der Werf et al., 2009) but can reach much higher values during extreme years when peat forest is affected (Ballhorn et al., 2009; Page et al., 2002) and emissions from the decomposition of drained peat which are estimated at 0.1 to 0.23 PgC yr^{-1} for Southeast Asia alone (Hooijer et al., 2010). The processes and time scales captured by these methods to estimate net land use change CO_2 emissions are diverse, creating difficulties with comparison of different estimates (Houghton et al., 2012; Table 6.2). For example, methods that do not include long-term 'legacy' fluxes from soils caused by deforestation prior to the starting period underestimate net land use change CO_2 emissions by 13–62% depending on the starting year and decade (Ramankutty et al., 2006).

Table 6.2: Estimates of net land to atmosphere CO_2 flux from land use change (PgC yr^{-1}). Positive values indicate CO_2 losses to the atmosphere from land ecosystems and in some estimates from wood products generated by land use change as well. Processes included are I=initial biomass loss D=decomposition of slash and soil carbon during the year of initial loss, R=regrowth, S=change in storage in wood products pools and L='legacy' long-term decomposition flux carried over from land use change transitions prior to start of time period used for reporting in the table. In the absence of data on L in the assessed estimates, the studies have either assumed I = instantaneous loss of all biomass and soil carbon (a committed future flux) or did not considered the legacy flux L.

	Data for Land Use Change Area[a]	Biomass Data	Processes Included	1980–1989 PgC yr^{-1}	1990–1999 PgC yr^{-1}	2000–2009 PgC yr^{-1}
Bookkeeping Method (global)						
Houghton et al. (2012)	FAO-2010	observed[b]	All	1.4	1.5	1.1
Satellite-based Methods (tropics only)						
Achard et al. (2004)	Landsat	observed[b]	I, D, R, S		0.9 (0.5–1.4)[c]	
DeFries et al. (2002)	AVHRR	observed[b]	I, D, R, S[d]	0.6 (0.3–0.8)	0.9 (0.5–1.4)	
Van der Werf et al. (2010)	GFED	CASA[e]	I, D		1.2 (0.6–1.8)[f]	
Baccini et al. (2012)	FAO-2010	satellite data	All			1.0
Process Models (global)						
Shevliakova et al. (subm.)	HYDE	LM3V	All	1.6	1.3	1.0
van Minnen et al. (2009)[g]	HYDE	IMAGE 2[e]	All	1.8	1.4	1.2
Strassmann et al. (2008)	HYDE	BernCC[e]	I, D, R, L	1.3	1.3	
Stocker et al. (2011)[g]	HYDE	BernCC[e]	I, D, R, L	1.4	0.9	0.6
Jain et al. (subm.)	SAGE	ISAM[e]	all	1.7	1.7	
Jain et al. (subm.)	FAO-2005	ISAM[e]	all	1.7	1.8	
Jain et al. (subm.)	HYDE	ISAM[e]	all	2.2	1.5	1.2
Arora and Boer (2010)	SAGE	CTEM[e]	all	1.1[h]	1.1[h]	
Arora and Boer (2010) [g]	HYDE	CTEM[e]	all	0.4[h]	0.4[h]	
Poulter et al. (2010)[g]	HYDE	LPGmL[e]	all	1.0	0.9	0.5
Kato et al. (2012)[g]	HYDE	VISIT[e]	all	1.2	1.0	0.5
Zaehle et al. (2011)	HYDE	O-CN	all	1.2	1.0	
Average of process models[i]				1.4 ± 0.8	1.2 ± 0.6	0.8 ± 0.6

Notes:
(a) References for the databases used: FAO (2010) as applied in Houghton et al. (2012); FAO (2005) as applied in Houghton (2003), updated; GFED (van der Werf et al., 2009); HYDE (Goldewijk et al., 2011), SAGE (Ramankutty and Foley, 1999). Landsat and AVHRR are satellite-based data and GFED is derived from satellite products as described in the references.
(b) Based on average estimates by biomes compiled from literature data (see details in corresponding references).
(c) 1990–1997 only.

(d) Legacy fluxes for land cover change prior to 1980 are not included and are estimated to add about 0.2 PgC yr^{-1} to the 1980s and 0.1 PgC yr^{-1} to the 1990s estimates, based on (Ramankutty et al., 2006).
(e) The vegetation and soil biomass is computed using a vegetation model described in the reference.
(f) 1997–2006 average based on estimates of carbon emissions from deforestation and degradation fires, including peat carbon emissions. Estimates were doubled to account for emissions other than fire including respiration of leftover plant materials and soil carbon following deforestation following (Olivier et al., 2005). Estimates include peat fires and oxidation. If peat fires are excluded, estimate in tropical Asia is 0.23 and Pan-tropical total is 0.71
(g) Method as described in the reference but updated to 2010 using the land cover change data listed in column 2.
(h) The large variability produced by the calculation method is removed for comparison with other studies by averaging the flux over the two decades.
(i) Average of estimates from all process models and 90% confidence uncertainty interval; note that the spread of the different estimates does not follow a Gaussian distribution.

Global net CO_2 emissions from land use change are estimated at 1.4, 1.5, and 1.1 PgC yr^{-1} for the 1980s, 1990s and 2000s, respectively, by the bookkeeping method of Houghton et al. (2012) (Table 6.2; Figure 6.10). This estimate is consistent with global emissions from process-based terrestrial ecosystem models using mainly three land cover change data products as input for time-varying maps of land use change (Table 6.2). The bookkeeping method estimate is also generally consistent although higher than the satellite-based methods (tropics only). Part of the discrepancy can be accounted for by emissions from extratropical regions (~0.1 PgC yr^{-1}; Table 6.3) and by legacy fluxes for land cover change prior to 1980s (~0.2 PgC yr^{-1}) that are not covered by satellite based methods used in Table 6.2. We adopt an uncertainty of ± 0.8 PgC yr^{-1} as representative of 90% uncertainty intervals. This is identical to the uncertainty of ± 0.5 PgC yr^{-1} representing ± 1-sigma interval (68% if Gaussian distributed error) from Houghton et al. (2012). The uncertainty of ± 0.8 PgC yr^{-1} on net land use change CO_2 fluxes is smaller than the one that was reported in AR4 of 0.5 to 2.7 PgC yr^{-1} for the 1990s (68% confidence interval). In this chapter, uncertainty is estimated based on expert judgment of the available evidence, including improved accuracy of land cover change incorporating satellite data, the larger number of independent methods to quantify emissions and the consistency of the reported results (Table 6.2; Figure 6.10). In particular, the FAO forest area loss data were revised downwards in 2010 following improvements in data coverage, for instance, new data were introduced for Indonesia and higher resolution satellite data were used for the Amazon basin (FAO, 2010).

The lower land use change CO_2 emissions reported in the 2000s compared to the 1990s, by 0.4 PgC yr^{-1} in the bookkeeping method based on FAO (2010), and by 0.3–0.5 PgC yr^{-1} from five process-based ecosystem models based on the HYDE land cover change data updated to 2009 (Goldewijk et al., 2011), is within the error bar of the data and methods. Sixty one percent of the emissions originated from the tropics in the 1980s on average across methods, a share that increased to 67% in the 1990s and 73% in the 2000s. However the range of estimates is large and estimates from the bookkeeping method and process-based ecosystem models do not agree in the extra tropics (Table 6.3). Furthermore, the FAO (2010) forest report, based on country level reporting supported with satellite data for some countries, suggests decreasing forest loss between 2000 and 2005, while the FAO recent entirely satellite-based analysis suggests the contrary. These inconsistencies in the available land cover change data and in the modeling results prevent a firm assessment of recent trends and their partitioning among regions (see data in Table 6.3).

[INSERT FIGURE 6.10 HERE]
Figure 6.10: CO_2 emissions from land use change from a range of methods (PgC yr^{-1}). The estimate from Houghton et al. (2012) (thick black) is used in Table 6.1. The sources for the other estimates are shown in the legend and described in Table 6.2.

Table 6.3: Estimates of net land to atmosphere flux from land use change (PgC yr^{-1}; except where noted) for decadal periods from 1980s to 2000s by region. Positive values indicate net CO_2 losses from land ecosystems affected by land use change to the atmosphere. Uncertainties are reported as 90% confidence interval (unlike 68% in AR4). Numbers in parentheses are ranges in uncertainty provided in some studies. Tropical Asia includes the Middle East, India and surrounding countries, Indonesia and Papua New Guinea. East Asia includes China, Japan, Mongolia and Korea. N/A indicates not available from the study cited.

	Central and South Americas	Africa	Tropical Asia	North America	Eurasia	East Asia	Oceania

2000s							
van der Werf et al. (2010)[a,b]	0.33	0.15	0.35	N/A	N/A	N/A	N/A
DeFries and Rosenzweig (2010)[c]	0.46	0.08	0.36	N/A	N/A	N/A	N/A
Houghton et al. (2012)	0.48	0.31[e]	0.25	0.01	–0.07[d]	0.01[e]	N/A
van Minnen et al. (2009)[a]	0.45	0.21	0.20	0.09	0.08	0.10	0.03
Stocker et al. (2011)[a]	0.19	0.18	0.21	0.019	–0.067	0.12	0.011
Jain et al. (subm.)[a]	0.14	0.03	0.25	0.25	0.39	0.12	0.02
Poulter et al. (2010)[a]	0.09	0.13	0.14	0.01	0.03	0.05	0.00
Kato et al. (2012) [a]	0.36	–0.09	0.23	–0.05	–0.04	0.10	0.00
Average	0.31 ± 0.25	0.13 ± 0.20	0.25 ± 0.12	0.05 ± 0.17	0.12 ± 0.31	0.08 ± 0.07	0.01 ± 0.02
1990s							
DeFries et al. (2002)	0.5 (0.2–0.7)	0.1 (0.1–0.2)	0.4 (0.2–0.6)				
Achard et al. (2004)	0.3 (0.3–0.4)	0.2 (0.1–0.2)	0.4 (0.3–0.5)				
Houghton et al. (2012)	0.67	0.32[e]	0.45	0.05	–0.04[d]	0.05[e]	
van Minnen et al. (2009)[a]	0.48	0.22	0.34	0.07	0.08	0.20	0.07
Stocker et al. (2011)[a]	0.30	0.14	0.19	–0.072	0.11	0.27	0.002
Jain et al. (subm.) [a].	0.20	0.04	0.31	0.27	0.47	0.19	0.00
Poulter et al. (2010)[a]	0.26	0.13	0.12	0.07	0.16	0.11	0.01
Kato et al. (2012)[a]	0.53	0.07	0.25	–0.04	–0.01	0.16	0.02
Average	0.41 ± 0.27	0.15 ± 0.15	0.31 ± 0.19	0.08 ± 0.19	0.16 ± 0.30	0.16 ± 0.13	0.02 ± 0.05
1980s							
DeFries et al. (2002)	0.4 (0.2–0.5)	0.1 (0.08–0.14)	0.2 (01–0.3)				
Houghton et al. (2012)	0.79	0.22[e]	0.32	0.04	0.00[d]	0.07[e]	
van Minnen et al. (2009)[a]	0.70	0.18	0.43	0.07	0.06	0.37	0.04
Stocker et al. (2011)[a]	0.44	0.16	0.25	0.085	0.11	0.40	0.009
Jain et al. (subm.)[a]	0.26	0.01	0.34	0.30	0.71	0.59	0.00
Poulter et al. (2010)[a]	0.37	0.11	0.19	0.02	0.03	0.29	0.01
Kato et al. (2012)[a]	0.61	0.07	0.25	–0.04	–0.02	0.35	0.01
Average	0.51 ± 0.32	0.12 ± 0.12	0.28 ± 0.14	0.08 ± 0.19	0.15 ± 0.46	0.35 ± 0.28	0.01 ± 0.03

Notes:
(a) Method as described in the reference but updated to 2010 using the HYDE land cover change data.
(b) 1997–2006 average based on estimates of CO_2 emissions from deforestation and degradation fires, including peat carbon emissions. Estimates were doubled to account for emissions other than fire including respiration of leftover plant materials and soil carbon following deforestation following (Olivier et al., 2005). Estimates include peat fires and peat soil oxidation. If peat fires are excluded, estimate in tropical Asia is 0.23 and Pan-tropical total is 0.71.
(c) CO_2 estimates were summed for dry and humid tropical forests, converted to C and normalized to annual values. Estimates are based on satellite-derived deforestation area (Hansen et al., 2010), and assume 0.6 fraction of biomass emitted with deforestation. Estimates do not include carbon uptake by regrowth or legacy fluxes from historical deforestation. Estimates cover emissions from 2000 to 2005.
(d) Includes China only.
(e) East Asia and Oceania are averaged in one region. The flux is split in two equally for computing the average; North Africa and the Middle East are combined with Eurasia.

The estimates of net land use change CO_2 emissions are shown in Figure 6.10. Estimated gross emissions from tropical deforestation were 3.0 ± 0.5 PgC yr^{-1} for the 1990s and 2.8 ± 0.5 PgC yr^{-1} for the 2000s using forest inventory data, FAO (2010) reporting and the bookeeping model method (Pan et al., 2011). The so called 'gross emissions' defined by all forest removal including both permanent deforestation and more temporary shifting cultivation and wood harvest cycles are about double the net emissions because of the presence of a large regrowth that compensates for about half of the gross emissions. A recent analysis estimated far lower gross deforestation of 0.6–1.2 PgC yr^{-1} (Harris et al. 2012). However that study primarily

estimated permanent deforestation and excluded additional gross emissions from degraded forests, shifting agriculture and some carbon pools (Houghton et al., 2012; House, subm.; van der Werf and Defries, subm.). Understanding the different system boundary issues and what is and is not included in different analyses can reconcile most of the difference between different 'gross emissions' published estimates (House, subm.).

Over the 1750–2011 time period, cumulative net CO_2 emissions from land use change of 180 ± 80 PgC are estimated using the cumulative land use emissions of 150 PgC of Houghton et al. (2012) during 1850–2011 (Table 6.1) and an additional 30 PgC for 1750–1850 from the average of four publications (22 PgC by Pongratz at al., 2009); 15 PgC by van Minnen et al. (2009); 64 PgC by Shevliakova et al. (2009b) and 24 PgC by Zaehle et al. (2011)). The uncertainty is based on the spread of the available estimates (Figure 6.10). The CO_2 flux from land use has been dominated by deforestation and other land use change in the mid northern latitudes prior to 1980s, and in the tropics since approximately 1980, largely from deforestation in tropical America and Asia with smaller contributions from tropical Africa. Deforestation from 800 to 1750 has been estimated at 27 PgC using a process-based ecosystem model (Pongratz et al., 2009).

6.3.2.3 Atmospheric CO_2 Concentration Growth Rate

Since the beginning of the Industrial Era (1750), the concentration of CO_2 in the atmosphere increased by 40%, from 278 ± 5 ppm to 390.4 ppm in 2011 (Figure 6.11), updated from MacFarling-Meure et al. (2006), corresponding to an increase in CO_2 of 240 ± 10 PgC in the atmosphere. Atmospheric CO_2 grew at a rate of 3.4 ± 0.2 PgC yr^{-1} in the 1980s, 3.1 ± 0.2 PgC yr^{-1} in the 1990s, and 4.0 ± 0.2 PgC yr^{-1} in the 2000s (Conway and Tans, 2011): data from NOAA/ESRL and Scripps Institution of Oceanography (www.esrl.noaa.gov/gmd/ccgg/trends/). The rise of atmospheric CO_2 is established with a very small uncertainty from measurements of CO_2 trapped in air bubbles in ice cores, between 1750 and 1957 e.g., Etheridge et al. (1996), and from highly precise continuous atmospheric CO_2 concentration measurements at background stations after that date (Keeling et al., 1976).

[INSERT FIGURE 6.11 HERE]

Figure 6.11: Atmospheric CO_2, CH_4, and N_2O concentrations history over the last 260 years determined from air enclosed in ice cores and firn air (color symbols) and from direct atmospheric measurements (blue lines, measurements from the Cape Grim observatory) (MacFarling-Meure et al., 2006).

The ice core record of atmospheric CO_2 concentration during the past century exhibits some interesting features, which can be related to climate induced-changes in the carbon cycle. Most conspicuous is the interval from about 1940 until the early 1960s, during which the concentration increase of CO_2 (also CH_4 and N_2O) stalled (MacFarling-Meure et al., 2006), possibly caused by slightly decreasing temperatures over land in the Northern Hemisphere (Rafelski et al., 2009).

There is substantial evidence (e.g., from ^{13}C carbon isotopesin atmospheric CO_2, Keeling et al., 2005) that source/sink processes on land generate most of the interannual variability in the atmospheric CO_2 growth rate as shown in Figure 6.12 (Section 6.3.2.5). The data shown in this figure indicate that the strong positive anomalies of the CO_2 growth rate in El Niño years (e.g., 1987/1988 and 1997/1998) originated in tropical latitudes, while the anomalies in 2003 and 2005 originated in northern mid- latitudes, maybe reflecting the European heat wave in 2003 (Ciais et al., 2010).

[INSERT FIGURE 6.12 HERE]

Figure 6.12: (Top) Global average atmospheric CO_2 growth rate, computed from the observations of the SIO network (dark green curve; Keeling et al., 2005) and from the marine boundary layer air reference measurements of the NOAA-GMD network (Conway et al., 1994; Keeling et al., 2005). (Bottom) Atmospheric growth rate of CO_2 as a function of latitude determined from the GLOBALVIEW data product, representative of stations located in the marine boundary layer at each given latitude (Masarie and Tans, 1995). Sufficient observations are available only since 1979.

6.3.2.4 CO_2 Airborne Fraction

The ratio of CO_2 annual groth rate in the atmosphere to total anthropogenic CO_2 emissions (fossil fuel and cement, plus net land use change emissions), i.e., the fraction of total emissions remaining in the atmosphere, is called the 'airborne fraction' (AF). This is an important diagnostic of the efficiency and variability of the CO_2 sinks at absorbing excess CO_2 from total anthropogenic emissions. Several factors can influence the AF.

First and most importantly, the AF responds to the emissions trajectory through the effect of atmospheric CO_2 on sinks. The AF is expected to be constant if emissions grow exponentially with a constant time scale (e-folding) and if the sinks respond linearly to increasing CO_2 (Bacastow and Keeling, 1979; Gloor et al., 2010). As emissions depart from exponential growth with constant time scale, the AF departs from constancy. In addition, other factors can influence the AF, such as changes in the response of carbon sinks to rising CO_2, nutrient availability, land management, and changes in physical climate and changes in terrestrial and marine ecosystems (nonlinear effects of climate on carbon fluxes). Climate and CO_2 effects were suggested to be important drivers of AF changes in future projections from coupled carbon-climate models used in the AR4 (Friedlingstein et al., 2006), with a diagnosed increase in the AF of 0.07 (median of 11 models; range of 0.01–0.22; Canadell et al. (2007)) in 2100 under the SRES-A2 emission scenario.

Up to the date of publication of the AR4, no significant trend in AF had been identified over the period since 1959 (for which the most accurate atmospheric CO_2 data are available). Until recently, the uncertainty in land use change emissions was too large to provide a meaningful measure of the trend in AF, and a definition of the AF using fossil fuel emissions only was used, such as Figure 7.4 in AR4. Improved forest area loss data from country statistics (FAO, 2010) and satellite data (Hansen et al., 2010; Regalado, 2010) have contributed to reducing the uncertainty in tropical land use CO_2 emission estimates (Section 6.3.2.2). A positive trend in AF of ~0.3%yr^{-1} relative to the mean was found by all recent studies using total anthropogenic CO_2 emissions to define AF, over the ~1960–2010 period, but there is no consensus on the significance (Ballantyne et al., 2012; Knorr, 2009) and the cause of this trend (Canadell et al., 2007; Gloor et al., 2010; Raupach et al., 2008). The significance of the AF positive trend is influenced by the specific consideration of uncertainty and (in some studies) by the method used to filter out 'known' variability associated with El Niño and volcanic major eruptions. The cause of the trend in the AF is also disputed, but land and ocean carbon cycle model results attributing the trends to underlying processes suggest that climate effects on ocean and land sinks could have a large influence (Le Quere et al., 2009), but that the role of climate variability is important as well (Raupach et al., subm.) and could dominate the signal (Frölicher et al., subm.).

6.3.2.5 Ocean Sinks

6.3.2.5.1 Global ocean sink

The estimate of the mean anthropogenic ocean CO_2 sink from AR4 of 2.2 ± 0.7 PgC yr^{-1} (uncertainty converted from 68% in AR4 to 90% confidence intervals in this Chapter) is unchanged from the AR4 report and confirmed by several contemporary estimates (see Chapter 3). The uptake of anthropogenic CO_2 by the ocean is primarily a response to increasing CO_2 in the atmosphere and is limited mainly by the rate at which anthropogenic CO_2 is transported from the surface waters into the deep waters (Gloor et al., 2010). However, this anthropogenic ocean CO_2 sink occurs on top of a very active natural oceanic carbon cycle. Recent trends in the climate system, such as ocean warming, changes in ocean circulation and changes in marine ecosystems and biogeochemical cycles can have affected both the anthropogenic ocean CO_2 sink occurs as well as natural CO_2 fluxes exchanged with the atmosphere. Since AR4, progress has been made to quantify the rate of change of the net ocean CO_2 sink in the past decades, including the attribution to the response of the ocean to increasing CO_2 in the atmosphere, and the response to climate and circulation trends and variability, as explained below.

Observations of the partial pressure of CO_2 at the ocean surface (pCO_2) show that pCO_2 has been increasing generally at about the same rate as CO_2 in the atmosphere when averaged over large ocean regions during the past two to three decades (Inoue and Ishii, 2005; McKinley et al., 2011; Takahashi et al., 2009). However, analyses of regional observations highlight substantial regional and temporal variations around this mean trend of pCO_2, with surface ocean pCO_2 increasing regionally either at the same rate or faster than atmospheric CO_2 between about 1990 and 2005 in the North Atlantic (Schuster et al., 2009; thus a constant, or a decreasing sink for CO_2 in that region) and between 1981 and 2004 in the western equatorial Pacific (Feely et al., 2006). A weakening sink in the Southern Ocean was also inferred from atmospheric CO_2 observations using one inversion model (Le Quere et al., 2007). By contrast, pCO_2 appears to have increased at a slower rate than atmospheric CO_2 (thus a growing ocean CO_2 sink in that region) in the Northern North Pacific Ocean (Takahashi et al., 2006).

The difference between decadal values of the ocean anthropogenic CO_2 sink is assessed in this Chapter with an ensemble of five studies using various methods, giving a decadal mean uptake of 2.0 ± 0.7 PgC yr^{-1} for 1980–1989 and of 2.3 ± 0.7 PgC yr^{-1} for 2000–2009 (Table 6.4). The methods used are: (1) an empirical Green's function approach fitted to observations of transient ocean tracers (Khatiwala et al., 2009), (2) a model-based Green's function approach fitted to anthropogenic carbon reconstructions (Mikaloff-Fletcher et al., 2006), (3) empirical relationships between ocean surface pCO_2 and temperature and salinity (Park et al., 2010), and (4) process-based global ocean biogeochemical models forced by observed meteorological fields (Assmann et al., 2010; Doney et al., 2009; LeQuere et al., 2010). All these different methods suggest that in the absence of recent climate change and climate variability, the ocean anthropogenic CO_2 sink should have increased by 0.23 ± 0.15 PgC yr^{-1} between the 1980s and the 1990s, and by 0.33 ± 0.13 PgC yr^{-1} between the 1990s and the 2000s (Figure 6.13). The decadal estimates in the ocean CO_2sink reported in Table 6.4 as 'CO_2 effects only' are entirely explained by the faster rate of increase of atmospheric CO_2 in the later decade. On the other hand, 'climate effects only' in Table 6.4 are assessed to have no noticeable effect on the sink difference between the 1980s and the 1990s (0.02 ± 0.05 PgC yr^{-1}), but are estimated by process-based models to have reduced the ocean anthropogenic CO_2 sink by 0.19 ± 0.18 PgC yr^{-1} between the 1990s and the 2000s (Table 6.4).

Table 6.4: Decadal change in the ocean CO_2 sink from models and from data-based methods (a positive change between two decades means an increasing sink with time). It is reminded that the total CO_2 sink for the 1990s is estimated at 2.2 ± 0.7 PgC yr^{-1} based on observations.

	Method	1990s minus 1980s PgC yr^{-1} $decade^{-1}$	2000s minus 1990s PgC yr^{-1}
CO_2 effects only			
Khatiwala et al. (2009)	data based	0.24	0.20
Mikaloff-Fletcher et al. (2006)[a]	data inversion	0.40	0.44
Assmann et al. (2010) (to 2007 only)	model	0.28	0.35
Graven et al. (2012)	model	0.15	0.25
Doney et al. (2009)	model	0.15	0.39
Le Quere et al. (2010) NCEP	model	0.16	0.32
Le Quere et al. (2010) ECMWF	model	–	0.39
Le Quere et al. (2010) JPL	model	–	0.32
Average[b]		0.23 ± 0.15	0.33 ± 0.13
Climate effects only			
Park et al. (2010)	data-based	–	–0.15
Assmann et al. (2010) (to 2007 only)	model	0.07	0.00
Graven et al. (2012)	model	0.02	–0.27
Doney et al. (2009)	model	–0.02	–0.21
Le Quere et al. (2010) NCEP	model	0.02	–0.27
Le Quere et al. (2010) ECMWF	model	–	–0.14
Le Quere et al. (2010) JPL	model	–	–0.36
Average[b]		0.02 ± 0.05	–0.19 ± 0.18
CO_2 and climate effects combined		0.25 ± 0.16	0.14 ± 0.22

Notes:
(a) As published by Sarmiento et al. (2010).
(b) Average of all estimates ± 90% confidence interval. The average includes results by Le Quere et al. (2010) – NCEP only because the other Le Quere et al. model versions do not differ sufficiently to be considered separately.
(c) The NCEP, ECMWF and JPL reproduce surface climate conditions as described in the reference.

[INSERT FIGURE 6.13 HERE]

Figure 6.13: Trends in the ocean-to-atmosphere flux of CO_2 in response to: (Top) variability and trends in surface climate, (middle) increasing atmospheric CO_2, and (Bottom) the sum of both effects (PgC yr^{-1}). All estimates are normalized to zero during 1990–2000 to highlight the trends. Estimates are updates from ocean models (in colours) and from indirect methods based on observations (Khatiwala et al., 2009; Park et al., 2010).

6.3.2.5.2 Regional air-sea CO_2 fluxes

Because of the superposition of an active natural cycle and the ocean anthropogenic CO_2 sink, a global map of net air-sea fluxes of CO_2 show regions in the ocean where CO_2 is absorbed from the atmosphere, and regions where CO_2 is released to the atmosphere, even though overall the ocean absorb about 2 PgC every year. The Equatorial Pacific (14°N–14°S) is a major net source for atmospheric CO_2 because deep waters rich in carbon are upwelled to the surface, losing about 0.5 PgC yr^{-1} (Takahashi et al., 2009). The temperate oceans, between 14° and 50° in both hemispheres, are major sink zones. Altogether, the Atlantic and Arctic oceans act as a net CO_2 sink of 0.6 ± 0.2 PgC yr^{-1} (Schuster et al., subm.). The North Atlantic is the most intense ocean CO_2 sink region on a per unit area basis, due to the combination of strong ocean mixing with strong biological productivity and cooling of surface waters. The Southern Ocean (<44°S) is estimated to be a CO_2 sink of ~ 0.3 PgC yr^{-1} (Gruber et al., 2009). It is not as intense as the North Atlantic because of a partial cancellation of the summer CO_2 uptake by the winter release of CO_2 from the upwelling of CO_2-enriched deep water (Gruber et al., 2009). The North Pacific and Southern Ocean subtropics are also sinks for CO_2 (Takahashi et al., 2009).

6.3.2.5.3 Regional changes in ocean dissolved inorganic carbon storage

Data-based estimates for the global ocean inventory of anthropogenic carbon obtained from repeated shipboard hydrographic cross sections (Khatiwala et al., 2009; Sabine et al., 2004; Waugh et al., 2006) agree well among each other, with an average value of 155 ± 30 PgC for the period 1750–2011 (See Chapter 3). The uptake of anthropogenic carbon into the ocean is observed to be larger in the high latitudes than in the tropics and subtropics over the entire Industrial Era, because of the more vigorous ocean mixing in the high latitudes (Khatiwala et al., 2009). A number of ocean cross sections have been repeated over the last decade and the observed changes in carbon storage, assessed in Table 6.5, suggest that some locations see rates of carbon accumulation that are higher and others that are lower than the global average estimated by Khatiwala et al. (2009). No global synthesis of these observations exists at present. Model results suggest that there may be an effect of climate change and variability in the storage of total inorganic carbon in the ocean (Table 6.4), but that this effect is small (~2 PgC over the past 50 years; Figure 6.13) compared to the cumulative uptake of anthropogenic carbon during the same period.

Table 6.5: Regional rates of change in inorganic carbon storage from repeated hydrographic cross sections

Section	Time	Storage rate (mol C m^{-2} yr^{-1})	Data source
Global average	2008	0.53 ± 0.16	Khatiwala et al. (2009)
Pacific Ocean			
Section along 30°S	1992–2003	1.0 ± 0.4	Murata et al. (2007)
N of 50°S, 120°W–180°W	1974–1996	0.9 ± 0.3	Peng et al. (2003)
154°W, 20°–50°S	1991–2006	0.56 ± 0.04	Sabine et al. (2008)
140°E–170°W, 45°S–65°S	1968–1991/1996	0.40 ± 0.20	Matear and McNeil (2003)
149° W, 4°S–10°N	1993–2005	0.3 ± 0.1	Murata et al. (2009)
149° W, 24°N–30°N	1993–2005	0.6 ± 0.2	Murata et al. (2009)
Northeast Pacific	1973–1991	1.3 ± 0.5	Peng et al. (2003)
~160°E ~45°N	1997–2008	0.40 ± 0.08	Wakita et al. (2010)
North of 20°N	1994–2004/2005	0.39 ± 0.15	Sabine et al. (2008)
150°W, 20°S–20°N	1991/1992–2006	0.25 ± 0.09	Sabine et al. (2008)
Indian Ocean			
20°S–10°S	1978–1995	0.1	Peng et al. (1998)

10°S–5°N	1978–1995	0.65	Peng et al. (1998)
Section along 20°S	1995–2003/2004	1.0 ± 0.1	Murata et al. (2010)
Atlantic Ocean			
Section along 30°S	1992/1993–2003	0.6 ± 0.1	Murata et al. (2010)
~30°W, 56°S–15°S	1989–2005	0.76	Wanninkhof et al. (2010)
20°W, 64°N–15°N	1993–2003	0.57	Wanninkhof et al. (2010)
~25°W, 15°N–15°S	1993–2003	0.2	Wanninkhof et al. (2010)
40°N–65°N	1981–1997/1999	2.2 ± 0.7	Friis et al. (2005)
20°N– 40°N	1981–2004	1.2 ± 0.3	Tanhua et al. (2007)
Nordic Seas	1981–2002/2003	0.9 ± 0.2	Olsen et al. (2006)
Sub-decadal variations			
Irminger Sea	1981–1991	0.55 ± 0.39	Perez et al. (2008)
Irminger Sea	1991–1996	2.3 ± 0.6	Perez et al. (2008)
Irminger Sea	1997–2006	0.75 ± 0.16	Perez et al. (2008)

6.3.2.5.4 Interannual variability in air-sea CO_2 fluxes

The interannual variability in the global ocean CO_2 sink is estimated to be of about ± 0.2 PgC yr^{-1} (Wanninkhof et al., subm.) which is small compared to the interannual variability of the terrestrial CO_2 sink. In general, the ocean takes up more CO_2 during El Niño episodes (Park et al., 2010) because of the temporary suppression of the natural source of CO_2 to the atmosphere over the eastern Pacific upwelling, during El Niño episodes. Interannual variability of ~0.3 PgC yr^{-1} has been reported for the North Atlantic ocean region alone (Watson et al., 2009) but there is no agreement among estimates regarding the exact magnitude of driving factors of air-sea CO_2 flux variability in this region (Schuster et al., subm.). Interannual variability of 0.1–0.2 PgC yr^{-1} was also estimated by models and one atmospheric inversion in the Southern Ocean (Le Quere et al., 2007), possibly driven by the Southern Annular Mode of climate variability (Lenton and Matear, 2007; Lourantou and Metzl, 2011; Lovenduski et al., 2007).

6.3.2.5.5 Processes driving variability and trends in air-sea CO_2 fluxes

Three type of processes are estimated to have an important effect on the air-sea fluxes of CO_2 on century time scales: (1) the dissolution of CO_2 at the ocean surface and its chemical equilibrium with other forms of carbon in the ocean (mainly carbonate and bicarbonate), (2) the transport of carbon between the surface and the intermediate and deep ocean, and 3) the cycling of carbon through marine ecosystem processes (see Section 6.1.1.1). The surface dissolution and equilibration of CO_2 with the atmosphere is well understood and quantified. It varies with the surface ocean conditions, in particular with temperature (solubility effect) and alkalinity (a measure of the capacity of an aqueous solution to neutralize acids). The capacity of the ocean to take up additional CO_2 for a given alkalinity decreases at higher temperature (4.23% per degree warming (Takahashi et al., 1993) and at elevated CO_2 concentrations (about 15% per 100 ppm, computed from the so called Revelle factor). These effects are well established and have been included in all previous IPCC Assessments Reports.

The recent increase in North Atlantic surface water pCO_2 values since about 1990 at rates faster than atmospheric CO_2 (causing a sink decrease) appear to be related to sea surface warming and its effect on solubility (Corbiere et al., 2007) and/or changes in ocean circulation (Schuster and Watson, 2007; Schuster et al., 2009). Recent changes have been associated with decadal variability in the North Atlantic Oscillation (NAO) and the Atlantic Multidecadal Variability (AMV) positive state (McKinley et al., 2011; Thomas et al., 2007; Tjiputra et al., 2012; Ullman et al., 2009), but a systematic analysis of estimates of trends in this region show no agreement regarding the drivers of change (Schuster et al., subm.). In addition, rapid increases of pCO_2 observed in winter 2003–2008 (observed pCO_2 increases between 5 to 7 µatm yr^{-1}) have been attributed to an increase of deep convection (import of rich-CO_2 subsurface and deep waters) that dominates the effect of recent cooling on pCO_2 (Metzl et al., 2010).

The weakening of the Southern Ocean CO_2 sink identified from atmospheric and oceanic CO_2 observations (Le Quere et al., 2007; Metzl, 2009; Takahashi et al., 2009) is attributed by models as a response to an increase in Southern Ocean winds driving increased upwards transport of carbon-rich deep waters (Lenton and Matear, 2007; LeQuere et al., 2010; Lovenduski et al., 2007; Verdy et al., 2007). The increased upwelling is in part compensated by increasing eddy fluxes outside the Southern Ocean and by increasing export of carbon to depth from biological production (Lenton et al., 2009). The increase in winds has been attributed to indirect human activities, mainly to the depletion of stratospheric ozone (Thompson and Solomon, 2002) with a contribution from greenhouse gases (Fyfe and Saenko, 2006).

Large decadal variability has been observed in the Equatorial Pacific (Ishii et al., 2009) associated with changes in the phasing of the Pacific Decadal Oscillation and its impact on gas transfer velocity (Feely et al., 2006; Valsala et al., 2012). There is less evidence available to attribute the observed changes in other regions to changes in underlying processes or climate change and variability.

Recent changes in nutrient supply in the ocean are also thought to have changed the export of organic carbon from biological processes below the surface layer, and thus the ocean CO_2 sink. Anthropogenic reactive nitrogen Nr (see Box 6.1) entering the ocean via atmospheric deposition or rivers acts as a fertilizer and is enhancing carbon export to depth and hence the CO_2 sink. This Nr contribution has been estimated between 0.1 and 0.4 PgC yr^{-1} in around year 2000 using models (Duce et al., 2008; Krishnamurthy et al., 2009; Reay et al., 2008; Suntharalingam et al., 2012). Similarly, human-driven increase in iron deposition over the ocean from land use change is estimated to have enhanced the ocean cumulative CO_2 uptake by 8 PgC during the 20th century (~3 percent) (Mahowald et al., 2010). Although changes in ocean circulation and in global biogeochemical drivers have the potential to alter the ocean carbon fluxes through changes in marine ecosystems, modelling studies show only small variability in ocean biological pump, which has not significantly impacted the response of the ocean carbon cycle over the recent period (Bennington et al., 2009). Therefore, there is no evidence that changes in marine ecosystems have had a large impact on the ocean CO_2 sink in recent decades apart from those triggered by changes in nitrogen and iron supply.

Model studies suggest that the response of the air-sea CO_2 fluxes to climate change and variability in recent decades has decreased the rate at which anthropogenic CO_2 is absorbed by the ocean (Sarmiento et al. (2010), Sitch et al. (subm); Table 6.4). This result is robust to the model or climate forcing used (Figure 6.13). The climate-induced weakening of the ocean CO_2 sink was attributed in one model to increases in winds in the Southern Ocean and in the equatorial Pacific, with a ~20% contribution from warming and a 30% non-linear amplification of the response to climate change and variability due to surface ocean warming (LeQuere et al., 2010). No formal attribution to anthropogenic climate change has been made outside the Southern Ocean.

6.3.2.5.6 Model evaluation of global and regional ocean carbon balance

Ocean process-based carbon cycle models are capable to reproduce to a first order the mean air-sea fluxes of CO_2 derived from pCO_2 observations (Takahashi et al., 2009) for at least ten years, including their general patterns and amplitude (Sarmiento et al., 2000), the anthropogenic uptake of CO_2 (Orr et al., 2001; Wanninkhof et al., subm.), and the regional distribution of air-sea fluxes (Gruber et al., 2009). The spread between different model results for air-sea CO_2 fluxes is the largest in the Southern Ocean (Matsumoto et al., 2004), where intense mixing occurs. Tracer observations (Schmittner et al., 2009) and water mass analysis (Iudicone et al., 2011) have been used to reduce the model uncertainty associated with ocean mixing and improve the simulation of carbon fluxes. The models reproduce the observed seasonal cycle of pCO_2 in the sub-tropics but generally do poorly in sub-polar regions where the balance of processes is more difficult to simulate well (McKinley et al., 2006; Schuster et al., subm.). Less information is available to evaluate specifically the representation of biological fluxes in the models, outside from their reasonable representation of surface ocean chlorophyll. Ocean process-based carbon cycle models used in AR5 reproduce the relatively small interannual variability inferred from observations (Figure 6.11; Wanninkhof et al., subm.). See also Chapter 9, Section 9.4.5.2.

Sensitivity of modelled air-sea fluxes to CO_2. The sensitivity of ocean models to the level and rate of change of CO_2 in the atmosphere can be evaluated from several studies that have isolated the uptake of anthropogenic CO_2 from changes in natural fluxes using combinations of observations. Data-based studies have focused on three time-periods: 1750–1994, 1990–1999, and 1990–2009, and estimated a cumulative

uptake of carbon of ~120 ± 25 PgC (Khatiwala et al., 2009; Sabine et al., 2004; Waugh et al., 2006), a mean anthropogenic CO_2 sink of 2.2 ± 0.7 Pg C yr^{-1}, and decadal trends of 0.13 PgC yr^{-1} per decade during the two decades 1990–2009 (Wanninkhof et al., subm.; from atmospheric inversions), respectively. Models that have estimated these quantities give a total ocean uptake of 130 ± 24 PgC for 1750–1994 and a mean ocean CO_2 sink of 2.3 ± 0.4 PgC yr^{-1} for 1990–1999 (model ensemble from Orr et al., 2005), and a trend in uptake rate of 0.12 PgC yr^{-1} per decade for 1990–2009 (Wanninkhof et al., subm.). Therefore, although the ocean models do not reproduce all the details of the regional structure and changes in air-sea CO_2 fluxes, their globally integrated ocean CO_2 sink and decadal rate of change of this sink is in good agreement with the available observations.

Sensitivity of modelled air-sea fluxes to climate. The relationship between air-sea CO_2 flux and climate is strongly dependent on the oceanic region and on the time-scale. In general, the ocean takes up more CO_2 during El Niño events when the upwelling of carbon-rich waters in the Pacific decreases (see Section 6.3.6.4), and more CO_2 during glacial periods when the ocean temperature was cooler and the ocean circulation modified (see Section 6.2.2.1.1). Yet, these time scales are not fully relevant to assess how climate dynamics this century impacts air-sea CO_2 fluxes. Changes in atmospheric CO_2 by less than 25 ppm during Dansgaard-Oeschger abrupt climate events during glacial periods may have been caused by the ocean (Schmittner and Galbraith, 2008) on a millennial time scale see Section 6.2.1.2. Although these abrupt events are relevant to gain insight on processes, they were associated with a re-organisation of the sea surface temperature and ocean circulation, rather than with a GHG driven global mean temperature change as during the Industrial Era. Ocean carbon cycle models used in AR5 estimate a reduction in cumulative ocean CO_2 uptake of 1.6–5.4 PgC over the period 1959–2008 (1.5–5.4%) in response to climate change and variability (Figure 6.13), partly due to changes in the equatorial Pacific and to changes in the Southern Ocean. The only observational-based estimate available to evaluate the climate response of the global air-sea CO_2 flux is from Park et al. (2010), which is at the low end of the model estimate for the past two decades (Table 6.4). However this estimate does not include the non-linear effects of changes in ocean circulation and warming on the global air-sea CO_2 flux, which could amplify the response of the ocean CO_2 sink to climate by 20–30% (LeQuere et al., 2010; Zickfeld et al., 2011). It is not yet possible to evaluate how much of this signal is in response to climate trends and how much is caused by climate variability. From the model estimates assessed in this chapter, the response of the ocean global CO_2 sink to climate trends and variability was negative (weakening sink) and about half the magnitude of the positive response (increasing sink) to atmospheric CO_2 in the past two decades (Table 6.4)

Processes missing in ocean models. The most important processes missing in current global ocean carbon cycle models used in the AR5 are those representing small-scale physical circulation (e.g., eddies, brine formation), which have an important influence on the vertical transport of water, heat and carbon (Loose and Schlosser, 2011; Sallée et al., 2012). In particular, changes in vertical transport in the Southern Ocean is thought to have caused most of the 80–100 ppm changes in atmospheric CO_2 between glacial and interglacial conditions (Sigman et al., 2010), consistent with observed changes in deep stratification (Burke and Robinson, 2012). This signal is not entirely reproduced by models (Section 6.2) and suggests that the sensitivity of ocean models could be underestimated.

Processes related to marine ecosystems in global ocean models are also limited to the simulation of lower trophic levels, with crude parameterizations for bacterial and other loss processes and their temperature-dependence. Projected changes carbon fluxes from the response of marine ecosystems to changes in temperature (Beaugrand et al., 2010), ocean acidification (Iglesias-Rodriguez et al., 2008), and pressure from fisheries (Pershing et al., 2010) are all considered potentially important, though not yet quantified. Several processes have been specifically identified that could lead to changes in the ocean CO_2 sink, in particular the temperature effects on marine ecosystem processes (Riebesell et al., 2009; Taucher and Oschlies, 2011) and the variable nutrient ratios induced by ocean acidification or ecosystem changes (Tagliabue et al., 2011). Nevertheless, the fit of ocean model results to recent observations and trends suggest that, up to now, changes in ecosystem processes have not had a dominant effect on ocean CO_2.

6.3.2.6 Land Sinks

6.3.2.6.1 Global land sink

The global budget of anthropogenic CO_2 constrained by observations of atmospheric CO_2 concentrations, estimates of fossil fuel emissions, land use change emissions and ocean observations and models provide an estimate of the so called 'residual land sink' necessary to satisfy mass conservation. This residual land sink of anthropogenic CO_2 is of 1.5 ± 1.1, 2.6 ± 1.2 and 2.5 ± 1.2 PgC yr^{-1} for the 1980s, 1990s, and 2000s, respectively (Table 6.1). The larger residual land sink in the early 1990s compared to the 1980s has been attributed to the response of terrestrial ecosystems to the eruption of Mount Pinatubo in June 1991, when a decrease in temperature and an increase in diffuse light fraction occurred, and were estimated using process-based terrestrial ecosystem models to have increased the residual land sink (Lucht et al., 2002; Mercado et al., 2009).

From an ensemble of several global process-based terrestrial ecosystem models forced by the same gridded weather and climate fields and observed atmospheric CO_2 concentrations, Sitch et al. (subm) estimate a global sink of anthropogenic CO_2 of 1.8 ± 0.7 PgC yr^{-1} for the 1980s, 2.3 ± 0.9 PgC yr^{-1} for the 1990s and 2.6 ± 1.4 PgC yr^{-1} for the 2000s (Table 6.6; Sitch et al., subm). However, none of these models includes land use change effects or forest dynamics (i.e., mortality and recruitment rates affecting biomass and CO_2 fluxes).

The net land-to-atmosphere flux of anthropogenic CO_2 (including land use change emissions plus the residual land sink) assessed in Table 6.1 corresponds to a net sink of CO_2 by terrestrial ecosystems, which has intensified globally from a neutral CO_2 flux of 0.1 ± 0.8 PgC yr^{-1} in the 1980s to a net CO_2 sink of 1.1 ± 0.9 PgC yr^{-1} and 1.4 ± 0.9 PgC yr^{-1} during the 1990s and 2000s, respectively (Table 6.1; Sarmiento et al., 2010). This increasing net land-to-atmosphere flux towards a larger sink is consistent with trends in the net atmosphere-to-land CO_2 flux from atmospheric inversion methods, which estimate an increasing trend in the atmosphere-to-land flux of –0.057 ± 0.01 PgC yr^{-2} during 1980–2008 (Gurney and Eckels, 2011).

Table 6.6: Estimates of atmosphere-to-land CO_2 flux from process-based terrestrial ecosystem models driven by rising CO_2 and by changes in climate.

Model name	Nitrogen limitation	Natural Fire CO_2 emissions	1980–1989	1990–1999	2000–2009
	(yes/no)	(yes/no)	PgC yr–1	PgC yr–1	PgC yr–1
CLM4C[b, c]	No	Yes	1.98	2.11	2.64
CLM4CN[b, c]	Yes	Yes	1.27	1.25	1.67
Hyland[d]	No	No	3.28	4.07	5.23
LPJ[e]	No	Yes	1.14	1.90	2.60
LPJ_GUESS[f]	No	Yes	1.15	1.54	2.07
OCN[g]	Yes	No	1.75	2.18	2.36
ORC[h]	No	No	2.08	3.05	3.74
SDGVM[i]	Yes	Yes	1.25	1.95	2.30
TRIFFID[j]	Yes	No	1.85	2.52	3.00
VEGAS[k]	No	No	–0.05	0.22	0.57
Average[a]			1.57 ± 1.34	2.08 ± 1.61	2.62 ± 1.93

Notes:
(a) Average of all model. The uncertainty represents ±1 Mean Absolute Deviation from the mean.
(b) Oleson et al. (2010)
(c) Lawrence et al. (2011)
(d) Levy et al. (2004)
(e) Sitch et al. (2003)
(f) (Smith et al., 2001a)
(g) Zaehle and Friend (2010)
(h) Krinner et al. (2005)
(i) Woodward and Lomas (2004)

(j) Cox (2001)
(k) Zeng (2003)
All these models run are forced by rising CO_2 concentration and time-varying historical reconstructed weather and climate fields using the same protocol from the TRENDY project (Sitch et al., subm) (http://www.globalcarbonproject.org/global/pdf/DynamicVegetationModels.pdf).

6.3.2.6.2 Regional atmosphere-land CO_2 fluxes

In this Chapter, the results from CO_2 inversions, terrestrial ecosystem models and forest inventories (obviously restricted to forest biomes, with very sparse coverage in the tropics) consistently show that the largest net terrestrial CO_2 sink is located in the northern extra-tropics (Gurney and Eckels, 2011; Jacobson et al., 2007; Pan et al., 2011; Sitch et al., 2008; Figure 6.14). Inversion estimates of atmosphere-land CO_2 fluxes in the tropics remain highly unconstrained, given very few atmospheric CO_2 stations, and inversion results show flux estimates ranging from neutral to a net tropical source of 0.5–1.0 PgC yr^{-1} (Gurney and Eckels, 2011; Jacobson et al., 2007). Stephens et al. (2007) selected from an ensemble of inversion models those that were consistent with independent aircraft cross-validation data, and constrained a quasi neutral tropical land CO_2 flux of 0.1 ± 0.8 PgC yr^{-1} during the period 1992–1996, and a Northern Hemisphere net land CO_2 sink of 1.5 ± 0.6.

[INSERT FIGURE 6.14 HERE]

Figure 6.14: Decadal average CO_2 fluxes for 22 partitions of the globe for (1) the 1990s (cyan) and 2000s (brown) as estimated by atmospheric CO_2 inversions, (2) the dynamic vegetation models (DGVMs), and (3) pCO_2 measurements based air-sea exchange climatology. The regional partitions are depicted as an inset and shaded by CO_2 flux density (blue-green-brown: -ve flux, red-grey: +ve flux). The mean values are calculated from monthly-mean fluxes from 17 inverse models for the period of 1990–2008, and standard deviations shown as error bars are for model-to-model differences within each decade. The DGVM fluxes are calculated using 14 climate-carbon model simulations (not true values).

A number of studies since AR4 have compared and attempted to reconcile regional atmosphere-land CO_2 flux estimates from multiple approaches and so provided an important test for the degree of confidence of regional land flux estimates. For North America, a net land CO_2 sink of 0.5 PgC yr^{-1} with 95% certain that the estimate is within 25% (SOCCR, 2007) and 0.3 ± 0.2 PgC yr^{-1} (Hayes et al., 2012); Europe, a 0.3 ± 0.2 PgC yr^{-1} sink (Schulze et al., 2009); for China, a 0.2± PgC yr^{-1} sink (Piao et al., 2009a); Russia a 0.6 – 0.8 PgC $csyr^{-1}$ (Dolman et al., 2012); Arctic tundra, a 0.1 PgC yr^{-1} sink with an uncertainty between a sink of 0.3 PgC yr^{-1} and a source of 0.1 PgC yr^{-1} (McGuire et al., 2009). A broader analysis of regional contributions estimated a 1.7 PgC yr^{-1} sink in the Northern Hemisphere regions above 20°N with consistent estimates from terrestrial models and inventories (uncertainty: ±0.3 PgC yr^{-1}) and atmospheric CO_2 inversions (uncertainty: ±0.7 PgC yr^{-1}) (Ciais et al., 2010).

Pan et al. (2011) assessed the contribution of regional forests to the global land CO_2 sink during the past two decades based on repeated forest biomass inventory data, completed with coarse estimates of soil carbon change and by the bookkeeping model of Houghton (2003) estimates of the net land use change CO_2 flux to the atmosphere. For the period 2000–2007, they estimated a global forest carbon accumulation of 0.5 $PgCyr^{-1}$ in boreal forests, and of 0.8 PgC yr^{-1} in temperate forests. Tropical forests were found to be near neutral with net emissions from land use change being compensated by sinks elsewhere in established tropical forests, therefore consistent with the Stephens et al. inversion estimate of tropical land CO_2 fluxes.

6.3.2.6.3 Interannual variability in atmosphere-land CO_2 fluxes

The interannual variability of the residual CO_2 land sink shown in Figures 6.8 and 6.13 accounts for most of the interannual variability of the atmospheric CO_2 growth rate. Atmospheric CO_2 inversion results suggest that tropical land ecosystems dominate the global CO_2 variability, with positive anomalies during El Niño episodes (Baker et al., 2006; Bousquet et al., 2000; Rodenbeck et al., 2003), which is consistent with the results of one inversion of atmospheric ^{13}C and CO_2 measurements (Rayner et al., 2008). A combined ENSO-Volcanic index time series explains 75% of the observed variability (Raupach et al., 2008). A positive phase of ENSO (El Niño) is associated with enhanced land CO_2 source, and a negative phase (La Niña) with enhanced land CO_2 sink (Jones and Cox, 2001; Peylin et al., 2005). Observations from eddy covariance networks suggest that interannual carbon flux variability in the tropics and temperate regions is dominated by precipitation, while boreal ecosystem fluxes are more sensitive to temperature and shortwave radiation

variation (Jung et al., 2011), in agreement with the results from process-based terrestrial ecosystem models (Piao et al., 2009b).

6.3.2.6.4 Inland water fluxes

Estimates of the transport of carbon from land ecosystems to the coastal ocean by rivers are ~0.2 Pg yr^{-1} for Dissolved Organic Carbon (DOC), 0.3 Pg yr^{-1} for Dissolved Inorganic Carbon (DIC), and 0.1–0.4 Pg yr^{-1} for Particulate Organic Carbon (POC) (Mayorga et al., 2010; Seitzinger et al., 2005; Syvitski et al., 2005). For the DIC fluxes, only ~2/3 of it originates from atmospheric CO_2 and the rest of the carbon is supplied by the weathered carbonate rocks (Gaillardet et al., 1999; Hartmann et al., 2009; Oh and Raymond, 2006; Suchet and Probst, 1995). Regional DIC fluxes transported by rivers are possibly increased in response to agricultural practices (Hamilton et al., 2007; Oh and Raymond, 2006; Perrin et al., 2008) and coupled with climate change can lead to large increases in regional scale DIC export in watersheds with a large agricultural footprint (Raymond et al., 2008). Furthermore, regional urbanization also elevate DIC fluxes in rivers (Baker et al., 2008; Barnes and Raymond, 2009) which suggest that anthropogenic activities could contribute a significant portion of the annual global river transported DIC flux to the ocean.

Land clearing and management are thought to produce an acceleration of POC transport, much of which is trapped in alluvial and colluvial deposition zones, lakes, reservoirs, and wetlands (Smith et al., 2001b; Stallard, 1998; Syvitski et al., 2005). One study argues that due to its long residence time in these new depositional environments, land clearing and management coupled to lateral transport by erosion is leading to a net carbon accumulation on land of ~0.1 PgC yr^{-1} (Van Oost et al., 2007). Numerous studies have demonstrated an increase in the concentration of DOC in rivers over the northeastern United States and northern/central Europe over the past 2–4 decades (Evans et al., 2005; Findlay, 2005; Lepisto et al., 2008; Monteith et al., 2007; Worrall et al., 2003). Due to the central role of wetlands on DOC export to rivers, the loss of global wetlands is probably the largest human-induced cause of changes in global river DOC fluxes to date (Seitzinger et al., 2005), although a global estimate of this alteration is not available. The robust partitioning between natural and anthropogenic C flows in freshwater systems is not yet possible, nor a quantification of its ultimate fate in the coastal and open oceans.

6.3.2.6.5 Processes driving terrestrial atmosphere-land CO_2 fluxes

Three type of processes are estimated to have an important effect on the net flux of CO_2 between the atmosphere and the land: (1) processes driven by changes in atmospheric composition such as CO_2 and N deposition inducing a 'fertilisation effect' on ecosystem productivity, (2) processes driven by changes in climate that can affect net primary productivity (NPP) and respiration responses to changes in temperature, radiation including radiation quality (diffuse fraction) and precipitation, and (3) processes driven by changes in land use (e.g., deforestation, degradation, afforestation) and land management (agricultural and forestry practices).

Assessment of experimental data (mostly local experiments), observations and model results suggest that the main processes that have an effect on the land CO_2 sink include the CO_2 fertilisation effect on photosynthesis (see Box 6.3), N fertilisation (Bonan and Levis, 2010; Gerber et al., 2010; Piao et al., 2009b; Thornton et al., 2007), forest regrowth and afforestation (Bellassen et al., 2011; Houghton, 2010; Pacala et al., 2001; Williams et al., 2012a), changes in forest management and reduced harvest rates (Nabuurs et al., 2008), and possibly increased radiation in the tropics (Gloor et al., 2009; Nemani et al., 2003). The lengthening of the growing season in northern latitude ecosystems is also estimated to contribute to explain at least partly the current CO_2 sink.

[START BOX 6.3 HERE]

Box 6.3: The CO_2 Fertilization Effect

The CO_2 fertilisation as a process susceptible to increase terrestrial primary productivity has a dominant role as a process to explain a global land CO_2 sink in terrestrial biogeochemical models (Sitch et al., 2008), yet it remains one of the most unconstrained process.

Field experiments provide direct evidence of increased photosynthesis rates and water use efficiency in plants growing under elevated CO_2, which in turn translates into an broad range of higher plant carbon

accumulation in at least 2/3 of the experiments (Ainsworth and Long, 2004; Ainsworth et al., 2012; Canadell et al., 2007; Denman et al., 2007; Luo et al., 2004; Norby et al., 2005; Nowak et al., 2004; Wang et al., 2012).

Since the AR4, new evidence is available from decade-long Free-air CO_2 Enrichment (FACE) experiments showing the capacity of ecosystems to sustain higher rates of carbon accumulation at elevated CO_2 over time (Aranjuelo et al., 2011; Dawes et al., 2011; Lee et al., 2011; Liberloo et al., 2009; McCarthy et al., 2010; Zak et al., 2011). The mean net primary production response for one decade-long tree FACE experiments is an increase of 8% (non-significant), 26% and 26% at double CO_2 (McCarthy et al., 2010; Norby et al., 2010; Zak et al., 2011). The FACE experiments also show the diminishing or lack of CO_2 fertilization effect in some ecosystems and plant species (Adair et al., 2009; Bader et al., 2009; Norby et al., 2010) and tree ring evidence suggests a lack of CO_2 fertilization in the sampled boreal and temperate forests (Gedalof and Berg, 2010; Peñuelas et al., 2011).

Nutrient limitation is the likely primary cause of a reduced or lack of CO_2 fertilization effect observed on NPP in some experiments (Dukes et al., 2005; Finzi et al., 2007; Luo et al., 2004; Norby et al., 2010). Nitrogen and phosphorus are very likely to play the most important role in this limitation of the CO_2 fertilization effect on NPP, and these nutrients are estimated to have an additive effect at the global scale, with N limitation prevalent in temperate and boreal ecosystems, and P limitation in the tropics (Goll et al., 2012b; Luo et al., 2004; Vitousek et al., 2010; Wang et al., 2010a). Although the enhancement of the CO_2 fertilization effect on the global terrestrial net primary productivity is very likely, the magnitude of such an effect remains uncertain in view of the broad range of experimental responses, and the uncertainty stemming from the lack of experiments outside of temperate climates.

END BOX 6.3 HERE]

Process attribution of the land sink of CO_2 at the global scale is difficult due to limited data, and because , global models do not represent yet the full range of processes thought to be important. Attribution of regional sinks has been more successful. Legacies of past forest clearing and decreased harvest removal are key processes very likely to explain a large fraction of the current forest carbon sink in the U.S.A. and Europe, with additional contribution from CO_2 and N fertilization effect, and in some regions of warming induced longer growing seasons (Bellassen et al., 2011; Ciais et al., 2008; Pacala et al., 2001; Schulze et al., 2010; Williams et al., 2011). Afforestation and forest regrowth likely play a major role in the carbon sink of East Asia, with a large uncertainty on the contribution of CO_2 fertilization (Fang et al., 2005; Piao et al., 2011). In the tropics, there is evidence from forest inventories that increasing forest growth rates are not explained by the natural recovery from disturbances, suggesting that increasing atmospheric CO_2 and climate change play a role in the observed sink in established forests (Lewis et al., 2009; Pan et al., 2011). Nemani et al. (2003) based on satellite greenness, estimated an increase in net primary producitvity (NPP) in the region over the the period 1982–1999 which they largely atributed to increased solar radiation from reduced cloud cover. Although increased forest growth rates and NPP are not surrogates for net land sinks, they are components of it and so provide information on the underlying processes.

Processes involving human induced / natural export of carbon from a land area, such as export of carbon through river transport (see Section 6.3.2.6.4), wood harvest and net trade balance of food and wood are significant components of the C balance for some regions (Pacala et al., 2001).

Disturbances such as fires, insect damage, storms, droughts and heat waves are significant processes driving inter-annual variability and possibly trends of regional land carbon fluxes (Chambers et al., 2007; Ciais et al., 2005; Clark et al., 2010; Lewis et al., 2011). It is not well understood to what degree disturbance caused instantaneous losses of CO_2 are compensated by regrowth in the short term (e.g., savanna fires) or if they are net long term losses (e.g., peat fires; Page et al., 2002; deforestation fires; van der Werf et al., 2010; see Section 6.3.2.2). In the future, climate induced disturbances are expected to become more important in driving trend dynamics of regional carbon fluxes, as it has already being observed with increased fire frequency and insect damage in Canadian forests (Kurz et al., 2008b).

Warming (and possibly the CO_2 fertilization effect) has also been correlated with global trends in satellite greenness observations, which resulted in an estimated 6% increase of global NPP, or the accumulation of

3.4 PgC on land over the period 1982–1999. This enhanced NPP was attributed to the relaxation of climatic constraints to plant growth, particularly in high latitudes, as also seen by an increase in the net carbon sink during the warmer 2000s compared to the 1990s in the Arctic tundra (McGuire et al., 2012). Concomitant to the increased of NPP with warming, global soil respiration increased between 1989 and 2008 (Bond-Lamberty and Thomson 2010) reducing the magnitude of the net land sink. More recent NPP trends suggested a reduction of 55 PgC over 2000–2009 (Zhao and Running (2010) although the model used to reconstruct NPP trends from satellite observation has not been widely accepted (Medlyn, 2011; Samanta et al., 2011; Zhao and Running, 2011).

An additional contributor to the growing global land sink is the effect of increased diffused radiation on photosynthesis, estimated to account for one quarter of the of the land sink during 1960–1999 (Mercado et al., 2009). The effect is largely driven by the enhanced efficiency of photosynthesis under diffuse light brought about by the increased in anthropogenic aerosols (Roderick et al., 2001; Romanou et al., 2007).

6.3.2.6.6 Model evaluation of global and regional terrestrial carbon balance

Evaluation of global process based ecosystem models was performed against ground and satellite observations including: (1) measured CO_2 fluxes and carbon storage change at particular sites around the world, in particular sites from the Fluxnet global network (Jung et al., 2007; Schwalm et al., 2010; Stockli et al., 2008; Tan et al., 2010), (2) observed spatio-temporal change in leaf area index (LAI) (Lucht et al., 2002; Piao et al., 2006), and (3) interannual and seasonal change in atmospheric CO_2 (Cadule et al., 2010; Randerson et al., 2009).

Figure 6.15 compares the global land sink of CO_2 simulated by different process based carbon cycle models (see Sitch et al., subm) without land use change, with the residual land sink (diagnosed as the sum of fossil fuel and cement emissions and land use change emissions minus the sum of CO_2 growth rate and ocean sink) from 1980 to 2009 (Friedlingstein and Prentice, 2010; Le Quere et al., 2009). The magnitude of the residual land sink and its trend can be reproduced faithfully by the multi-model mean, despite the large discrepancies among individual models, and the lack of land use change prescribed to models. Limited availability of in-situ measurements, particularly in the tropics, limits the progress towards reducing uncertainty on model parameterizations.

[INSERT FIGURE 6.15 HERE]

Figure 6.15: Time series for the land CO_2 sink showing the residual land sink deduced (1) from the global budget (Figure 6.8) with the black line being obtained as the difference between emissions from fossil fuel and land use change, minus the atmospheric growth rate and the ocean sink, and (2) from global process-based terrestrial ecosystem models (Table 6.6 for references) shown as red lines. The red shading shows one standard deviation from the model mean.

At the regional scale, the models of terrestrial carbon dynamics can be better constrained because of the higher availability of data, at least in some regions. In Europe, forest inventory data show that the forest carbon sink density over Europe is of 89 ± 19 gC m^{-2} yr^{-1}, which is comparable with model estimates with afforestation (–63 gC m^{-2} yr^{-1}; Luyssaert et al., 2010), while modeled NPP was 43% larger than the inventory estimate. In North America, the ability of 22 terrestrial carbon cycle models were evaluated to simulate the seasonal cycle of land-atmosphere CO_2 exchange from 44 eddy covariance flux towers, and found that the difference between observations and simulations was about 10 times the observational uncertainty (Schwalm et al., 2010); key model shortcomings are the variability due to spring phenology, soil thaw, and snow pack melting, as well as lag responses to extreme climate events (Keenan et al., 2012). In China, the magnitude of the carbon sink estimated by five terrestrial ecosystem models (0.22 to 0.13 PgC yr^{-1}) was comparable to the observation-based estimate (0.18 ± 73 PgC yr^{-1}; Piao et al., 2009b), but modelled interannual variation was weakly corrected to observed regional land-atmosphere CO_2 fluxes (Piao et al., 2011).

Sensitivity of the terrestrial carbon cycle to CO_2. The sensitivity of the terrestrial carbon cycle to rising atmospheric CO_2 concentration is one of the key metrics to inter-compare and evaluate terrestrial carbon cycle models. Results from Free Air CO_2 experiments (FACE) on diverse ecosystems generally show a higher net primary productivity (NPP) under elevated atmospheric CO_2 (see Box 6.3). The magnitude of the NPP enhancement at the four temperate forest FACE experiments was reproduced correctly by the LPJ-GUESS model (Hickler et al., 2008). Some experiments failed to show a CO_2 fertilisation effect on NPP, and

factorial experiments with elevated CO_2 and nitrogen additions inferred that nitrogen limitation was the cause of the lack of CO_2 fertilization effect (see Box 6.3). This implies that carbon cycle models not considering the limitation of nitrogen availability on vegetation growth are likely to overestimate the response of plant productivity to rising atmospheric CO_2 concentration (Zaehle and Friend, 2010). The small number of in situ measurements of the long-term response of CO_2 fluxes to elevated CO_2 limits the evaluation of the models for the CO_2 fertilization effect. Phosphorus information to parameterize process models, in addition to N, is also required to test the role of P in limiting the current and future land carbon sink.

Sensitivity of terrestrial carbon cycle to climate trends and variability. Warming exerts a direct control on the net land-atmosphere CO_2 exchange since both photosynthesis and respiration are sensitive to changes in temperature. Warming is likely to increase vegetation productivity in temperate and boreal regions through increasing growing season length (Lucht et al., 2002; Piao et al., 2006; Zhou et al., 2001). A meta-analysis of field warming experiments from temperate and boreal regions suggests for instance an average 19% increase in aboveground plant primary productivity (Rustad et al., 2001), along with an increase or no change in the net atmosphere-land CO_2 flux (Luo, 2007; Marchand et al., 2004).

From estimates of the annual residual land CO_2 sink, it is assessed that a 1°C global temperature anomaly leads to a decrease of 4 PgC yr^{-1} of the global land CO_2 sink (Figure 6.16), a response close to the multi-model estimated average of the interannual temperature sensitivity of the global land CO_2 sink (–3.5 PgC yr^{-1}°C^{-1} in Piao et al., subm.). Different models, however, showed different sensitivities of their global land CO_2 sink to interannual temperature variability, with values ranging from –0.5 PgC yr^{-1} °C^{-1} to –6.2 PgC yr^{-1} °C^{-1} (Piao et al., subm.). The sensitivity of the the global land CO_2 sink to climate is likely to vary with different time scale as well. For instance, the sensitivity of atmospheric CO_2 concentration to century-scale temperature change was estimated at about 3.6~45.6 PgC °C^{-1} (or 1.7~21.4 ppm CO_2°C^{-1}) using the ice core observed CO_2 drop during the Little Ice Age, when human impacts on atmospheric CO_2 were assumed to be negligible (Frank et al., 2010).

Carbon release in response to future drying in the Tropics is one of the dominant explanation of the positive carbon cycle-climate feedback found in the coupled carbon-climate models used in AR4 (Cox, 2001; Friedlingstein et al., 2006; Sitch et al., 2008). An artificial drought experiment in an east-central Amazonian rainforest at Tapajos showed that a 50% reduction in precipitation led to a 25% reduction in aboveground NPP during the first two years of prescribed drought (Nepstad et al., 2002), followed by a 38% increase in tree mortality rates which further reduced NPP (Nepstad et al., 2007). A global estimate of GPP show that 30% of the spatial GPP variability in tropical forests was correlated with precipitation (Beer et al., 2010). Carbon cycle models used in AR5 generally underestimate GPP in the water limited regions, implying that these models do not correctly simulate soil moisture conditions, or that they are too sensitive to changes in soil moisture (Jung et al., 2007). It is also suggested that the AR5 models overestimate the interannual precipitation sensitivity of the land flux in the tropics (Wang et al., subm.). At the global scale, most of the process-based terrestrial ecosystem models in Table 6.6 (eight of nine models) estimated that the interannual precipitation sensitivity of the global land CO_2 sink to be higher than that of the observed residual land sink (–0.01 PgC yr^{-1} mm^{-1}; Figure 6.16).

[INSERT FIGURE 6.16 HERE]

Figure 6.16: The sensitivity of Net Ecosystem Production (NEP) to interannual variation in temperature and interannual variation in precipitation at the global and regional scales. The gloal residual land sink is estimated as the sum of fossil fuel and cement emissions and land use change emissions minus the sum of CO_2 growth rate and modelled ocean sink (Friedlingstein and Prentice, 2010; Le Quere et al., 2009). The sensitivities of NEP to interannual variation of temperature and precipitation are estimated by a multiple linear regression approach using detrended NEP as dependent variable and detrended annual temperature and annual precipitation as independent variables (Piao et al., subm.). 10 carbon cycle models are Community Land Model 4C (CLM4C), Community Land Model 4CN (CLM4CN), Hyland (HYL), Lund-Potsdam-Jena (LPJ), LPJ_GUESS, ORCHIDEE-CN (OCN), ORCHIDEE (ORC), Sheffield-DGVM (SDGVM), TRIFFID (TRI), and VEGAS. Negative value indicates decrease in carbon sink.

Processes missing in terrestrial models. Currently, most global terrestrial ecosystem models used in AR5 only consider the effects of climate change and atmospheric CO_2 on land-atmosphere CO_2 fluxes, but still miss several key processes governing the terrestrial carbon cycle. First, many of global models do not explicitly take into account the various forms of disturbances: fire, logging, harvesting and the resulting

variation in forest age structure which is known to affect the net carbon exchange (Bellassen et al., 2010). Eddy covariance flux observations show that the strength of net carbon uptake of forest ecosystem is locally controlled by forest stand age (Amiro et al., 2010). Second, processes relevant to decomposition of carbon in permafrost and wetlands, including tropical peatland are not dealt in the majority of models, despite these pools hold large carbon stores and are vulnerable to warming and land use change (Hooijer et al., 2010; Koven et al., 2011; Page et al., 2010; Tarnocai et al., 2009). However, progress is taking place as now some models do include permafrost carbon (Koven et al., 2011; Schaefer et al., 2011). Third, despite several studies demonstrating the important role of N limitation in regulating the terrestrial carbon cycle, and the fertilizing effect of N-deposition on ecosystem productivity (Magnani et al., 2007), N dynamics is only taken into account by few models. For instance, the global land carbon sink estimated by the model (CLM4CN) with considering N limitation is lower than in that of the model (CLM4C) without considering N limitation (Table 6.6). Phosphorus (P) availability is also observed to limit, or, with N, to co-limit, productivity in some ecosystems (Elser et al., 2007; LeBauer and Treseder, 2008), but even fewer models represent P dynamics or N-P interactions. Fourth, the effects of elevated tropospheric ozone have also not been taken into account for most of current carbon cycle models. It was found that increased exposure of plants to elevated tropospheric ozone would reduce vegetation productivity, and thus further decrease NEP (Sitch et al., 2007). Fifth, transfer of radiation, water and heat in the vegetation-soil-atmosphere continuum are treated very simply in the global ecosystem models used in this Chapter, which further limit credibility of model simulation. Finally, lateral surface process (e.g., water and tillage erosion; Quinton et al., 2010) and human managements including fertilisation and irrigation (Gervois et al., 2008) may also substantially influence C cycle at regional scales, but it was not considered in most of current model studies.

6.3.3 Global CH_4 Budget

AR5 is the first IPCC assessment report providing a consistent synthesis of the CH_4 budget per decade, using different approaches. A suite of different atmospheric CH_4 inversion models (top-down) and various process-based models and inventories (bottom-up) are used to derive the main CH_4 emission sources and their regional contributions, during the 1980s, the 1990s and 2000s (Table 6.7; Kirsche et al. subm.). In the table, the uncertainties on emissions and sinks are listed using minimum and maximum of each published estimate for each decade. Bottom-up approaches are used to attribute decadal budgets to different processes emitting CH_4 (see Section 6.1.1.2 for a general overview). Top-down inversions provide an atmospheric-based constraint for the total CH_4 source per region. Estimations of CH_4 sinks in the troposphere by reaction with tropospheric-OH, in soils and in the stratosphere are also reported for the past three decades.

6.3.3.1 Atmosphere Burden and Trend

Since preindustrial times, the concentration of the global average surface CH_4 increased by a factor of 2.5 (from 730 ppb to 1803 ppb in 2011) and it is measured today by a network of more than 100 surface sites (Cunnold et al., 2002; Dlugokencky et al., 2011; Langenfelds et al., 2002), aircraft profiles in the lower part of the atmosphere, and before 1979 from analyses of firn air and ice cores (see Chapter 5 and Section 6.2), Figure 6.11. The growth of CH_4 in the atmosphere is largely in response to increasing anthropogenic emissions. Currently, the vertically averaged atmospheric CH_4 concentration field can be mapped by remote sensing from the surface using Fourier Transform Infrared Spectroscopy (FTIR) instruments (Total Carbon Column Observing Network, TCCON, http://www.tccon.caltech.edu/) and from space by several satellite instruments: AIRS (since 2002), TES (since 2004), IASI (since 2006), SCIAMACHY (since 2003), and GOSAT-TANSO-FTS (since 2009). As an example, SCIAMACHY (Frankenberg et al., 2008) clearly shows the column CH_4 gradient between the two hemispheres as well as increased concentrations over South East Asia, due to emissions from agriculture, wetlands, waste, and energy production (Figure 6.2).

The growth rate of CH_4 has declined since the mid 1980s and a near zero growth rate (quasi-stable concentrations) was observed during 1999–2006 suggesting an approach to steady state where the sum of emissions are in balance with the sum of sinks (Dlugokencky et al., 2003; Khalil et al., 2007; Figure 6.17). The reasons for this growth rate change after the mid-1980s are still debated, and results from various studies provide possible scenarios: (1) a reduction of emitting activities such as coal mining, gas industry and animal husbandry in the countries of the former Soviet Union (Dlugokencky et al., 2003; Savolainen et al., 2009), (2) a compensation between increasing anthropogenic emissions and decreasing wetland emissions (Bousquet et al., 2006), (3) reduced emissions from rice paddies attributed to changes in agricultural

practices (Kai et al., 2011), (4) stable microbial and fossil fuel emissions in the early 2000s (Levin et al., 2012), and/or (5) significant (Rigby et al., 2008) to small (Montzka et al., 2011) changes in OH concentrations.

[INSERT TABLE 6.7 HERE]

Table 6.7: Global CH_4 budget for the past three decades (in $Tg(CH_4)yr^{-1}$). T-D stands for Top-Down inversions and B-U for Bottom-Up approaches. Full references are given at the end of the chapter. Ranges represent minimum and maximum values from the cited references. The sum of sources and sinks from B-U approaches does not automatically balance the atmospheric changes. Only studies covering at least five years of each decade have been used. For B-U studies, individual source types are also presented. For T-D inversions, the 1980s decade starts in 1984. As some atmospheric inversions did not reference their global sink, balance with the atmosphere and the sum of the sources has been assumed. One biomass burning estimate[22] excludes biofuels (a). Stratospheric loss for B-U is the sum of the loss by OH radicals, a 10 Tg yr^{-1} loss due to O^1D radicals (Neef et al., 2010) and a 20–35% contribution due to Cl radicals[24].

Since 2007, the growth rate of CH_4 has been observed to increase again (Dlugokencky et al., 2009; Rigby et al., 2008) with positive anomalies of emissions of 21 $Tg(CH_4)\ yr^{-1}$ and 18 $Tg(CH_4)\ yr^{-1}$ inverted for 2007 and 2008, respectively (Bousquet et al., 2011) as compared to the 1999–2006 period. The increase of emissions in 2007–2008 was dominated by tropical regions (Bousquet et al., 2011) with a major role from tropical wetlands, and some role from high latitude wetlands in the 2007 anomaly (Bousquet et al., 2011; Dlugokencky et al., 2009) as suggested by the growth rate vs. latitude in Figure 6.17 (Dlugokencky et al., 2009). The recent increase of CH_4 concentration since 2007 is also in line with the EDGAR4–v4.2 anthropogenic emission inventory, which shows rapidly increasing anthropogenic CH_4 emissions in the period 2000–2008, related to increased energy production in growing Asian economies (EDGAR4, edgar.jrc.ec.europa.eu). The atmospheric increase has continued after 2009, at a rate of 4–5 ppb per year (Sussmann et al., 2012).

[INSERT FIGURE 6.17 HERE}

Figure 6.17: Upper panel: Globally averaged growth rate of atmospheric CH_4 in ppb yr^{-1} determined from the GLOBALVIEW data product, representative for the marine boundary layer (Masarie and Tans, 1995). Lower panel: Atmospheric growth rate of CH_4 as a function of latitude determined from the GLOBALVIEW data product.

6.3.3.2 Emissions

The global atmospheric burden and trend of CH_4 results from the balance between emissions and sinks. Methane emission sources around the globe are biogenic, thermogenic, or pyrogenic in origin (Neef et al., 2010), and they can be the direct result of either human activities and/or natural processes (see Section 6.1.1.2 and Table 6.7). Biogenic sources are due to degradation of organic matter in anaerobic conditions (natural wetlands, ruminants, waste, landfills, rice paddies, fresh waters, termites). Thermogenic sources come from the slow transformation of organic matter into fossil fuels on geological timescales (natural gas, coal, oil). Pyrogenic sources are due to incomplete combustion of organic matter (biomass and biofuel burning). Some sources can eventually combine a biogenic and a thermogenic origin (e.g., natural geological sources such as oceanic seeps, mud volcanoes or hydrates). Each of these three processes is characterized by distinct ranges in the magnitude of isotopic fractionation against $^{13}C\text{-}CH_4$: –55 to –70‰ for biogenic, –25 to –45% for thermogenic, and –13 to –25‰ for pyrogenic. These isotopic distinctions provide a basis to separate the relative contribution of different methane sources using the top-down approach (Bousquet et al., 2006; Monteil et al., 2011; Neef et al., 2010).

During the decade of the 2000s, natural sources of CH_4 are assessed to account for 35–55% of the decadal mean global emissions (Table 6.7). The single most dominant CH_4 source of the global flux and inter-annual variability is CH_4 emissions from wetlands from the tropics and high latitudes (177–284 $Tg(CH_4)\ yr^{-1}$). The term 'wetlands' denotes here a variety of ecosystems emitting CH_4: wet soils, swamps, peatlands, fresh waters from lakes and rivers. These emissions are highly sensitive to climate change and variability, as seen for instance from the response to the recent 2007–2008 anomalies in precipitation and temperature. The relatively dry conditions that prevailed in some regions of the Northern Hemisphere continents during the late 1990s and early 2000s may have decreased wetland emissions at this period (Bousquet et al., 2006), although ^{13}C in CH_4 atmospheric observations seem to suggest stable microbial and fossil fuel emissions

during the early 2000s (Levin et al., 2012). Several process-based models of methane emissions from natural wetlands have been developed since AR4, and these models are improving rapidly (Hodson et al., 2011; Melton et al., subm.; Ringeval et al., 2011; Spahni et al., 2011). Nonetheless, the confidence in present-day modelled spatial and temporal patterns of wetland CH_4 emissions remains low, in particular because of limited observational datasets available for the models calibration and evaluation at the regional scale. Likely, wetland CH_4 emissions increase in response to elevated atmospheric CO_2 concentrations, a consequence of the CO_2 fertilization effect (see Box 6.3), while the sign and magnitude of the CH_4 emission response to changes in temperature and precipitation vary among models (Melton et al., subm.). In addition both wetland area and CH_4 flux density are sensitive to climate.

In AR4, natural geological sources were estimated between 4 and 19 $Tg(CH_4)yr^{-1}$. Since then, these sources received more attention and have been re-evaluated (Etiope et al., 2008). Emissions from terrestrial (13–29 $Tg(CH_4)yr^{-1}$) and marine (~20 $Tg(CH_4)yr^{-1}$) seepages, mud volcanoes (6–9 $Tg(CH_4)yr^{-1}$), hydrates (5–10 $Tg(CH_4)yr^{-1}$) and geothermal and volcanic areas (3–6 $Tg(CH_4)yr^{-1}$) are assessed to represent between 42 and 64 $Tg(CH_4)yr^{-1}$ (Etiope et al., 2008). This larger than in AR4 contribution from natural, geological, and partly fossil CH_4 is consistent with a recent $^{13}CH_4$ re-analysis showing natural and anthropogenic fossil contributions to the global CH_4 budget to be around 30% (Lassey et al., 2007) and not around 20% as previously thought.

Of the natural sources of CH_4, emissions from thawing permafrost and CH_4 hydrates in the northern circumpolar region are potentially important in the next century because they could increase dramatically due to the rapid climate warming of the Arctic and the large C pools stored there (Tarnocai et al., 2009). Hydrates are however estimated in this Chapter to represent only a very small emission, between 5 to 10 $Tg(CH_4)\ yr^{-1}$ (Table 6.7). Super saturation of dissolved CH_4 at the bottom and surface waters in the East Siberian Arctic Shelf indicate some CH_4 activity across the region, with a net sea-air flux of 10.5 $Tg(CH_4)yr^{-1}$ which is similar in magnitude to the flux for the entire ocean (Shakhova et al., 2010). The ebullition of CH_4 from decomposing, thawing lake sediments in north Siberia with an estimated flux of ~4 $Tg(CH_4)yr^{-1}$ is another demonstration of the activity of this region and of its potential importance in the future (van Huissteden et al., 2011; Walter et al., 2006). Over the past decades, however, there is no evidence for significant emission of CH_4 from permafrost and hydrates (Dlugokencky et al., 2009).

Pyrogenic sources of CH_4 are assessed to have a small contribution in the global flux for the 2000s (16–20 $Tg(CH_4)yr^{-1}$) and play a role much smaller than wetlands in inter-annual variability, particularly from the burning of tropical and boreal forests in response to regional droughts and deforestation. Tropical fire emissions during the 1997–1998 record high El Niño, during which burning of forests and peatland took place in Indonesia and Malaysia, released 12 $Tg(CH_4)$ (Langenfelds et al., 2002; van der Werf et al., 2004), with other smaller fire CH_4 emissions positive anomalies were suggested during the dry spell over the northern mid-latitudes in 2002–2003, in particular over Eastern Siberia in 2003 (van der Werf et al., 2010) and Russia in 2010. Traditional biofuel burning was estimated to be a source of 10 $Tg(CH_4)yr^{-1}$ (Yevich and Logan, 2003) during the 1980s.

Keppler at al. (2006) reported that plants under aerobic conditions were able to emit CH_4, and thus potentially could constitute a large additional emission that had not been previously considered in AR4 in the global CH_4 budget. Later studies do not support plant emissions as a wide spread mechanism (Dueck et al., 2007; Nisbet et al., 2009; Wang et al., 2008) or show negligible emissions in the context of the global CH_4 budget (Bloom et al., 2010; Nisbet et al., 2009; Vigano et al., 2008). Alternative mechanisms have been suggested to explain the apparent aerobic CH_4 production involving adsorption and desorption, but not new production (Kirschbaum and Walcroft, 2008; Nisbet et al., 2009), degradation of organic matter under strong UV light (Dueck et al., 2007; Nisbet et al., 2009), and methane in the groundwater emitted through internal air spaces in tree bodies (Terazawa et al., 2007). Therefore, we assessed that significant plant CH_4 emissions are very unlikely, and this source was not reported in Table 6.7. Finally, CH_4 emissions from termites range from 2 to 22 $Tg(CH_4)yr^{-1}$ (Table 6.7).

Anthropogenic CH_4 sources are estimated to range between 45% and 65% of the decadal-mean global emissions for the 2000s (Table 6.7) and included rice-paddies agriculture, ruminant animals, sewage and waste, landfills, and fossil fuel extraction, storage, transformation, transportation and use (coal mining, gas, oil and industry). Anthropogenic sources are dominant over natural sources in top-down inversions but they

are of the same magnitude in bottom-up models and inventories (Table 6.7). Natural emissions are estimated by different bottom-up models with no constrain on their sum, which might be overestimated considering the large imbalance with the modelled chemical sink (Table 6.7). Rice paddies emit between 32 and 44 $Tg(CH_4)yr^{-1}$, continuously flooded paddies having much higher emissions per square metre than drought-prone, rain-fed paddies, or irrigated paddies that are intermittently drained. Ninety per cent of emissions come from Monsoon Asia, and more than 50% from China and India alone (Yan et al., 2009). Ruminant livestock, such as cattle, sheep, goats and deer produce CH_4 by food fermentation in their anoxic rumens with a total estimate of between 89 and 97 $Tg(CH_4)\ yr^{-1}$. Major regional contributions of this flux come from India, China, Brazil, and the US (EPA, 2006). India, with the world's largest livestock population (485 millions in 2003, with no deer), emitted 11.8 $Tg(CH_4)yr^{-1}$ in 2003, including emission from enteric fermentation (10.7 $Tg(CH_4)yr^{-1}$) and manure management (1.1 $Tg(CH_4)\ yr^{-1}$; Chhabra et al., 2009). Methanogenesis in landfills, livestock manure and waste waters produce between 65 and 90 $Tg(CH_4)yr^{-1}$ due to anoxic conditions and a high availability of acetate, CO_2 and H_2. Loss of natural gas (~90% CH_4) is the largest contributor to fossil fuel related emissions (52–69 $Tg(CH_4)yr^{-1}$). Unintended emissions from industrial processes (fugitive emissions) are high in the Russian Federation, where they relate to older energy infrastructure, and in the USA (EPA, 2006). Coal mining contributes between 18 and 35 $Tg(CH_4)yr^{-1}$ and residual emissions are associated with oil industry (EPA, 2006).

Global CH_4 emissions, as estimated from the sum of bottom-up models and inventories, are very uncertain (range 519–822 $Tg(CH_4)\ yr^{-1}$) for the 2000s (Kirschke et al., subm.). No constrain applies on the sum of emissions in bottom-up models, unlike for top-down inversions which display a narrower range (526–569 $Tg(CH_4)\ yr^{-1}$), based on the assimilation of atmospheric observations of CH_4, (Kirschke et al., subm.). Therefore, top-down inversions can help close the global sum of sources in the global CH_4 budget, although they do not provide as detailed of a budget as bottom-up approaches since they do not account for processes (Table 6.7).

6.3.3.3 Sinks of Atmospheric CH_4

The main sink of atmospheric CH_4 is its oxidation by OH radicals, a process which takes place mostly in the troposphere and stratosphere (Table 6.7). OH removes about 90% of atmospheric CH_4, yielding a partial atmospheric lifetime of about 9 years (7–11 years) for an atmospheric burden of 4800 $Tg(CH_4)$ (4700–4900 $TgCH_4$; see Chapter 8, Section 8.2.3.3). Oxidation in dry soils removes about 21–33 $Tg(CH_4)yr^{-1}$ (Kirschke et al., subm.). A small sink is suspected, but still debated, in the marine boundary layer due to a reaction with chlorine (Allan et al., 2007). Another minor sink is the reaction of CH_4 with Cl radicals and $O(^1D)$ in the stratosphere (Kirschke et al., subm.; Shallcross et al., 2007).

There have been a number of published estimates of global OH concentrations and variations over the past decade (Bousquet et al., 2005; Dentener et al., 2003; Montzka et al., 2011; Prinn et al., 2001; Prinn et al., 2005; Rigby et al., 2008). The very short lifetime of OH makes it almost impossible to estimate global OH concentrations from the aggregation of sparse direct measurements. Either chemistry transport models (CTMs), chemistry climate models (CCMs), or proxy methods have to be used to obtain a global mean value and time variations. Global mean chemical loss is very uncertain between 509 and 794 $Tg(CH_4)yr^{-1}$for the 2000s as estimated by CCMs and CTMs (Table 6.7), but top-down inversions using methyl-chloroform (MCF) as a proxy provide a more narrow range of 510–540 $Tg(CH_4)\ yr^{-1}$ for the total chemical loss in the 2000s. CCMs and CTMs produce small variations of OH radicals, typically of 1–3% due to a high buffering of this radical by the atmospheric photochemical reactions. Atmospheric inversions indicate much larger variations for the 1980s and the 1990s (5–10%), likely because of an oversensitivity to uncertainties on methyl-chloroform emissions of the methyl-chloroform proxy (Montzka et al., 2011), although reduced variations are inferred after 1998 (Prinn et al., 2005). For the 2000s, the reduction of MCF in the atmosphere, due to the Montreal protocol (1987), allows a consistent estimate of OH variations (<±3%) between atmospheric inversions (within 5%) and CCMs/CTMs. However, the very low atmospheric values reached by MCF (a few ppt in 2010) impose the need to find another OH proxy in the upcoming years. Finally, evidence for the role of changes in OH concentrations in explaining the increase in atmospheric methane since 2007 is variable, ranging from a significant contribution (Rigby et al., 2008) to only a small role (Bousquet et al., 2011).

6.3.4 Global N_2O Budget

The atmospheric abundance of N_2O has been increasing mainly as a result of agricultural intensification and extensification to meet the food demand for a growing human population. Fertilizer use and manure excretion increase the production of N_2O in soils and sediments, via nitrification and denitrification pathways, leading to increased N_2O emissions. Increased emissions do not only occur in agricultural fields, but also in aquatic systems after N leaching and runoff, and in natural soils and ocean surface waters as a result of atmospheric deposition of N originating from agriculture and industrial activities. Food production is likely responsible for 80% of the increase in atmospheric N_2O (Davidson, 2009; Kroeze et al., 1999; Park et al., 2012; Syakila and Kroeze, 2011; Williams and Crutzen, 2010; Zaehle and Dalmonech, 2011). Global emissions of N_2O are difficult to estimate. Table 6.8 presents global emissions based on upscalling of flux measurements at the Earth's surface. Global and regional budgets are constrained by inverse modelling studies (Hirsch et al., 2006; Huang et al., 2008; Rhee et al., 2009; Thompson et al., subm.). However, the atmospheric life-time of N_2O is not well constrained due to uncertainty in the dominant loss term of N_2O, , i.e., the destruction of N_2O by photolysis and reaction with O(1D) in the stratosphere, which causes considerable uncertainty in the top-down global N_2O budget. The long atmospheric lifetime of N_2O (122 years, Volk et al. 1997) implies that it will take decades before atmospheric abundances stabilize after the stabilization of global emissions. This is of concern not only because of its contribution to the global radiative forcing, but also because emissions of N_2O are currently the most important of any ozone depleting substance (Ravishankara et al., 2009).

Firstly, AR4 estimated total N_2O emissions in the 1990s (Table 6.8). Since then, a number of studies have been published that give reason to update some of the N_2O emission estimates. First and most importantly, the IPCC Guidelines have been revised in 2006 (DeKlein et al., 2007). In particular the emission factors for estimating agricultural emissions have been updated. Applying these 2006 emission factors to global agricultural statistics results in direct emissions from agriculture (from fertilized soils and animal production) that are higher than in AR4, but in indirect emissions (mainly from leaching and runoff) that are considerably lower (Table 6.8). It should be noted that emissions of N_2O show large spatial and temporal variability, resulting in large uncertainties from default emission factors when applied at the global scale (Crutzen et al., 2008). Recent top-down estimates, show that the emission factor approach still severely underestimates agricultural, and thus total emissions, in (sub)-tropical regions (Thompson et al., subm.).

[INSERT TABLE 6.8 HERE]

Table 6.8: Section 1 gives the Global N budget (TgN yr^{-1}): a) creation of reactive N, b) emissions of NO_x, NH_3 in 2000s to atmosphere, c) deposition of N to land and oceans and d) discharge of total N to coastal ocean. Section 2 gives the N_2O budget for the year 2005, and for the 1990s compared to AR4. Unit: Tg(N_2O-N) yr^{-1}.

Secondly, it has been recently recognized that the open ocean is an anthropogenic source of N_2O (Duce et al., 2008) because atmospheric deposition of anthropogenic reactive nitrogen Nr (nitrogen oxides and ammonia) increases N_2O emissions from the open ocean. This anthropogenic N_2O source was implicitly included in the natural ocean source estimate in AR4, but is now included as anthropogenic source in Table 6.8.

Third, a first estimate was published of global N_2O uptake at the Earth's surface (Syakila and Kroeze, 2011; Syakila et al., 2010), based on reviews of measurements of N_2O uptake in soils and sediments (Chapuis-Lardy et al., 2007; Kroeze et al., 2007). The uncertainty in this estimate is large. On the global scale, surface uptake may seem negligible, but at the local scale it may not be irrelevant. It was therefore included in Table 6.8.

6.3.4.1 Atmosphere Burden and Trends

The concentration of N_2O is currently 19% higher than pre-industrial levels (Figure 6.12; MacFarling-Meure et al., 2006) Figure 6.18 shows the concentration and annual growth rate of atmospheric N_2O estimated from direct measurements (NOAA/ESRL programme). On decadal time scales the concentration of N_2O has been rising steadily at a rate of 0.73 ± 0.03 ppb yr^{-1}. The inter-annual variability in mid to high latitudes in Northern and Southern hemispheric N_2O abundances has been shown to be correlated with the strength of the Brewer-Dobson circulation (Nevison, 2011). Variability in stratosphere to troposphere air mass exchange, coupled with the stratospheric N_2O sink is likely to be responsible for a fraction of the variability

in tropospheric N_2O, but the prognostic understanding of the seasonal and inter-annual variability of the stratosphere-troposphere exchange is low (Huang et al., 2008). This removal process signal is obscured in the southern hemisphere by the timing of oceanic thermal and biological ventilation signals (Nevison, 2011). Quantitative understanding of the terrestrial source variability is low, although it may be driven by soil water content variability in the Northern hemisphere, as inferred from correlations with the observed variability in the N_2O atmospheric growth rate (Ishijima et al., 2009). A first process model-based estimate suggests that the mainly climate-driven variability in the terrestrial source may account for only 0.07 ppb yr^{-1} in atmospheric N_2O, which would be difficult to detect in the observed growth rate (Zaehle et al., 2011).

[INSERT FIGURE 6.18 HERE]

Figure 6.18: Globally averaged growth rate of N_2O in ppb yr^{-1} determined from the observations of the NOAA/ESRL halocarbons program. Brown dots indicate annual values augmented by a smoothed line to guide the eye.

6.3.4.2 Emissions and Sinks

Most N_2O is produced by biological (microbial) processes such as nitrification and denitrification in terrestrial and aquatic systems, including rivers, estuaries, coastal seas and the open ocean. In general, more N_2O is formed when more reactive nitrogen is available. The production of N_2O shows a large spatial and temporal variability. Experimental data are mostly available for terrestrial systems in temperate zones. As a result emission estimates for tropical regions and for aquatic systems are relatively uncertain. Inverse modelling studies add to our assessments of the N_2O budget by providing mostly independent constraints on the global and regional emission estimates from bottom-up methods, and show that the errors in these are large, especially in (sub)-tropical regions (e.g., Hirsch et al., 2006; Huang et al.; 2008, Thompson et al., subm.). Emissions from rivers, estuaries and continental shelves have been subject of debate for several decades (DeKlein et al., 2007; Seitzinger and Kroeze, 1998). A recent study in North America confirms that rivers can be important sources of N_2O (Beaulieu et al., 2011b).

Table 6.8 does not include the formation of atmospheric N_2O from the abiotic decomposition of ammonium nitrate in the presence of light, appropriate relative humidity and a surface, however it has been recently proposed as a potentially important source of N_2O (Rubasinghege et al., 2011). A global estimate of the source strength, however, does not yet exist. Table 6.8 indicates that the global N_2O emissions in the mid 1990s amount to 17.4 (8.5–27.7) Tg N yr^{-1}. This is essentially the same as the estimate in AR4 (17.7 TgN yr^{-1} in AR4). The uncertainty range overlaps with that of inverse modelling studies (14.1–17.8) by Huang et al. (2008). Anthropogenic emissions have steadily increased over the last two decades and in 2006 were 15% higher than the value in the early 1990s. Overall, anthropogenic emissions are now a factor of 8 greater than their estimated level in 1900. These trends are consistent with observed increases in atmospheric N_2O (Syakila et al., 2010). Human activities strongly influence the source of N_2O, since N-fertilizer used in agriculture is now the main source of N for nitrification and denitrification. Trends in nitrogen isotopes confirm that agriculture is primarily responsible for historic increase in N_2O (Park et al., 2012; Sutka et al., 2006).

6.3.4.3 Sensitivity of N_2O fluxes to Climate and Elevated CO_2

Early studies have suggested a considerable positive feedback between N_2O and climate (Khalil and Rasmussen, 1989) supported by observed glacial-interglacial swings in atmospheric N_2O (Fluckiger et al., 1999). Climate changes influence marine and terrestrial sources, but their individual contribution and even the sign of their response to climate variations are difficult to estimate, and there appears to be no consensus about the sources responsible for the long-term (glacial-interglacial) N_2O concentration changes. Simulations of a terrestrial biosphere model suggest a moderate increase of global N_2O emissions with recent climatic changes (Zaehle and Dalmonech, 2011). However, most of the change in atmospheric N_2O is attributed to anthropogenic reactive nitrogen (Nr) and industrial emissions (Davidson, 2009; Holland et al., 2005; Zaehle and Dalmonech, 2011). Significant uncertainty remains in the N_2O-climate feedback from land ecosystems, as it is very sensitive to the changes in the seasonal and frequency distribution of precipitation, and also because agricultural emissions themselves may also be sensitive to climate.

Methods to monitor ecosystem exchanges of N_2O have greatly improved in recent years, but technological challenges persist and the network remains very sparse (Sutton et al., 2007). Climate change will directly

affect nitrification and denitrification processes, and thus N_2O production, due to its effect on temperature and soil moisture regimes (Butterbach-Bahl and Dannenmann, 2011). N_2O emissions may also be influenced indirectly by the effects of CO_2 fertilisation or by N deposition induced changes in soil moisture, plant productivity, activity and composition of soil microbial and fungal communities, and nitrogen availability due to plant-soil interactions (Barnard et al., 2005; Singh et al., 2010). Only a few long-term manipulation experiments have been conducted to investigate the effect of global changes on terrestrial N_2O emissions, and these have mostly focused on temperate and boreal ecosystems. Warming experiments show varying N_2O emission responses, likely due to co-variations in soil moisture and temperature-related increase in N_2O production (Brown et al., 2011; Chantarel et al., 2011; Lohila et al., 2010). N_2O emissions were estimated to predominantly increase with elevated CO_2 (vanGroenigen et al., 2011), however, reductions have also been observed (Billings et al., 2002; Mosier et al., 2002), depending mainly on changes in the microbial/fungal community and the overall plant-soil nitrogen cycling (Kammann et al., 2008; Reich et al., 2006). In ecosystems where N is not limiting, the N_2O response to temperature and atmospheric CO_2 increases will likely be positive (Butterbach-Bahl and Dannenmann, 2011).The effect of interacting climate and atmospheric CO_2 change modulates and potentially dampens the individual responses to each driver, however, the global implications of these interactions remain poorly understood (Brown et al., 2011). Thawing permafrost soils may under particular hydrological settings may liberate reactive nitrogen and turn into significant sources of N_2O, however, the global significance of this source is not established (Elberling et al., 2010).

6.3.4.4 Global N Budget

For base year 2005, anthropogenic activities created ~220 TgN of reactive nitrogen Nr from N_2, in contrast to natural terrestrial sources totalling ~100 TgN (90–120 TgN yr^{-1}) – human actions amounted to a factor of 2 more reactive nitrogen than natural terrestrial processes (Table 6.8, Section 1a). This contrast might be even larger. A recent analysis estimates that natural terrestrial process may only total ~58 TgN yr^{-1} (40–100 TgN yr^{-1}; Vitousek et al., subm.). Of this created reactive nitrogen, NO_x and NH_3 emissions from anthropogenic sources are ~4-fold greater than natural emissions (Table 6.8, Section 1b). The resulting deposition of NHx is more favored to the continents than the oceans relative to the NO_y deposition due to the longer atmospheric residence time of the latter. These deposition estimates are lower limits, as they do not include organic nitrogen species, which can increase deposition rates by up to 30% (Duce et al., 2008; Table 6.8, Section 1c). Discharge of reactive nitrogen to the coastal oceans is ~45 TgN yr^{-1} (Table 6.8, Section 1c). There are two broad findings in AR5 compared to AR4. First, human creation of reactive nitrogen is 2 to 4 times greater than creation by natural terrestrial systems, and second, the atmosphere is about twice as important as riverine systems in distributing reactive nitrogen through the global environment.

6.4 Projections of Future Carbon and Other Biogeochemical Cycles

6.4.1 Introduction

In this section, we assess how accurately changes in the evolution of CO_2, CH_4 and N_2O concentration can be projected using models, and hence the role of carbon and other biogeochemical cycles in future climate under socio-economic emission scenarios. AR4 reported how climate change can affect the natural carbon cycle in a way which could feed back onto climate itself. A comparison of 11 coupled climate-carbon cycle models of different complexity (Coupled Climate-Carbon Cycle Model Intercomparison Project; C4MIP; Friedlingstein et al., 2006) showed that all 11 models simulated a positive feedback. In other words, climate change reduced natural carbon uptake in these models and amplified atmospheric CO_2 increases (see Box 6.4). However, there is substantial quantitative uncertainty in future CO_2 and temperature, both across coupled carbon-climate models (Friedlingstein et al., 2006) and within each model parametrizations (Booth et al., 2012). This uncertainty on the coupling between carbon cycle and climate is of comparable magnitude to the uncertainty caused by physical climate processes discussed in Chapter 12 of this report (Denman et al., 2007; Gregory et al., 2009; Huntingford et al., 2009), showing that carbon-climate interactions are key to climate projections.

Very few coupled carbon-climate models include a representation of nutrient cycles in the terrestrial carbon cycle, which are yet an important component of the terrestrial carbon cycle, affecting both its ability to take up anthropogenic carbon and its response to future climate change (Section 6.4.6). Recent studies (Sokolov

et al., 2008; Thornton et al., 2009; Zaehle et al., 2010a) have found that representation of nitrogen in terrestrial carbon cycle models substantially alters the response of future CO_2 projections and can even change the sign of the climate-carbon feedback. Available nitrogen can both limit the natural uptake of carbon by terrestrial ecosystems, and also reduce the potential sensitivity of land carbon sink to future climate change. The availability of labile forms of phosphorus (P) is also known to limit ecosystem productivity, with important interactions among carbon, nitrogen, and phosphorus cycles (Elser et al., 2007; LeBauer and Treseder, 2008). Other important processes such as anthropogenic or natural disturbances (Sections 6.4.3.2, 6.4.8.1), forest age distribution or interactions with atmospheric composition (Sections 6.4.8.3, 6.4.8.5) are often missing or treated simplistically in these models (see also Section 6.3.2.6.6).

Other biogeochemical cycles and feedbacks other than induced by the carbon cycle play an important role in the future of the climate system, although the carbon cycle represents the strongest of these. Natural CH_4 emissions from wetland and fires are sensitive to climate change (Sections 6.4.7 and 6.3.3.2). The fertilizing effects of nitrogen deposition and rising CO_2 also likely affect CH_4 emissions by wetlands through increased productivity. Changes in the nitrogen cycle, in addition to interactions with CO_2 sources and sinks, are very likely to affect the emissions of N_2O both on land and from the ocean (Section 6.4.6) and potentially on the rate of CH_4 oxidation (Gardenas et al., 2011). A recent review highlighted the complexity of terrestrial biogeochemical feedbacks (Arneth et al., 2010). A model study including feedbacks from carbon storage, and CH_4 and N_eO emissions from land estimated land-climate feedbacks contribute an additional 30–40% to climate sensitivity (Stocker et al., subm.). Mahowald (2011) estimated that the radiative forcing from aerosol effects on biogeochemical cycles is of comparable magnitude to the conventional aerosol direct and indirect radiative forcing effects. A similar degree of complexity exists in the ocean and in interactions between land, atmosphere and ocean cycles (Figure 6.19). Many of these processes are not yet represented in coupled climate-biogeochemistry models and so their magnitudes have to be estimated in offline or simpler models, which makes their quantitative assessment difficult. It is likely that there will be non-linear interactions between many of these processes, but these are not yet quantified. Confidence in the magnitude, and sometimes even the sign, of these feedbacks is low.

[INSERT FIGURE 6.19 HERE]

Figure 6.19: A summary of the magnitude of biogeochemical feedbacks. Gregory et al. (2009) proposed a framework for expressing non-climate feedbacks in common units (W m^{-2} K^{-1}) with physical feedbacks, and Arneth et al. (2010) extended this beyond carbon cycle feedbacks to other terrestrial biogeochemical feedbacks. The figure shows the results compiled by Arneth et al. (2010), with ocean carbon feedbacks from the C4MIP coupled climate-carbon models used for AR4 also added. Some further biogeochemical feedbacks from the HadGEM2-ES Earth System model (Collins et al., 2011) are also shown. Black dots represent single estimates, and coloured bars denote the simple mean of the dots with no weighting or assessment being made to likelihood of any single estimate. An indication of the confidence in the magnitude of these estimates is shown in the right hand column and is low for feedbacks with only one, or few, dots. The role of nitrogen limitation on terrestrial carbon sinks is also shown – this is not a separate feedback, but rather a modulation to the climate-carbon and concentration-carbon feedbacks. This list is not exhaustive. These feedback metrics are also likely to be state or scenario dependent and so cannot always be compared like-for-like (see Section 6.4.2.2). Results have been compiled from (a) Arneth et al. (2010), (b) Friedlingstein et al. (2006), (c) HadGEM2-ES (Collins et al., 2011) simulations, (d) Burke et al. (subm.), (e) von Deimling et al. (2012). Note the expanded x-axis scale for the lower portion of the figure.

The response of land and ocean carbon storage to changes in climate, atmospheric CO_2 levels and anthropogenic activity varies strongly on different timescales making it hard to simply use past changes to make projections of future changes. This chapter has assessed carbon cycle changes across many timescales from monthly to millennial, and these are summarised in Table 6.9. A common result is that an increase in atmospheric CO_2 will *always* lead to an *increase* in land and ocean carbon storage. However, changes in climate do not lead to a consistent sign of response in carbon storage change due to the very many different mechanisms that operate. For example, land carbon increases on seasonal time scales in temperate and high latitudes in northern spring-summer months due to higher temperatures and light levels; over glacial cycles, land carbon also increases as climate warms due to reduced cover of ice sheets. However, on centennial timescales land carbon is projected to reduce in a warmer climate due to faster decomposition of soil organic matter. Thus changes in carbon cycling on different timescales cannot simply be extrapolated to make projections on different timescales, but can provide valuable information on the processes at work and can be used to evaluate and improve models.

[INSERT TABLE 6.9 HERE]

Table 6.9: Comparison of the magnitude of changes in carbon storage (PgC) by land and ocean over different timescales. These changes are shown as approximate numbers to allow a comparison across timescales. For more details see the indicated chapter section. An indication, where known, of what causes these changes (climate, CO_2, land use change) is also given with an indication of the sign: '+' means that an increase in CO_2 or global-mean temperature is associated with an increase in carbon storage (positive β or γ), and a '–' means an increase in CO_2 or global-mean temperature is associated with a decrease in carbon storage (negative β or γ). The processes which operate to drive these changes can vary markedly from seasonal phenology of vegetation to long-term changes in ice sheet cover or ocean circulation. Some of these processes are 'reversible' in the context that they can increase and decrease cyclically, whereas some are 'irreversible' in the context that changes in one sense might be much longer than in the opposite direction.

[START BOX 6.4 HERE]

Box 6.4: Climate-Carbon Cycle Models and Experimental Design

What are coupled climate-carbon cycle models and why do we need them?

General circulation models (GCMs, generally referred to as 'climate models') have long been used for making climate projections, and have formed the core of previous IPCC climate projection chapters (e.g., Meehl et al. (2007). For the 5th Coupled Model Intercomparison Project (CMIP5) many models now have an interactive carbon cycle. What exactly does this mean, how do they work and how does their use differ from previous climate models? Atmosphere-ocean GCMs typically represent the physical behaviour of the atmosphere and oceans but atmospheric composition, such as the amount of CO_2 in the atmosphere, is prescribed as an input to the model. This approach neglects the fact that changes in climate might affect the natural biogeochemical cycles, which control atmospheric composition, and so there is a need to represent these processes in climate projections.

Specifically there is growing recognition that interactions between climate change and the global carbon and other biogeochemical cycles can have profound influences on future climate. In 2006, the C4MIP project (Coupled climate-carbon cycle model intercomparison project; Friedlingstein et al., 2006) assembled results from 11 models, which explicitly represented these interactions and thus enabled the first multi-model quantification of the climate-carbon cycle feedback. At the core of coupled climate-carbon cycle models is the physical atmosphere-ocean GCM, but additional components of land and ocean biogeochemistry respond to the changes in the climate conditions to influence the atmospheric CO_2. Now, the atmospheric CO_2 becomes a part of the model and its evolution in time is simulated rather than being prescribed as an input. Instead, the input comes in the form of CO_2 emissions (such as from burning fossil fuel) which can increase the CO_2 and then the natural carbon cycle exchanges CO_2 between the atmosphere and land and ocean components. These 'climate-carbon cycle models' (also commonly referred to as 'Earth System Models' (ESMs) – see Glossary) provide a predictive link between fossil fuel CO_2 emissions and future CO_2 concentrations and are an important part of the CMIP5 experimental design (Hibbard et al., 2007). The phrase 'earth system' refers to more than just the carbon cycle, and some models (e.g., HadGEM2-ES; Collins et al., 2011) also represent atmospheric chemistry processes. In this box we focus specifically on the implementation and use of coupled climate-carbon cycle models within the CMIP5 experiments.

The Role of Land-Cover

Land cover is the term used to describe what occupies an area of land, be it trees, grasses, ice or urban areas. All models require some description of the physical properties of the land surface, but how this is represented differs between them. Conventional climate models would have prescribed land-cover: i.e., the land cover at every point is pre-defined, although it may be defined to change in time to represent a scenario of land use change. Land cover change includes deforestation and other land use change assessed in Section 6.3.2.2 for their effect on CO_2 emissions during the past decades. Some models used for coupled climate-biogeochemical cycles projections incorporate the ability to simulate changes in the natural land cover from biome migration, as different types of vegetation grow or die in response to environmental changes. So-called Dynamic Global Vegetation Models (DGVMs, e.g., Sitch et al. (2008)) can simulate such changes in the natural land-cover and hence additional biophysical effects through heat and moisture fluxes as well as changes in carbon storage.

How are these models used?

Earth System GCMs (ESMs) are the primary tool for making projections of climate change for the next century. The additional capability to simulate carbon cycle processes and feedbacks and in some models other biogeochemical cycles, allows for a greater range of quantities to be simulated such as changes in natural carbon stores, fluxes or ecosystem functioning. As described above, the ESM models have the capability of simulating the time variations in atmospheric CO_2 interactively with GCM simulated climate. But there may also be applications where it is desirable for the user to pre-define the pathway of atmospheric CO_2 and prescribe it as a forcing to the ESMs. Thus, numerical simulations with ESM models can be either 'concentration driven' or 'emissions driven' as described below. It should be noted that a model can be used in either configuration – this is not a distinction between different models, but a distinction between different ways of using them.

Concentration-driven simulations follow the 'traditional' approach of prescribing the time-evolution of atmospheric CO_2 as an input to the model used in IPCC AR1 to AR4 Assessment reports, although AR4 discussed in their Chapter 7 the emission-driven C4MIP results. This is shown schematically in Box 6.4 Figure 1 (left hand side). Atmospheric CO_2 concentration is prescribed as input to the model from a given scenario (e.g., RCP scenarios) and follows a pre-defined pathway regardless of changes in the climate or natural carbon cycle processes. The processes between the horizontal dashed lines in the figure represent the model components which are calculated during the concentration-driven simulation. Externally prescribed changes in atmospheric CO_2 concentration, and hence climate, can and will affect land and ocean carbon storage. By construction, changes in land and ocean storage, however, do not feedback on the atmospheric CO_2 concentration and hence wider climate. The changes in natural carbon fluxes and stores are output by the model and can be used to diagnose the sensitivity of the carbon cycle to (prescribed) CO_2 and (calculated) climate changes. Additionally in concentration driven simulations, externally prescribed human-caused changes in land use and land-cover may be applied from scenarios, which affect the terrestrial carbon storage, but this has no impact on the atmospheric CO_2, although the physical impact of land-cover change on the climate will be included.

[INSERT BOX 6.4, FIGURE 1 HERE]

Box 6.4, Figure 1: Schematic representation of carbon cycle numerical experimental design. Concentration-driven (left hand side) and emissions-driven (right hand side) simulation experiments make use of the same ESM models, but configured differently. Concentration-driven simulations prescribe atmospheric CO_2 as a pre-defined input to the climate and carbon cycle model components, but their output does not affect the CO_2. Emissions-driven simulations prescribe CO_2 emissions as the input and atmospheric CO_2 is now an internally calculated element of the earth system model.

Emissions-driven simulations allow the full range of interactions in the models to operate and determine the evolution of atmospheric CO_2 and climate as an internal part of the simulation itself (Box 6.4, Figure 1, right hand side). In this case external fossil fuel and cement emissions of CO_2 are the externally prescribed input to the model and the subsequent changes in atmospheric CO_2 concentration are simulated by it. The model simulates changes in land and ocean carbon storage, and associated carbon fluxes with the atmosphere and these affect the atmospheric CO_2 allowing the effects of feedbacks between climate and the carbon cycle to be quantified. If externally prescribed human caused land use or land cover changes are applied as a forcing scenario then in addition to the physical effects on the climate, changes in carbon storage from deforestation or other land use change (see Section 6.3.2.2) will influence the course of atmospheric CO_2.

The outputs from the two types of simulation experiment are different but closely related. In both cases natural land and ocean carbon fluxes and stores are simulated by the models. In *emissions-driven* experiments, the atmospheric CO_2 growth rate is calculated within the model due to the net effect of the anthropogenic emissions, E, and natural fluxes:

$$\frac{dCO_2}{dt}_{simulated} = E - \left(land\_carbon\_uptake + ocean\_carbon\_uptake\right)$$

In *concentration-driven* simulation experiments, the so called 'compatible fossil fuel emissions', E, that can be diagnosed afterwards from mass conservation principle, from the prescribed atmospheric CO_2

concentration pathway by calculating the residual between the prescribed CO_2 pathway and the natural fluxes, i.e., as given by the following equation:

$$E = \frac{dCO_2}{dt}_{prescribed} + \left(land\_carbon\_uptake + ocean\_carbon\_uptake\right)$$

The effect of climate change on the natural carbon cycle will manifest itself either through changes in atmospheric CO_2 in the *emissions-driven* experiments or in the compatible emissions in the *concentration-driven* experiments.

Concentration-driven simulation experiments have the advantage that they can be performed by GCMs without an interactive carbon cycle. For this reason, most of the RCP simulations presented later in this Chapter with carbon cycle models and in Chapter 12 are performed this way. Emissions-driven simulations have the advantage of representing the full range of interactions in the coupled climate-carbon cycle models and may be seen as a more realistic experimental design. Hence the RCP8.5 pathway is repeated by many ESM models as an emissions-driven simulation to quantify the possible effects of the climate-carbon cycle feedback on climate change under this high-emissions scenario (Friedlingstein et al., subm.).

Feedback Analysis

The Earth System models are made up of many 'components', corresponding to separate parts of the computer programme which perform calculations to represent different processes or aspects of the system. E.g., models may have components to represent clouds, rainfall, ocean currents, sea ice and land and ocean ecosystems. All these components interact in the full model – i.e., the output from one set of calculations may change the conditions, which affect another. For example if it rains in a dry place, the plants may grow more.

In order to understand the behaviour of the very complex ESM models a technique was developed to assess different aspects of the models' sensitivities (Arora et al., subm.; Friedlingstein et al., 2003; Friedlingstein et al., 2006). The two dominant interactions in the carbon cycle are the response of the carbon cycle to changes in CO_2 and its response to changes in climate. These can be measured using two metrics: 'beta' (β) measures the strength of changes in carbon fluxes by land or ocean in response to changes in atmospheric CO_2; 'gamma' (γ) measure the strength of changes in carbon fluxes by land or ocean in response to changes in climate. These metrics can be calculated as cumulative changes in carbon storage (as in Friedlingstein et al., 2006) or instantaneous rates of change (Arora et al., subm.). It is not possible to measure these sensitivities simultaneously in a single simulation because it is not possible to know whether carbon fluxes are responding to CO_2, climate or both. Hence it is necessary to perform 'decoupled' simulations where some processes in the models are artificially disabled in order to be able to evaluate the changes in other processes.

For climate-carbon cycle models, these decoupled experiments are summarised in Box 6.4 and in Table 1. In a fully coupled simulation, the carbon cycle components of the models experience both changes in atmospheric CO_2 and changes in climate. Additionally the models can perform two further simulations. In the first the atmospheric radiation experiences constant CO_2 while the carbon cycle model components experience increasing CO_2. This is known as 'biogeochemically coupled' referring to the fact that this experiment quantifies the strength of the effect of rising CO_2 concentration alone on the carbon cycle in the absence of climate change (referred to as CMIP5 experiments called 'esmFixClim'). The role of this simulation is to allow quantification of the β metric (independently for land and ocean), defined as the change in carbon store per unit change in atmospheric CO_2 in the absence of climate change.

Box 6.4, Table 1: Configurations of simulations designed for feedback analysis by artificially allowing some processes to operate but holding others constant. The curves denote whether increasing or constant CO_2 values are input to the radiation and carbon cycle model components.

	CO_2 input to radiation scheme	CO_2 input to carbon-cycle scheme	Reason

Fully coupled			Simulates the fully coupled system
Biogeochemically coupled 'esmFixClim'			Isolates carbon-cycle response to CO_2 (β)
Radiatively coupled 'esmFdbk'			Isolates carbon-cycle response to climate change (γ)

The second decoupled experiment is the converse of the first one, and is known as 'radiatively coupled' (the CMIP5 experiments called 'esmFdbk'). In this experiment, the climate model's radiation scheme experiences an increase in CO_2 (and hence produces a change in climate) while fixed CO_2 concentrations are input to the carbon cycle model components. The role of this simulation is to allow quantification of the effect of climate change alone on the carbon cycle: the γ metric, defined as the change in carbon store per degree of global temperature change.

A large positive value of β denotes that a model responds to increasing CO_2 by simulating large increases in natural carbon uptake, e.g., through a large modelled 'CO_2 fertilization effect' (see Box 6.3). Negative values of γ denote that a model response to climate warming is to reduce CO_2 uptake from the atmosphere, whilst a positive value means warming acts to increase CO_2 uptake. β and γ values are not specified in a model, but are properties that emerge from the suite of complex processes represented in the model. The values of the β and γ metrics diagnosed from simulations can vary from place to place within the same model (see Section 6.4.2.3) although it is the global aggregate that determines the global extent of the climate-carbon cycle feedback.

Other feedback analysis techniques exist than that of Friedlingstein et al. (2006) . Boer and Arora (2010) analysed the carbon cycle response to climate and CO_2 at a grid-point level and present maps of these metrics in a method analogous to that used for physical radiative feedback analyses. Yoshikawa et al. (2008) also presents geographical analysis of the feedback metrics. Goodwin and Lenton (2009) show that feedbacks can be expressed as an equivalent emission. Arora et al. (subm.) analyse CMIP5 models using both the Boer and Arora (2010) flux-based and Friedlingstein et al. (2006) cumulative-based methodologies to define the sensitivities. The metrics calculated for each approach vary in time during the simulations and would differ for different scenarios. Such analysis frameworks should be seen as techniques for assessing relative sensitivities of models and understanding their differences, rather than as absolute measures of invariant system properties.

Evaluation

The complex ESM models have new components and new processes beyond conventional atmosphere-ocean GCMs and thus require additional evaluation to assess their ability to make climate projections. Evaluation of the carbon cycle model components themselves is presented in Sections 6.3.2.5.6 for ocean carbon models and 6.3.2.6.6 for land carbon models, whilst evaluation of the fully coupled models is presented in Chapter 9.

[END BOX 6.4 HERE]

6.4.2 Carbon Cycle Feedbacks in CMIP5 Models

6.4.2.1 Global Analysis

The carbon cycle response to future climate and CO_2 changes can be viewed as two strong and opposing feedbacks (Gregory et al., 2009). The climate-carbon response γ determines changes in carbon storage due to changes in climate, and the concentration-carbon response β determines changes in storage due to elevated CO_2. Climate-carbon cycle feedback responses have been analysed for 8 CMIP5 models which performed idealized simulations involving atmospheric CO_2 increasing at a prescribed rate of 1% per year (Arora et al., subm.). Increased atmospheric CO_2 will lead to increased land and ocean carbon uptake (high confidence) but by an uncertain amount. Models agree on the sign of land and ocean response to rising CO_2 but show only medium and low agreement for the magnitude of ocean and land carbon uptake respectively (Figure 6.20). Future climate change will decrease land and ocean carbon uptake (medium confidence). Models agree on the sign, globally, of land and ocean response to climate change but show low agreement on the magnitude of this response. Land and ocean carbon uptake may differ in sign between different regions and between models (Section 6.4.2.3). Inclusion of N-cycle processes in 2 land carbon cycle model components out of these 8 reduces the magnitude of the sensitivity to both CO_2 and climate (Section 6.4.6.2).

[INSERT FIGURE 6.20 HERE]

Figure 6.20: Comparison of carbon cycle feedback metrics between the C4MIP ensemble of 7 GCMs and 4 EMICs under the SRES-A2 scenario (Friedlingstein et al., 2006) and 8 CMIP5 models (Arora et al., subm.) under the 1% increase per year CO_2 scenario. Black dots represent a single model simulation and coloured bars the mean of the multi-model results, grey dots are used for models with a coupled terrestrial nitrogen cycle. The comparison with C4MIP is for context, but these metrics are known to be variable across different scenarios and rates of change (see Section 6.4.2.2). Some of the CMIP5 models are derived from models that contributed to C4MIP and some are new to this analysis. Table 6.10 lists the main attributes of each CMIP5 model used in this analysis. The SRES A2 scenario is closer in rate of change to a 0.5% yr^{-1} scenario and as such it should be expected that the CMIP5 gamma terms are comparable, but the beta terms are likely to be around 20% smaller for CMIP5 than for C4MIP. This high dependence on scenario (Section 6.4.2.2) reduces confidence in any quantitative statements of how CMIP5 carbon cycle feedbacks differ from C4MIP. Models used: MPI-ESM-LR, BCC-CSM1, HadGEM2-ES, IPSL-CM5A-LR, CanESM2, NorESM-ME, CESM1-BGC, MIROC-ESM.

[INSERT TABLE 6.10 HERE]

Table 6.10: CMIP5 model descriptions in terms of carbon cycle attributes and processes.

The role of the idealised experiment presented here is to study model processes and understand what causes the differences between models. Arora et al. (subm.) assess the global carbon budget from these idealized simulations and find across CMIP5 ESMs the contribution of land and ocean carbon-concentration feedback is typically 4–5 times larger than that of the carbon-climate feedback (Figure 6.21). The land carbon-climate feedback (γ) is larger than the ocean carbon-climate feedbacks in all models. Whilst land and ocean contribute equally to the total carbon-concentration feedback (β), model *spread* in the land response is greater than for the ocean.

[INSERT FIGURE 6.21 HERE]

Figure 6.21: Cumulative emissions across CMIP5 models broken down into the contributions of land and ocean response to CO_2 and climate. The contribution of the carbon-concentration feedback is larger than the climate-carbon feedback for all models and the land and ocean contributions to this are typically comparable. The exception is for NorESM-ME and CESM1-BGC which include nitrogen interactions in the terrestrial carbon cycle – these models with nitrogen included in the terrestrial carbon cycle model component simulate a smaller response to both climate and carbon than the other models, but still of the same sign as the other models. The contribution of the ocean to the climate-carbon response is small for all models. Models used: MPI-ESM-LR, BCC-CSM1, HadGEM2-ES, IPSL-CM5A-LR, CanESM2, NorESM-ME, CESM1-BGC, MIROC-ESM.

6.4.2.2 Scenario Dependence of Feedbacks

The values of carbon-cycle feedback metrics can vary markedly for different scenarios and as such cannot be used to compare model simulations with different time periods, nor inter-compare model simulations with different scenarios (Arora et al., subm.). Gregory et al. (2009) demonstrated how sensitive the feedback metrics are to the rate of change of CO_2 in the forcing scenario. For two models, β varied under different rates of increase of CO_2 (0.5% yr^{-1}, 1% yr^{-1} and 2% yr^{-1}), decreasing by around 20% from 0.5% yr^{-1} to 1% yr^{-1} and from 1% yr^{-1} to 2% yr^{-1}. Faster rates of CO_2 increase lead to reduced beta values as the carbon

uptake (especially in the ocean) lags further behind the forcing. γ is much less sensitive to the scenario, especially between 0.5 % yr^{-1} and 1% yr^{-1}, as both global temperature and carbon uptake lag the forcing.

6.4.2.3 Regional Feedback Analysis

The linear feedback analysis with the β and γ metrics of Friedlingstein et al. (2006) has been applied at the regional scale to future carbon uptake by Roy et al. (2011), Yoshikawa et al. (2008). Figure 6.22 shows this analysis extended to land and ocean points for the CMIP5 models.

[INSERT FIGURE 6.22 HERE]

Figure 6.22: The spatial distributions of multi model-mean land and ocean β and γs for 7 CMIP5 models using the *concentration-driven* idealised 1% per year CO_2 simulations. For land and ocean, β and γ are defined from changes in terrestrial carbon storage and changes in air-sea accumulated fluxes respectively, from the beginning to the end of the 1% simulation relative to global (not local) CO_2 and temperature change. Stippling denotes areas where the magnitude of the multi-model ensemble mean exceeds the 90% confidence level interval for β, and where at least 80% models agree on the sign of change for γ. The solid lines show the multi-model mean and shaded areas denote ±1 standard deviation. Models used are: CanESM2, GFDL-ESM2M, HadGEM2-ES, IPSL-CM5A-LR, MPI-ESM-LR, NorESM1-ME for all, CESM1-BGC for land β, and bcc-csm1-1 for ocean β and γ.

6.4.2.3.1 Regional ocean response

Increased CO_2 is projected by the CMIP5 models to increase oceanic CO_2 sinks almost everywhere (high confidence) with the exception of some very limited areas. The spatial distribution of this ocean response to CO_2, β_o, is consistent between the models and with Roy et al. (2011) analysis, with the largest βs in the high-latitudes ocean regions of both the northern and southern Hemispheres in agreement with historical uptake of anthropogenic carbon (Section 6.3.2.5.3). On average, the regions with the strongest increase of oceanic CO_2 sinks in response to higher atmospheric CO_2 are the North Atlantic and the Southern Ocean. The magnitude and distribution of β_o in the ocean closely resemble the distribution of historical anthropogenic CO_2 flux from inversion studies and forward modelling studies (Gruber et al., 2009), with the dominant anthropogenic CO_2 uptake regions in the subpolar Southern Ocean.

Climate warming is projected by the CMIP5 models to reduce oceanic carbon uptake in most oceanic regions (medium confidence) consistent with the Roy et al. (2011) analysis. This sensitivity of ocean CO_2 sinks to climate, γ_o, is mostly negative (i.e., a reduced regional ocean CO_2 sink in response to climate change) but with regions of positive values in the Arctic, the Antarctic and in the equatorial Pacific (i.e., climate change increases ocean CO_2 sink in these regions). The North Atlantic ocean and the mid-latitude Southern Ocean have the largest negative γ_o values. Reduced CO_2 uptake in response to climate change in the sub-polar Southern Ocean and the tropical regions has been attributed to warming induced decreased CO_2 solubility, reduced CO_2 uptake in the mid-latitudes to decreased CO_2 solubility and decreased vertical mixing which decreases the absorption of anthropogenic CO_2 in intermediate and deep waters (Roy et al., 2011). Increased uptake in the Arctic and the polar Southern Ocean is partly associated with a reduction in the fractional sea ice coverage (Roy et al., 2011). The North Atlantic ocean may exhibit a peak and subsequent reduction in carbon uptake as a combined response to CO_2 and climate feedbacks occurring through carbonate system CO_2 buffering and a slowdown in the Atlantic Meridional Overturning Circulation respectively (Halloran et al., subm.).

6.4.2.3.2 Regional land response

Increased CO_2 is projected by the CMIP5 models to increase land CO_2 sinks everywhere (high confidence). This response, β_L, has largest values over tropical land, in humid rather than arid regions, associated with enhanced carbon uptake in forested areas of already high biomass. In the zonal totals, there is a secondary peak of high β_L values over Northern Hemisphere temperate and boreal ecosystems partly due to a greater land area there but also coincident with large areas of forest. Models agree on the sign of response but have low agreement on the magnitude.

Climate warming is projected by the CMIP5 models to reduce land CO_2 sinks in tropics and mid-latitudes (high confidence). CMIP5 models show medium agreement that warming may increase land carbon uptake in high latitudes but none of these models include representation of permafrost carbon which is projected to decrease in warmer conditions (Section 6.4.3.3), therefore confidence is low regarding the sign and magnitude of future high-latitude land carbon response to climate change. Jones and Falloon (2009) showed

that changes in soil organic matter were the most important driver of the climate-carbon cycle feedback across C4MIP models, but these changes are not necessarily driven by soil processes. Matthews et al. (2005) have previously shown that vegetation productivity is a larger cause of model spread than modelled soil carbon decomposition processes.

6.4.3 Implications of the Future Projections for the Carbon Cycle

The CMIP5 simulations include 4 future scenarios referred to as 'Representative Concentration Pathways' or RCPs (Moss et al., 2010): RCP2.6, RCP4.5, RCP6.0, RCP8.5 (see Chapter 1). These future scenarios include CO_2 concentration and emissions, and have been generated by four Integrated Assessment Models (IAMs) and are labelled according to the approximate global radiative forcing level at 2100.

6.4.3.1 Climate and Carbon Cycle Model Components Used in the Integrated Assessment Models for the RCP Future CO_2 Concentration and Emissions Scenarios

van Vuuren (2011) have shown that the basic climate and carbon cycle responses of IAMs is generally consistent with the spread of climate and carbon cycle responses from ESMs. Some of the IAMs which were run to create the RCPs are more complex than others in terms of their carbon cycle model component and some use common climate and carbon cycle components. For the RCPs, three of the four IAMs (GCAM, RCP4.5; AIM, RCP6.0; MESSAGE, RCP8.5) use a version of the MAGICC simple climate and carbon cycle model that has been commonly used in IPCC Assessment reports. Hence, for the physical and biogeochemical components of the RCP scenarios 4.5, 6.0 and 8.5, the underlying IAMs are closely related. Only the IMAGE IAM, which created RCP2.6 differs markedly by using a newer version of MAGICC climate and a more sophisticated carbon cycle components for land and ocean carbon cycle (see Table 6.11). The same version of MAGICC was subsequently used to generate the CO_2 pathway for all 4 RCP scenarios using the CO_2 emissions output by the 4 IAMs (Meinshausen et al., 2011).

Table 6.11: Description of carbon cycle parameterizations in integrated assessment models.

IAM Model Name	Scenario	Climate	Terrestrial Carbon Cycle Model Component	Resolution	Vegetation Dynamics	Ocean Carbon
IMAGE	2.6	MAGICC6	Detailed description	0.5 x 0.5 degree	Biome model	Bern model
GCAM	4.5	MAGICC5.3	GCAM submodel	Regional/land use type	N	MAGICC
AIM	6	MAGICC4	MAGICC	Regional	N	MAGICC
MESSAGE	8.5	MAGICC4.1[a]	Explicit for forests (DIMA), otherwise via MAGICC	Regional	N	MAGICC

Notes:
(a) Some parameters have been adjusted.

6.4.3.2 Land Use Changes in Future Scenarios

ESMs and IAMs use a diversity of approaches for representing land use changes (Table 6.12), including different land use classifications, parameter settings, and geographical scales. To implement land use change in a consistent manner across ESMs, a 'harmonized' set of annual gridded land use change during the period (1500–2100) covering the historical period based on land use reconstructions, and the future based on socio-economic projections by IAMs were developed for input to the CMIP5 ESMs (Hurtt et al., 2011).

Not all the ESMs models used for CMIP5 used the full range of information available from the land use change scenarios, such as wood harvest projections, sub-grid scale shifting cultivation or representation of primary and secondary forests. This has implications for their ability to simulate carbon fluxes associated with land use change because sensitivity studies indicated that shifting cultivation, wood harvesting and simulation start date all strongly affect secondary land area and age, and estimated carbon fluxes (Section 6.3.2.2; Hurtt et al., 2011). The choice of RCP had a smaller impact on CO_2 emissions from land use change than the effects of wood harvest, shifting cultivation and choice of start date.

Table 6.12: Processes of land use incorporated in IAMs and ESMs.

Model	Deforestation	Wood Harvest	Explicit Age Classes	Crop Management	Explicit Biofuels
IAMs					
IMAGE	Y	Y	N	Y	Y
GCAM	Y	Y	N	Y	Y
AIM	Y	Y	N	Y	Y
MESSAGE	Y	Y	N	Y	Y
ESMs					
CanESM2	Y	N	N	Y	N
CCSM4	Y	Y	N	N	N
CESM1-BGC	Y	Y	N	N	N
GFDL-ESM2G	Y	Y	Y	Y (harvest)	N
HadGEM2-ES	Y	Y	N	N	N
INM-CM4	Y	Y	N	?	N
IPSL-CM5A	Y	Y	N	N	N
MIROC-ESM	Y	Y	Y	Y	N
MPI-ESM	Y	Y	N	N	N
NorESM1	Y	Y	N	N	N

Land use has been in the past and will be in the future a significant driver of forest land cover change and terrestrial carbon storage. Land use trajectories in the RCPs show very distinct trends and cover a wide-range of projections. These land use trajectories are very sensitive to assumptions made by each individual IAMs regarding the amount if land needed for food production (Figure 6.23). Wise et al. (2009) and Thomson et al. (2010) use the GCAM IAM model to highlight the large sensitivity of future land use requirements to modelling assumptions, such as increases in crop yield technology. Tilman et al. (2011) using empirical projection of cropland need for food production by 2050 also showed the sensitivity of future demand for cropland to assumptions about how agricultural technology and intensification is applied. The area of cropland and pasture increases in RCP8.5 with the MESSAGE IAM model, mostly driven by an increasing global population, but cropland area also increases in the RCP2.6 with the IMAGE IAM model, despite a smaller population increase, as a result of bio-energy production necessary to maintain low CO_2 concentration pathway. RCP6 with the AIM IAM model shows an expansion of cropland but a decline in pasture land. RCP4.5 with the GCAM IAM is the only scenario to show a decrease in global cropland. It should not be assumed that there is a monotonic progression from 'low' to 'high' land use through the scenarios related to the radiative forcing of each scenario.

Within the IAMs, land use change is translated into land use change CO_2 emissions as shown in Figure 6.23(b). The degree of process detail strongly depends on the IAM model and hence differs between the RCP scenarios. IAMs typically model the demand and supply of land use related commodities (food crops, feed, animal products and timber) at the level of world regions. In the IAMs, land is used for mitigation in the future in ways that have no equivalent in the historical period, using for instance bio-energy and forms of capture and storage (BECCS), which strongly affects land use projections in the IAM. The CO_2 emissions from land use change are then estimated from the calculated land use patterns using the terrestrial carbon cycle model component specific to each IAM (see Table 6.11). Depending on the IAM, this may be done at an aggregated, regional, level – or using a detailed representation of vegetation and carbon flows at the grid level. The CO_2 emissions from land use change calculated by IAM models in the RCPs tend to decline over time due to a slow down (or even reversal) of agricultural land expansion. As most scenarios expect the population level to stabilise (or even decline), agricultural production levels are expected to stabilize as well. Cumulative emissions for the 21st century (Figure 6.23c) vary markedly across RCPs, with increasing cropland and pastureland areas in RCP2.6 and RCP8.5 giving rise to the highest emissions from land use change, RCP4.5 to intermediate emissions, and RCP6.0 to close to zero net emissions. All scenarios suggest that 21st century land use emissions will be less than half of those from 1850 to present day, which has important consequences for projections of CO_2 and climate in the AR5 IPCC Assessment Report.

The adoption of widely differing approaches among ESMs for the treatment of land use and land cover change (LULCC) processes in terrestrial carbon cycle models leads to substantial between-model variation in predicted LULCC fluxes and associated carbon stocks. Present-day fluxes associated with anthropogenic land cover transitions (sources to the atmosphere) vary by more than a factor of 10 among models, as do model predictions of present-day wood product pools. The highest present-day fluxes are predicted by models which include representation of rotational harvest on managed forest lands (Lawrence et al., 2012; Shevliakova et al., 2009a), while variation in the size of wood product pools depends on differing rates of harvest as well as differing rates of wood product decomposition. Differences among IAMs in the treatment of LULCC processes compounds the variability in LULCC fluxes and pools among ESMs for predictions over the 21st century. The harmonization process applied to LULCC datasets for CMIP5 has been an important step toward consistency among IAMs. However, among ESMs, and between IAMs and ESMs, assignment of meaningful uncertainty ranges to present-day and future LULCC fluxes and states remains a critical knowledge gap with implications for compatible emissions to achieve CO_2 pathways (Section 6.4.3.3; Jones et al., subm.).

[INSERT FIGURE 6.23 HERE]

Figure 6.23: Land use trends and emissions according to the four different integrated assessment models (IAM) used to define the RCP scenarios. Global changes in croplands and pasture from the historical record and the RCP scenarios (top left), and associated annual land use emissions of CO_2 (bottom left). Bars (right panel) show cumulative land use emissions for the historical period (defined here as 1850–2005) and the 4 RCP scenarios from 2006 to 2100.

6.4.3.3 Projections of Future Carbon Cycle Response Under the RCP Scenarios

Future projections with Earth system models can be either *emissions-driven* or *concentration-driven* (see Box 6.4). Simulated changes in land and ocean carbon uptake and storage under the four RCP scenarios are presented here using results from CMIP5 ESMs concentration-driven simulations. The implications of these changes on atmospheric CO_2 and climate as simulated by CMIP5 emissions-driven simulations are presented in Chapter 12.

The results of the CMIP5 ESMs show medium agreement on the magnitude of cumulative ocean carbon uptake from 1850 to 2005 (Figure 6.24a): average 128 PgC, range: 95–198 PgC. The models show low agreement on the sign and magnitude of changes in land carbon storage (Figure 6.24b): average –8 PgC, range –124 to +134 PgC. These central estimates are very close to observational estimates of 125 ± 25 PgC for the ocean and –5 ± 40 PgC for the land respectively (Table 6.1), but show wide spread across models. For the four RCP scenarios all the concentration-driven ESM models project an increase in ocean uptake over the 21st century. For RCP4.5 and RCP6, all the models also project an increase in land carbon uptake, but for RCP2.6 and RCP8.5 some models (CanESM2 for RCP2.6, MIROC-ESM for RCP2.6 and 8.5, CESM1-BGC for RCP8.5) project a decrease in land carbon storage at 2100 relative to 2005. Model spread in land carbon projections is much greater than model spread in ocean carbon projections. Cox et al. (subm.) find a relationship between short term variability and long-term land carbon cycle sensitivity which may offer an observational constraint on the climate-carbon cycle response over the next century.

Representation of land use processes in ESMs is an advance since the AR4 (C4MIP models) which considered no land use processes in terrestrial carbon cycle models, but the range of processes included differs greatly between ESMs making comparison with historical land use CO_2 emissions trends (Tables 6.2 and 6.3) and RCP scenarios difficult (Section 6.4.3.1). Quantifying the carbon emissions from those land use processes included is not straightforward due to their far-reaching influence on land carbon, atmospheric CO_2 and climate. Simulated land use emissions cannot be deduced by the same method as for compatible fossil fuel emissions as they leave no net effect on the total carbon in the system (Jones et al., subm.). The net effect of a time-varying land use scenario on the carbon balance can be understood by comparison with a second simulation without land use changes (Arora and Boer, 2010). It remains a challenge to diagnose land use carbon emissions consistently across the CMIP5 models, and this is not tackled in the assessment presented in this Chapter.

[INSERT FIGURE 6.24 HERE]

Figure 6.24: Changes in land and ocean carbon uptake simulated for the four RCP scenarios. Total ocean and land reservoirs cumulative changes in carbon content are shown in the top two panels respectively for the whole period from 1850 to 2100. The lower four panels show the 21st century changes in carbon uptake for land (dashed) and ocean

(solid) separately for each scenario. Models used: CanESM2, GFDL-ESM2G, GFDL-ESM2M, HadGEM2-CC, HadGEM2-ES, IPSL-CM5A-LR, IPSL-CM5A-MR, IPSL-CM5B-LR, MIROC-ESM-CHEM, MIROC-ESM, MPI-ESM-LR, NorESM1-ME, inmcm4, CESM1-BGC.

The *concentration-driven* ESM simulations can be used to quantify the compatible fossil fuel emissions required to follow the four RCP CO_2 pathways (Jones et al., subm.; see Box 6.4, Figure 6.25, Table 6.13). There is significant spread between ESMs, but no systematic inconsistency between the ESMs compatible fossil fuel emissions and the 'original' emissions themselves estimated by IAMs to define each RCP scenario. By the end of RCP8.5 on average, the CMIP5 models project lower compatible emissions than the MESSAGE IAM. The IMAGE IAM predicts that global negative emissions are required to achieve the RCP2.6 decline in radiative forcing from 3 W m^{-2} to 2.6 W m^{-2} by 2100. There is disagreement between the complex ESMs over the necessity for global emissions to become negative to achieve this, with 4 ESM models simulating negative compatible emissions and 4 ESM models simulating positive emissions from 2080 to 2100. The RCP2.6 scenario achieves this negative emission rate through use of large-scale bio-energy with carbon-capture and storage (BECCS). This would be classed as a carbon dioxide removal (CDR) form of geoengineering under the definition used in this IPCC report, and is discussed further in Section 6.5. Rogelj et al. (2011) also demonstrate the importance of BECCS to achieve a 2°C climate target, but any such negative emissions should be offset against existing forest carbon sinks which may be displaced (Hudiburg et al., 2011). The ESMs themselves make no assumptions about how the compatible emissions could or would be achieved, but merely compute the global total emission that is required to follow the CO_2 concentration pathway.

Table 6.13: The range of compatible fossil fuel emissions (PgC) simulated by the CMIP5 models for the historical period and the 4 RCP scenarios, expressed as cumulative fossil fuel emission from 2006 to 2100.

	Compatible fossil fuel emissions diagnosed from *concentration-driven* CMIP5 simulations			Land carbon changes			Ocean carbon changes		
	Historical / RCP scenario	CMIP5 ESM mean	CMIP5 ESM range	Historical / RCP scenario	CMIP5 ESM mean	CMIP5 ESM range	Historical / RCP scenario	CMIP5 ESM mean	CMIP5 ESM range
1850–2005	315 [a]	300	195–395	–5 ± 40 [b]	–10	–125–135	125 ± 20 [b]	130	95–200
RCP2.6	325	330	190–470	[c]	80	–40–215	[c]	160	120–200
RCP4.5	785	840	640–1070		235	60–470		265	200–425
RCP6.0	1215	1145	995–1310		225	100–340		305	275–350
RCP8.5	1905	1760	1450–1960		190	–90–370		415	330–660

Notes:
(a) Historical estimates of fossil fuel are as prescribed to all CMIP5 ESM models (Andres et al., 2011).
(b) Estimate of historical net land and ocean carbon uptake from Table 6.1.
(c) IAM breakdown of future carbon changes by land and ocean are not available.
(d) Consistent with Table 6.1 budgets values are rounded to the nearest 5 PgC.

[INSERT FIGURE 6.25 HERE]

Figure 6.25: Compatible fossil fuel emissions simulated by the CMIP5 models for the 4 RCP scenarios. Top: timeseries of instantaneous emission rate. Thick lines represent the historical estimates and emissions calculated by the integrated assessment models (IAM) used to define the RCP scenarios, thin lines show results from CMIP5 ESMs. Bottom: cumulative emissions for the historical period (1860–2005) and 21st century (defined in CMIP5 as 2006–2100) for historical estimates and RCP scenarios (bars) and ESMs (symbols). In the CMIP5 model results, total carbon in the land-atmosphere-ocean system can be tracked and changes in this total must equal fossil fuel emissions to the system (see also Table 6.13). Other sources and sinks of CO_2 such as from volcanism, sedimentation or rock weathering, which are very small on centennial time scales are not considered here. Hence the compatible emissions are given by cumulative-Emissions = $\Delta C_A + \Delta C_L + \Delta C_O$ or emission rate = d/dt $[C_A + C_L + C_O]$, where C_A, C_L, C_O are carbon stored in atmosphere, land and ocean respectively. Models used: CanESM2, GFDL-ESM2G, GFDL-ESM2M, HadGEM2-CC, HadGEM2-ES, IPSL-CM5A-LR, IPSL-CM5A-MR, IPSL-CM5B-LR, MIROC-ESM-CHEM, MIROC-ESM, MPI-ESM-LR, NorESM1-ME, inmcm4, CESM1-BGC.

The dominant cause of future changes in the airborne fraction (AF) is the emissions scenario and not carbon cycle feedbacks (Figure 6.26). Models show high agreement that 21st century cumulative AF will increase under rapidly increasing CO_2 in RCP8.5 and decreases under the peak-and-decline RCP2.6 scenarios. AF declines slightly under RCP4.5 and remains of similar magnitude in the RCP6.0 scenario. Inter-model spread in changes in the land-fraction is greater than inter-scenarios spread. Models show high agreement that the ocean fraction will increase under RCP2.6 and remain of similar magnitude in the other RCP scenarios.

[INSERT FIGURE 6.26 HERE]

Figure 6.26: changes in airborne, land and ocean fraction of fossil fuel carbon emissions. The fractions are defined as the changes in storage in each component (atmosphere, land, ocean) divided by the compatible fossil fuel emissions derived from each CMIP5 simulation for the 4 RCP scenarios. Solid circles show the observed estimate based on Table 6.11 for the 1990s. The coloured lines and symbols denote the change in uptake fractions under the different RCP scenarios for each model, calculated using the cumulative change in carbon from 2005 to 2100. Multi-model mean values are shown as star symbols and the multi-model range (min-to-max) is shown by the vertical coloured lines. Due to the difficulty of estimating fossil and land use emissions from the ESMs this figure uses a fossil fuel definition of airborne fraction, rather than the preferred definition of fossil + land use emissions discussed in Section 6.3. 21st century cumulative airborne, land and ocean fractions are shown here in preference to the more commonly shown instantaneous fractions because for RCP2.6 emissions reach and cross zero and so an instantaneous definition of AF becomes singular at that point. Models used: CanESM2, GFDL-ESM2G, GFDL-ESM2M, HadGEM2-CC, HadGEM2-ES, IPSL-CM5A-LR, IPSL-CM5A-MR, IPSL-CM5B-LR, MIROC-ESM-CHEM, MIROC-ESM, MPI-ESM-LR, NorESM1-ME, inmcm4, CESM1-BGC.

Several studies (Jones et al., 2006; Matthews, 2006; Miyama and Kawamiya, 2009; Plattner et al., 2008) have shown that climate-carbon cycle feedbacks affect the compatible fossil fuel CO_2 emissions that are consistent with a given CO_2 concentration pathways. Five CMIP5 ESMs from decoupled simulations (see ESM_BOX) agree for RCP4.5 that the climate impact on carbon uptake by both land and oceans will reduce the compatible fossil fuel CO_2 emissions for that scenario by between 6% and 29% between 2006 and 2100 respectively (Figure 6.27) equating to an average of 157 PgC (range 61–262 PgC) less carbon that can be emitted from fossil fuel use. Such uncoupled simulations have not been performed for the other RCP scenarios, but previous work has shown that compatible emissions are reduced by a greater degree under higher CO_2 scenarios which exhibit a greater degree of climate change (Jones et al., 2006).

[INSERT FIGURE 6.27 HERE]

Figure 6.27: Diagnosed compatible fossil fuel emissions (top panel) in the presence (red lines) and absence (blue lines) of the climate impact on the carbon cycle for the RCP4.5 scenario, and the difference between them (bottom panel). Thin lines show annual values and thick lines 10-year smoothed values. This shows the impact of climate change on the compatible fossil fuel CO_2 emissions to achieve the RCP4.5 CO_2 concentration pathway. Models used: CanESM2, GFDL-ESM2M, HadGEM2-ES, IPSL-CM5A-LR and MIROC-ESM.

6.4.3.4 Permafrost Carbon

Current estimates of permafrost soil carbon stocks are 1670 PgC (Tarnocai et al., 2009), the single largest component of the terrestrial carbon pool and higher than previously thought. Terrestrial carbon models show a land CO_2 sink with warming at high northern latitudes, however none of the models participating in C4MIP or CMIP5 included explicit representation of permafrost soil carbon decomposition, which at a minimum requires sufficient vertical resolution in modelled soil carbon distribution and processes to separate surface pools from very old (Pleistocene) permafrost carbon pools. Including permafrost carbon processes into an ESM can change the sign of this C response to warming from a sink to a source in northern high latitudes (Koven et al., 2011). The magnitude of this source of CO_2 to the atmosphere from decomposition of permafrost carbon varies widely by 2100 according to different model estimates: process-model estimates include 7–17 Pg (Zhuang et al., 2006), 55–69 Pg (Koven et al., 2011), and 126–254 Pg (Schaefer et al., 2011); estimates of uncertainty ranges suggest the source could range from 33 to 114 Pg C (68% range) under RCP8.5 warming (von Deimling et al., 2012), or 50–270 PgC (5th–95th percentile range; Burke et al., subm.). Combining observed vertical soil C profiles with modelled thaw rates estimate that the total quantity of newly-thawed soil C by 2100 will be 246 Pg for RCP4.5 and 436 Pg for RCP8.5 (Harden et al., 2012 in press). Sources of uncertainty for the permafrost C feedback include the physical thawing rates, the fraction of C that is release after being thawed and the timescales of release, possible mitigating nutrient feedbacks, and the role of fine-scale processes in determining the terrestrial response.

6.4.4 Future Ocean Acidification

A fraction of CO_2 emitted into the atmosphere dissolves in the ocean, reducing surface ocean pH and carbonate ion concentrations. The associated chemistry is not debated by the scientific community (very high confidence) and expected changes are in line with what is measured at ocean time series stations (see Chapter 3). Multi-model projections using ocean process-based carbon cycle models discussed in AR4 demonstrate large decreases in pH and carbonate ion concentration [CO_3^{2-}] during the 21st century throughout the world oceans (Orr et al., 2005). The largest decrease in surface [CO_3^{2-}] occur in the warmer low and mid-latitudes, which are naturally rich in this ion (Feely et al., 2009). However, it is the colder high-latitude oceans that first become undersaturated with respect to aragonite (i.e., Ω_A <1, where Ω_A = [Ca^{+2}][CO_3^{2-}]/Ksp, where Ksp is the solubility product for the metastable form of $CaCO_3$ known as aragonite). This undersaturation in surface waters is reached within decades in the Southern Ocean as highlighted in AR4, but occurs sooner and is more intense in the Arctic (Steinacher et al., 2009). Ten percent of Arctic surface waters are projected to become undersaturated when atmospheric CO_2 reaches 428 ppm (by 2025 under all IPCC SRES scenarios) . That proportion increases to 50% when atmospheric CO_2 reaches 534 ppm (Steinacher et al., 2009). By 2100 under the A2 scenario, much of the Arctic surface is projected to become undersaturated with respect to calcite (Feely et al., 2009). Surface waters would then be corrosive to all $CaCO_3$ minerals. These general trends are confirmed by the latest projections from the CMIP5 earth system models (Christian et al., subm.), Figure 6.28).

[INSERT FIGURE 6.28 HERE]

Figure 6.28: Projected ocean acidification from 12 CMIP5 earth system models under the RCP8.5 scenario: time series of surface **(a)** carbonate ion concentration and **(b)** pH shown as the mean (solid line) and range of models (filled), given as area-weighted averages over the Arctic Ocean (green), the tropical oceans (red), and the Southern Ocean (blue); maps of the median model's **(c)** change in surface pH from 1850 to 2100 and its surface Ω_A in **(d)** 2013, **(e)** 2050, and **(f)** 2100; and zonal mean sections (latitude vs. depth) of Ω_A in 2100 over the (g) Atlantic and (h) Pacific, while the ASH is shown in 2013 (dotted line) as well as 2100 (solid line). Panels (a) and (b) also include mean model results from three other scenarios: RCP2.6, RCP4.5, and RCP6.0 (dashed lines). Over most of the ocean, gridded data products of carbonate system variables (Key et al., 2004) are used to correct each model for its present-day bias by subtracting the model-data difference at each grid cell following (Orr et al., 2005). Where gridded data products are unavailable (Arctic Ocean, all marginal seas, and the ocean near Indonesia), results are shown without bias correction. The bias correction reduces the range of model projections by up to a factor of 4, e.g., in panels (a) and (b) compare the large range of model projections for the Arctic (without bias correction) to the smaller range in the Southern Ocean (with bias correction).

Regional ocean carbon cycle models project that some nearshore systems are highly vulnerable to future pH decrease. In the California Current System, an eastern boundary upwelling system, strong seasonal upwelling of carbon-rich waters (Feely et al. 2008) renders surface waters as vulnerable to future ocean acidification as those in the Southern Ocean (Gruber et al., 2012). In the Northwestern European Shelf Seas, large spatiotemporal variability is enhanced by local effects from river input and organic matter degradation, exacerbating acidification from anthropogenic CO_2 invasion (Artioli et al., 2012). In the Gulf of Mexico and East China Sea, coastal eutrophication, another anthropogenic perturbation, has been shown to enhance subsurface acidification as additional respired carbon accumulates at depth (Cai et al., 2011).

In the open ocean, future reductions in surface ocean pH and $CaCO_3$ saturation states are controlled mostly by the invasion of anthropogenic carbon. Other effects due to future climate change counteract less than 10% of the CO_2-induced reductions in $CaCO_3$ saturation (Cao et al., 2007; McNeil and Matear, 2006; Orr et al., 2005). Warming dominates other effects from climate-change by reducing CO_2 solubility and thus by enhancing [CO_3^{2-}]. An exception is the Arctic Ocean where reductions in pH and $CaCO_3$ saturation states (for both aragonite and calcite, the stable form of calcium carbonate) are projected to be exacerbated by effects from increased freshwater input due to enhanced sea ice melt, more precipitation, and greater air-sea CO_2 fluxes due to less sea ice cover (Steinacher et al., 2009; Yamamoto et al., 2012). The projected effect of freshening is consistent with current observations of lower saturation states and lower pH values near river mouths and in areas under substantial fresh-water influence (Chierici and Fransson, 2009; Salisbury et al., 2008; Yamamoto-Kawai et al., 2009).

Surface $CaCO_3$ saturation also varies seasonally, particularly in the high latitudes, where observed saturation is higher in summer and lower in winter (Feely et al., 1988; Findlay et al., 2008; Merico et al., 2006). Future

projections using ocean carbon cycle models indicate that undersaturated conditions will be reached first in winter (Orr et al., 2005). In the Southern Ocean, it is projected that wintertime undersaturation with respect to aragonite will begin when atmospheric CO_2 will reach 450 ppm, which is about 100 ppm sooner (~30 years under the IS92a scenario) than for the annual mean undersaturation (McNeil and Matear, 2008).

Although projected changes are generally largest at the surface, the greatest pH changes in the subtropics occur between 200–300 m where subsurface changes in anthropogenic CO_2 are similar to surface changes but the carbonate buffering capacity is lower (Orr, 2011). This more intense projected subsurface pH reduction is consistent with the observed subsurface changes in pH in the subtropical North Pacific (Byrne et al., 2010; Dore et al., 2009; Ishii et al., 2011). As subsurface saturation states decline, the horizon separating undersaturated waters below from supersaturated waters above is projected to move upward (shoal). By 2100 under the RCP8.5 scenario, the median projection from 12 CMIP5 models is that this interface (aragonite saturation horizon) will shoal from 197 m up to 36 m in the subarctic Pacific, from 965 m up to the surface in the Southern Ocean, and from 2870 m to 151 m in the North Atlantic, consistent with results from previous model comparison (Orr, 2011; Orr et al., 2005). Under the SRES A2 scenario, the volume of ocean with supersaturated waters is projected to decline from 42% in the preindustrial era to 25% in 2100 (Steinacher et al., 2009). Yet even if atmospheric CO_2 does not go over 450 ppm, most of the deep ocean volume is projected to become undersaturated with respect to both aragonite and calcite after several centuries (Caldeira and Wickett, 2005). Nonetheless, the most recent projections under RCPs mitigation scenarios illustrate that limiting atmospheric CO_2 will greatly influence the level of ocean acidification that will be experienced (Joos et al., 2011).

6.4.5 Future Ocean Oxygen Depletion

It is likely that global warming will lead to declines in dissolved O_2 in the ocean interior through warming-induced reduction in O_2 solubility and increased ocean stratification (see Box 6.5). This would have implications for nutrient and carbon cycling, ocean productivity and marine habitats (Keeling et al., 2010).

[START BOX 6.5 HERE]

Box 6.5: IPCC AR5 Ocean Deoxygenation

A general decrease in the dissolved oxygen concentration of the ocean has been observed across much of the coastal and open ocean over the latter decades of the 20th century (Gilbert et al., 2010; Helm et al., 2011; Keeling et al., 2010). These changes in oceanic oxygen (ΔO_2^{tot}) can be related to climate forcing, both directly through the reduced solubility of oxygen in warm waters (ΔO_2^{sol}), and indirectly through changes in ocean mixing and ventilation processes (ΔO_2^{vent}) and changes in biological activity (ΔO_2^{bio}). These processes are highlighted in Figure 1 and combine simply as follows:

$$\Delta O_2^{tot} = \Delta O_2^{sol} + \Delta O_2^{vent} + \Delta O_2^{bio} \quad (6.3.1)$$

The processes that influence ocean oxygen also affect the ocean carbon cycle, albeit in different proportions. Thus, climate signatures of ocean deoxygenation provide an important insight into the functioning of the oceans and their capacity to take up CO_2. Models consistently estimate that changes in ocean ventilation explain most of the observed 'deoxygenation' of the ocean, causing oxygen decreases about four times greater than those expected from ocean warming alone, and exceeding any oxygen increases that may be caused by decreases in biological productivity at low latitudes. However, although the observed deoxygenation is consistent with the impact expected from climate change, formal attribution has not been made and the observed deoxygenation signal could be mainly caused by natural variability in the ocean carbon cycle system. Ocean deoxygenation leads to increases in the oceanic emissions of N_2O, and has impacts on marine ecosystems.

[INSERT BOX 6.5, FIGURE 1 HERE]

Box 6.5, Figure 1: *The ocean O_2 cycle*. The oceanic reservoir of oxygen communicates with the atmosphere via air-sea gas exchange (F_{O2}). In the ocean interior, a change in dissolved O_2 concentration over time can be driven by changes in: (1) surface ocean O_2 solubility ΔO_2^{sol}, (2) the ventilation age of a water parcel advected into the subsurface (ΔO_2^{vent}) (3) biological utilisation of oxygen in remineralization of Dissolved Organic Carbon (DOC; ΔO_2^{bio}).

[END BOX 6.5 HERE]

Future changes in dissolved O_2 have been investigated using intermediate complexity ocean models (EMIC) (Oschlies et al., 2008; Plattner et al., 2001; Schmittner et al., 2008; Shaffer et al., 2009) and 3D ocean carbon cycle models (Bopp et al., 2002; Frolicher et al., 2009; Matear and Hirst, 2003; Matear et al., 2000; Sarmiento et al., 1998). There is broad consensus that the global oceanic oxygen inventory will decline significantly under future scenarios (Cocco et al., subm.). Simulated declines in mean dissolved O_2 concentration for the global ocean range from 6 to 12 μmol kg^{-1} by the year 2100 (Table 6.14), with a projection of 3–4 μmol kg^{-1} in one model with low climate sensitivity (Frolicher et al., 2009). This general trend is confirmed by the latest projections from the CMIP5 earth system models, with reductions in mean dissolved O_2 concentrations from 3 to 6% (5 to 10 μmol kg^{-1}) in 2100 for RCP8.5 (Figure 6.29b).

The global decline in oxygen concentration is explained in models by enhanced surface ocean stratification leading to reductions in convective mixing and deep water formation with a contribution of 18–50% from ocean warming-induced reduction in solubility, in part compensated by a small increase in O_2 concentration from projected reductions in biological export production (Bopp et al., 2001; Steinacher et al., 2010) or changes in ventilation age of the tropical thermocline (Gnanadesikan et al., 2007). The largest regional decreases in oxygen concentration (~20–100 μmol kg^{-1}) are projected for the intermediate (200–400 m) to deep waters of the North Atlantic, North Pacific and Southern Ocean for 2100 (Cocco et al., subm.; Frolicher et al., 2009; Matear and Hirst, 2003; Matear et al., 2010; Plattner et al., 2002; Figure 6.29a).

Table 6.14 Model configuration and predictions for marine O_2 depletion by 2100 (adapted from Keeling et al. (2010)

Study	Ocean carbon cycle model	Forcing	Mean [O_2] Decrease (μmol kg^{-1})[a,b]	Solubility Contribution (%)
Sarmiento et al. (1998)	GFDL		7[c]	
Matear et al. (2000)	CSIRO	IS92a		18
(Plattner et al., 2002)	Bern 2D	SRES A1	12	35
Bopp et al. (2002)	IPSL	SRES A2[d]	4	25
Matear and Hirst (2003)	CSIRO	IS92a	9	26
Schmittner et al. (2008)	UVic	SRES A2	9	
Oschlies et al. (2008), Shaffer et al. (2009)	UVic	SRES A2	9[e]	
	UVic-variable C:N	SRES A2	12[e]	
Frölicher et al. (2009)	NCAR CSM1.4-CCCM	SRES A2	4	50
		SRES B1	3	
Shaffer et al. (2009)	DCESS	SRES A2	10[e]	

Notes:
(a) Assuming a total ocean mass of 1.48 x 10^{21} kg^{-1}
(b) Relative to pre-industrial baseline in 1750
(c) Model simulation ends at 2065
(d) Radiative forcing of non-CO_2 GHGs is excluded from this simulation
(e) For simulations with reduced ocean exchange, assuming modern average ocean O_2 concentration of 178 μmol kg^{-1} (Sarmiento and Gruber, 2006)

There is not such a broad consensus on the evolution of the extent of hypoxic (dissolved oxygen <60–80 μmol kg^{-1}) and suboxic (dissolved oxygen <5 μmol kg^{-1}) waters. Most models show even some increase in oxygen in most O_2-poor waters and thus a slight decrease in the extent of suboxic waters under the SRES-A2 scenario (Cocco et al., subm.), as well as under RCP8.5 scenario (Figure 6.29b). This rise in oxygen in most suboxic waters has been shown to be caused in one model study by an increased supply of oxygen due to lateral diffusion (Gnanadesikan et al., 2011). Given the limitations of global ocean models in simulating

today's O_2 distribution (Cocco et al., subm.), as well as simulating the changes detected in O_2 concentrations over the past 50 years (Andrews et al., subm.; Stramma et al., 2012), the model predictions are speculative, especially concerning the evolution of O_2 in and around oxygen minimum zones.

A number of biogeochemical ocean carbon cycle feedbacks, not yet included in most EMICs or ESMs, could also impact future trends of ocean deoxygenation. For example, model experiments which include a pCO_2-sensitive C:N drawdown in primary production, as suggested by some mesocosm experiments (Riebesell et al., 2007), project future increases of up to 50% in the volume of the suboxic waters by 2100 (Oschlies et al., 2008; Tagliabue et al., 2011). In addition, future marine hypoxia could be amplified by changes in the $CaCO_3$ to organic matter 'rain ratio' in response to rising pCO_2 (Hofmann and Schellnhuber, 2009). Reduction in biogenic calcification due to ocean acidification would weaken the strength of $CaCO_3$ mineral ballasting effect which would lead organic material to be remineralised at a shallower depth exacerbating the future expansion of shallow hypoxic waters.

These estimates do not take into account processes that are specific of the coastal ocean and may amplify deoxygenation. Recent observations for the period 1976–2000 have shown that dissolved O_2 concentrations have declined at a faster rate in the coastal ocean (–0.28 μmol kg^{-1} yr^{-1}) than the open ocean (–0.02 μmol kg^{-1} y^{-1}; Gilbert et al., 2010). Hypoxia in the shallow coastal ocean (apart from continental shelves in Eastern Boundary Upwelling Systems) is largely eutrophication-driven and is controlled by the anthropogenic flux of nutrients (N and P) and organic matter from rivers. If continued industrialisation and intensification of agriculture yield larger nutrient loads in the future, eutrophication should intensify (Rabalais et al., 2010), and further increase the coastal ocean deoxygenation.

On longer time scales, ocean deoxygenation is projected to keep increasing after 2100, with some models simulating a tripling in the volume of suboxic waters by 2500 (Schmittner et al., 2008). Ocean deoxygenation and further expansion of suboxic waters could persist on millennial timescales, with average dissolved O_2 concentrations projected to reach minima of up to 56 μmol kg^{-1} below pre-industrial levels in experiments with high CO_2 emissions and high climate sensitivity (Shaffer et al., 2009).

The potential expansion of hypoxic or suboxic water over large parts of the future is also likely to impact the marine cycling of important nutrients, particularly nitrogen. In particular, the marine flux of N_2O depends critically upon the volume of low-O_2 waters since denitrification, which provide an important pathway for N_2O production, is inhibited by oxic conditions (Nevison et al., 2003). The intensification of low oxygen waters will likely lead to significant increases in global N_2O emissions (e.g., Codispoti, 2010; Naqvi et al.; 2009). A tripling in the volume of suboxic waters would lead to a quadrupling in global water column denitrification and a doubling in marine N_2O production by the year 4000 (Schmittner et al., 2008). Changes in denitrification and nitrogen fixation in a deoxygenated ocean are also likely to impact upon the marine inventory of fixed nitrogen, however the sign and magnitude of this feedback is uncertain (e.g., Codispoti et al., 2001; Deutsch et al., 2007; Lam and Kuypers, 2010).

[INSERT FIGURE 6.29 HERE]

Figure 6.29: (a) Multi-model mean projected changes in dissolved O_2 (μmol kg^{-1} in the main thermocline (100–600 m depth average) from 1995–2005 to 2090–2100 under the RCP8.5 scenario. To indicate consistency in the sign of change, regions are stippled where at least 80% of models agree on the sign of the mean change. (b) Modelled evolution from 1850 to 2100 (under RCP8.5 scenario) of the relative change in global mean O_2 concentration, as well as of volume anomalies of hypoxic (O_2 <80 μmol kg^{-1}) and suboxic (O_2 <5 μmol kg^{-1}) waters. These diagnostics are detailed in Cocco et al. (subm.) in a previous model intercomparison using the SRES-A2 scenario and have been applied to CMIP5 models under RCP8.5 here. Models used: GFDL-ESM2G, GFDL-ESM2M, HadGEM2-ES, IPSL-CM5A-LR, IPSL-CM5A-MR, MPI-ESM-LR, MPI-ESM-MR.

6.4.6 Future Trends in the Nitrogen Cycle and Impact on Carbon Fluxes

6.4.6.1 Projections for Formation of Reactive N by Human Activity

Since 1970s, human activities of food production, industrial activity and fossil fuel combustion have introduced more reactive nitrogen (Nr) into the biosphere than natural processes (Section 6.1; Box 6.1, Figure 1). A simple conceptual model of the future global use of nitrogen fertilizer was derived from the current use and the expected developments of drivers that influence this use (Winiwarter et al., subm.). Five

driving parameters (population growth, biofuels use, food equity, increased N-use efficiency and diet optimization) are used to project future N demands (Figure 6.30). During the 21st century, the projections are expected to change from just a slight increase to roughly doubling with respect to the year 2005 situation. Despite the uncertainties and the non-inclusion of many important drivers, all scenarios generated by the (Winiwarter et al., subm.) model point towards an increase in future production of reactive nitrogen. The actual amounts of Nr released to the environment in the future will depend on the demand for food (and its type), and the demand for energy (and its type).

[INSERT FIGURE 6.30 HERE]

Figure 6.30: Global fertilizer Nr fixation (TgN yr^{-1}) derived as fertilizer demand, projected till 2100. Lines in the left panel reflect trends based on drivers from the RCP scenarios, dots different independent assessment. The asterisks report the ranges of two different interpretations of the SRES scenarios, with Erisman et al. (2008) using a methodology very similar to the one used for RCPs (Winiwarter et al., subm.).

With the continuing increases in the formation of Nr from anthropogenic activities will come increased injection into environmental reservoirs, especially soils, terrestrial vegetation, the atmosphere, groundwater and the coastal ocean.

The main driver of future global N deposition is the emission trajectories of NO_y and NH_3. For the atmosphere, in some RCP scenarios, deposition of NO_y and NH_x is projected to remain relatively constant globally although there is a balance between increases in NH_x deposition and decreases in NO_y deposition. On a regional basis, there are future projected decreases in North America and Northern Europe, and generally increases in Asia. The regional impacts (spatial patterns) for deposition are more complex and sensitive to, apart from its sources, climate change and corresponding changes in precipitation, temperature and atmospheric circulation. Large uncertainties remain in our understanding of atmospheric NO_y and NH_x removal mechanisms, which also depend on atmospheric physical state and hence is sensitive to climate change. These changes in both emissions, and atmospheric transport and deposition processes lead to major uncertainties in the projection of future Nr deposition fluxes, particularly in regions remote from anthropogenic emissions (Dentener et al., 2006). The large spread between atmospheric GCM models associated with precipitation projections confounds extraction of an anthropogenic-forced climate signal in deposition projections (Hedegaard et al., 2008; Langner et al., 2005).

The area of natural vegetation exposed to critical loads of nitrogen deposition in excess of 1000 mg N m^2 yr^{-1} is projected to increase under future emissions scenarios for 2050. Under all RCP scenarios except RCP4.5, Nr deposition is expected to increase in many land regions, following projected increases in NH_3 emissions but overall decreases in anthropogenic NO_x emissions (Lamarque et al., 2011). By 2100, emission-driven change could more than double atmospheric Nr deposition to some world biodiversity hotspots (under a IS92a scenario) with half of these hotspots subjected to nitrogen deposition rates over at least 10% of their total area higher than 15 kg N ha^{-1} yr^{-1}, thus exceeding critical loads set for sensitive ecosystems (Bleeker et al., 2011; Phoenix et al., 2006).

Given the tight coupling between the atmospheric N and S cycles, and the impact of both on climate, e.g., through aerosols, this Chapter also presents scenarios for sulphur. Deposition of SO_x is also projected to decrease (Figure 6.31). Estimates for sulfur deposition in 2100, based on scenarios prior to RCPs, strongly depend on regional projections for SO_2 emissions, with all scenarios projecting decreases in North America and Europe, but potential for large growth (or reductions) in regions such as South America, Africa, South and East Asia (Dentener et al., 2006; Tagaris et al., 2008; Figure 6.33). Under the RCP scenarios, SO_x deposition is projected to ultimately decreases strongly throughout the globe by 2100 (Lamarque et al., 2011) but in some regions SO_2 emission increases will very likely lead to higher sulfate deposition in the near-term under some of the RCPs.

With increasing introduction of Nr into terrestrial ecosystems will come increased flux from rivers into coastal systems. As illustrated by the Global NEWS 2 model, by the base year 2000, the discharge of dissolved inorganic nitrogen (DIN) to marine coastal waters was >500 kg N km^{-2} of watershed area for most watershed systems downstream of either high population or extensive agricultural activity (Figure 6.34a) (Mayorga et al., 2010; Seitzinger et al., 2010). The change in DIN discharge under the Global Orchestration (GO) scenario of the Millennium Ecosystem Assessment (MEA) (the scenario with the most extreme pressures) was assessed by taking the change between the base year 2000, and the projection year, in this

case 2050 (Figure 6.34b). Manure is the most important contributor as a result of assumed high per capita meat consumption, although there are considerable regional variations (Seitzinger et al., 2010). At the other extreme is the projected change in the riverine flux between 2000 and 2050 for the Adapting Mosaic scenario, the most ambitious in terms of nutrient managements of the MEA scenarios. These two scenarios provide a range of projections for future DIN riverine fluxes by the year 2050.

[INSERT FIGURE 6.31 HERE]

Figure 6.31: Deposition of SO_x (left panel, TgS yr^{-1}), NH_x (middle panel, TgN yr^{-1}) and NO_y (right panel, TgN yr^{-1}) from 1850 to 2000 and projections of deposition to 2100 under the four RCP emission scenarios (Lamarque et al., 2011; van Vuuren et al., 2011). Also shown are the 2030 scenarios using the SRES B1/A2 energy scenario with assumed current legislation and maximum technically feasible air pollutant reduction controls (Dentener et al., 2006).

[INSERT FIGURE 6.32 HERE]

Figure 6.32: Spatial variability of N deposition in 2000 with projections for 2100, using the 2.6, 4.5, 6.0 and 8.5 RCP scenarios, kg N ha^{-1} yr^{-1} adapted from (Lamarque et al., 2011).

[INSERT FIGURE 6.33 HERE]

Figure 6.33: Spatial variability of S deposition in 2000 with projections for 2100, using the 2.6, 4.5, 6.0 and 8.5 RCP scenarios, kg S ha^{-1} yr^{-1}(Lamarque et al., 2011).

[INSERT FIGURE 6.34 HERE]

Figure 6.34: (a) Dissolved inorganic nitrogen river discharge to coastal zone (mouth of rivers) in 2000, based up on Global NEWS 2 model, (b) change in DIN discharge from 2000 to 2050, based upon Global Orchestration and the Adapting Mosaic scenarios, Millennium Ecosystem Assessment (Mayorga et al., 2010; Seitzinger et al., 2010). Units are kg N per km^2 watershed per year, as an average for each watershed.

In addition to these future changes in the atmospheric and riverine fluxes of short-lived Nr, there are also projected to be increases in N_2O emissions. This is illustrated by the comparison of emissions from 1850 to those in 2000 and 2050, using the IMAGE model (Figure 6.35). This spatially explicit soil nutrient budget and N gas emission scenario was elaborated by Bouwman et al. (2011b) on the basis of the International Assessment of Agricultural Knowledge, Science and Technology for Development (IAASTD) baseline scenario (McIntyre et al., 2009). A comprehensive spatially explicit inventory of N budgets in livestock and crop production systems (Bouwman et al., 2011a) shows that between 1900 and 1950, the global soil Nr surplus almost doubled to 36 TgN yr^{-1} and between 1950 and 2000 to 138 TgN yr^{-1}. The IMAGE model scenario shown in Figure 6.35 portrays a world with a further increasing global crop production (+82% for 2000–2050) and livestock production (+115%). Despite rapidly assumed increasing Nr recovery in crop (+35%) and livestock (+35%) production, global Nr surpluses are projected to continue to increase (+23%). Associated agricultural emission of N_2O (soil emission from agricultural fields) are consequently projected to increase from 2.5 Tg in 1900 to 7.0 Tg of N_2O-N yr^{-1} in 2000, with a continued increase to 9.3 Tg yr^{-1}, reflecting the above developments.

Regional to global scale model applications suggest a strong effect of climate variability on inter-annual variability of land N_2O emissions (Tian et al., 2010; Zaehle and Dalmonech, 2011). Kesik et al. (2006) found that higher temperatures and lower soil moisture could in the future the European average of forest soil N_2O emissions under scenarios of climate change, despite local increases of emission rates by up to 20%. Other modelling studies have shown no significant effect of climate change on terrestrial net emissions (Abdalla et al., 2010). Two independent global modelling studies (Stocker et al., subm.; Zaehle, subm.) have suggested an increase of terrestrial N_2O emissions by 0.5 to 5 TgN yr^{-1} due to climate and atmospheric CO_2 abundance changes under different future global change scenarios between the years 2005 and 2100, partly due to the amplification of agricultural emissions under altered climate regimes. These changes provide a small but long-lasting positive feedback mechanism between terrestrial biogeochemistry and the climate system. However, due to the limited observational constraint and modelling evidence, there is little confidence in the overall magnitude of this feedback.

On a related matter concerning actions that would need to be taken to decrease N_2O emission, Davidson (2012), in a model-based analysis, shows that the magnitude of changes that would be required to stabilize atmospheric N_2O by 2050, consistent with the most aggressive of the RCP mitigation scenarios, would have

to be about 50% reductions in emission factors in all sectors and about a 50% reduction in mean per capita meat consumption in the developed world.

[INSERT FIGURE 6.35 HERE]

Figure 6.35: N_2O emissions in 1900, 2000 and projected to 2050 (Bouwman et al., 2011a).

6.4.6.2 Impact of Future Changes in Reactive Nitrogen on Carbon Uptake and Storage

Anthropogenic Nr addition and natural N-cycle responses to global changes will have an important impact on the global carbon cycle. As a principal nutrient for plant growth, nitrogen can both limit future carbon uptake and stimulate it depending on changes in Nr availability. A range of global terrestrial carbon cycle models have been developed since AR4 that integrate nitrogen dynamics into the simulation of land carbon cycling (Churkina et al., 2009; Esser et al., 2011; Gerber et al., 2010; Jain et al., 2009; Sokolov et al., 2008; Thornton et al., 2007; Zaehle and Friend, 2010).

In response to climate warming, increased decomposition of soil organic matter increases N mineralisation, (high confidence) which can enhance Nr uptake and growth of vegetation. Generally, higher C:N ratio in woody vegetation causes increased Nr uptake and hence ecosystem carbon storage (Melillo et al., 2011). In two models (Sokolov et al., 2008; Thornton et al., 2009), this effect is strong enough to turn the carbon-climate interaction into a small negative feedback, i.e., an increased land CO_2 uptake in response to climate warming (positive γ_L values in Figure 6.19), whereas in other (Zaehle et al., 2010b) CMIP5 models that describe C, N interactions, (Arora et al., subm.) the carbon-climate interaction remains positive, i.e., decreased land CO_2 uptake in response to climate change (negative γ_L values in Figures 6.19, 6.20). Sokolov et al. (2008) note, however, that the land biosphere eventually becomes a net CO_2 source despite nitrogen feedbacks and γ_L would eventually change sign.

Consistent with the observational evidence (Finzi et al., 2006; Norby et al., 2010; Palmroth et al., 2006), modelling studies have shown a strong effect of Nr availability on the response of plant growth and land carbon sequestration to elevated atmospheric CO_2 (Sokolov et al., 2008; Thornton et al., 2009; Zaehle and Friend, 2010). These analyses are affected by the projected future trajectories of anthropogenic Nr deposition. The effects of N availability interact synergistically with the N constraints on CO_2 fertilisation and climate (Churkina et al., 2009; Zaehle et al., 2010a). Estimates of the total net C storage on land due to Nr deposition between 1860 and 2100 range between 27 and 66 PgC (Thornton et al., 2009; Zaehle et al., 2010a), based on diverging assumptions about the future evolution of N deposition.

There is high confidence that at the global scale, nutrient limitation will reduce the global land carbon sequestration projected by carbon-cycle only models (Figure 6.36). Only two of the current CMIP5 ESM models explicitly consider C, N interactions (CESM1-BGC and NorESM1-ME) in the AR5. The effect of the N limitations on terrestrial carbon sequestration in the results of the other CMIP5 models may be approximated by comparing the implicit N requirement given plausible ranges of terrestrial C:N stoichiometry (Wang and Houlton, 2009) to plausible increase in terrestrial N supply due increased biological nitrogen fixation (Wang and Houlton, 2009) and anthropogenic Nr deposition (Lamarque et al., 2011). For the ensemble of CMIP5 projections under the RCP 8.5 scenario, this implies a lack of available nitrogen of 1.9–18.8 PgN which would reduce terrestrial C sequestration by 92–400 PgC. Assuming an average 21st century airborne fraction of 0.6 in the RCP 8.5 scenarios (Section 6.4.3.3; Jones et al., subm.), this lack of available nitrogen would cause an increase in atmospheric CO_2 of 26–113 ppm by the year 2100, implying an additional radiative forcing of 0.15–0.61 W m^{-2}. The inferred geographic pattern suggests that N limitation will be stronger in temperate/boreal ecosystems and tropical ecosystems and in pristine areas than highly polluted areas (Section 6.3), but this varies widely between models.

The different magnitude and spatial distribution of N limitation across the two CMIP5 terrestrial carbon cycle model components inclusive of these processes is caused by uncertainty about key mechanisms controlling C-N couplings (Zaehle and Dalmonech, 2011). Alternative mechanisms to represent N limitation, loss and stoichiometry, have important consequences for determining the N requirement associated with an increase in land carbon stocks (Sokolov et al., 2008). Zaehle et al. (2010b) demonstrated the potential use of ecosystem manipulation experiments to constrain model responses. However, the observational data to evaluate carbon-nitrogen coupling in these models remains vague.

The effect on land C storage due to climate-induced N release from soils is of comparable magnitude to the C storage associated with increased anthropogenic Nr. Models disagree, however, which of the two factors is more important, with both effects dependent on the choice of scenario. Crucially, the effect of N limitation on vegetation growth and ecosystem carbon storage under elevated CO_2 is the strongest effect of the natural and disturbed N cycle on terrestrial C dynamics (Bonan and Levis, 2010; Zaehle et al., 2010a). In consequence, the projected atmospheric CO_2 concentrations (and thus degree of climate change) in 2100 are higher in projections with models describing C, N interactions than in those projected by traditional carbon-cycle-only climate models. The influence of current and future nitrogen deposition on the ocean sink for anthropogenic carbon is estimated to be rather small, with less than 5% of the ocean carbon sink in 2100 attributable to fertilization from anthropogenic nitrogen deposition over the oceans (Reay et al., 2008).

[INSERT FIGURE 6.36 HERE]

Figure 6.36: (a) Implied global terrestrial nitrogen deficit of the RCP8.5 carbon sequestration projections; (b) implied overestimation of terrestrial C sequestration due to neglecting N limitations; (c) Additional radiative forcing resulting from the nitrogen limitation of terrestrial C sequestration. The N deficit was calculated as follows: The simulated increase in terrestrial C stocks were converted into N requirements as described by Wang and Houlton (2009). The yearly evolution of the nitrogen requirements were compared on a model grid-cell bases against the newly available nitrogen due to changes in biological nitrogen fixation and atmospheric deposition. The error bars represent the range of results obtained using alternative assumption about terrestrial C:N stoichimetry, N retention from N deposition and changes in fixation. Values are presented for the year 2005 and 2100 and displaced in time for clearer visibility. Radiative forcing was calculated using the formulation of Ramaswamy et al. (2001), assuming an air-borne fraction of 0.6, and are evaluated as change in atmospheric CO_2 burden against the RCP8.5 scenario abundances in 2005 (377 ppm) and 2100 (935 ppm). The panels also show simulations of the IPSL-CM4-A2-OC model (Zaehle et al., 2010a), driven with the SRES-A2 scenario projections of the IPSL-CM4 model for which both a C-cycle only and dynamically coupled C-N cycle simulation are available, and for which the N deficit of the C-cycle model can therefore be determined explicitly.

6.4.7 Future Changes in CH_4 Emissions

Future atmospheric CH_4 concentrations are sensitive to future changes in both emissions and subsequent oxidation. Atmospheric chemistry is not covered in this chapter and we assess here future changes in natural CH_4 emissions, which may change in response to climate change (e.g., O'Connor et al., 2010). Methane sources most likely to be affected by climate change are wetlands (Section 6.4.7.1) and natural fires (Section 6.4.7.4). In high latitudes, where future temperature changes are likely to be highest, wetlands may be influenced by permafrost (Section 6.4.7.2). Methane hydrate deposits, both in permafrost soils and in subsea sediments, may become unstable and escape to the atmosphere, though the quantities stored in hydrates are not well known (Section 6.4.7.3). Future changes in anthropogenic emissions may also be important but are not assessed here. Potential future changes in CH_4 emissions are assessed in the following Sections and summarised in Figure 6.37.

[INSERT FIGURE 6.37 HERE]

Figure 6.37: Summary of the sizes and time scales associated with future CH_4 emissions (adapted from O'Connor et al., 2010). Uncertainty in these future changes is large, and so this figure demonstrates the relative magnitude of possible future changes. Anthropogenic emissions continuing at a present day level of 300 Tg(CH_4) yr^{-1} (consistent with Table 6.7) are shown for reference. Wetland emissions are taken as 140–280 Tg(CH_4) yr^{-1} present day values (Table 6.7) and increasing by between 0–100% (Section 6.4.7.1; Figure 6.38). Permafrost emissions may become important during the 21st century. Large CH_4 hydrate release to the atmosphere is not expected during the 21st century. No quantitative estimates of future changes in CH_4 emissions from wildfires exist, so plotted here are continued present day emissions of 1–4 Tg(CH_4) yr^{-1} (Table 6.7).

6.4.7.1 Future CH_4 Emissions from Global Wetlands

Wetlands exist most commonly in the tropics and high latitudes, and emit CH_4 due to anaerobic decomposition (methanogenesis) of organic matter in water-logged soils. Wetland extent is determined by geomorphology and soil moisture, which depends on precipitation, evapotranspiration, drainage and runoff. All of these may change in the future. Increasing temperature can lead to higher rates of evapotranspiration, reducing soil moisture and therefore reduced wetland extent. Regional projections of precipitation changes are especially uncertain (see Chapter 12). These hydrological processes operate on fine spatial scales and are thus particularly difficult to include in ESMs. Those ESMs that do include wetland dynamics predict wetland

extent increasing in some areas due to increased water availability either through more precipitation and/or lower evapotranspiration due to the CO_2 effect on stomatal closure, and decreasing in other areas due to increased evapotranspiration and drainage, or earlier snowmelt (Koven et al., 2011; Ringeval et al., 2011). The UVic ESCM has projected for instance a loss of wetland area north of 45°N in the 21st century from 6.6% for RCP2.6 to 19.8% for RCP8.5 (Avis et al., 2011).

Since AR4, several modelling studies attempted to quantify the sensitivity of global wetand CH_4 emissions to environmental changes, and these are summarised in Figure 6.38. The studies cover a wide range of simulation experiments but there is high agreement between model results that the combined effect of CO_2 increase and climate change by the end of the 21st century will increase wetland CH_4 emissions. Using a common experimental protocol (Melton et al., subm.) seven models indicate that under increased temperature alone (red bars in Figure 6.38) CH_4 emissions may increase or decrease, while the effect of increased precipitation alone (green bars in Figure 6.38) there was always an increase in wetland CH_4 emissions, although generally small. The effect of increased atmospheric CO_2 concentration (blue bars) always resulted in an increase of wetland CH_4 emissions: between 22 and 162%. Other studies assessed different environmental changes such as temperature and precipitation together (orange bars in Figure 6.38) and often found an increase in wetland CH_4 emissions (Eliseev et al., 2008; Gedney et al., 2004; Shindell et al. 2004; Volodin, 2008), although Ringeval et al. (2011) found a net decrease. One reason for this current disagreement between models on the sign of the temperature sensitivity of emissions is that some models simulate a reduction of wetland area followed by a reduction of CH_4 emissions under higher temperatures, whereas other models that use fixed wetland areas show an increase in CH_4 emissions under higher temperatures. The combined effect of climate and CO_2 results in an increase of CH_4 emissions of 40% (Volodin, 2008; fixed wetland area) and 68% (Ringeval et al., 2011; variable wetland area).

The mechanisms that cause the simulated changes of wetland CH_4 emissions shown in Figure 6.38 are: (1) decreased wetland area caused by (a) reduced soil moisture due to higher temperatures and (b) decreased precipitation, and (2) increased wetland area caused by (a) thawing permafrost due to higher temperatures and (b) a reduction of evapotranspiration due to the CO_2 effect on stomatal closure. Depending on which effects prevail in a model, wetland area will either decrease and reduce CH_4 emissions or increase and enhance CH_4 emissions. Direct effects on CH_4 emissions are caused by (1) higher NPP under higher temperature and higher atmospheric CO_2 concentrations, (2) higher CH_4 production rates under higher temperature, and (3) reduction of CH_4 oxidation through increased precipitation that increases water table position (Melton et al., subm.). In most models, enhanced CO_2 concentration has the strongest enhancement effect on CH_4 emissions. However, large uncertainties exist concerning the lack of wetland specific plant functional types in most models and the lack of understanding how wetland plants will react to CO_2 fertilization (e.g., Berendse et al., 2001; Boardman et al., 2011; Heijmans et al., 2001; Heijmans et al., 2002a, 2002b).

Small-scale studies show that simulated CH_4 emissions from a bog in western Siberia approximately doubled when temperature (+3–5°C) and precipitation (+10–15%) were increased at the same time (Bohn et al., 2007). However, in the same study, an increase in only temperature led to such a big decrease in emissions that methane oxidation became larger than the emissions and the simulated site became a CH_4 sink. This extreme sensitivity to fine-scale conditions is typical of methane models, and implies large uncertainty to their current predictive capability (Riley et al., 2011). Field-based experiments in Alaska showed a weaker response to water table manipulations and warming experiments: warming and flooding increased CH_4 fluxes on average by 79%, while lowering the water table reduced the flux by up to 36% (Turetsky et al., 2008).

[INSERT FIGURE 6.38 HERE]

Figure 6.38: Relative changes of global CH_4 emissions from either pre-industrial or present day conditions and environmental changes that reflect potential conditions in 2100. The first seven models took part in the WETCHIMP intercomparison project and were run under a common protocol (Melton et al., subm.) . Other studies used different future conditions as listed in the figure: Eliseev et al. (2008), Gedney et al. (2004), Ringeval et al. (2011), Shindell et al. (2004), Volodin (2008).

The effect of climate change on methane emissions from tropical wetlands (Section 6.3; Bergamaschi et al., 2007; Chen and Prinn, 2006) received little attention but tropical wetlands are likely to experience multiple disturbances such as alterations to the thermal and hydrological regime and changes in the freshwater-

seawater gradient (Hamilton, 2010; Mitsch et al., 2010). A separation between wetlands that are inundated for long periods and wet mineral soils that are defined as mineral soils that are not inundated but whose soil moisture can intermittently reach a level that facilitates CH_4 emissions was introduced by (Spahni et al., 2011). There is still a large uncertainty around the magnitude of CH_4 emissions from these wet mineral soils but Spahni et al. (2011) allocated 63 Tg(CH_4) yr^{-1} to wet mineral soils and 80 Tg(CH_4) yr^{-1} to inundated wetlands for the present day. Regional changes in soil moisture will affect heterotrophic respiration in mineral soils (Falloon et al., 2011) and could also lead to a change in CH_4 emissions from wet soils, but the sign of such a change is uncertain.

Soil CH_4 oxidation of about 30 Tg(CH_4) yr^{-1} (Table 6.7) represents the smallest of the three sinks for atmospheric methane (see Table 6.7) but is also sensitive to future environmental changes. Soil CH_4 oxidation is projected to increase by up to 23% under the SRES A1B due to rising atmospheric CH_4 concentrations, higher soil temperature and lower soil moisture (Curry, 2009).

6.4.7.2 Future CH_4 Emissions from Permafrost Areas

Permafrost thaw may lead to increased drainage and a net reduction in wetlands, a process that has already begun to be seen in lakes in the discontinuous permafrost zone (Smith et al., 2005), or alternatively to lake growth in continuous permafrost areas underlain by ice-rich material subject to thermokarst (Christensen et al., 2004; Plug and West, 2009). There is high agreement between land surface models that permafrost extent is expected to reduce during the 21st century, accompanying particularly rapid warming at high latitudes (Chapter 12). However, estimates vary widely as to the pace of degradation. Lawrence and Slater (2005), using the NCAR CCSM3, climate model predicted widespread loss (60–90%) of permafrost within the upper 3 m of soils during the 21st century. Burn and Nelson (2006) argue that this is an overestimate, as it does not include many of the known stabilizing effects for permafrost; however, subsequent improvements to this model to include some of these mechanisms still show large permafrost losses (Lawrence et al., 2008). The LPJ-WHyMe model projected permafrost area loss of 30% (SRES B1) and 47% (SRES A2) by 2100 (Wania, 2007). Marchenko et al. (2008) calculate that by 2100, 57% of Alaska will lose permafrost within the top 2 m. For the RCP scenarios, the CMIP5 multi-model ensemble show a wide range of predictions for permafrost loss: 15–87% under RCP4.5 and 30–99% under RCP8.5 (Koven et al., subm.). Hydrological changes to wetland systems may lead to tradeoffs between the CO_2 and CH_4 balance of these ecosystems, with anoxic methane production rates being roughly an order of magnitude less than rates of oxic decomposition to CO_2, but the global warming potential of CH_4 is an order of magnitude greater than CO_2. The extent of permafrost thaw simulated by climate models has been used to estimate possible subsequent carbon release (Burke et al., subm.; Harden et al., 2012 in press; Section 6.4.3.4) but few studies explicitly partition this into CO_2 or CH_4 release to the atmosphere. Schneider von Deimling et al. (2012) estimate cumulative CH_4 emissions by 2100 between 131 and 533 Tg(CH_4) across the 4 RCPs.

Thawing of deeper unsaturated Yedoma deposits (large amounts of organic carbon located in permafrost in northeast Siberia) was postulated to produce significant CH_4 emissions (Khvorostyanov et al., 2008), however more recent estimates with Yedoma carbon lability constrained by incubation observations (Dutta et al., 2006) argue for smaller emissions at 2100 (Koven et al., 2011). Other significant sources of uncertainty are the fraction of thawed carbon that becomes available as a substrate for methanogenesis and the impact of vegetation shifts on soil gas transport and substrate supply.

6.4.7.3 Future CH_4 Hydrate Emissions and in Response to Climate Warming

Substantial quantities of methane are believed to be stored within submarine hydrate deposits at continental margins (see also Section 6.1, FAQ 6.2). Estimates of the hydrate pool remain poorly constrained by limited observations and uncertain model boundary conditions. There is concern that warming of overlying waters may melt these deposits, releasing CH_4 into the ocean and atmosphere systems.

Considering a potential warming of bottom waters by 1, 3 and 5 K during the next 100 years, (Reagan and Moridis, 2007), hereafter RM07, found that hydrates residing in a typical deep ocean setting (4°C and 1000 m depth) would be stable during this timeframe. Within a typical shallow low-latitude setting (6°C and 560 m) sea-floor CH_4 fluxes did not exceed calculated ranges of CH_4 oxidation and consumption within the sediments, but in a typical cold-shallow Arctic setting (0.4°C and 320 m) these scenarios resulted in CH_4

fluxes that exceeded rates of benthic sediment oxidation. Observations of gas venting along the Svalbard margin seafloor (Westbrook et al., 2009) suggest observed regional warming of 1°C during the last 30 years is driving hydrate disassociation, an idea supported by modelling (Reagan and Moridis, 2009). Elliott et al. (2011), incorporating the Arctic CH_4 fluxes of RM07 into an ocean biogeochemistry model, demonstrated significant impacts on marine hypoxia and acidity, although atmospheric CH_4 release was small. These findings are supported by the modelling study of (Biastoch et al., 2011). Using the multi-model response to AR4 1% yr^{-1} CO_2 increase (Lamarque, 2008), predicted an upper-estimate of the global sea-floor flux of between 560–2140 $Tg(CH_4)yr^{-1}$, mostly in the high-latitudes.

Simulations of heat penetration through the sediment by Fyke and Weaver (2006) suggest that only small changes in the gas hydrate stability zone will result on century timescales except in high-latitude regions of shallow ocean shelves. In the study of Hunter et al. (subm.), pre-2100 hydrate dissociation was similarly focussed in shallow Arctic waters and comparable in magnitude to Biastoch et al. (2011) although maximum CH_4 sea floor fluxes at 2100 were smaller than Lamarque (2008), peaking at 270 to 420 $Tg(CH_4)yr^{-1}$ for RCP 4.5 to 8.5. Most of the sea-floor flux of CH_4 would be expected to be oxidised in the water column. Mau et al. (2007) suggest only 1% might be released to the atmosphere but this fraction depends on the depth of water and ocean conditions. These studies do not consider subsea-permafrost hydrates suggested recently to be regionally significant sources of atmospheric CH_4 (Shakhova et al., 2010).

Large methane hydrate release due to marine landslides is unlikely as any given landslide could only release a tiny fraction of the global inventory (Archer, 2007). There was no positive excursion in the methane concentration recorded in ice cores from the largest known submarine landslide, the Storegga slide off Norway 8,200 years ago.

Overall, chronic methane release from hydrates could lead to climate impacts over the next century of potentially similar magnitude to other CH_4 sources such as thawing permafrost peats (Archer, 2007). In the longer term (Archer et al., 2009a) estimated that between 35 and 940 PgC, up to half the inventory assumed in that study, could be released over several thousand years in the future following a sustained 3 K seafloor warming, but confidence is higher in modelling abilities to simulate equilibrium hydrate inventories than transient changes in them.

6.4.7.4 Fire CH_4 Emissions and Climate

Fire is a source of CH_4, both from natural but mainly anthropogenic fires (see Table 6.7). Projected increases in future fire activity (Section 6.4.8.1) imply that CH_4 from fires will also increase, but there are no quantitative projections published on future fire CH_4 sources. Interactions with other processes, such as thawing of permafrost may also cause fire occurrence and CH_4 emissions to increase (Turetsky et al., 2011).

6.4.8 How Future Trends in Other Biogeochemical Cycles Will Affect the Carbon Cycle

6.4.8.1 Changes in Fire Under Climate Change / Scenarios of Anthropogenic Fire Changes

Fire is a disturbance process that affects the net landscape carbon balance. Regional studies for boreal regions suggest an increase in future fire activity (e.g., Amiro et al., 2009; Balshi et al., 2009; Flannigan et al., 2009a; Spracklen et al., 2009; Tymstra et al., 2007; Westerling et al., 2011; Wotton et al., 2010; Kurz et al., 2008b) indicated that increased fire activity has the potential to turn the Canadian forest from a sink to a source of atmospheric CO_2. Research on future changes in fire activity and CO_2 emissions has so far focused mainly on boreal North America. Models predict spatially variable responses in fire activity, including strong increases and decreases, due to regional variations in the climate – fire relationship, and anthropogenic interference (Flannigan et al., 2009b; Kloster et al., 2011; Krawchuk et al., 2009; Pechony and Shindell, 2010; Scholze et al., 2006). The response of future fire frequency and severity and CO_2 emissions in response to climate change will depend on the prevalent fire regime, which can be limited by fuel availability or by fuel moisture content. Wetter conditions can reduce fire activity, but increased biomass availability can promote fires (Scholze et al., 2006).

Using a land-surface model and future climate projections from two GCMs, Kloster et al. (2011) projected fire carbon emissions in 2075–2099 that exceed present day emissions by 17–62% depending on scenario.

The amount of CO_2 released from fires depends critically on the burn severity. Increasing burned area and more late season burning in the future will enhance ground-layer combustion and carbon emissions, which will become even more dramatic if climate change continues to affect thawing of permafrost (Turetsky et al., 2011; Section 6.4.7).

Future fire activity will also depend on anthropogenic factors. Land use change, resulting in landscape fragmentation, reduced biomass and a less flammable landscape, might explain the observed decreasing trend in fire activity following 1870 (Kloster et al., 2010; Marlon et al., 2008; Pechony and Shindell, 2010) , although declines in rate of deforestation in the Amazon do not seem to be accompanied by reduced incidence of fire (Davidson, 2012). Fire management efforts to protect life and property will try to adapt to changes in fire activity, but might reach their limits with projected increases (Flannigan et al., 2009a). For the Amazon it is estimated that at present 58% of the area is too humid to allow deforestation fires. Climate change might reduce this area to 37% by 2050 (LePage et al., 2010). Golding and Betts (2008) estimated that future Amazon forest vulnerability to fire may depend non-linearly on combined pressure from climate change and deforestation.

Fire modelling in the CMIP5 ESMs does not adequately represent the complex fire-climate relationship and possible anthropogenic interferences for a quantitative assessment of projections of future fire carbon emissions.

6.4.8.2 Impacts of Phosphorus Limitations on the Land Carbon Cycle

In contrast to N, which can be obtained from the atmosphere by N-fixing microorganisms, P enters land ecosystems almost exclusively through weathering of bedrock (Vitousek et al., 2010). On centennial time scales, the P limitation of terrestrial carbon uptake could become more severe than the N limitation because of limited P sources. In model simulations, elevated temperatures and high CO_2 concentrations cause a shift after 2100 from N to P limitation at high latitudes, induced by a strong increase in NPP and the low P sorption capacity of soils (Goll et al., 2012a). The confidence in this shift is low as processes of soil P sorption and biochemical mineralization are poorly constrained from observations. Recent synthesis efforts are leading toward global-scale datasets needed to drive coupled C-N-P models (Yang and Post, 2011).

6.4.8.3 Impacts of Tropospheric Ozone on the Land Carbon Cycle

Plants are known to suffer damage due to exposure to high levels of ozone (O_3) (Ashmore, 2005) and are likely to respond to water limitation by reducing stomatal aperture, restricting leaf uptake of both CO_2 and O_3. Using a 2030 current legislation scenario, van Dingenen (2009) estimated future reductions in global crop yields of 2–6% and 1–2% for wheat and rice, respectively. Felzer et al. (2005) presented global simulations of plant O_3 damage on the carbon cycle and showed a reduction in cumulative net terrestrial carbon storage between 2005 and 2100 ranging from 4 to 140 PgC depending strongly on degree of ozone increase, use of fertilizers and levels of CO_2. Sitch et al. (2007) found a significant suppression of the global land CO_2 sink due to O_3 damage to vegetation by up to 260 PgC by 2100 using one terrestrial carbon cycle model based on the SRES A2 emission scenarios. The indirect radiative forcing from the resulting increased CO_2 concentration in response to O_3-induced decreased CO_2 sinks reported by Sitch et al. (2007) could exceed that of direct radiative effect of tropospheric O_3 increases.

6.4.8.4 Iron-Deposition to Ocean

Desert dust carries iron, which is an essential micronutrient for marine biogeochemistry and thus can modulate ocean carbon storage. Future projections of desert dust deposition over the ocean are still largely uncertain, even about the sign of changes (Mahowald et al., 2009; Tegen et al., 2004). Tagliabue et al. (2008) present results showing relatively little impact of varying aeolian Fe input on cumulative ocean CO_2 fluxes and atmospheric pCO_2 over 2000–2100, but Mahowald et al. (2011) show projected changes in ocean productivity as large as the changes in productivity due to CO_2 increases and climate change.

6.4.8.5 Impacts of Changes in Radiation Quality on the Land Carbon Cycle

Mercado et al. (2009) estimated that variations in the diffuse fraction, associated largely with the 'global dimming' period (Stanhill and Cohen, 2001), enhanced the land carbon sink by approximately 25% between 1960 and 1999. This more than offsets the negative effect of reduced surface radiation on the land carbon sink. However Mercado et al. (2009) also showed local site optima in the relationship between photosynthesis and diffuse light conditions. Under heavily polluted or dark cloudy skies, plant productivity will decline as the diffuse effect is insufficient to offset decreased surface irradiance (UNEP, 2011). Under a future scenario involving rapid reductions in sulphate and black carbon aerosols, the 'diffuse-radiation' fertilisation declines to near zero by 2100. This implies that steeper GHG emission cuts are required to stabilize climate if anthropogenic aerosols decline as expected.

6.4.9 The Long Term Carbon Cycle and Commitments

Long term changes in vegetation structure and induced carbon storage potentially show larger changes beyond 2100 than during the 21st century as the long timescale response of tree growth and ecosystem migrations means that by 2100 only a part of the eventual committed change will be realised (Jones et al., 2009). Long-term ‘commitments’ to ecosystems migration also carry long-term committed effects to changes in terrestrial carbon storage (Jones et al., 2010; Liddicoat et al., subm.) and permafrost (O'Connor et al., 2010; Section 6.4.7). The short and long term response of terrestrial carbon storage may vary in sign over different time horizons (Jones et al., 2010; Smith and Shugart, 1993). Rapid response of tropical ecosystems may lead to early loss of carbon which could be later offset due to a larger, but slower, uptake in enhanced high latitude forests.

Northward expansion of boreal forest may be considered likely because warming of high latitudes is common to most climate models (Chapter 12) and will enable forest ecosystems to extend north into present tundra regions (Kurz et al., 2008a; MacDonald et al., 2008). The CMIP5 simulations forced by extended RCP scenarios to 2300 (Meinshausen et al., 2011) allow analysis of this longer term response of the carbon cycle. Two ESMs with dynamic vegetation that have performed these extended scenarios using the *concentration-driven* approach both simulate increases in tree cover and terrestrial carbon storage north of 60°N (Figure 6.39). Changes in temperate forests and the southern boundary of the boreal forest vary across climate scenarios with models showing either an increase or decrease in tree cover depending on scenario. Increases in fire disturbace or insect damage may drive loss of forest in these regions (Kurz et al., 2008a) however, but this process is poorly represented or not accounted at all in these models. Large scale loss of tropical forest has been found to be uncertain (Scholze et al., 2006) and depends strongly on the predicted future changes in precipitation (Good et al., 2011), although both models here simulate reduced tree cover and carbon storage for the RCP8.5 scenario. Earth System models also poorly simulate resilience of ecosystems to climate changes and usually do not account for possible existence of alternative ecosystem states such as tropical forest or savannah (Hirota et al., 2011).

Regional specific changes in ecosystem composition and carbon storage are uncertain but it is very likely that ecosystems will continue to change for decades to centuries following stabilisation of greenhouse gases and climate change.

[INSERT FIGURE 6.39 HERE]

Figure 6.39: Maps of changes in woody cover fraction, %, (left) and terrestrial carbon storage, kg C m^{-2}, (right) for three RCP extension scenarios 2.6 (top), 4.5 (middle), and 8.5 (bottom) between years 2100 and 2300 averaged for two models, HadGEM2-ES and MPI-ESM, which simulate vegetation dynamics. Model results were interpolated on 1° x 1° grid; white colour indicate areas where models disagree in sign of changes. Note the RCP6.0 extension was not a CMIP5 required simulation. Anthropogenic land use in these extension scenarios is kept constant at 2100 levels, so these results show the response of natural ecosystems to the climate change.

6.5 Potential Effects of Carbon Dioxide Removal Methods and Solar Radiation Management on the Carbon Cycle

6.5.1 Introduction to Carbon Dioxide Removal Methods

To slow or perhaps reverse projected increases in the future atmospheric CO_2 concentrations (Section 6.4), several methods have been proposed to augment the removal of atmospheric CO_2 and enhance the storage of carbon in land, ocean and geological reservoirs. These methods have been categorized as ‘Carbon Dioxide

Removal (CDR)' methods and fall under a broad class of 'climate intervention' proposals. Another category of methods involves the intentional manipulation of planetary solar absorption to counter climate change, and is called the 'Solar Radiation Management (SRM)' (discussed in Chapter 7). In this Section, CDR methods are discussed from the point of view of their effects on carbon and other biogeochemical cycles, and a brief discussion on the indirect carbon cycle effects of SRM methods are also provided. Most of the currently proposed CDR methods are summarized in Table 6.15 and some are illustrated schematically in Chapter 7 (FAQ 7.3 Figure 2). Since a subset of these CDR methods concepts are designed for operating on large spatial scales in order to remove significant amounts of CO_2 from the atmosphere, these CDR methods could cause a large scale modification to the global climate and carbon cycle, and hence they are also called 'Geoengineering' proposals (Keith, 2001). Removal of non-CO_2 greenhouse gases such as CH_4 and N_2O has been also proposed to slow down climate change.

Table 6.15: Main examples of proposed CDR methods and their implications for carbon cycle and climate. The list is non-exhaustive. The 'Rebound' effect and thermal inertia of climate system are associated with all CDR methods.

Carbon Cycle Process to be Manipulated	CDR Method Name	Nature of CDR Removal Process	Storage Location	Storage Form	Some Carbon Cycle and Climate Implications
Enhanced biological production on land	Afforestation/reforestation[a] Improved forest management[b] Sequestration of wood in buildings[c] Biomass burial[d] No till agriculture[e] Biochar[f] Conservation agriculture[g] Fertilisation of land plants[h] Creation of wetlands[i] Biomass Energy with Carbon Capture and Storage (BECCS)[j]	Biological	[a]Land (biomass, soils) [b]Land (biomass, soils) [c]Land (urban) [d]Land/ocean floor [e]Land (soils) [f]Land (soils) [g]Land (soils) [h]Land (biomass, soils) [i]Land (wetland soils) [j]Ocean/geological formations	[a]Organic [b]Organic [c]Organic [d]Organic [e]Organic [f]Organic [g]Organic [h]Organic [i]Organic [j]Inorganic	[a,b,c,e,f,g,h,i] Lack of permanence, alters surface albedo and evapotranspiration Lack of permanence [d] Potentially permanent if buried on the ocean floor [j] Permanent if stored in geological reservoir
Enhanced biological production in ocean	Ocean iron fertilisation[k] Algae farming and burial[l] Blue carbon (mangrove, kelp farming)[m] Modifying ocean upwelling to bring nutrients from deep ocean to surface ocean[n]	Biological	Ocean	[k]Inorganic [l]Organic [m]Organic [n]Inorganic	[k]May lead to expanded regions with low oxygen concentration, altered production of DMS and non-CO_2 greenhouse gases, possible pH change and disruptions to marine ecosystems and regional carbon cycle [n]Disruptions to regional carbon cycle
Accelerated weathering	Enhanced weathering over land[o] Enhanced weathering over ocean[p]	Chemical	[o]Soils and oceans [p]Ocean	[o]Inorganic [p]Inorganic	[o]Permanent removal; likely to change pH of soils, rivers, and ocean [p]Permanent removal; likely to change pH of ocean
Enhanced solubility pump	Modifying ocean downwelling	Chemical	Ocean	Inorganic	Likely to alter regional carbon cycle and the thermal structure of the ocean
Others	Direct-air capture with storage	Chemical	Ocean/geological formations	Inorganic	Permanent removal if stored in geological reservoirs

Notes:
Superscripts in column 2 refer to the corresponding superscripts in column 4, 5 and 6.

By definition, in so-called carbon dioxide removal (CDR) methods, humans *remove* atmospheric CO_2 and store the amount of removed carbon it the land, ocean or geological reservoirs. Large scale industrial methods such as carbon capture and storage (CCS), biofuel energy production for substitution to fossil fuels (without CCS) and reducing emissions from deforestation and degradation (REDD) are not CDR methods

since they *reduce fossil fuel or land use change CO_2 emissions* to the atmosphere or provide alternatives to fossil fuels but they do not involve a net removal of CO_2 that is already in the atmosphere. However, direct air capture of CO_2 which uses industrial methods instead of natural carbon cycle processes (Table 6.15; and Chapter 7 FAQ 7.3 Figure 2) will remove CO_2 from the atmosphere and is considered as a CDR method, hence included in Table 6.15. According to the IPCC definition of mitigation, most CDR methods can be considered as climate change mitigation options.

Most CDR methods are believed to be relatively less risky in terms of unintended side effects on the climate system than are most solar radiation management (SRM) methods. This is because CDR methods remove atmospheric carbon dioxide, thus reducing the associated radiative forcing and climate warming. CDR methods also reduce direct consequences of high CO_2 levels including ocean acidification (see Section 6.4.4) whereas SRM methods are thought to have little impact on the consequences of high CO_2 levels (Matthews et al., 2009).The effects of CDR methods that propose to manipulate natural carbon cycle processes (see Table 6.15) are slow, due to the long time scales (centennial to millennial timescales) required for example to accumulate soil carbon, to transport CO_2 from surface waters to deep ocean or to remove CO_2 by weathering of silicate and carbonate rocks (see Box 6.2). Modeling studies (see Box 6.2) show that the climate system begins to respond with a <5-year relaxation (e-folding) time scale for an assumed instantaneous reduction in radiative forcing to preindustrial levels (Held et al., 2010) but the approach to climate equilibrium would takes many decades (MacMynowski et al., 2011). At present, there is no known CDR method, including industrial direct air capture of CO_2 that can feasibly reduce the atmospheric CO_2 to pre-industrial levels within a few decades. Therefore, CDR methods do not present an option for rapid mitigation of climate change. However, if implemented on large scales and for long enough, dypically during several consecutive decades, these methods could potentially make a contribution to slow-down or even decrease atmospheric CO_2 concentrations. The level of confidence of the quantitative effects of potential CDR methods on carbon and other biogeochemical cycles is based upon few model studies only, and can be assessed as low.

6.5.1.1 Permanence vs. Non Permanence of Carbon Sequestered by CDR Methods

Important scientific considerations for evaluating CDR methods from the point of view of carbon and other biogeochemical cycles include the associated carbon storage capacity, the permanence of the carbon storage and potential adverse side effects (Shepherd et al., 2009). Geological reservoirs could store several thousand PgC (House et al., 2006; Metz et al., 2005; Orr, 2009). For pulse CO_2 emissions of a few thousand PgC, 75–90% of the released CO_2 will end up in the oceans after about 10,000 years (see Box 6.2; Archer et al., 2009b). Hence, the ocean may be able to store a few thousand PgC of anthropogenic carbon in the long-term. The terrestrial biosphere may have the potential to store carbon equivalent to the cumulative historical land use flux of 180 ± 80 PgC (Table 6.1; Section 6.5.2.1).

CDR methods associated with either permanent or non-permanent carbon sequestration (see Table 6.15) have very different climate implications (Kirschbaum, 2003). Permanent sequestration methods have the potential to reduce the radiative forcing of CO_2 over time, and consequently to mitigate climate change. By contrast, non-permanent sequestration methods will release back the temporarily sequestered carbon as CO_2 to the atmosphere, thus increasing radiative forcing in the future, after some delayed time interval (Herzog et al., 2003). The interval of delayed time depends on the lifetime of stored carbon, and hence on the specific CDR method (Matthews, 2010; Shaffer, 2010). As a consequence, elevated levels of atmospheric CO_2 and climate warming will only be delayed and not avoided by non-permanent sequestration CDR methods (Figure 6.40). Nevertheless, CDR methods that could create a temporary CO_2 sink in terrestrial ecosystems (Table 6.15) may still have value (Dornburg and Marland, 2008) because they can decrease the cumulative impact of higher temperature. Temporary sinks allow to 'buy time', i.e., they mitigate climate change in the short term while allowing time for existing options to improve and/or new mitigation options to emerge in the long term.

[INSERT FIGURE 6.40 HERE]

Figure 6.40: Idealized model simulations (Matthews, 2010) to illustrate the effects of CDR methods associated respectively with either permanent or non-permanent carbon sequestration after $CO_2$is removed from the atmosphere. There is an emission of 1000 PgC in the reference case (black line) between 1800 and 2100. Permanent sequestration of the additional emitted CO_2 of 380 PgC, assuming no leakage of sequestered carbon, has the potential to reduce the radiative forcing of $CO_2$and to mitigate climate change (blue line, compared to black line). By contrast, the green line

shows an idealized case of a non permanent sequestration CDR method where, after CO_2 removal from the atmosphere, carbon will be sequestered in a non-permanent reservoir, in such a manner that all of the sequestered carbon will get returned as CO_2 back to the atmosphere over three centuries. In this non-permanent sequestration case, climate change would only be only delayed whereas the eventual magnitude of climate change will be equivalent to the no-sequestration case (green line, compared to black). Figure adapted from Figure 5 of Matthews (2010).

Depending on the details of the specific CDR method considered, carbon stored in the terrestrial biosphere or in the ocean is susceptible to be released back as CO_2 to the atmosphere during the time in the future when fossil fuel will continue to be used, although some forms of storage may last for several centuries. In contrast, carefully selected geological storage places are less subject to future human actions and interference with the ecological processes (Caldeira et al., 2005). Carbon stored in the ocean in conjunction with alkaline minerals also appears to be close to permanent on centennial timescales (Caldeira et al., 2005; Caldeira and Rau, 2000; Kheshgi, 1995). Furthermore, for many of the CDR methods listed in Table 6.15, long-term storage effectiveness could be affected by feedbacks involving climate and carbon cycle processes. Hence, any CDR related sink permanence or non-permanence issues should be considered in the context of climate change, of changes in nitrogen, phosphorus availability (see Section 6.4.6) and in atmospheric CO_2, of changes in and in land use (see Section 6.4.1), and not only in the context of present-day conditions.

6.5.1.2 The Rebound Effect

In addition to permanence vs. non permanence of sequestration from CDR methods, another important scientific consideration for CDR methods is the so called 'rebound effect'. In the Industrial Era (since 1750) about half of the CO_2 emitted into the atmosphere from fossil fuel emissions has been so far taken up and sequestered by land and ocean carbon reservoirs (see Section 6.3 and Table 6.1). As for CO_2 emissions and the consequent CO_2 rise which are *opposed* by natural reservoirs, any removal of CO_2 from the atmosphere by CDR will be also *opposed* by natural reservoirs. Therefore, if CO_2 is removed from the atmosphere, the subsequent inherent rate of removal of CO_2 from the atmosphere by natural carbon reservoirs on land and ocean will be reduced or could be even reversed. Simple models have shown that when carbon is removed from the atmosphere and stored permanently, the reduction in the atmospheric carbon is less than 50% of the sequestered carbon (Kirschbaum, 2003).A recent climate-carbon modelling study (Cao and Caldeira, 2010b) has shown the re-release of carbon from the land and ocean and the consequent increase in atmospheric CO_2 after an idealized complete instantaneous removal of all CO_2 in excess to pre-industrial period, i.e., the opposite model simulation to the CO_2 pulse addition described in Box 6.2. Ultimately, returning to pre-industrial CO_2 levels would require permanently sequestering an amount of carbon equal to total anthropogenic CO_2 emissions that have been released before the time of CDR (Cao and Caldeira, 2010b; Lenton and Vaughan, 2009; Matthews, 2010). Therefore, if the goal of CDR would be to return and maintain atmospheric CO_2 near pre-industrial concentrations, not only will anthropogenic CO_2 in the atmosphere need to be removed, but anthropogenic CO_2 currently stored in ocean and land carbon reservoirs will also need to be removed when it will eventually outgas to the atmosphere (Figure 6.41).

[INSERT FIGURE 6.41 HERE]

Figure 6.41: Idealized simulations with a simple global carbon cycle model (Cao and Caldeira, 2010b) to illustrate the 'rebound effect'. Effects of an instantaneous cessation of CO_2 emissions (amber line), one-time removal of excess atmospheric CO_2 (blue line) and removal of excess atmospheric CO_2 followed by continued removal of CO_2 that degasses from the atmosphere and ocean (green line). To a first approximation, a cessation of emissions prevents further warming but does not lead to significant cooling on the century time scale. A one-time removal of excess atmospheric CO_2 eliminates approximately half of the warming experienced at the time of the removal. To cool the planet back to pre-industrial levels would require the removal of all previously emitted CO_2, i.e., an amount equivalent to approximately twice the amount of excess CO_2 in the atmosphere above pre-industrial level. Simulations were started in 1800 but results are shown from 1850. Figure adapted from Cao and Caldeira (2010b).

6.5.2 Carbon Cycle Processes Involved in CDR Methods

The CDR methods listed in Table 6.15 rely primarily on human caused 'improvement' of natural carbon cycle processes to accelerate the removal of atmospheric CO_2: (1) enhanced net biological uptake and subsequent sequestration by land ecosystems, (2) enhanced biological production in ocean and subsequent sequestration by the ocean, (3) accelerated chemical weathering reactions over land and ocean and (4) enhanced solubility pump (see Sections 6.1.1.1 for a definition of this process) in the ocean. The exception is

industrial direct air capture of CO_2, which relies on chemistry-based methods to remove CO_2 directly from air. The CO_2 removed from atmosphere by CDR methods would be stored in organic form on land, against inorganic form in ocean and geological reservoirs (Table 6.15). The principle of these various CDR methods is briefly described below and the characteristics of some CDR methods with peer-reviewed literature are summarized in Table 6.16.

[INSERT TABLE 6.16 HERE]

Table 6.16: Characteristics of some CDR methods which have peer-reviewed literature. It should be noted that a variety of economic, environmental, and other constraints could also limit deployment.

6.5.2.1 Enhanced Net Biological Uptake of CO_2 and Carbon Sequestration by Land Ecosystems

The key driver in these CDR methods (Table 6.15) is the net primary productivity by terrestrial plants which produces biomass at a rate of approximately 50–60 PgC yr^{-1} (Nemani et al., 2003). The common strategy of many of these CDR methods is to increase net primary productivity and/or store a fraction of the biomass produced under the form of wood in forests, or organic matter in soils or elsewhere (e.g., afforestation/reforestation, biochar, biomass burial, sequestration of construction wood in buildings) or the use of biomass for energy production and subsequent sequestration of emitted CO_2 (BECCS).

Estimates of the global potential for enhanced primary productivity over land and for specific methods are uncertain because the achievable sequestration by any specific method is severely constrained by competing land needs (e.g., agriculture, biofuels, urbanization and conservation) and sociocultural considerations. A first approximation of the potential of afforestation/reforestation is the cumulative historical (1750–2011) deforestation flux from forest conversion to cropland and pasturelands which is estimated as 180 ± 80 PgC (Table 6.1; Section 6.3.2.2; Canadell and Raupach, 2008; DeFries et al., 1999; Houghton, 2008). However, House et al., (2002), using a simple global carbon cycle model estimated that the atmospheric CO_2 concentration by 2100 would be less by only about 40–70 (~80–140 PgC) ppm if all of the carbon released by land use changes could be restored to the terrestrial biosphere.

The capacity for enhancing the soil carbon content on agricultural and degraded lands was estimated by one study at 50–60% of the historical soil carbon loss of 42–78 PgC (Lal, 2004a). The sequestration of carbon in soil will saturate as the soil carbon storage potential is realized. Recent estimates suggest a cumulative potential of 30–60 PgC of additional storage over 25–50 years (Lal, 2004b). Soil carbon sequestration is clearly a non-permanent CDR method, since the sequestered carbon can be lost quickly with a change in soil and agricultural management.

Finally, there is little peer-reviewed literature for CDR methods such as biochar and biomass burial methods whose principle is to store organic carbon into very long turnover time pools of terrestrial ecosystems, since none of these methods is implemented today at large scale. The maximum sustainable technical potential of biochar cumulative sequestration is estimated at 130 PgC over a century by one study (Woolf et al., 2010). The residence time of carbon converted to biochar in soils, and the effect on soil productivity of adding large loadings of char is uncertain and further research is required to assess the potential of this CDR method (Shepherd et al., 2009).

6.5.2.2 Enhanced Biological Production in the Ocean

Ocean fertilization, algae farming and enhanced storage in coastal plants are CDR methods that rely primarily on enhanced primary productivity in the ocean. The carbon cycle principle here is to enhance primary productivity of phytoplankton (the marine biological pump; Section 6.1.1) so that a fraction of the extra organic carbon produced by plankton is transported to the deep ocean where another fraction could be sequestered. Some of the inorganic carbon in the surface layers of ocean that is removed by the export of net primary productivity below the surface layer can be subsequently replaced by CO_2 pumped from the atmosphere. Ocean primary productivity is limited by the supply of nutrients. The principle behind enhanced biological production in ocean CDR methods in Table 6.15 is to add nutrients that are otherwise limiting (e.g., iron, nitrogen and phosphate) to the surface ocean to stimulate productivity and thereby pump atmospheric CO_2 into the ocean. The expected result is an increase in the downward flux of carbon exported

below the surface layer (Martin, 1990), that can be partly sequestered as Dissolved Inorganic Carbon after mineraization in the intermediate and deep waters. In other CDR methods like algae and kelp farming and burial, the organic carbon would be rather stored in organic form.

Ocean-fertilisation by added iron has been tested in more than a dozen experiments (Boyd et al., 2007) on small spatial scales (~10 km^2 scale). These experiments demonstrated only limited transient effects in removing atmospheric CO_2: the addition of iron effectively led to increased productivity (phytoplankton blooms), but this effect was moderated either by other limiting elements, or by compensatory respiration from increased zooplankton grazing. There are some indications that sustained natural iron fertilization may have a higher efficiency in exporting carbon from surface to intermediate and deep ocean (Pollard et al., 2009). The effectiveness of ocean fertilization by iron addition depends both on the amount of increased productivity in the ocean surface layers and on the ultimate fate of this carbon. Most of the carbon that produced by primary productivity in the surface layers is oxidized (rematerialized into DIC) in the same layer, and only a small fraction is ultimately exported to the intermediate and deep layers (Lampitt et al., 2008). Increases in carbon export below the surface layer were measured in one experiment in the Southern Ocean, but the amount of increased export of carbon was small relative to both natural phytoplankton blooms occurring in that area, and to the scale of anthropogenic carbon dioxide emissions (Buesseler et al., 2004).

Global or regional ocean carbon cycle model studies have assessed the potential carbon sink that could be generated by widespread iron fertilization as a CDR method (Aumont and Bopp, 2006b; Jin et al., 2008; Zeebe and Archer, 2005). Maximum potential drawdown of atmospheric CO_2 have been estimated from 15 ppm (Zeebe and Archer, 2005) to 33 ppm (Aumont and Bopp, 2006b) for a high-end future CO_2 concentration level of 700–800 ppm in 2100. In idealized model-based studies of ocean fertilization in global ocean or only the Southern Ocean (Cao and Caldeira, 2010a; Joos et al., 1991; Peng and Broecker, 1991; Watson et al., 1994), the maximum potential atmospheric CO_2 reduction was estimated at less than 100 ppm for ideal conditions. Jin and Gruber (2003) obtained an atmospheric drawdown of more than 60 ppm over 100 years in modeling an idealized iron fertilization over the entire Southern Ocean.

Biological production in the surface water could also be enhanced if the supply of nutrients to surface layers could be artificially increased in upwelling areas (Karl and Letelier, 2008; Lovelock and Rapley, 2007). The amount of carbon sequestered by CDR methods that rely on enhanced upwelling depends critically on the location and may well be negative (Yool et al., 2009). Human induced increased upwellings, under most optimistic assumptions, has been estimated by models to sequester atmospheric CO_2 at a rate of about 0.9 PgC yr^{-1}(Oschlies et al., 2010b) but under realistic conditions, this rate could be an order of magnitude lower or even negative.

6.5.2.3 Accelerated Weathering

The removal of CO_2 involving the weathering or dissolution of silicate and carbonate minerals (Archer et al., 2009b; Berner et al., 1983) occurs on time scales from thousands to tens of thousands of years (see Box 6.2). The weathering reactions take place at a rate that is very slow and small relative to the rate at which fossil fuel CO_2 is being emitted. Natural chemical weathering of minerals consumes about 0.2 $PgCyr^{-1}$of CO_2 from the atmosphere (Figure 6.1; Gaillardet et al., 1999; Hartmann et al., 2009). Carbonate mineral weathering fluxes are small and over a time scale of thousands of years, transfers CO_2 from the atmosphere to the ocean. Silicate mineral weathering operates on a time scale of hundreds of thousands of years. It is silicate-weathering time scale that ultimately governs the removal of excess CO_2 from Earth's surface carbon reservoirs (Archer et al., 2009b; Berner et al., 1983; see Box 6.2).

Fossil fuel CO_2 released to the atmosphere leads to chemical disequilibrium in the ocean, and geochemical equilibrium will be eventually reset by the dissolution of ocean carbonate sediments (Archer et al., 1997). The principle of CDR methods based upon accelerated weathering is to dissolve the carbonate mineral in advance so the approach to the geochemical equilibrium can be accelerated. It has been proposed that large amounts of silicate minerals such as olivine ($(Mg,Fe)_2SiO_4$) could be mined, crushed, transported to, and distributed on agricultural land, with the intent that atmospheric CO_2 will react with olivine and be immobilized partly as carbonate minerals and partly as bicarbonate ions in solution which would be transported to the ocean (Schuiling and Krijgsman, 2006). Alternatively, the weathering reaction rate might

be enhanced by exposing minerals such as basalt or olivine to elevated CO_2 levels (Kelemen and Matter, 2008). In these land-based enhanced weathering CDR methods, some carbon would be stored in soils and the remaining would be transported to the ocean by rivers. A recent study using a model estimated a potential removal rate of up to 1 PgC yr^{-1} from the atmosphere, in the idealized case where olivine could be distributed as fine powder over land areas of the humid tropics, but the removal rate will be limited by the saturation concentration of silicic acid (Köhler et al., 2010), and the feasibility of applying such a CDR method approach at this scale has not been assessed.

In ocean based increased weathering CDR methods, carbonate rocks could be crushed and reacted with CO_2 captured at power plants to produce bicarbonate solution which would be released to the ocean (Caldeira and Rau, 2000; Rau, 2008; Rau and Caldeira, 1999). Alternatively, carbonate minerals could be directly released into the ocean (Harvey, 2008; Kheshgi, 1995). It has also been proposed that strong bases, derived from silicate rocks, could be released to ocean (House et al., 2007), which would cause the ocean to absorb additional CO_2. Carbonate minerals such as limestone could be heated to produce lime ($Ca(OH)_2$); this lime could be added to the ocean to increase the ocean's alkalinity and thereby promote ocean uptake of atmospheric CO_2 (Kheshgi, 1995). While there is sufficient level of scientific understanding of the weathering processes, uncertainties are large in assessments of feasibility and effectiveness.

6.5.2.4 Enhanced Solubility Pump

It has been proposed that increasing artificially the overturning circulation of the ocean will cause increased transport of DIC from the surface ocean to the deep ocean in high latitudes (Zhou and Flynn, 2005) and this remove CO_2 from the atmosphere. This proposal is motivated by the fact that most of the carbon in the deep sea is transported there by the overturning circulation (the 'solubility pump') and not by the 'marine biological pump' pump (see Section 6.1.1; Sarmiento and Gruber, 2006; Volk and Hoffert, 1985). Therefore, the principle of 'enhanced solubility pump' CDR methods listed in Table 6.15 is to increase the rate of downwelling in high latitudes. In this process, carbon would be stored in the deep ocean in inorganic form (DIC). However, deep ocean waters typically have higher concentrations of DIC than do surface waters (Sarmiento and Gruber, 2006; Volk and Hoffert, 1985), thus such proposals risk transporting carbon from the deep ocean to the atmosphere. Realistic enhancement of downwelling by 1 million m^3 s^{-1} (one Sverdrup (Sv)) is estimated to increase ocean uptake of carbon by only ~0.01–0.02 PgC yr^{-1}(Zhou and Flynn, 2005). The proposed enhancement in downwelling of one Sv is much smaller than the projected slowdown in Atlantic meridional overturning circulation of up to 5 to 10 Sv by 2100 because of climate change (Meehl et al., 2007). The overall level of scientific knowledge on the effectiveness and feasibility of this CDR method is low and uncertainties are very large.

6.5.2.5 Other CDR Methods

6.5.2.5.1 Direct air capture

Direct Air Capture (DAC) refers to the chemical process by which a pure CO_2 stream is produced by capturing CO_2 from the ambient air. The captured CO_2 would be transported and used for commercial purposes such as manufacturing carbonated drinks or sequestered in inorganic form in geological reservoirs or the deep ocean. At least three methods have been proposed to capture CO_2 from the atmosphere: (1) adsorption on solids (Gray et al., 2008; Lackner, 2009; Lackner, 2010); (2) absorption into highly alkaline solutions (Mahmoudkhani and Keith, 2009; Stolaroff et al., 2008); (3) absorption into moderate alkaline solution with a catalyst (Bao and Trachtenberg, 2006). The main scientific limitation to DAC is the thermodynamic barrier due to the lower concentration of CO_2 in air (CO_2 content of the air is only about 0.039%) and hence there is large uncertainty on the effectiveness of this method.

6.5.3. Impacts of CDR Methods on Carbon Cycle and Climate

One impact that is common to all CDR methods is related to the thermal inertia of the climate system. Many components of the Earth System will continue to respond for decades or centuries to the original increases in CO_2 even after CDR is applied (see Section 6.4.9). Therefore, these components of the Earth System will lag CDR-induced decreases in atmospheric CO_2 concentrations and surface temperature (Boucher et al., 2012). Modelling the impacts of CDR method on the climate system is still in its infancy. Some of the first modelling studies (Cao et al., 2011; Wu et al., 2010) have shown that there could be a temporary

intensification of the global hydrological cycle in response to a reduction in atmospheric CO_2 concentrations (Figure 6.42). Another effect that is common to all CDR methods is the potential 'loss of CO_2 fertilization' (see Box 6.3) induced by lower CO_2 levels, that could decrease the terrestrial and the ocean CO_2 sink.

[INSERT FIGURE 6.42 HERE]

Figure 6.42: HadCM3L results from an idealized simulation (Cao et al., 2011) with 2% annual change in atmospheric CO_2: (a) global and annual mean changes in precipitation as a function of atmospheric CO_2; (b) global and annual mean changes in precipitation as a function of global and annual mean changes in surface temperature. Red dots represent the first 70-year simulation phase with 2% annual CO_2 increase (ramp_up) and time moves forward from the lower left to the upper right. Blue dots represent the subsequent 70-year period with 2% annual CO_2 decrease (ramp_down) and time moves forward from the upper right to the lower left. Black dots represent the following 150-years with the constant control CO_2 concentration and time moves forward from the upper right to the lower left. The simulation states when atmospheric CO_2 reaches $1 \times CO_2$ and $4 \times CO_2$ concentrations are marked with pink circles. Due to the ocean thermal inertia one atmospheric CO_2 state corresponds to two different states of temperature and precipitation, and due to the precipitation sensitivity to atmospheric CO_2 content changes (Bala et al., 2009), one temperature state corresponds to two different precipitation states. Figure adopted from Cao et al. (2011).

6.5.3.1 Enhanced Net Biological Uptake by Land

CDR methods aiming at increasing biomass in forests are non permanent and carry the risk that stored carbon may return to the atmosphere by disturbances such as fire and insect outbreaks, exacerbated by climate extremes and climate change, or by future human induced deforestation. When considering afforestation/reforestation, it is also important to account for biophysical effects on climate in addition to carbon sequestration because afforestation/reforestation changes surface characteristic such as albedo, evapotranspiration and surface roughness (Bernier et al., 2011; Bonan, 2008). Modeling studies have shown that afforestation in seasonally snow covered boreal and temperate regions is likely to decrease the land surface albedo and have a net (biophysical plus biogeochemical) warming effect, whereas afforestation in low latitudes (Tropics) is likely to enhance latent heat flux from evapotranspiration and have a net cooling effect (Bala et al., 2007; Bathiany et al., 2010; Betts, 2000; Bonan et al., 1992; Montenegro et al., 2009). Consequently, the location of biomass enhancement CDR methods needs to be considered carefully when evaluating their net effects on climate (Bala et al., 2007; Lee et al., 2011). For instance, in idealized coupled climate carbon model experiments, Bala et al., (2007) showed that global land mean temperature would increases by 0.9 K for tropical deforestation but decreases by 0.2 and 1.4 K for mid- and high-latitude deforestation, respectively. This result is confirmed in a recent study which estimated the warming reductions per unit afforested area as three times higher in the tropics than in the boreal and northern temperate regions, suggesting that afforestation in the tropics are effective forest management strategies from a climate perspective (Arora and Montenegro, 2011). However, many of these studies examine average conditions in a region, ignoring some of the local conditions that may produce results of opposite sign. For example, reforestation in boreal regions may produce a net cooling effect because land that was actually converted tended to be less snow-covered and have higher carbon stocks than average land in this region (Pongratz et al., 2011b). CDR methods to increase forest biomass may require production of nutrients (fertilizers) which is likely to be associated with negative consequences such as indirect CO_2 emission from industrial fertilizer production and excess nitrogen runoff. Regarding biochar, there are some indications that biochar addition could promote rapid loss of forest humus and background carbon in some ecosystems in the first decade of application (Wardle et al., 2008).

6.5.3.2 Enhanced Biological Production in the Ocean

In the case of ocean fertilization, the utilization of macronutrients such as nitrogen and phosphate in the fertilized region could lead to a decrease in production 'downstream' of the fertilized region (Gnanadesikan and Marinov, 2008; Gnanadesikan et al., 2003; Watson et al., 2008). This effect can occur, for example, if nutrients such as nitrogen and phosphate are depleted in the fertilized region. In a worst case scenario, (Gnanadesikan et al., 2003) simulated a decline in export production of 30 tons of carbon for every ton removed from the atmosphere. A sustained global-ocean iron fertilization for IPCC A2 CO_2 emission scenario was also found to acidify the deep ocean by storing more DIC there (pH decrease of about 0.1–0.2 units) while mitigating the surface pH change by only 0.06 units (Cao and Caldeira, 2010a). Other environmental risks associated with ocean fertilization include expanded regions with low oxygen concentration (Oschlies et al., 2010a), increased production of dimethyl sulphide (DMS), Isoprene, CO, N_2O,

CH_4 and other non-CO_2 greenhouse gases (Jin and Gruber, 2003; Oschlies et al., 2010a) and possible disruptions to marine ecosystems (Denman, 2008).

In the case of CDR methods relying on increased ocean upwelling to bring nutrients from deep ocean to the surface ocean (or downwelling as discussed in Section 6.5.2.4), there could be disturbance to the regional carbon balances, since the upwelling (downwelling) must be balanced by downwelling (upwelling) at another location. Along with growth-supporting nutrients, enhanced concentrations of DIC are also brought to surface waters which could degas to the atmosphere and partially offset carbon sequestration. Further, whenever artificial upwelling is stopped, atmospheric CO_2 concentrations could rise rapidly because carbon removed from the atmosphere and stored in soils could be suddenly released (Oschlies et al., 2010b). The overall level of scientific knowledge on the impacts of the enhanced upwelling or downwelling is low.

6.5.3.3 Enhanced Weathering

The pH and carbonate mineral saturation of soils, rivers and ocean surface waters would be raised by enhanced terrestrial weathering, which could alleviate some of the ocean acidification trend. In a modelling study, Köhler et al. (2010) showed that the pH of the Amazon river would rise to 8.7 from its current mean value of 6.2 if dissolution of olivine in entire Amazon basin was used to remove 0.5 PgC yr^{-1} from the atmosphere. In the marine environment, the elevated pH and increased alkalinity could potentially counteract the effects of ocean acidification, which is beneficial. Change in alkalinity could also disturb existing ecosystems. There is uncertainty in our understanding of the net effect on ocean CO_2 uptake but most likely there will be a partial offset of the abiotic effect by calcifying species. As for other CDR methods, the overall level of scientific knowledge on the impacts of accelerated weathering is low.

6.5.4 Impacts of Solar Radiation Management on Carbon Cycle

Solar radiation management (SRM) methods aim to reduce the amount of incoming solar radiation to the Earth's surface (Chapter 7). Balancing reduced outgoing radiation by reduced incoming radiation may be able to counter global mean temperature changes but may lead to a less intense global hydrological cycle (Bala et al., 2008) and may not completely cancel regional changes in temperature and precipitation (Govindasamy et al., 2003; Irvine et al., 2010; Matthews and Caldeira, 2007; Ricke et al., 2010) or may create new ones (Robock et al., 2008). Therefore, effects of climate change on the carbon and other biogeochemical cycles budgets may not be mitigated by SRM methods.

Whilst SRM techniques may avoid climate warming, they do not interfere with the direct biogeochemical effects of CO_2 on ocean and land carbon cycle processes. For example, ocean acidification caused by elevated CO_2 (Section 6.4.5) is not prevented by SRM. On land, enhanced vegetation productivity associated with elevated CO_2 (see Box 6.3) is affected only marginally by SRM (Govindasamy et al., 2002; Matthews and Caldeira, 2007; Naik et al., 2003). Similarly, SRM should not alter the stomatal response of plants to elevated CO_2 that leads to a decline in evapotranspiration, causing land temperatures to warm and runoff to increase (Betts et al., 2007; Cao et al., 2010; Gedney et al., 2006; Piao et al., 2007).

However, due to the strong coupling between climate and the carbon cycle, SRM could indirectly affect the carbon cycle. In a coupled climate-carbon model, Matthews and Caldeira (2007) showed that carbon uptake by land and ocean increased in response to SRM because there is a direct CO_2-driven increase in carbon uptake without an offsetting temperature-driven suppression of carbon sinks. Consequently, for the SRES A2 scenario with SRM geoengineering, they simulated a lower CO_2 concentration of 110 ppm in year 2100 relative to the case without SRM. Further, land carbon sinks may be additionally enhanced by increasing the amount of diffuse relative to direct radiation (Mercado et al., 2009) in case SRM is accompanied by an increased fraction of diffuse light (e.g., injection of aerosols into the stratosphere). However, a parallel reduction in the direct component of radiation available for plans by SRM methods could decrease terrestrial CO_2 sinks. Information is lacking to ascertain whether the net effect of changes in diffuse versus direct radiation on the carbon cycle would enhance or reduce the terrestrial carbon sink. Further, SRM may negatively affect the efficiency of the southern ocean sink, for example, by altering the winds in the Southern Ocean, although the magnitude or duration of this effect is uncertain (Vaughan and Lenton, 2011).

[START FAQ 6.1 HERE]

FAQ 6.1: What Happens to Carbon Dioxide After it is Emitted into the Atmosphere?

First, the emitted excess CO_2 is rapidly distributed between atmosphere, the upper ocean and vegetation. Then, the carbon further circulates among the different reservoirs of the global carbon cycle—such as soils, the deeper ocean, and rocks—on a multitude of time scales. Depending on the amount of CO_2 released, between 15% and 40% will remain in the atmosphere for up to 2000 years, after which a new balance is established between the atmosphere, the land biosphere and the ocean. Geological processes will take anything from tens to hundreds of thousand of years—perhaps longer—to reduce that carbon further. Enhanced atmospheric CO_2, and associated climate impacts of present emissions, will, therefore, persist for a very long time into the future.

Carbon dioxide is a largely non-reactive gas, which is rapidly mixed throughout the entire troposphere in less than a year. Unlike chemical compounds in the atmosphere such as methane, which are removed and broken down by sink processes, carbon is instead redistributed among the different reservoirs of the global carbon cycle. FAQ 6.1, Figure 1 shows a simplified diagram of the global carbon cycle. The open arrows indicate typical timeframes for carbon atoms to be transferred through the different reservoirs, and recycled back into the atmosphere.

[INSERT FAQ 6.1, FIGURE 1 HERE]

FAQ 6.1, Figure 1: Simplified schematic of the global carbon cycle showing the typical turnover time scales for carbon transfers through the major reservoirs.

Before the industrial era, the global carbon cycle was roughly balanced: carbon inflows closely matched the outflows of each carbon pool. Anthropogenic emissions of carbon dioxide into the atmosphere, however, disturbed that equilibrium. As global CO_2 concentrations rise, the exchange processes between CO_2 and the surface ocean and vegetation are altered, as are subsequent exchanges within and among further carbon reservoirs on land, in the ocean and eventually, the earth crust. In this way, the excess carbon is redistributed within the global carbon cycle, until the exchange fluxes between the different carbon pools have reached a new, approximate balance.

Over the ocean, CO_2 molecules pass through the air-sea interface by gas exchange. In sea water, CO_2 reacts with water to form carbonic acid, which exchanges very quickly with the large pool of dissolved inorganic carbon—bi-carbonate and carbonate ions—in the ocean. Currents and mixing processes transport the carbon between the surface layer and the middle depths of the ocean. The marine biota also redistributes carbon: marine organisms grow organic tissue and calcareous shells in surface waters, which, after their death, sink to deeper waters, where they are returned to the dissolved inorganic carbon pool by dissolution and microbial decomposition. A small fraction reach the sea floor, and are incorporated into the sediments. The extra carbon from anthropogenic emissions has the effect of increasing the atmospheric partial pressure of CO_2, which in turn increases the air-to-sea flux of CO_2 molecules. In the surface ocean, the carbonate chemistry quickly accommodates that extra CO_2. As a result, shallow surface ocean waters reach quickly balance with the atmosphere—within one or two years. Further circulation takes longer—between decades and many centuries—as CO_2 is transported from the surface into middle depths and deeper waters by ocean circulation and ventilation. On still longer time scales, acidification by the invading CO_2 dissolves carbonate sediments on the sea floor, which further enhances ocean uptake. However, it is believed that, unless substantial ocean circulation changes occur, plankton biomass remains roughly unchanged, since plankton growth is limited mostly by environmental factors, such as nutrients and light, and not by the abundant inorganic carbon. Therefore, it does not contribute to the ocean uptake of CO_2.

On land, vegetation absorbs CO_2 by photosynthesis and converts it into organic matter. A fraction of this carbon is immediately returned to the atmosphere as CO_2 by plant respiration. Plants use the remainder for growth. Dead plant material is incorporated into soils, eventually to be decomposed by microorganisms, then respired back into the atmosphere as CO_2. In addition, carbon in vegetation and soils is also converted back into CO_2 by disturbance processes such as fires, insects, herbivores and harvesting. Some organic carbon is also transferred through freshwater bodies into the ocean. An increase in atmospheric CO_2 stimulates photosynthesis, and thus carbon uptake. This in turn increases the biomass in vegetation and soils and so

fosters a carbon sink on land. The magnitude of this sink, however, also depends critically on other factors, such as water and nutrient availability.

Modeling indicates that, overall, the warmer the climate, the less carbon is taken up by the ocean and land. This implies that atmospheric CO_2 levels will increase, constituting a positive climate feedback on the global carbon cycle. Many different factors contribute to this effect: warmer seawater, for instance, has a lower CO_2 solubility, so altered chemical carbon reactions result in less oceanic uptake of excess atmospheric CO_2. On land, higher temperatures foster longer seasonal growth periods in temperate and higher latitudes, but also faster respiration of soil carbon.

The time it takes to reach a new carbon distribution balance depends on the transfer times of carbon through the different reservoirs, and takes place over a multitude of time scales. Carbon is first exchanged among the 'fast' carbon reservoirs, such as the atmosphere, oceans, land vegetation and soils, over time scales up to a few thousand years. Over longer time scales, very slow secondary geological processes—dissolution of carbonate sediments and sediment burial into the earth crust—become important.

FAQ 6.1, Figure 2 illustrates the decay of an excess amount of CO_2 initially emitted into the atmosphere, and how it is redistributed among land and the ocean over time. Because of ocean chemistry the size of the initial input is important: higher emissions imply that a larger fraction of CO_2 will remain in the atmosphere. After 2000 years, the atmosphere will still contain between 15% and 40% of those initial CO_2 emissions. A further reduction by carbonate sediment dissolution, and reactions with igneous rocks, such as silicate weathering and sediment burial, will take anything from tens to hundreds of thousands of years, or even longer.

[INSERT FAQ 6.1, FIGURE 2 HERE]

FAQ 6.1, Figure 2: Decay of a CO_2 excess amount of 5000 PgC emitted at time zero into the atmosphere, and its subsequent redistribution into land and ocean as a function of time, computed by coupled carbon–cycle climate models. The size of the colour bands indicate the carbon uptake by the respective reservoir. The first two panels show the multi-model mean from a model intercomparison project (Joos et al., submitted). The last panel shows the longer term redistribution including ocean dissolution of carbonaceous sediments as computed by the CLIMBER-2 model (after Archer et al, 2009b).

[END FAQ 6.1 HERE]

[START FAQ 6.2 HERE]

FAQ 6.2: Could Rapid Release of Methane and Carbon Dioxide from Thawing Permafrost or Ocean Warming Substantially Increase Warming?

Permafrost is permanently frozen ground, mainly found in the high latitudes of the Arctic. Permafrost, including the sub-sea permafrost on the shallow shelves of the Arctic Ocean, contains old organic carbon deposits. Some are relicts from the last glaciation, and hold at least twice the amount of carbon currently present in the atmosphere as carbon dioxide. Should a sizeable fraction of this carbon be released as methane and carbon dioxide, it would increase atmospheric concentrations, which would lead to higher atmospheric temperatures. That in turn would cause yet more methane and carbon dioxide to be released, creating a positive feedback which would further amplify global warming.

The Arctic domain presently represents a net sink of carbon dioxide—sequestering around 0.4 ± 0.4 PgCyr^{-1} in growing vegetation—and a modest source of methane: between 15 and 50 Tg(CH_4) yr^{-1}), mostly from seasonally unfrozen wetlands. There is no evidence yet that thawing contributes significantly to the current global budgets of these two greenhouse gases. However, under sustained Arctic warming, modelling studies and expert judgments indicate with medium agreement that a potential combined release of up to 200 PgC as carbon dioxide equivalent could occur until the year 2100.

[INSERT FAQ 6.2, FIGURE 1 HERE]

FAQ 6.2, Figure 1: A simplified graph of current major carbon pools and flows in the Arctic domain, including permafrost on land, continental shelves and ocean (adapted from McGuire et al. (2009) and Tarnocai et al. (2009)). TgC = 10^{12} gC, and PgC = 10^{15} gC.

Permafrost soils on land, and in ocean shelves, contain large pools of organic carbon, which must be thawed and decomposed by microbes before it can be released—mostly as carbon dioxide. Where oxygen is limited, as in waterlogged soils, some microbes also produce methane, which can escape to the atmosphere.

On land, permafrost is overlain by a surface 'active layer', which thaws during summer and forms part of the tundra ecosystem. When warming spring and summer air temperatures thaw that active layer, it thickens, making more organic carbon available for microbial decomposition. However, during summer, growing Arctic vegetation increases its carbon dioxide uptake through photosynthesis. That means the net Arctic carbon balance is delicate one between enhanced uptake and enhanced release of carbon.

Hydrological conditions during the summer thaw are also important. In standing water, lack of oxygen will induce methane production. The complexity of Arctic landscapes under climate warming means we have low confidence around which of these different processes might dominate on a regional scale. Heat diffusion and permafrost melting takes time—in fact, the deeper Arctic permafrost can be seen as a relict of the last glaciation, which is still slowly eroding—so any significant loss of permafrost soil carbon will happen over similarly long time scales.

Given enough oxygen, mineralisation of organic soil carbon is accompanied by the release of heat by microbes (similar to compost), which, during summer, might stimulate further permafrost thaw. Depending on the amount of carbon and ice content of the permafrost, and the hydrological regime, this mechanism could, under warming, trigger relatively fast local permafrost degradation.

Modelling studies of permafrost dynamics and greenhouse gas emissions indicate a relatively slow positive feedback, on time scales of hundreds of years. Until the year 2100, up to 100 PgC could be released as carbon dioxide, and up to five Pg as methane. Given methane's stronger greenhouse warming potential, that corresponds to a further 100 PgC of equivalent carbon dioxide. These amounts are similar in magnitude to other biogeochemical feedbacks, e.g., the additional carbon dioxide released by the global warming of terrestrial soils.

Methane hydrates are another form of frozen carbon, occurring in deep permafrost soils, ocean shelves, shelf slopes and deeper ocean bottom sediments. They consist of methane and water molecule clusters, which are only stable in a specific window of low temperatures and high pressures. On land and in the ocean, most of these hydrates originate from marine or terrestrial biogenic carbon, decomposed in the absence of oxygen and trapped in an aquatic environment under suitable temperature-pressure conditions.

Any warming of permafrost soils, ocean waters and sediments and/or changes in pressure could destabilise those hydrates, releasing their methane to the ocean. During larger, more sporadic releases, a fraction of that methane might also be outgassed to the atmosphere. There is a large pool of these hydrates: in the Arctic alone, the amount of methane stored as hydrates could be more than 10 times greater than the methane presently in the global atmosphere.

Like permafrost thawing, liberating hydrates on land is a slow process, taking decades to centuries. The deeper ocean regions and bottom sediments will take still longer—between centuries and millennia to warm enough to destabilise the hydrates within them. Furthermore, methane released in deeper waters has to reach the surface and atmosphere before it can become climatically active, but most is expected to be consumed by microorganisms before it gets there. Only the methane from hydrates in shallow shelves, such as in the Arctic Ocean north of Eastern Siberia, may actually reach the atmosphere to have a climate impact.

Several recent studies have documented locally significant methane emissions over the Arctic Siberian shelf and from Siberian lakes. How much of this methane originates from decomposing organic carbon or from destabilizing hydrates is not known. There is also no evidence available to determine whether these sources have been stimulated by recent regional warming, or whether they have always existed—it may be possible that these methane seepages have been present since the last deglaciation. In any event, these sources make a very small contribution to the global methane budget—less than 5%. This is also confirmed by atmospheric methane concentration observations, which do not show any substantial increases over the Arctic.

However modelling studies and expert judgment indicate that methane and carbon dioxide emissions will increase under Arctic warming, and that they will provide a positive climate feedback. Over centuries, this feedback will be moderate: of a magnitude similar to other climate-terrestrial ecosystem feedbacks. Over millennia and longer, however, carbon dioxide and methane releases from permafrost and shelves/shelf slopes are much more important, because of the large carbon and methane hydrate pools involved.

[END FAQ 6.2 HERE]

References

Abdalla, M., M. Jones, J. Yeluripati, P. Smith, J. Burke, and M. Williams, 2010: Testing DayCent and DNDC model simulations of N2O fluxes and assessing the impacts of climate change on the gas flux and biomass production from a humid pasture. *Atmospheric Environment*, **44**, 2961-2970.

Achard, F., H. D. Eva, P. Mayaux, H.-J. Stibig, and A. Belward, 2004: Improved estimates of net carbon emissions from land cover change in the tropics for the 1990s. *Global Biogeochemical Cycles*, **18**, doi:10.1029/2003GB002142.

Adair, E. C., P. B. Reich, S. E. Hobbie, and J. M. H. Knops, 2009: Interactive Effects of Time, CO2, N, and Diversity on Total Belowground Carbon Allocation and Ecosystem Carbon Storage in a Grassland Community. *Ecosystems*, **12**, 1037-1052.

Adkins, J. F., K. McIntyre, and D. P. Schrag, 2002: The salinity, temperature and δ18O of the glacial deep ocean. *Science*, **298**, 1769-1773.

Ahn, J., and E. J. Brook, 2008: Atmospheric CO2 and climate on millennial time scales during the last glacial period. *Science*, **322**, 83-85.

Ahn, J., et al., 2012: Atmospheric CO2 over the last 1000 years: A high resolution record from the West Antarctic Ice Sheet (WAIS) Divide ice core. *Global Biogeochemical Cycles*, **26**.

Ainsworth, E. A., and S. P. Long, 2004: What have we learned from 15 years of free-air CO2 enrichment (FACE)? A meta-analytic review of the responses of photosynthesis, canopy properties and plant production to rising CO2. *New Phytologist*, **165**, 351–372.

Ainsworth, E. A., C. R. Yendrek, S. Sitch, W. J. Collins, and L. D. Emberson, 2012: The effects of tropospheric ozone on net primary productivity and implications for climate change. *Annual review of plant biology*, **63**, 637-661.

Allan, W., H. Struthers, and D. C. Lowe, 2007: Methane carbon isotope effects caused by atomic chlorine in the marine boundary layer: Global model results compared with Southern Hemisphere measurements. *Journal of Geophysical Research-Atmospheres*, **112, D04306, doi:10.1029/2006jd007369**.

Amiro, B., A. Cantin, M. Flannigan, and W. de Groot, 2009: Future emissions from Canadian boreal forest fires. *Canadian Journal of Forest Research-Revue Canadienne De Recherche Forestiere*, **39**, 383-395.

Amiro, B., et al., 2010: Ecosystem carbon dioxide fluxes after disturbance in forests of North America. *Journal of Geophysical Research-Biogeosciences*, **115**, -.

Anderson, R. F., M. Q. Fleisher, Y. Lao, and G. Winckler, 2008: Modern CaCO3 preservation in equatorial Pacific sediments in the context of late-Pleistocene glacial cycles. *Marine Chemistry*, **111**, 30-46.

Andres, R., J. Gregg, L. Losey, G. Marland, and T. Boden, 2011: Monthly, global emissions of carbon dioxide from fossil fuel consumption. *Tellus Series B-Chemical and Physical Meteorology*, **63**, 309-327.

Andres, R. J., et al., 2012: A synthesis of carbon dioxide emissions from fossil-fuel combustion. *Biogeosciences Discuss.*, **9**, 1845-1871.

Andrews, O. D., N. L. Bindoff, P. R. Halloran, T. Ilyina, and C. Le Quere, subm.: Detecting an external influence on recent changes in oceanic oxygen using an optimal fingerprinting method. *Biogeosciences*.

Aranjuelo, I., et al., 2011: Maintenance of C sinks sustains enhanced C assimilation during long-term exposure to elevated [CO2] in Mojave Desert shrubs. *Oecologia*, **167**.

Archer, D., 2007: Methane hydrate stability and anthropogenic climate change. *Biogeosciences*, **4**, 521-544.

Archer, D., and E. Maierreimer, 1994: Effect of deep-sea sedimentary calcite preservation on atmospheric CO2 concentration. *Nature*, **367**, 260-263.

Archer, D., and V. Brovkin, 2008: The millennial atmospheric lifetime of anthropogenic CO2. *Climatic Change*, **90**, 283-297.

Archer, D., B. Buffett, and V. Brovkin, 2009a: Ocean methane hydrates as a slow tipping point in the global carbon cycle. *Proceedings of the National Academy of Sciences*, **106**, 20596-20601.

Archer, D., A. Winguth, D. Lea, and N. Mahowald, 2000: What caused the glacial/interglacial atmospheric pCO(2) cycles? *Reviews of Geophysics*, **38**, 159-189.

Archer, D., et al., 2009b: Atmospheric Lifetime of Fossil Fuel Carbon Dioxide. *Annual Review of Earth and Planetary Sciences*, **37**, 117-134.

Archibald, S., A. C. Staver, and S. A. Levin, 2012: Evolution of human-driven fire regimes in Africa. *Proceedings of the National Academy of Sciences of the United States of America*, **109**, 847-852.

Arneth, A., et al., 2010: Terrestrial biogeochemical feedbacks in the climate system. *Nature Geoscience*, **3**, 525-532.

Arora, V. K., and G. J. Boer, 2010: Uncertainties in the 20th century carbon budget associated with land use change. *Global Change Biology*, **16**, 3327-3348.

Arora, V. K., et al., 2011: Carbon emission limits required to satisfy future representative concentration pathways of greenhouse gases. *Geophysical Research Letters*, **38**, L05805, doi:05810.01029/02010GL046270.

Arora, V. K., et al., subm.: Carbon-concentration and carbon-climate feedbacks in CMIP5 Earth system models. *Journal of Climate*.

Artioli, Y., et al., 2012: The carbonate system in the North Sea: Sensitivity and model validation. *Journal of Marine Systems*, **102–104**, 1-13.

Ashmore, M., 2005: Assessing the future global impacts of ozone on vegetation. *Plant Cell and Environment*, **28**, 949-964.

Assmann, K. M., M. Bentsen, J. Segschneider, and C. Heinze, 2010: An isopycnic ocean carbon cycle model. *Geoscientific Model Development*, **3**, 143-167.
Aumont, O., and L. Bopp, 2006: Globalizing results from ocean in situ iron fertilization studies. *Global Biogeochemical Cycles*, **20**, GB2017, doi:2010.1029/2005GB002591.
Avis, C., A. Weaver, and K. Meissner, 2011: Reduction in areal extent of high-latitude wetlands in response to permafrost thaw. *Nature Geoscience*, **4**, 444-448.
Aydin, M., et al., 2011: Recent decreases in fossil-fuel emissions of ethane and methane derived from firn air. *Nature*, **476**, 198-201.
Ayres, R. U., W. H. Schlesinger, and R. H. Socolow, 1994: Human impacts on the carbon and nitrogen cycles. *Industrial Ecology and Global Change*, R. H. Socolow, Andrews, C., Berkhout, R, and V. Thomas (eds.), Ed., 121-155.
Bacastow, R. B., and C. D. Keeling, 1979: Models to predict future atmospheric CO2 concentrations. *Workshop on the Global Effects of Carbon Dioxide from Fossil Fuels,* United States Department of Energy, 72-90.
Baccini, A., et al., 2012: Estimated carbon dioxide emissions from tropical deforestation improved by carbon-density maps. *Nature Climate Change*, **Published online 29 January 2012**.
Bader, M., E. Hiltbrunner, and C. Kö rner, 2009: Fine root responses of mature deciduous forest trees to free air carbon dioxide enrichment (FACE). *Functional Ecology*, **23**, 913–921.
Baker, A., S. Cumberland, and N. Hudson, 2008: Dissolved and total organic and inorganic carbon in some British rivers. *Area*, **40**, 117-127.
Baker, D. F., et al., 2006: TransCom 3 inversion intercomparison: Impact of transport model errors on the interannual variability of regional CO2 fluxes, 1988–2003. *Global Biogeochemical Cycles*, **20**.
Ballantyne, A. P., C. B. Alden, J. B. Miller, P. P. Tans, and J. W. C. White, 2012: Increase in observed net carbon dioxide uptake by land and oceans during the past 50 years. *Nature*, **488**, 70-73.
Ballhorn, U., F. Siegert, M. Mason, and S. Limin, 2009: Derivation of burn scar depths and estimation of carbon emissions with LIDAR in Indonesian peatlands. *Proceedings of the National Academy of Sciences*, **106**, 21213-21218.
Balshi, M., A. McGuire, P. Duffy, M. Flannigan, D. Kicklighter, and J. Melillo, 2009: Vulnerability of carbon storage in North American boreal forests to wildfires during the 21st century. *Global Change Biology*, **15**, 1491-1510.
Barnard, R., P. W. Leadley, and B. A. Hungate, 2005: Global change, nitrification, and denitrification: A review. *Global Biogeochemical Cycles*, **19**, GB1007, doi:1010.1029/2004GB002282.
Barnes, R. T., and P. A. Raymond, 2009: The contribution of agricultural and urban activities to inorganic carbon fluxes within temperate watersheds. *Chemical Geology*, **266**, 318-327.
Bastviken, D., J. Cole, M. Pace, and L. Tranvik, 2004: Methane emissions from lakes: Dependence of lake characteristics, two regional assessments, and a global estimate. *Global Biogeochem. Cycles*, **18**, GB4009.
Bastviken, D., L. J. Tranvik, J. A. Downing, P. M. Crill, and A. Enrich-Prast, 2011: Freshwater Methane Emissions Offset the Continental Carbon Sink. *Science*, **331**, 50.
Batjes, N., 1996: Total carbon and nitrogen in the soils of the world. *European Journal of Soil Science*, **47**, 151-163.
Beaugrand, G., M. Edwards, and L. Legendre, 2010: Marine biodiversity, ecosystem functioning, and carbon cycles. *Proceedings of the National Academy of Sciences*, 10.1073/pnas.0913855107.
Beaulieu, J. J., et al., 2011a: Nitrous oxide emission from denitrification in stream and river networks. *P Natl Acad Sci USA*, **108**, 214-219.
Beaulieu, J. J., et al., 2011b: Nitrous oxide emission from denitrification in stream and river networks. *Proceedings of the National Academy of Sciences*, **108**, 214-219.
Beer, C., et al., 2010: Terrestrial Gross Carbon Dioxide Uptake: Global Distribution and Covariation with Climate. *Science*, **329**, 834-838.
Bellassen, V., G. Le Maire, J. F. Dhote, P. Ciais, and N. Viovy, 2010: Modelling forest management within a global vegetation model. Part 1: Model structure and general behaviour. *Ecological Modeling*, **221**, 2458-2474.
Bellassen, V., N. Viovy, S. Luyssaert, G. Le Maire, M.-J. Schelhaas, and P. Ciais, 2011: Reconstruction and attribution of the carbon sink of European forests between 1950 and 2000. *Global Change Biology*, **17**, 3274-3292.
Bennington, V., G. A. McKinley, S. Dutkiewicz, and D. Ullman, 2009: What does chlorophyll variability tell us about export and air-sea CO2 flux variability in the North Atlantic? *Global Biogeochemical Cycles*, **23**, GB3002, doi:3010.1029/2008GB003241.
Bentsen, M., et al., subm.: The Norwegian Earth System Model, NorESM1-M. Part1: Description and basic evaluation. *Geoscientific Model Development*.
Berendse, F., et al., 2001: Raised atmospheric CO2 levels and increased N deposition cause shifts in plant species composition and production in Sphagnum bogs. *Global Change Biology*, **7**, 591-598.
Bergamaschi, P., et al., 2007: Satellite chartography of atmospheric methane from SCIAMACHYon board ENVISAT: 2. Evaluation based on inverse model simulations. *Journal of Geophysical Research-Atmospheres*, **112**, D02304, doi:02310.01029/02006JD007268.
Bergamaschi, P., et al., 2009: Inverse modeling of global and regional CH4 emissions using SCIAMACHY satellite retrievals. *J. Geophys. Res.*, **114**, D22301.
Berger, W. H., 1982: Increase of carbon-dioxide in the atmosphere during deglaciation - the coral-reef hypothesis. *Naturwissenschaften*, **69**, 87-88.

Berner, R. A., 1992: Weathering, plants, and the long-term carbon-cycle. *Geochimica Et Cosmochimica Acta*, **56**, 3225-3231.
Biastoch, A., et al., 2011: Rising Arctic Ocean temperatures cause gas hydrate destabilization and ocean acidification. *Geophysical Research Letters*, **38**, -.
Billings, S. A., S. M. Schaeffer, and R. D. Evans, 2002: Trace N gas losses and N mineralization in Mojave desert soils exposed to elevated CO2. *Soil Biology & Biochemistry*, **34**, 1777-1784.
Bird, M. I., J. Lloyd, and G. D. Farquhar, 1996: Terrestrial carbon storage from the last glacial maximum to the present. *Chemosphere*, **33**, 1675-1685.
Bleeker, A., K. Hicks, F. Dentener, and J. Galloway, 2011: N deposition as a threat to the World's protected areas under the Convention on Biological Diversity. *Environmental Pollution*, **159**, 2280-2288.
Bloom, A. A., J. Lee-Taylor, S. Madronich, D. J. Messenger, P. I. Palmer, D. S. Reay, and A. R. McLeod, 2010: Global methane emission estimates from ultraviolet irradiation of terrestrial plant foliage. *New Phytologist*, **187**, 417-425.
Blunier, T., J. Chappellaz, J. Schwander, B. Stauffer, and D. Raynaud, 1995: Variations in atmospheric methane concentration during the Holocene epoch. *Nature*, **374**, 46-49.
Boardman, C., V. Gauci, J. Watson, S. Blake, and D. Beerling, 2011: Contrasting wetland CH4 emission responses to simulated glacial atmospheric CO2 in temperate bogs and fens. *New Phytologist*, **192**, 898-911.
Bock, M., J. Schmitt, L. Moller, R. Spahni, T. Blunier, and H. Fischer, 2010: Hydrogen Isotopes Preclude Marine Hydrate CH4 Emissions at the Onset of Dansgaard-Oeschger Events. *Science*, **328**, 1686-1689.
Boden, T., G. Marland, and R. Andres: Global CO2 Emissions from Fossil-Fuel Burning,Cement Manufacture, and Gas Flaring: 1751-2008. [Available online at http://cdiac.ornl.gov/trends/emis/meth_reg.html.]
Bohn, T., D. Lettenmaier, K. Sathulur, L. Bowling, E. Podest, K. McDonald, and T. Friborg, 2007: Methane emissions from western Siberian wetlands: heterogeneity and sensitivity to climate change. *Environmental Research Letters*, **2**, -.
Bonan, G. B., and S. Levis, 2010: Quantifying carbon-nitrogen feedbacks in the Community Land Model (CLM4). *Geophysical Research Letters*, **37**, -.
Booth, B. B. B., et al., 2012: High sensitivity of future global warming to land carbon cycle processes. *Environ. Res. Lett.*, **7**, 8pp.
Bopp, L., K. E. Kohfeld, C. Le Quere, and O. Aumont, 2003: Dust impact on marine biota and atmospheric CO2 during glacial periods. *Paleoceanography*, **18**.
Bopp, L., C. Le Quere, M. Heimann, A. C. Manning, and P. Monfray, 2002: Climate-induced oceanic oxygen fluxes: Implications for the contemporary carbon budget. *Global Biogeochem. Cycles*, **16**, 1022.
Bopp, L., et al., 2001: Potential impact of climate change on marine export production. *Global Biogeochem. Cycles*, **15**, 81-99.
Bousquet, P., D. A. Hauglustaine, P. Peylin, C. Carouge, and P. Ciais, 2005: Two decades of OH variability as inferred by an inversion of atmospheric transport and chemistry of methyl chloroform. *Atmospheric Chemistry and Physics*, **5**, 2635-2656.
Bousquet, P., P. Peylin, P. Ciais, C. Le Quere, P. Friedlingstein, and P. Tans, 2000: Regional changes in carbon dioxide fluxes of land and oceans since 1980. *Science*, 1342-1346.
Bousquet, P., et al., 2006: Contribution of anthropogenic and natural sources to atmospheric methane variability. *Nature*, **443**, 439-443.
Bousquet, P., et al., 2011: Source attribution of the changes in atmospheric methane for 2006–2008. *Atmos. Chem. Phys.*, **11**, 3689-3700.
Bouttes, N., D. Paillard, D. M. Roche, V. Brovkin, and L. Bopp, 2011: Last Glacial Maximum CO2 and d13C successfully reconciled. *Geophysical Research Letters*, **38**.
Bouwman, A. F., et al., 2011a: Exploring global changes in nitrogen and phosphorus cycles in agriculture induced by livestock production over the 1900–2050 period. *P Natl Acad Sci USA*, 10.1073/pnas.1012878108.
Bouwman, L., et al., 2011b: Exploring global changes in nitrogen and phosphorus cycles in agriculture induced by livestock production over the 1900–2050 period. *Proceedings of the National Academy of Sciences of the United States of America*, 10.1073/pnas.1012878108.
Bozbiyik, A., M. Steinacher, F. Joos, T. F. Stocker, and L. Menviel, 2011: Fingerprints of changes in the terrestrial carbon cycle in response to large reorganizations in ocean circulation. *Climate of the Past*, **7**, 319-338.
Broecker, W. S., and T. H. Peng, 1986: Carbon cycle - 1985 glacial to interglacial changes in the operation of the global carbon cycle. *Radiocarbon*, **28**, 309-327.
Broecker, W. S., E. Clark, D. C. McCorkle, T. H. Peng, I. Hajdas, and G. Bonani, 1999: Evidence for a reduction in the carbonate ion content of the deep sea during the course of the Holocene. *Paleoceanography*, **14**, 744-752.
Brovkin, V., A. Ganopolski, D. Archer, and S. Rahmstorf, 2007: Lowering of glacial atmospheric CO2 in response to changes in oceanic circulation and marine biogeochemistry. *Paleoceanography*, **22**.
Brovkin, V., J. H. Kim, M. Hofmann, and R. Schneider, 2008: A lowering effect of reconstructed Holocene changes in sea surface temperatures on the atmospheric CO2 concentration. *Global Biogeochemical Cycles*, **22**.
Brovkin, V., T. Raddatz, C. H. Reick, M. Claussen, and V. Gayler, 2009: Global biogeophysical interactions between forest and climate. *Geophysical Research Letters*, **36**.

Brovkin, V., S. Sitch, W. von Bloh, M. Claussen, E. Bauer, and W. Cramer, 2004: Role of land cover changes for atmospheric CO2 increase and climate change during the last 150 years. *Global Change Biology*, **10**, 1253-1266.
Brovkin, V., J. Bendtsen, M. Claussen, A. Ganopolski, C. Kubatzki, V. Petoukhov, and A. Andreev, 2002: Carbon cycle, vegetation, and climate dynamics in the Holocene: Experiments with the CLIMBER-2 model. *Global Biogeochemical Cycles*, **16**.
Brovkin, V., et al., 2010: Sensitivity of a coupled climate-carbon cycle model to large volcanic eruptions during the last millennium. *Tellus*, **62B**, 674-681.
Brown, J. R., J. C. Blankinship, A. Niboyet, K. J. Groenigen, P. Dijkstra, X. Roux, and P. W. Leadley, 2011: Effects of multiple global change treatments on soil N2O fluxes. *Biogeochemistry*, **109**, 85-100.
Brzezinski, M. A., et al., 2002: A switch from Si(OH)4 to NO3− depletion in the glacial Southern Ocean. *Geophys. Res. Lett.*, **29**, 1564.
Burke, A., and L. F. Robinson, 2012: The Southern Ocean's Role in Carbon Exchange During the Last Deglaciation. *Science*, **335**, 557-561.
Burke, E. J., C. D. Jones, and C. D. Koven, subm.: Estimating the permafrost-carbon-climate response in the CMIP5 climate model using a simplified approach. *Journal of Climate*.
Burn, C., and F. Nelson, 2006: Comment on "A projection of severe near-surface permafrost degradation during the 21st century" by David M. Lawrence and Andrew G. Slater. *Geophysical Research Letters*, **33**, -.
Butterbach-Bahl, K., and M. Dannenmann, 2011: Denitrification and associated soil N2O emissions due to agricultural activities in a changing climate. *Current Opinion in Environmental Sustainability*, **3**, 389-395.
Byrne, R., S. Mecking, R. Feely, and X. Liu, 2010: Direct observations of basin-wide acidification of the North Pacific Ocean. *Geophysical Research Letters*, **37**, -.
Cadule, P., et al., 2010: Benchmarking coupled climate-carbon models against long-term atmospheric CO2 measurements. *Global Biogeochemical Cycles*, **24**, -.
Cai, W.-J., et al., 2011: Acidification of subsurface coastal waters enhanced by eutrophication. *Nature Geosci*, **4**, 766-770.
Caldeira, K., and M. E. Wickett, 2005: Ocean model predictions of chemistry changes from carbon dioxide emissions to the atmosphere and ocean. *J Geophys Res-Oceans*, **110**.
Canadell, J. G., and M. R. Raupach, 2008: Managing forests for climate change mitigation. *Science*, **320**, 1456-1457.
Canadell, J. G., et al., 2007: Contributions to accelerating atmospheric CO2 growth from economic activity, carbon intensity, and efficiency of natural sinks. *Proceedings of the National Academy of Sciences of the United States of America*, **104**, 18866-18870.
Canfield, D. E., A. N. Glazer, and P. G. Falkowski, 2010: The Evolution and Future of Earth's Nitrogen Cycle. *Science*, **330**, 192-196.
Cao, L., and K. Caldeira, 2010a: Can ocean iron fertilization mitigate ocean acidification? *Climatic Change*, **99**, 303-311.
——, 2010b: Atmospheric carbon dioxide removal: long-term consequences and commitment. *Environmental Research Letters*, **5**.
Cao, L., K. Caldeira, and A. K. Jain, 2007: Effects of carbon dioxide and climate change on ocean acidification and carbonate mineral saturation. *Geophysical Research Letters*, **34**.
Carcaillet, C., et al., 2002: Holocene biomass burning and global dynamics of the carbon cycle. *Chemosphere*, **49**, 845-863.
Chambers, J. Q., J. I. Fisher, H. Zeng, E. L. Chapman, D. B. Baker, and G. C. Hurtt, 2007: Hurricane Katrina's Carbon Footprint on U.S. Gulf Coast Forests. *Science*, **318**, 1107.
Chantarel, A. M., J. M. G. Bloor, N. Deltroy, and J.-F. Soussana, 2011: Effects of climate change drivers on nitrous oxide fluxes in an upland temperate grassland. *Ecosystems*, **14**, 223-233.
Chapuis-Lardy, L., N. Wrage, A. Metay, J. L. Chotte, and M. Bernoux, 2007: Soils, a sink for N2O? A review. *Global Change Biology*, **13**, 1-17.
Chen, Y. H., and R. G. Prinn, 2006: Estimation of atmospheric methane emissions between 1996 and 2001 using a three-dimensional global chemical transport model. *Journal of Geophysical Research-Atmospheres*, **111**, -.
Chhabra, A., K. R. Manjunath, S. Panigrahy, and J. S. Parihar, 2009: Spatial pattern of methane emissions from Indian livestock. *Current Science*, **96**, 683-689.
Chierici, M., and A. Fransson, 2009: Calcium carbonate saturation in the surface water of the Arctic Ocean: undersaturation in freshwater influenced shelves. *Biogeosciences*, **6**, 2421-2431.
Christensen, T., et al., 2004: Thawing sub-arctic permafrost: Effects on vegetation and methane emissions. *Geophysical Research Letters*, **31**.
Christian, J., et al., subm.: Trends in ocean CaCO3 undersaturation in the CMIP5 suite of Earth System Models. *Geophysical Research Letters*.
Churkina, G., V. Brovkin, W. von Bloh, K. Trusilova, M. Jung, and F. Dentener, 2009: Synergy of rising nitrogen depositions and atmospheric CO2 on land carbon uptake moderately offsets global warming. *Global Biogeochemical Cycles*, **23**.
Ciais, P., P. Rayner, F. Chevallier, P. Bousquet, M. Logan, P. Peylin, and M. Ramonet, 2010: Atmospheric inversions for estimating CO2 fluxes: methods and perspectives. *Climatic Change*, **103**, 69-92.

Ciais, P., et al., 2012: Large inert carbon pool in the terrestrial biosphere during the Last Glacial Maximum. *Nature Geosci*, **5**, 74-79.
Ciais, P., et al., 2008: Carbon accumulation in European forests. *Nature Geoscience*, **1**, 425-429.
Ciais, P., et al., 2005: Europe-wide reduction in primary productivity caused by the heat and drought in 2003. *Nature*, DOI 10.1038/nature03972, 529-533.
Clark, D. B., D. A. Clark, and S. F. Oberbauer, 2010: Annual wood production in a tropical rain forest in NE Costa Rica linked to climatic variation but not to increasing CO2. *Global Change Biology*, **16**, 747-759.
Cocco, V., et al., subm.: Oxygen and indicators of stress for marine life in multi-model global warming projections. *Biogeosciences*.
Codispoti, L. A., 2010: Interesting Times for Marine N2O. *Science*, **327**, 1339-1340.
Codispoti, L. A., A. H. Devol, S. W. A. Naqvi, H. W. Paerl, and T. Yoshinari, 2001: The oceanic fixed nitrogen and nitrous oxide budgets: Moving targets as we enter the anthropocene? *Scientia Marina*, **65**, 85-105.
Collins, W. J., et al., 2011: Development and evaluation of an Earth-system model - HadGEM2. *Geosci. Model Dev. Discuss.*, **4**, 997-1062.
Conrad, R., 1996: Soil microorganisms as controllers of atmospheric trace gases (H2, CO, CH4, OCS, N2O, and NO). *Microbiological Reviews*, **60**, 609-640.
Conway, T., and P. Tans: Global CO2. Available online at http://www.esrl.noaa.gov/gmd/ccgg/trends/global.html.
Conway, T. J., P. P. Tans, L. S. Waterman, and K. W. Thoning, 1994: Evidence for interannual variability of the carbon cycle from the national oceanic and atmospheric administration climate monitoring and diagnostics laboratory global air sampling network. *Journal of Geophysical Research - Atmospheres*, **99**, 22831-22855.
Corbiere, A., N. Metzl, G. Reverdin, C. Brunet, and A. Takahashi, 2007: Interannual and decadal variability of the oceanic carbon sink in the North Atlantic subpolar gyre. *Tellus Series B-Chemical and Physical Meteorology*, **59**, 168-178.
Cox, P., and C. Jones, 2008: Climate change - Illuminating the modern dance of climate and CO2. *Science*, DOI 10.1126/science.1158907, 1642-1644.
Cox, P. M., 2001: Description of the TRIFFID dynamic global vegetation model. *Technical Note 24 HadleyCentre, Met Office*.
Cox, P. M., D. Pearson, B. B. Booth, P. Friedlingstein, C. Huntingford, C. D. Jones, and C. M. Luke, subm.: Carbon dioxide variability constrains the sensitivity of tropical carbon to climate change. *Nature*.
Crutzen, P. J., A. R. Mosier, K. A. Smith, and W. Winiwarter, 2008: N_2O release from agro-biofuel production negates global warming reduction by replacing fossil fuels. *Atmos. Chem. Phys.*, **8**.
Cunnold, D. M., et al., 2002: In situ measurements of atmospheric methane at GAGE/AGAGE sites during 1985–2000 and resulting source inferences. *J. Geophys. Res.*, **107**, 4225.
Curry, C., 2009: The consumption of atmospheric methane by soil in a simulated future climate. *Biogeosciences*, **6**, 2355-2367.
Davidson, E. A., 2009: The contribution of manure and fertilizer nitrogen to atmospheric nitrous oxide since 1860. *Nature Geoscience*, **2**, 659-662.
——, 2012: Representative concentration pathways and mitigation scenarios for nitrous oxide. *Environmental Research Letters*, **7**.
Dawes, M. A., S. Hattenschwiler, P. Bebi, F. Hagedorn, I. T. Handa, C. Christian Korner, and C. Rixen, 2011: Species-specific tree growth responses to 9 years of CO2 enrichment at the alpine treeline. *Journal of Ecology*, **99**, 383–394.
DeFries, R., and C. Rosenzweig, 2010: Toward a whole-landscape approach for sustainable land use in the tropics. *Proceedings of the National Academy of Sciences*, **107**, 19627-19632.
DeFries, R., R. A. Houghton, M. Hansen, C. Field, D. L. Skole, and J. Townshend, 2002: Carbon emissions from tropical deforestation and regrowth based on satellite observations for the 1980s and 90s. *Proceedings of the National Academy of Sciences*, **99**, 14256-14261.
DeKlein, C., et al., 2007: N_2O Emissions from Managed Soils, and CO_2 Emissions from Lime and Urea Application. *2006 IPCC Guidelines for National Greenhouse Gas Inventories*, 1-54.
Delmas, R. J., J. M. Ascencio, and M. Legrand, 1980: Polar ice evidence that atmospheric CO2 20,000-yr BP was 50-percent of present. *Nature*, **284**, 155-157.
Denman, K. L., et al., 2007: Couplings Between Changes in the Climate System and Biogeochemistry.
Dentener, F., W. Peters, M. Krol, M. van Weele, P. Bergamaschi, and J. Lelieveld, 2003: Interannual variability and trend of CH4 lifetime as a measure for OH changes in the 1979-1993 time period. *Journal of Geophysical Research-Atmospheres*, **108**.
Dentener, F., et al., 2005: The impact of air pollutant and methane emission controls on tropospheric ozone and radiative forcing: CTM calculations for the period 1990-2030. *Atmospheric Chemistry and Physics*, **5**, 1731-1755.
Dentener, F., et al., 2006: The global atmospheric environment for the next generation. *Environ. Sci. Technol.*, **40**, 3586-3594.
Deutsch, C., J. L. Sarmiento, D. M. Sigman, N. Gruber, and J. P. Dunne, 2007: Spatial coupling of nitrogen inputs and losses in the ocean. *Nature*, **445**, 163-167.
Dickens, G. R., 2003: A Methane Trigger for Rapid Warming? *Science*, **299**, 1017.

Dlugokencky, E. J., P. M. Lang, and K. A. Masarie, 2010: Atmospheric Methane dry air mole fractions from teh NOAA ESRL carbon cycle cooperative global air sampling network, 1983-2009. NOAA/ESRL.
Dlugokencky, E. J., E. G. Nisbet, R. Fisher, and D. Lowry, 2011: Global atmospheric methane: budget, changes and dangers. *Philosophical Transactions of the Royal Society a-Mathematical Physical and Engineering Sciences*, **369**, 2058-2072.
Dlugokencky, E. J., S. Houweling, L. Bruhwiler, K. A. Masarie, P. M. Lang, J. B. Miller, and P. P. Tans, 2003: Atmospheric methane levels off: Temporary pause or a new steady-state? *Geophysical Research Letters*, **30**.
Dlugokencky, E. J., et al., 2009: Observational constraints on recent increases in the atmospheric CH4 burden. *Geophys. Res. Lett.*, **36**, L18803.
Dolman, A. J., et al., 2012: An estimate of the terrestrial carbon budget of Russia using inventory based, eddy covariance and inversion methods. *Biogeosciences Discuss*, **9**, 6579-6626.
Doney, S. C., et al., 2009: Mechanisms governing interannual variability in upper-ocean inorganic carbon system and air-sea CO2 fluxes: physical climate and atmospheric dust. *Deep-Sea Res.*, **II**, 640-655.
Dore, J. E., R. Lukas, D. W. Sadler, M. J. Church, and D. M. Karl, 2009: Physical and biogeochemical modulation of ocean acidification in the central North Pacific. *Proceedings of the National Academy of Sciences*, **106**, 12235-12240.
Duce, R. A., et al., 2008: Impacts of atmospheric anthropogenic nitrogen on the open ocean. *Science*, **320**, 893-897.
Dueck, T. A., et al., 2007: No evidence for substantial aerobic methane emission by terrestrial plants: a (13)C-labelling approach. *New Phytologist*, **175**, 29-35.
Dufresne, J.-L., M.-A. Foujols, S. Denvil, A. Caubel, O. Marti, O. Aumont, and Y. Balkanski, subm.: Climate change projections using the IPSL-CM5 Earth System Model: from CMIP3 to CMIP5.
Dukes, J. S., et al., 2005: Responses of grassland production to single and multiple global environmental changes. *Plos Biology*, **3**, 1829-1837.
Dunne, J. P., et al., subm.: GFDL's ESM2 global coupled climate-carbon Earth System Models. Part II: Carbon system formation and baseline simulation characteristics. *Journal of Climate*.
Dunne, J. P., et al., 2012: GFDL's ESM2 global coupled climate-carbon Earth System Models Part I: Physical formulation and baseline simulation characteristics. *Journal of Climate*, doi:10.1175/JCLI-D-11-00560.1.
Dutta, K., E. Schuur, J. Neff, and S. Zimov, 2006: Potential carbon release from permafrost soils of Northeastern Siberia. *Global Change Biology*, **12**, 2336-2351.
Eby, M., K. Zickfeld, A. Montenegro, D. Archer, K. J. Meissner, and A. J. Weaver, 2009: Lifetime of Anthropogenic Climate Change: Millennial Time Scales of Potential CO2 and Surface Temperature Perturbations. *Journal of Climate*, **22**, 2501-2511.
EDGAR4-database: Emission Database for Global Atmospheric Research (EDGAR), release version 4.0. http://edgar.jrc.ec.europa.eu, 2009
Elberling, B., H. H. Christiansen, and B. U. Hansen, 2010: High nitrous oxide production from thawing permafrost. *Nature Geoscience*, **3**, 332-335.
Eliseev, A., I. Mokhov, M. Arzhanov, P. Demchenko, and S. Denisov, 2008: Interaction of the methane cycle and processes in wetland ecosystems in a climate model of intermediate complexity. *Izvestiya Atmospheric and Oceanic Physics*, **44**, 139-152.
Elliott, S., M. Maltrud, M. Reagan, G. Moridis, and P. Cameron-Smith, 2011: Marine methane cycle simulations for the period of early global warming (vol 116, G01010, 2011). *Journal of Geophysical Research-Biogeosciences*, **116**, -.
Elser, J. J., et al., 2007: Global analysis of nitrogen and phosphorus limitation of primary producers in freshwater, marine, and terrestrial ecosystems. *Ecology Letters*, **10**, 1135-1142.
Elsig, J., et al., 2009: Stable isotope constraints on Holocene carbon cycle changes from an Antarctic ice core. *Nature*, **461**, 507-510.
EPA, 2006: Global anthropogenic non-CO2 greenhouse gas emissions. US EPA report EPA-430-R-06-003. http://nepis.epa.gov/EPA/html/DLwait.htm?url=/Adobe/PDF/2000ZL5G.PDF.
——, 2010: Methane and Nitrous Oxide Emissions From Natural Sources, U.S. Environmental Protection Agency.
——, 2011: Global Anthropogenic Non-CO2 Greenhouse Gas Emissions: 1990 - 2030.
Erisman, J. W., M. S. Sutton, J. N. Galloway, Z. Klimont, and W. Winiwarter, 2008: A century of ammonia synthesis. *Nature Geosciences*, **1**, 1-4.
Erisman, J. W., J. Galloway, S. Seitzinger, A. Bleeker, and K. Butterbach-Bahl, 2011: Reactive nitrogen in the environment and its effect on climate change. *Current Opinion in Environmental Sustainability*, **3**, 281-290.
Esser, G., J. Kattge, and A. Sakalli, 2011: Feedback of carbon and nitrogen cycles enhances carbon sequestration in the terrestrial biosphere. *Global Change Biology*, **17**, 819-842.
Etheridge, D. M., L. P. Steele, R. L. Langenfelds, R. J. Francey, J.-M. Barnola, and M. V. I., 1996: Natural and anthropogenic changes in atmospheric CO2 over the last 1000 years from air in Antarctic ice and firn. *Journal of Geophysical Research*, **101**, 4115-4128.
Etiope, G., K. R. Lassey, R. W. Klusman, and E. Boschi, 2008: Reappraisal of the fossil methane budget and related emission from geologic sources. *Geophysical Research Letters 35: L09307.*, **35**, L09307.
Evans, C. D., D. T. Monteith, and D. M. Cooper, 2005: Long-term increses in surface water dissolved organic carbon: Observations, possible causes and environmental impacts. *Environmental Pollution*, **137**, 55-71.

Falloon, P., C. Jones, M. Ades, and K. Paul, 2011: Direct soil moisture controls of future global soil carbon changes: An important source of uncertainty. *Global Biogeochemical Cycles*, **25**, -.
Fan, S., T. Blaine, and J. Sarmiento, 1999: Terrestrial carbon sink in the Northern Hemisphere estimated from the atmospheric CO2 difference between Manna Loa and the South Pole since 1959. *Tellus B*, **51**, 863-870.
Fang, J., T. Oikawa, T. Kato, W. Mo, and Z. Wang, 2005: Biomass carbon accumulation by Japan's forests from 1947 to 1995. *Global Biogeochemical Cycles*, **19**.
FAO, 2005: Global Forest Resource Assessment 2005, 129-147 pp.
——, 2010: Global Forest Resources Assessment 2010. *FAO Forestry Paper 163*, 340 pp.
Feely, R. A., S. C. Doney, and S. R. Cooley, 2009: Ocean Acidification: Present Conditions and Future Changes in a High-CO2 World. *Oceanography*, **22**, 36-47.
Feely, R. A., R. H. Byrne, J. G. Acker, P. R. Betzer, C.-T. A. Chen, J. F. Gendron, and M. F. Lamb, 1988: Winter-summer variations of calcite and aragonite saturation in the Northeast Pacific. *Marine Chemistry*, **25**, 227-241.
Feely, R. A., T. Takahashi, R. Wanninkhof, M. J. McPhaden, C. E. Cosca, S. C. Sutherland, and M. E. Carr, 2006: Decadal variability of the air-sea CO2 fluxes in the equatorial Pacific Ocean. *J Geophys Res-Oceans*, **111**, -.
Felzer, B., et al., 2005: Future effects of ozone on carbon sequestration and climate change policy using a global biogeochemical model. *Climatic Change*, **73**, 345-373.
Ferretti, D. F., et al., 2005: Unexpected changes to the global methane budget over the past 2000 years. *Science*, **309**, 1714-1717.
Findlay, H. S., T. Tyrrell, R. G. J. Bellerby, A. Merico, and I. Skjelvan, 2008: Carbon and nutrient mixed layer dynamics in the Norwegian Sea. *Biogeosciences*, **5**, 1395-1410.
Findlay, S. E. G., 2005: Increased carbon transport in the Hudson River: unexpected consequence of nitrogen deposition? *Frontiers in Ecology and the Environment*, **3**, 133-137.
Finzi, A., et al., 2006: Progressive nitrogen limitation of ecosystem processes under elevated CO2 in a warm-temperate forest. *Ecology*, **87**, 15-25.
Finzi, A. C., et al., 2007: Increases in nitrogen uptake rather than nitrogen-use efficiency support higher rates of temperate forest productivity under elevated CO2. *Proceedings of the National Academy of Sciences*, **104**, 14014–14019.
Fischer, H., et al., 2008: Changing boreal methane sources and constant biomass burning during the last termination. *Nature*, **452**, 864-867.
Flannigan, M., B. Stocks, M. Turetsky, and M. Wotton, 2009a: Impacts of climate change on fire activity and fire management in the circumboreal forest. *Global Change Biology*, **15**, 549-560.
Flannigan, M., M. Krawchuk, W. de Groot, B. Wotton, and L. Gowman, 2009b: Implications of changing climate for global wildland fire. *International Journal of Wildland Fire*, **18**, 483-507.
Fluckiger, J., A. Dallenbach, T. Blunier, B. Stauffer, T. F. Stocker, D. Raynaud, and J. M. Barnola, 1999: Variations in atmospheric N2O concentration during abrupt climatic changes. *Science*, **285**, 227-230.
Fluckiger, J., et al., 2002: High-resolution Holocene N2O ice core record and its relationship with CH4 and CO2. *Global Biogeochemical Cycles*, **16**.
Fluckiger, J., et al., 2004: N2O and CH4 variations during the last glacial epoch: Insight into global processes. *Global Biogeochemical Cycles*, **18**.
Foley, J. A., C. Monfreda, N. Ramankutty, and D. Zaks, 2007: Our share of the planetary pie. *Proceedings of the National Academy of Sciences*, **104**, 12585.
Frank, D. C., J. Esper, C. C. Raible, U. Buntgen, V. Trouet, B. Stocker, and F. Joos, 2010: Ensemble reconstruction constraints on the global carbon cycle sensitivity to climate. *Nature*, **463**, 527-U143.
Frankenberg, C., et al., 2008: Tropical methane emissions: A revised view from SCIAMACHY onboard ENVISAT. *Geophysical Research Letters*, **35**, L15811.
Friedli, H., H. Lotscher, H. Oeschger, U. Siegenthaler, and B. Stauffer, 1986: Ice core record of the C-13/C-12 ratio of atmospheric CO2 in the past 2 centuries. *Nature*, **324**, 237-238.
Friedlingstein, P., and I. Prentice, 2010: Carbon-climate feedbacks: a review of model and observation based estimates. *Current Opinion in Environmental Sustainability*, DOI 10.1016/j.cosust.2010.06.002, 251-257.
Friedlingstein, P., J. Dufresne, P. Cox, and P. Rayner, 2003: How positive is the feedback between climate change and the carbon cycle? *Tellus Series B-Chemical and Physical Meteorology*, 692-700.
Friedlingstein, P., M. Meinshausen, V. Arora, C. Jones, S. Liddicoat, and R. Knutti, subm.: CMIP5 climate projections and uncertainties due to carbon cycle feedbacks. *Journal of Climate*.
Friedlingstein, P., et al., 2006: Climate-carbon cycle feedback analysis: Results from the (CMIP)-M-4 model intercomparison. *Journal of Climate*, **19**, 3337-3353.
Friis, K., A. Kortzinger, J. Patsch, and D. W. R. Wallace, 2005: On the temporal increase of anthropogenic CO2 in the subpolar North Atlantic. *Deep-Sea Research Part I-Oceanographic Research Papers*, **52**, 681-698.
Frolicher, T. L., F. Joos, G. K. Plattner, M. Steinacher, and S. C. Doney, 2009: Natural variability and anthropogenic trends in oceanic oxygen in a coupled carbon cycle–climate model ensemble. *Global Biogeochem. Cycles*, **23**, GB1003.
Frölicher, T. L., F. Joos, C. C. Raible, and J. L. Sarmiento, subm.: Atmospheric CO2 response to volcanic eruptions: the role of ENSO, season, and variability. *Global Biogeochemical Cycles*.

Fuller, D. Q., J. van Etten, K. Manning, C. Castillo, E. Kingwell-Banham, and A. Weisskopf, et al., 2011: The contribution of rice agriculture and livestock pastoralism to prehistoric methane levels: an archaeological assessment. *The Holocene*.
Fung, I., M. Prather, J. John, J. Lerner, and E. Matthews, 1991: Three-dimensional model synthesis of the global methane cycle. *Journal of Geophysical Research*, **96**, 13,033-013,065.
Fyfe, J. C., and O. A. Saenko, 2006: Simulated changes in the extratropical Southern Hemisphere winds and currents. *Geophysical Research Letters*, **33**.
Fyke, J., and A. Weaver, 2006: The effect of potential future climate change on the marine methane hydrate stability zone. *Journal of Climate*, **19**, 5903-5917.
Gaillard, M. J., et al., 2010: Holocene land-cover reconstructions for studies on land cover-climate feedbacks. *Climate of the Past*, **6**, 483-499.
Gaillardet, J., B. Dupre, P. Louvat, and C. J. Allegre, 1999: Global silicate weathering and CO consumption rates deduced from the chemistry of large rivers. *Chemical Geology*, **159**, 3-30.
Galloway, J., et al., 2004: Nitrogen cycles: past, present, and future. *Biogeochemistry*, **70**, 153-226.
Galloway, J. N., W. H. Schlesinger, H. Levy II, A. Michaels, and J. L. Schnoor, 1995: Nitrogen fixation: Anthropogenic enhancement – environmental response. *Global Biogeochem. Sci.*, **9**, 235-252.
Galloway, J. N., J. D. Aber, J. W. Erisman, S. P. Seitzinger, R. W. Howarth, E. B. Cowling, and B. J. Cosby, 2003: The nitrogen cascade. *Bioscience*, **53**, 341-356.
Galloway, J. N., et al., 2008: Transformation of the nitrogen cycle: recent trends, questions and potential solutions. *Science*, **320**, 889-889.
Gardenas, A., et al., 2011: Knowledge gaps in soil carbon and nitrogen interactions - From molecular to global scale. *Soil Biology & Biochemistry*, **43**, 702-717.
Gedalof, Z., and A. A. Berg, 2010: Tree ring evidence for limited direct CO2 fertilization of forests over the 20th century. *Global Biogeochemical Cycles*, **24**, -.
Gedney, N., P. Cox, and C. Huntingford, 2004: Climate feedback from wetland methane emissions. *Geophysical Research Letters*, ARTN L20503, DOI:10.1029/2004GL020919, -.
Gerber, S., L. O. Hedin, M. Oppenheimer, S. W. Pacala, and E. Shevliakova, 2010: Nitrogen cycling and feedbacks in a global dynamic land model. *Global Biogeochemical Cycles*, **24**.
Gerber, S., F. Joos, P. Brugger, T. F. Stocker, M. E. Mann, S. Sitch, and M. Scholze, 2003: Constraining temperature variations over the last millennium by comparing simulated and observed atmospheric CO2. *Climate Dynamics*, **20**, 281-299.
Gervois, S., P. Ciais, N. de Noblet-Ducoudre, N. Brisson, N. Vuichard, and N. Viovy, 2008: Carbon and water balance of European croplands throughout the 20th century. *Global Biogeochemical Cycles*, **22**, -.
Gilbert, D., N. N. Rabalais, R. J. Diaz, and J. Zhang, 2010: Evidence for greater oxygen decline rates in the coastal ocean than in the open ocean. *Biogeosciences*, **7**, 2283-2296.
Gloor, M., J. L. Sarmiento, and N. Gruber, 2010: What can be learned about carbon cycle climate feedbacks from the CO2 airborne fraction? *Atmospheric Chemistry and Physics*, **10**, 7739-7751.
Gloor, M., et al., 2009: Does the disturbance hypothesis explain the biomass increase in basin-wide Amazon forest plot data? *Global Change Biology*, **15**, 2418-2430.
Gnanadesikan, A., J. L. Russell, and F. Zeng, 2007: How does ocean ventilation change under global warming? *Ocean Science*, **3**, 43-53.
Gnanadesikan, A., J. P. Dunne, and J. John, 2011: Will open-ocean oxygen stress intensify under climate change? *Biogeosciences Discussions*, **8**, 7007-7032.
Goldewijk, K. K., 2001: Estimating global land use change over the past 300 years: the HYDE Database. *Global Biogeochemical Cycles*, **15**, 417.
Goldewijk, K. K., A. Beusen, G. van Drecht, and M. de Vos, 2011: The HYDE 3.1 spatially explicit database of human-induced global land-use change over the past 12,000 years. *Global Ecology and Biogeography*, **20**, 73-86.
Golding, N., and R. Betts, 2008: Fire risk in Amazonia due to climate change in the HadCM3 climate model: Potential interactions with deforestation. *Global Biogeochemical Cycles*, ARTN GB4007, DOI 10.1029/2007GB003166.
Goldstein, B., F. Joos, and T. F. Stocker, 2003: A modeling study of oceanic nitrous oxide during the Younger Dryas cold period. *Geophysical Research Letters*, **30**, 1092.
Goll, D. S., et al., 2012a: Nutrient limitation reduces land carbon uptake in simulations with a model of combined carbon, nitrogen, and phosphorus cycling. *Biogeosciences Discuss.*, **9**, 3173-3232.
Goll, D. S., et al., 2012b: Nutrient limitation reduces land carbon uptake in simulations with a model of combined carbon, nitrogen and phosphorus cycling. *Biogeosciences Discussions*, **9**, 3173-3232.
Good, P., C. Jones, J. Lowe, R. Betts, B. Booth, and C. Huntingford, 2011: Quantifying Environmental Drivers of Future Tropical Forest Extent. *Journal of Climate*, **24**, 1337-1349.
Goodwin, P., and T. Lenton, 2009: Quantifying the feedback between ocean heating and CO2 solubility as an equivalent carbon emission. *Geophysical Research Letters*, **36**, -.
Graven, H. D., N. Gruber, X. Giraud, R. Key, and S. Khatiwala, 2012: Changing controls on oceanic radiocarbon: New insights on shallow-to-deep ocean exchange and anthropogenic CO2 uptake. *(accepted for publication) Journal of Geophysical Research*.

Gregg, J. S., R. J. Andres, and G. Marland, 2008: China: Emissions pattern of the world leader in CO2 emissions from fossil fuel consumption and cement production. *Geophysical Research Letters*, **35**, -.
Gregory, J., C. Jones, P. Cadule, and P. Friedlingstein, 2009: Quantifying Carbon Cycle Feedbacks. *Journal of Climate*, DOI 10.1175/2009JCLI2949.1, 5232-5250.
Gruber, N., and J. N. Galloway, 2008: An Earth-system perspective of the global nitrogen cycle. *Nature*, **451**, 293-296.
Gruber, N., C. Hauri, Z. Lachkar, D. Loher, T. L. Frölicher, and G. K. Plattner, 2012: Rapid progression of ocean acidification in the California Current System. *Science*, **337**, 220-223.
Gruber, N., et al., 2009: Oceanic sources, sinks, and transport of atmospheric CO2. *Global Biogeochemical Cycles*, **23**.
Gurney, K. R., and W. J. Eckels, 2011: Regional trends in terrestrial carbon exchange and their seasonal signatures. *Tellus Series B-Chemical and Physical Meteorology*, **63**, 328-339.
Halloran, P. R., B. B. B. Booth, C. D. Jones, F. H. Lambert, D. J. McNeall, I. J. Totterdell, and C. Volker, subm.: Assessing the vulnerability of the North Atlantic CO2 sink.
Hamilton, S. K., 2010: Biogeochemical implications of climate change for tropical rivers and floodplains. *Hydrobiologia*, **657**, 19-35.
Hamilton, S. K., A. L. Kurzman, C. Arango, L. Jin, and G. P. Robertson, 2007: Evidence for carbon sequestration by agricultural liming. *Global Biogeochemical Cycles*, **21**.
Hansell, D., C. Carlson, D. Repeta, and R. Schlitzer, 2009: Dissolved Organic Matter in the Ocean: a Controversy Stimulates New Insights. *Oceanography*, **22**, 202-211.
Hansen, M., S. Stehman, and P. V. Potapov, 2010: Quantification of global gross forest cover loss. *Proceedings of the National Academy of Sciences*, **107**, 8650-8655.
Harden, J. W., et al., 2012 in press: Field information links permafrost carbon to physical vulnerabilities of thawing. *Geophysical Research Letters,* doi:10.1029/2012GL051958 http://www.agu.org/pubs/crossref/pip/2012GL051958.shtml,.
Harrison, K. G., 2000: Role of increased marine silica input on paleo-pCO(2) levels. *Paleoceanography*, **15**, 292-298.
Hartmann, J., N. Jansen, H. H. Dürr, S. Kempe, and P. Köhler, 2009: Global CO2-consumption by chemical weathering: What is the contribution of highly active weathering regions? *Global and Planetary Change*, **69**, 185-194.
Hayes, D. J., et al., 2012: Reconciling estimates of the contemporary North American carbon balance among terrestrial biosphere models, atmospheric inversions, and a new approach for estimating net ecosystem exchange from inventory-based data. *Global Change Biology*, **18**, 1282–1299.
Hedegaard, G., J. Brandt, J. Christensen, L. Frohn, C. Geels, K. Hansen, and M. Stendel, 2008: Impacts of climate change on air pollution levels in the Northern Hemisphere with special focus on Europe and the Arctic. *Atmospheric Chemistry and Physics*, **8**, 3337-3367.
Heijmans, M. M. P. D., W. J. Arp, and F. Berendse, 2001: Effects of elevated CO2 and vascular plants on evapotranspiration in bog vegetation. *Global Change Biology*, **7**, 817-827.
Heijmans, M. M. P. D., H. Klees, and F. Berendse, 2002a: Competition between Sphagnum magellanicum and Eriophorum angustifolium as affected by raised CO2 and increased N deposition. *Oikos*, **97**, 415-425.
Heijmans, M. M. P. D., H. Klees, W. de Visser, and F. Berendse, 2002b: Response of a Sphagnum bog plant community to elevated CO2 and N supply. *Plant Ecology*, **162**, 123-134.
Hein, R., P. J. Crutzen, and M. Heimann, 1997: An inverse modeling approach to investigate the global atmospheric methane cycle. *Global Biogeochem. Cycles*, **11**, 43-76.
Helm, K. P., N. L. Bindoff, and J. A. Church, 2011: Observed decreases in oxygen content of the global ocean. *Geophysical Research Letters (in press)*, 10.1029/2011GL049513.
Herridge, D. F., M. B. Peoples, and R. M. Boddey, 2008: Global inputs of biological nitrogen fixation in agricultural systems. *Plant Soil*, **311**, 1-18.
Hibbard, K. A., G. A. Meehl, P. M. Cox, and P. Friedlingstein, 2007: A strategy for climate change stabilization experiments. *EOS, Transactions American Geophysical Union*, **88**.
Hickler, T., B. Smith, I. C. Prentice, K. Mjofors, P. Miller, A. Arneth, and M. T. Sykes, 2008: CO_2 fertilization in temperate FACE experiments not representative of boreal and trophical forests. *Global Change Biology*, **14**, 1531-1542.
Hirota, M., M. Holmgren, E. H. Van Nes, and M. Scheffer, 2011: Global Resilience of Tropical Forest and Savanna to Critical Transitions. *Science*, **334**, 232-235.
Hirsch, A. I., A. M. Michalak, L. M. Bruhwiler, W. Peters, E. J. Dlugokencky, and P. P. Tans, 2006: Inverse modeling estimates of the global nitrous oxide surface flux from 1998 to 2001. *Global Biogeochem. Cycles*, **20**, GB1008.
Hodson, E. L., B. Poulter, N. E. Zimmermann, C. Prigent, and J. O. Kaplan, 2011: The El Nino-Southern Oscillation and wetland methane interannual variability. *Geophysical Research Letters*, **38**.
Hoelzemann, J. J., M. G. Schultz, G. P. Brasseur, C. Granier, and M. Simon, 2004: Global Wildland Fire Emission Model (GWEM): Evaluating the use of global area burnt satellite data. *J. Geophys. Res.*, **109**, D14S04.
Hofmann, M., and H.-J. Schellnhuber, 2009: Oceanic acidification affects marine carbon pump and triggers extended marine oxygen holes. *Proceedings of the National Academy of Sciences*, **106**, 3017-3022.
Holland, E., J. Lee-Taylor, C. D. Nevison, and J. Sulzman, 2005: Global N cycle: Fluxes and N_2O mixing ratios originating from human activity. Oak Ridge National Laboratory Distributed Active Archive Center.

Honisch, B., N. G. Hemming, D. Archer, M. Siddall, and J. F. McManus, 2009: Atmospheric Carbon Dioxide Concentration Across the Mid-Pleistocene Transition. *Science*, **324**, 1551-1554.
Hooijer, A., S. Page, J. Canadell, M. Silvius, J. Kwadijk, H. Wosten, and J. Jauhiainen, 2010: Current and future CO2 emissions from drained peatlands in Southeast Asia. *Biogeosciences*, **7**, 1505-1514.
Houghton, R., G. R. van der Werf, R. De Fries, M. Hansen, J. House, J. Pongratz, and N. Ramankutty, 2012: Chapter G2 Carbon emissions from land use and land-cover change. *Biogeosciences Discuss.*, **9**, 835-878.
Houghton, R. A., 2003: Revised estimates of the annual net flux of carbon to the atmosphere from changes in land use and land management 1850-2000. *Tellus B*, **55**, 378-390.
Houghton, R. A., 2010: How well do we know the flux of CO2 from land-use change? *Tellus Series B-Chemical and Physical Meteorology*, **62**, 337-351.
House, J., subm.: Comment on "Baseline Map of Carbon Emissions from Deforestation in Tropical Regions". *Science*.
Huang, J., et al., 2008: Estimation of regional emissions of nitrous oxide from 1997 to 2005 using multinetwork measurements, a chemical transport model, and an inverse method. *J. Geophys. Res.*, **113**, D17313.
Huber, C., et al., 2006: Isotope calibrated Greenland temperature record over Marine Isotope Stage 3 and its relation to CH4. *Earth and Planetary Science Letters*, **243**, 504-519.
Hudiburg, T. W., B. E. Law, C. Wirth, and S. Luyssaert, 2011: Regional carbon dioxide implications of forest bioenergy production. *Nature Climate Change*, **1**, 419-423.
Hunter, S. J., D. S. Goldobin, A. M. Haywood, A. Ridgwell, and J. G. Rees, subm.: Sensitivity of the global submarine hydrate inventory to scenarious of future climate change. *Planetary Science Letters*.
Huntingford, C., J. Lowe, B. Booth, C. Jones, G. Harris, L. Gohar, and P. Meir, 2009: Contributions of carbon cycle uncertainty to future climate projection spread. *Tellus Series B-Chemical and Physical Meteorology*, DOI 10.1111/j.1600-0889.2009.00414.x, 355-360.
Hurtt, G. C., et al., 2011: Harmonization of land-use scenarios for the period 1500-2100: 600 years of global gridded annual land-use transitions, wood harvest, and resulting secondary lands. *Climatic Change*, DOI 10.1007/s10584-011-0153-2.
Huybers, P., and C. Langmuir, 2009: Feedback between deglaciation, volcanism, and atmospheric CO2. *Earth and Planetary Science Letters*, **286**, 479-491.
Iglesias-Rodriguez, M. D., et al., 2008: Phytoplankton Calcification in a High-CO2 World. *Science*, **320**, 336-340.
Indermuhle, A., et al., 1999: Holocene carbon-cycle dynamics based on CO2 trapped in ice at Taylor Dome, Antarctica. *Nature*, **398**, 121-126.
Inoue, H. Y., and M. Ishii, 2005: Variations and trends of CO2 in the surface seawater in the Southern Ocean south of Australia between 1969 and 2002. *Tellus 57B*, 58-69.
Ishii, M., N. Kosugi, D. Sasano, S. Saito, T. Midorikawa, and H. Inoue, 2011: Ocean acidification off the south coast of Japan: A result from time series observations of CO2 parameters from 1994 to 2008. *J Geophys Res-Oceans*, **116**, -.
Ishii, M., et al., 2009: Spatial variability and decadal trend of the oceanic CO2 in the western equatorial Pacific warm/fresh water. *Deep-Sea Res Pt Ii*, **56**, 591-606.
Ishijima, K., T. Nakazawa, and S. Aoki, 2009: Variations of atmospheric nitrous oxide concentration in the northern and western Pacific. *Tellus B*, **61**, 408-415.
Ito, A., and J. E. Penner, 2004: Global estimates of biomass burning emissions based on satellite imagery for the year 2000. *J. Geophys. Res.*, **109**, D14S05.
Iudicone, D., et al., 2011: Water masses as a unifying framework for understanding the Southern Ocean Carbon Cycle. *Biogeosciences*, **8**, 1031-1052.
Iversen, T., et al., subm.: The Norwegian Earth System Model, NorESM1-M. Part 2: Climate Response and Scenario Projections. *Geoscientific Model Development*.
Jaccard, S. L., and E. D. Galbraith, 2011: Large climate-driven changes of oceanic oxygen concentrations during the last deglaciation. *Nature Geosci*, **advance online publication**.
Jaccard, S. L., G. H. Haug, D. M. Sigman, T. F. Pedersen, H. R. Thierstein, and U. Röhl, 2005: Glacial/Interglacial changes in subarctic North Pacific stratification. *Science*, **308**, 1003-1006.
Jacobson, A. R., S. E. Mikaloff Fletcher, N. Gruber, J. L. Sarmiento, and M. Gloor, 2007: A joint atmosphere-ocean inversion for surface fluxes of carbon dioxide: 2. Regional results. *Global Biogeochemical Cycles*, **21**.
Jain, A., X. Yang, H. Kheshgi, A. McGuire, W. Post, and D. Kicklighter, 2009: Nitrogen attenuation of terrestrial carbon cycle response to global environmental factors. *Global Biogeochemical Cycles*, **23**, -.
Jain, A. K., P. Meiyappan, Y. Song, and J. I. House, subm.: Estimates of Carbon Emissions from Historical Land-Use and Land-Cover Change. *Biogeosciences*.
Jones, C., and P. Cox, 2001: Modeling the volcanic signal in the atmospheric CO2 record. *Global Biogeochemical Cycles*, 453-465.
Jones, C., S. Liddicoat, and J. Lowe, 2010: Role of terrestrial ecosystems in determining CO2 stabilization and recovery behaviour. *Tellus Series B-Chemical and Physical Meteorology*, DOI 10.1111/j.1600-0889.2010.00490.x, 682-699.
Jones, C., J. Lowe, S. Liddicoat, and R. Betts, 2009: Committed terrestrial ecosystem changes due to climate change. *Nature Geoscience*, DOI 10.1038/ngeo555, 484-487.

Jones, C., et al., 2011: The HadGEM2-ES implementation of CMIP5 centennial simulations. *Geoscientific Model Development*, **4**, 543-570.
Jones, C. D., and P. Falloon, 2009: Sources of uncertainty in global modelling of future soil organic carbon storage. *Uncertainties in Environmental Modelling and Consequences for Policy Making*, P. Bavaye, J. Mysiak, and M. Laba, Eds., Springer, 283-315.
Jones, C. D., P. M. Cox, and C. Huntingford, 2006: Impact of climate carbon cycle feedbacks on emission scenarios to achieve stabilization. *Avoiding Dangerous Climate Change*, W. C. H. J. Schellnhuber, N. Nakicenovic, T. Wigley and G. Yohe, Ed., Cambridge University Press.
Jones, C. D., et al., subm.: 21th century compatible CO2 emissions and airborne fraction simulated by CMIP5 Earth System models under 4 Representative Concentration Pathways. *Journal of Climate*.
Joos, F., T. L. Frölicher, M. Steinacher, and G.-K. s. s. Plattner, 2011: Impact of climate change mitigation on ocean acidification projections. *Ocean Acidification*, J.-P. G. a. L. Hansson, Ed., Oxford University Press.
Joos, F., S. Gerber, I. C. Prentice, B. L. Otto-Bliesner, and P. J. Valdes, 2004: Transient simulations of Holocene atmospheric carbon dioxide and terrestrial carbon since the Last Glacial Maximum. *Global Biogeochemical Cycles*, **18**.
Joos, F., et al., submitted: Carbon dioxide and climate impulse response functions for the computation of greenhouse gas metrics: A multi-model analysis. *Atmospheric Chemistry and Physics*.
Jung, M., et al., 2007: Assessing the ability of three land ecosystem models to simulate gross carbon uptake of forests from boreal to Mediterranean climate in Europe. *Biogeosciences*, **4**, 647-656.
Jung, M., et al., 2011: Global patterns of land-atmosphere fluxes of carbon dioxide, latent heat, and sensible heat derived from eddy covariance, satellite, and meteorological observations. *Journal of Geophysical Research-Biogeosciences*, **116**.
Jungclaus, J. H., et al., 2010: Climate and carbon-cycle variability over the last millennium. *Climate of the Past*, **6**, 723-737.
Kai, F. M., S. C. Tyler, J. T. Randerson, and D. R. Blake, 2011: Reduced methane growth rate explained by decreased Northern Hemisphere microbial sources. *Nature*, **476**, 194-197.
Kammann, C., C. Müller, L. Grünhage, and H.-J. Jäger, 2008: Elevated CO2 stimulates N2O emissions in permanent grassland. *Soil Biology and Biochemistry*, **40**, 2194–2205.
Kaplan, J. O., G. Folberth, and D. A. Hauglustaine, 2006: Role of methane and biogenic volatile organic compound sources in late glacial and Holocene fluctuations of atmospheric methane concentrations. *Global Biogeochemical Cycles*, **20**.
Kaplan, J. O., I. C. Prentice, W. Knorr, and P. J. Valdes, 2002: Modeling the dynamics of terrestrial carbon storage since the Last Glacial Maximum. *Geophysical Research Letters*, **29**.
Kaplan, J. O., K. M. Krumhardt, E. C. Ellis, W. Ruddiman, and K. Klein Goldewijk, 2011: Holocene carbon emissions as a result of anthropogenic land cover change. *The Holocene*, 10.1177/0959683610386983.
Kato, E., T. Kinoshita, A. Ito, M. Kawamiya, and Y. Yamagata, 2012: Evaluation of spatially explicit emission scenario of land-use change and biomass burning using a process-based biogeochemical model. *(in press) Journal of Land Use Science*.
Keeling, C. D., S. C. Piper, and M. Heimann, 1989: A three dimensional model of atmospheric CO2 transport based on observed winds: 4. Mean annual gradients and interannual variations. *Aspects of Climate Variability in the Pacific and the Western Americas*, D. H. Peterson, Ed., AGU, 305-363.
Keeling, C. D., R. B. Bacastow, A. E. Bainbridge, C. A. Ekdahl, P. R. Guenther, L. S. Waterman, and J. F. S. Chin, 1976: Atmospheric carbon-dioxide variations at Mauna-Loa observatory, Hawaii. *Tellus*, **28**, 538-551.
Keeling, C. D., S. C. Piper, R. B. Bacastow, M. Wahlen, T. P. Whorf, M. Heimann, and H. A. Meijer, 2005: Atmospheric CO_2 and $^{13}CO_2$ exchange with the terrestrial biosphere and oceans from 1978 to 2000: observations and carbon cycle implications. *A History of Atmospheric CO_2 and Its Effects on Plants, Animals, and Ecosystems*, J. R. Ehleringer, T. E. Cerling, and M. D. Dearing, Eds., Springer, 83-113.
Keeling, R. F., and S. R. Shertz, 1992: Seasonal and interannual variations in atmospheric oxygen and implications for the global carbon cycle. *Nature*, **358**, 723-727.
Keeling, R. F., S. C. Piper, and M. Heimann, 1996: Global and hemispheric CO2 sinks deduced from changes in atmospheric O2 concentration. *Nature*, **381**, 218-221.
Keeling, R. F., A. Kortzinger, and N. Gruber, 2010: Ocean Deoxygenation in a Warming World. *Annual Review of Marine Science*, **2**, 199-229.
Keenan, T. F., et al., 2012: Terrestrial biosphere model performance for inter-annual variability of land-atmosphere CO2 exchange. *Global Change Biology*, **18**, 1971–1198.
Keith, D. W., M. Ha-Duong, and J. K. Stolaroff, 2006: Climate strategy with CO2 capture from the air. *Climatic Change*, **74**, 17-45.
Kelemen, P. B., and J. Matter, 2008: In situ carbonation of peridotite for CO2 storage. *Proceedings of the National Academy of Sciences of the United States of America*, **105**, 17295-17300.
Keppler, F., J. T. G. Hamilton, M. Brass, and T. Rockmann, 2006: Methane emissions from terrestrial plants under aerobic conditions. *Nature*, **439**, 187-191.
Kesik, M., et al., 2006: Future scenarios of N(2)O and NO emissions from European forest soils. *Journal of Geophysical Research-Biogeosciences*, **111**.

Key, R. M., et al., 2004: A global ocean carbon climatology: Results from Global Data Analysis Project (GLODAP). *Global Biogeochemical Cycles*, **18**.
Khalil, M. A. K., and R. A. Rasmussen, 1989: Climate-induced feed backs for the global cycles of methane and nitrous oxide. *Tellus B*, **41B**, 554-559.
Khalil, M. A. K., C. L. Butenhoff, and R. A. Rasmussen, 2007: Atmospheric Methane: Trends and Cycles of Sources and Sinks. *Environ Sci Technol*, **41**, 2131-2137.
Khatiwala, S., F. Primeau, and T. Hall, 2009: Reconstruction of the history of anthropogenic CO2 concentrations in the ocean. *Nature*, **462**, 346-349.
Kheshgi, H. S., 1995: Sequestering atmospheric carbon-dioxide by incresing ocean alkalinity. *Energy*, **20**, 915-922.
Khvorostyanov, D., P. Ciais, G. Krinner, and S. Zimov, 2008: Vulnerability of east Siberia's frozen carbon stores to future warming. *Geophysical Research Letters*, **35**, -.
Kim, J. H., et al., 2004: North Pacific and North Atlantic sea-surface temperature variability during the holocene. *Quaternary Science Reviews*, **23**, 2141-2154.
Kirschbaum, M. U. F., and A. Walcroft, 2008: No detectable aerobic methane efflux from plant material, nor from adsorption/desorption processes. *Biogeosciences*, **5**, 1551-1558.
Kirschke, S., P. Bousquet, P. Ciais, S. M., P. Canadell, C. Le Quere, and S. Houweling, subm.: Three decades of methane sources and sinks: budgets and variations.
Kleinen, T., V. Brovkin, and R. Getzieh, 2011: A dynamic model of wetland extent and peat accumulation: results for the Holocene. *Biogeosciences Discussions*, **8**, 4805–4839.
Kleinen, T., V. Brovkin, W. von Bloh, D. Archer, and G. Munhoven, 2010: Holocene carbon cycle dynamics. *Geophysical Research Letters*, **37**.
Kloster, S., N. M. Mahowald, J. T. Randerson, and P. L. Lawrence, 2011: The impacts of climate, land use, and demography on fires during the 21st century simulated by CLM-CN. *Biogeosciences Discussion*, **8**, 9709-9746.
Kloster, S., et al., 2010: Fire dynamics during the 20th century simulated by the Community Land Model. *Biogeosciences*, **7**, 1877-1902.
Knorr, W., 2009: Is the airborne fraction of anthropogenic emissions increasing? *Geophysical Research Letters*, **36**, L21710, doi:21710.21029/22009GL040613.
Kohfeld, K. E., and A. Ridgwell, 2009: Glacial-interglacial variability in atmospheric CO2. *Surface Ocean - Lower Atmospheres Processes*, C. L. Q. r. a. E. S. Saltzman, Ed., 350 pp.
Köhler, P., J. Hartmann, and D. A. Wolf-Gladrow, 2010: Geoengineering potential of artificially enhanced silicate weathering of olivine. *Proceedings of the National Academy of Sciences*, **107**, 20228-20233.
Konijnendijk, T. Y. M., S. L. Weber, E. Tuenter, and M. van Weele, 2011: Methane variations on orbital timescales: a transient modeling experiment. *Climate of the Past*, **7**, 635-648.
Koven, C. D., W. J. Riley, and A. Stern, subm.: Analysis of permafrost thermal dynamics and response to climate change in the CMIP5 Earth System Models. *Journal of Climate*.
Koven, C. D., et al., 2011: Permafrost carbon-climate feedbacks accelerate global warming. *Proceedings of the National Academy of Sciences, August 18, 2011*, 10.1073/pnas.1103910108.
Krawchuk, M., M. Moritz, M. Parisien, J. Van Dorn, and K. Hayhoe, 2009: Global Pyrogeography: the Current and Future Distribution of Wildfire. *Plos One*, **4**, -.
Kraxner, F., S. Nilsson, and M. Obersteiner, 2003: Negative emissions from BioEnergy use, carbon capture and sequestration (BECS) - the case of biomass production by sustainable forest management from semi-natural temperate forests. *Biomass Bioenerg.*, **24**, 285-296.
Krinner, G., et al., 2005: A dynamic global vegetation model for studies of the coupled atmosphere-biosphere system. *Global Biogeochemical Cycles*, ARTN GB1015, DOI 10.1029/2003GB002199, -.
Krishnamurthy, A., J. K. Moore, N. Mahowald, C. Luo, S. C. Doney, K. Lindsay, and C. S. Zender, 2009: Impacts of increasing anthropogenic soluble iron and nitrogen deposition on ocean biogeochemistry. *Global Biogeochemical Cycles*, **23**.
Kroeze, C., A. Mosier, and L. Bouwman, 1999: Closing the global N2O budget: A retrospective analysis 1500–1994. *Global Biogeochem. Cycles*, **13**, 1-8.
Kroeze, C., L. Bouwman, and C. P. Slomp, 2007: Sinks for N_2O at the Earth's surface. *Greenhouse Gas Sinks*, *M. H. Raey D.S., J. Grace and K.A. Smith*, Ed., *CAB International*, 227-243.
Kroeze, C., E. Dumont, and S. Seitzinger, 2010: Future trends in emissions of N_2O from rivers and estuaries. *Journal of Integrative Environmental Sciences*, **7**, 71 - 78.
Kurahashi-Nakamura, T., A. Abe-Ouchi, Y. Yamanaka, and K. Misumi, 2007: Compound effects of Antarctic sea ice on atmospheric pCO(2) change during glacial-interglacial cycle. *Geophysical Research Letters*, **34**.
Kurz, W. A., G. Stinson, and G. Rampley, 2008a: Could increased boreal forest ecosystem productivity offset carbon losses from increased disturbances? *Philosophical Transactions of the Royal Society B-Biological Sciences*, **363**, 2261-2269.
Kurz, W. A., G. Stinson, G. J. Rampley, C. C. Dymond, and E. T. Neilson, 2008b: Risk of natural disturbances makes future contribution of Canada's forests to the global carbon cycle highly uncertain. *Proceedings of the National Academy of Sciences*, **105**, 1551-1555.
Lam, P., and M. M. M. Kuypers, 2010: Microbial Nitrogen Cycling Processes in Oxygen Minimum Zones. *Annual Review of Marine Science*, **3**, 317-345.

Lamarque, J.-F., et al., 2010: Historical (1850-2000) gridded anthropogenic and biomass burning emissions of reactive gases and aerosols: methodology and application. *Atmos. Chem. Phys.*, **10**, 7017-7039.
Lamarque, J., 2008: Estimating the potential for methane clathrate instability in the 1%-CO2 IPCC AR-4 simulations. *Geophysical Research Letters*, **35**, -.
Lamarque, J. F., et al., 2011: Global and regional evolution of short-lived radiatively-active gases and aerosols in the Representative Concentration Pathways. *Climatic Change*, **109**, 191-212.
Langenfelds, R. L., R. J. Francey, B. C. Pak, L. P. Steele, J. Lloyd, C. M. Trudinger, and C. E. Allison, 2002: Interannual growth rate variations of atmospheric CO_2 and its $d^{13}C$, H_2, CH_4, and CO between 1992 and 1999 linked to biomass burning. *Global Biogeochemical Cycles*, **16**, 1048, doi:1010.1029/2001GB001466.
Langner, J., R. Bergstrom, and V. Foltescu, 2005: Impact of climate change on surface ozone and deposition of sulphur and nitrogen in Europe. *Atmospheric Environment*, **39**, 1129-1141.
Lassey, K. R., D. C. Lowe, and A. M. Smith, 2007: The atmospheric cycling of radiomethane and the "fossil fraction" of the methane source. *Atmos Chem Phys*, **7**, 2141-2149.
Lawrence, D., and A. Slater, 2005: A projection of severe near-surface permafrost degradation during the 21st century. *Geophysical Research Letters*, **32**, -.
Lawrence, D., A. Slater, V. Romanovsky, and D. Nicolsky, 2008: Sensitivity of a model projection of near-surface permafrost degradation to soil column depth and representation of soil organic matter. *Journal of Geophysical Research-Earth Surface*, **113**, -.
Lawrence, D., et al., 2011: Parameterization Improvements and Functional and Structural Advances in Version 4 of the Community Land Model. *Journal of Advances in Modeling Earth Systems*, **3**, 27 pp.
Lawrence, P. J., et al., 2012: Simulating the biogeochemical and biogeophysical impacts of transient land cover change and wood harvest in the Community Climate System Model (CCSM4) from 1850 to 2100. *Journal of Climate*, **25**, 3071-3095.
Le Quere, C., et al., 2007: Saturation of the Southern Ocean CO2 sink due to recent climate change. *Science*, **316**, 1735-1738.
Le Quere, C., et al., 2009: Trends in the sources and sinks of carbon dioxide. *Nature Geoscience*, **2**, 831-836.
LeBauer, D. S., and K. K. Treseder, 2008: Nitrogen limitation of net primary productivity in terrestrial ecosystems is globally distributed. *Ecology*, **89**, 371-379.
Lee, X., et al., 2011: Observed increase in local cooling effect of deforestation at higher latitudes. *Nature*, **479**, 384-387.
Lemmen, C., 2009: World distribution of land cover changes during Pre- and Protohistoric Times and estimation of induced carbon releases. *Geomorphologie-Relief Processus Environnement*, 303-312.
Lenton, A., and R. J. Matear, 2007: Role of the Southern Annular Mode (SAM) in Southern Ocean CO2 uptake. *Global Biogeochemical Cycles*, **21**, -.
Lenton, A., F. Codron, L. Bopp, N. Metzl, P. Cadule, A. Tagliabue, and J. Le Sommer, 2009: Stratospheric ozone depletion reduces ocean carbon uptake and enhances ocean acidification. *Geophysical Research Letters*, **36**, -.
Lenton, T. M., and C. Britton, 2006: Enhanced carbonate and silicate weathering accelerates recovery from fossil fuel CO2 perturbations. *Global Biogeochemical Cycles*, **20**.
Lenton, T. M., and N. E. Vaughan, 2009: The radiative forcing potential of different climate geoengineering options. *Atmospheric Chemistry and Physics*, **9**, 5539-5561.
LePage, Y., G. R. van der Werf, D. C. Morton, and J. M. C. Pereira, 2010: Modeling fire-driven deforestation potential in Amazonia under current and projected climate conditions. *Journal of Geophysical Research-Biogeosciences*, **115**, -.
Lepisto, A., P. Kortelainen, and T. Mattsson, 2008: Increased organic C and N leaching in a northern boreal river basin in Finland. *Global Biogeochemical Cycles*, **22**.
LeQuere, C., T. Takahashi, E. T. Buitenhuis, C. Rodenbeck, and S. C. Sutherland, 2010: Impact of climate change and variability on the global oceanic sink of CO2. *Global Biogeochemical Cycles*, **24**, -.
LeQuere, C., et al., 2009: Trends in the sources and sinks of carbon dioxide. *Nature Geoscience*, **2**, 831-836.
Levin, I., et al., 2010: Observations and modelling of the global distribution and long-term trend of atmospheric 14CO 2. *Tellus B*, **62**, 26-46.
Levin, I., et al., 2012: No inter-hemispheric [dgr]13CH4 trend observed. *Nature*, **486**, E3-E4.
Levine, J. G., et al., 2011: Reconciling the changes in atmospheric methane sources and sinks between the Last Glacial Maximum and the pre-industrial era. *Geophys. Res. Lett.*, **38**, L23804.
Levy, P. E., M. G. R. Cannell, and A. D. Friend, 2004: Modelling the impact of future changes in climate, CO2 concentration and land use on natural ecosystems and the terrestrial carbon sink. *Global Environmental Change*, **14**, 21-30.
Lewis, S. L., P. M. Brando, O. L. Phillips, G. M. F. v. d. Heijden, and D. Nepstad, 2011: The 2010 Amazon Drought. *Science*, **331**, 554.
Lewis, S. L., et al., 2009: Increasing carbon storage in intact African tropical forests. *Nature*, **457**, 1003-1006.
Liberloo, M., et al., 2009: Coppicing shifts CO2 stimulation of poplar productivity to above-ground pools: a synthesis of leaf to stand level results from the POP/EUROFACE experiment. *New Phytologist*, **182**, 331–346.
Liddicoat, S., C. Jones, and E. Robertson, subm.: CO2 emissions determined by HadGEM2-ES to be compatible with the Representative Concentration Pathway scenarious and their extension. *Journal of Climate*.

Lindsay, K., et al., subm.: Preindustrial Control and 20th Century Carbon Cycle. Experiments with the Earth System Model CESM1-(BGC). *Journal of Climate*.
Lohila, A., M. Aurela, J. Hatakka, M. Pihlatie, K. Minkkinen, T. Penttila, and T. Laurila, 2010: Responses of N2O fluxes to temperature, water table and N deposition in a northern boreal fen. *European Journal of Soil Science*, **61**, 651-661.
Loose, B., and P. Schlosser, 2011: Sea ice and its effect on CO2 flux between the atmosphere and the Southern Ocean interior. *J Geophys Res-Oceans*, **116**.
Loulergue, L., et al., 2008: Orbital and millennial-scale features of atmospheric CH4 over the past 800,000 years. *Nature*, **453**, 383-386.
Lourantou, A., and N. Metzl, 2011: Decadal evolution of carbon sink within a strong bloom area in the subantarctic zone. *Geophysical Research Letters*, **38**.
Lovenduski, N. S., N. Gruber, S. C. Doney, and I. D. Lima, 2007: Enhanced CO2 outgassing in the Southern Ocean from a positive phase of the Southern Annular Mode. *Global Biogeochemical Cycles*, **21**, -.
Lucht, W., et al., 2002: Climatic control of the high-latitude vegetation greening trend and Pinatubo effect. *Science*, 1687-1689.
Luo, Y., et al., 2004: Progressive Nitrogen Limitation of Ecosystem Responses to Rising Atmospheric Carbon Dioxide. *Bioscience*, **54**, 731-739.
Luo, Y. Q., 2007: Terrestrial carbon-cycle feedback to climate warming. *Annu Rev Ecol Evol S*, **38**, 683-712.
Luthi, D., et al., 2008: High-resolution carbon dioxide concentration record 650,000-800,000 years before present. *Nature*, **453**, 379-382.
Luyssaert, S., et al., 2010: The European carbon balance. Part 3: forests. *Global Change Biology*, **16**, 1429-1450.
MacDonald, G. M., K. V. Kremenetski, and D. W. Beilman, 2008: Climate change and the northern Russian treeline zone. *Philosophical Transactions of the Royal Society B-Biological Sciences*, **363**, 2285-2299.
MacFarling-Meure, C., et al., 2006: Law Dome CO(2), CH(4) and N(2)O ice core records extended to 2000 years BP. *Geophysical Research Letters*, **33**.
Magnani, F., et al., 2007: The human footprint in the carbon cycle of temperate and boreal forests. *Nature*, **447**, 848-850.
Mahowald, N., 2011: Aerosol Indirect Effect on Biogeochemical Cycles and Climate. *Science*, **334**, 794-796.
Mahowald, N., et al., 1999: Dust sources and deposition during the last glacial maximum and current climate: A comparison of model results with paleodata from ice cores and marine sediments. *Journal of Geophysical Research-Atmospheres*, **104**, 15895-15916.
Mahowald, N., et al., 2009: Atmospheric Iron Deposition: Global Distribution, Variability, and Human Perturbations. *Annual Review of Marine Science*, **1**, 245-278.
Mahowald, N. M., D. R. Muhs, S. Levis, P. J. Rasch, M. Yoshioka, C. S. Zender, and C. Luo, 2006: Change in atmospheric mineral aerosols in response to climate: Last glacial period, preindustrial, modern, and doubled carbon dioxide climates. *Journal of Geophysical Research-Atmospheres*, **111**.
Mahowald, N. M., et al., 2011: Desert dust and anthropogenic aerosol interactions in the Community Climate System Model coupled-carbon-climate model. *Biogeosciences*, **8**, 387-414.
Mahowald, N. M., et al., 2010: Observed 20th century desert dust variability: impact on climate and biogeochemistry. *Atmospheric Chemistry and Physics*, **10**, 10875-10893.
Maier-Reimer, E., I. Kriest, J. Segschneider, and P. Wetzel, 2005: The HAMburg Ocean Carbon Cycle model HAMOCC 5.1 – Technical description, Release 1.1. Max-Planck Institute for Meteorology.
Manning, A. C., and R. F. Keeling, 2006: Global oceanic and land biotic carbon sinks from the Scripps atmospheric oxygen flask sampling network. *Tellus Series B-Chemical and Physical Meteorology*, **58**, 95-116.
Marchand, F. L., I. Nijs, H. J. de Boeck, F. Kockelbergh, S. Mertens, and L. Beyens, 2004: Increased turnover but little change in the carbon balance of High-Arctic tundra exposed to whole growing season warming. *Arct Antarct Alp Res*, **36**, 298-307.
Marchenko, S. S., V. Romanovsky, and G. S. Tipenko, 2008: Numerical modeling of spatial permafrost dynamics in Alaska. *Ninth International Conference on Permafrost.*
Marland, G., and R. M. Rotty, 1984: Carbon-dioxide emissions from fossil-fuels - A procedure for estimation and results for 1950 - 1982. *Tellus Series B-Chemical and Physical Meteorology*, **36**, 232-261.
Marlon, J. R., et al., 2008: Climate and human influences on global biomass burning over the past two millennia. *Nature Geoscience*, **1**, 697-702.
Martin, J. H., 1990: Glacial-interglacial CO2 change: the iron hypothesis. *Paleoceanography*, **5**, 1-13.
Masarie, K. A., and P. P. Tans, 1995: Extension and integration of atmospheric carbon-dioxide data into a globally consistent measurement record. *Journal of Geophysical Research-Atmospheres*, **100**, 11593-11610.
Matear, R. J., and A. C. Hirst, 2003: Long-term changes in dissolved oxygen concentrations in the ocean caused by protracted global warming. *Global Biogeochem. Cycles*, **17**, 1125.
Matear, R. J., and B. I. McNeil, 2003: Decadal accumulation of anthropogenic CO2 in the Southern Ocean: A comparison of CFC-age derived estimates to multiple-linear regression estimates. *Global Biogeochemical Cycles*, **17**.
Matear, R. J., A. C. Hirst, and B. I. McNeil, 2000: Changes in dissolved oxygen in the Southern Ocean with climate change. *Geochem. Geophys. Geosyst.*, **1**.

Matear, R. J., Y. P. Wang, and A. Lenton, 2010: Land and ocean nutrient and carbon cycle interactions. *Current Opinion in Environmental Sustainability*, **2**, 258-263.
Matsumoto, K., 2007: Biology-mediated temperature control on atmospheric pCO(2) and ocean biogeochemistry. *Geophysical Research Letters*, **34**.
Matsumoto, K., J. L. Sarmiento, and M. A. Brzezinski, 2002: Silicic acid leakage from the Southern Ocean: A possible explanation for glacial atmospheric pCO(2). *Global Biogeochemical Cycles*, **16**.
Matsumoto, K., et al., 2004: Evaluation of ocean carbon cycle models with data-based metrics. *Geophysical Research Letters*, **31**.
Matthews, H. D., 2006: Emissions targets for CO2 stabilization as modified by carbon cycle feedbacks. *Tellus*, **58B**, 591-602.
Matthews, H. D., A. J. Weaver, and K. J. Meissner, 2005: Terrestrial carbon cycle dynamics under recent and future climate change. *Journal of Climate*, **18**, 1609-1628.
Mau, S., D. Valentine, J. Clark, J. Reed, R. Camilli, and L. Washburn, 2007: Dissolved methane distributions and air-sea flux in the plume of a massive seep field, Coal Oil Point, California. *Geophysical Research Letters*, **34**.
Mayorga, E., et al., 2010: Global Nutrient Export from WaterSheds 2 (NEWS 2): Model development and implementation. *Environmental Modelling & Software*, **25**, 837-853.
McCarthy, H. R., et al., 2010: Re-assessment of plant carbon dynamics at the Duke free-air CO2 enrichment site: interactions of atmospheric [CO2] with nitrogen and water availability over stand development. *New Phytologist*, **185**, 514-528.
McGuire, A. D., et al., 2009: Sensitivity of the carbon cycle in the Arctic to climate change. *Ecological Monographs*, **79**, 523-555.
McGuire, A. D., et al., 2012: An assessment of the carbon balance of arctic tundra: comparisons among observations, process models, and atmospheric inversions. *Biogeosciences Discussions*, **9**, 4543-4459.
McInerney, F. A., and S. L. Wing, 2011: The Paleocene-Eocene Thermal Maximum: A Perturbation of Carbon Cycle, Climate, and Biosphere with Implications for the Future. *Annual Review of Earth and Planetary Sciences*, **39**, 489-516.
McIntyre, B. D., H. R. Herren, J. Wakhungu, and R. T. Watson, 2009: International assessment of agricultural knowledge, science and technology for development (IAASTD): global report, 590 pp.
McKinley, G., A. Fay, T. Takahashi, and N. Metzl, 2011: Convergence of atmospheric and North Atlantic carbon dioxide trends on multidecadal timescales. *Nature Geoscience*, **4**, 606-610.
McKinley, G. A., et al., 2006: North Pacific carbon cycle response to climate variability on seasonal to decadal timescales. *J Geophys Res-Oceans*, **111**, -.
McNeil, B., and R. Matear, 2006: Projected climate change impact on oceanic acidification. *Carbon balance and management*, 10.1186/1750-0680-1-2.
McNeil, B. I., and R. J. Matear, 2008: Southern Ocean acidification: A tipping point at 450-ppm atmospheric CO2. *Proceedings of the National Academy of Sciences of the United States of America*, **105**, 18860-18864.
McWethy, D. B., C. Whitlock, J. M. Wilmshurst, M. S. McGlone, and X. Li, 2009: Rapid deforestation of South Islands, New Zealands, by early Polynesian fires. *Holocene*, **19**, 883-897.
Medlyn, B. E., 2011: Comment on "Drought-induced reductions in global terrestrial net primary production from 2000 through 2009". *Science*, **333**, 1093-d.
Meehl, G. H., et al., 2007: Global Climate Projections. Climate Change 2007: The Physical Science Basis. Contribution of Working Group1 to the Forth Assessment Report of the Intergovernmental Panel on Climate Change, 747-846 pp.
Meinshausen, M., et al., 2011: The RCP greenhouse gas concentrations and their extensions from 1765 to 2300. *Climatic Change*, **109**, 213-241.
Melillo, J., et al., 2011: Soil warming, carbon-nitrogen interactions, and forest carbon budgets. *Proceedings of the National Academy of Sciences of the United States of America*, **108**, 9508-9512.
Melton, J. R., et al., subm.: Present state of global wetland extent and wetland methane modelling: Conclusions from a model intercomparison project (WETCHIMP). *Biogeosciences*.
Menviel, L., and F. Joos, 2012: Toward explaining the Holocene carbon dioxide and carbon isotope records: Results from transient ocean carbon cycle-climate simulations. *Paleoceanography*, **27**.
Menviel, L., F. Joos, and S. P. Ritz, subm.: Atmospheric CO2, C13 and the marine carbonate cycle during the last glacial-interglacial cycle: results from transient simulations with the Bern3D model. *Quaternary Science Reviews*.
Menviel, L., A. Timmermann, A. Mouchet, and O. Timm, 2008: Meridional reorganizations of marine and terrestrial productivity during Heinrich events. *Paleoceanography*, **23**.
Mercado, L. M., N. Bellouin, S. Sitch, O. Boucher, C. Huntingford, M. Wild, and P. M. Cox, 2009: Impact of changes in diffuse radiation on the global land carbon sink. *Nature*, **458**, 1014-U1087.
Merico, A., T. Tyrrell, and T. Cokacar, 2006: Is there any relationship between phytoplankton seasonal dynamics and the carbonate system? *Journal of Marine Systems*, **59**, 120-142.
Metzl, N., 2009: Decadal increase of oceanic carbon dioxide in Southern Indian Ocean surface waters (1991-2007). *Deep-Sea Res Pt Ii*, **56**, 607-619.

Metzl, N., et al., 2010: Recent acceleration of the sea surface fCO(2) growth rate in the North Atlantic subpolar gyre (1993-2008) revealed by winter observations. *Global Biogeochemical Cycles*, **24**, -.
Mieville, A., et al., 2010: Emissions of gases and particles from biomass burning during the 20th century using satellite data and an historical reconstruction. *Atmospheric Environment*, **44**, 1469-1477.
Mikaloff-Fletcher, S. E., et al., 2006: Inverse estimates of anthropogenic CO2 uptake, transport, and storage by the ocean. *Global Biogeochemical Cycles*, **20**.
Mischler, J. A., et al., 2009: Carbon and hydrogen isotopic composition of methane over the last 1000 years. *Global Biogeochemical Cycles*, **23**.
Mitchell, L. E., E. J. Brook, T. Sowers, J. R. McConnell, and K. Taylor, 2011: Multidecadal variability of atmospheric methane, 1000-1800 CE. *Journal of Geophysical Research-Biogeosciences*, **116**.
Mitsch, W., A. Nahlik, P. Wolski, B. Bernal, L. Zhang, and L. Ramberg, 2010: Tropical wetlands: seasonal hydrologic pulsing, carbon sequestration, and methane emissions. *Wetlands Ecology and Management*, **18**, 573-586.
Miyama, T., and M. Kawamiya, 2009: Estimating allowable carbon emission for CO2 concentration stabilization using a GCM-based Earth system model. *Geophysical Research Letters*, **36**, -.
Monnin, E., et al., 2001: Atmospheric CO2 concentrations over the last glacial termination. *Science*, **291**, 112-114.
Monnin, E., et al., 2004: Evidence for substantial accumulation rate variability in Antarctica during the Holocene, through synchronization of CO2 in the Taylor Dome, Dome C and DML ice cores. *Earth and Planetary Science Letters*, **224**, 45-54.
Monteil, G., S. Houweling, E. J. Dlugockenky, G. Maenhout, B. H. Vaughn, J. W. C. White, and T. Rockmann, 2011: Interpreting methane variations in the past two decades using measurements of CH(4) mixing ratio and isotopic composition. *Atmospheric Chemistry and Physics*, **11**, 9141-9153.
Monteith, D. T., et al., 2007: Dissolved organic carbon trends resulting from changes in atmospheric deposition chemistry. *Nature*, **450**, 537-U539.
Montenegro, A., V. Brovkin, M. Eby, D. Archer, and A. J. Weaver, 2007: Long term fate of anthropogenic carbon. *Geophysical Research Letters*, **34**.
Montzka, S. A., M. Krol, E. Dlugokencky, B. Hall, P. Joeckel, and J. Lelieveld, 2011: Small Interannual Variability of Global Atmospheric Hydroxyl. *Science*, **331**, 67-69.
Morford, S. L., B. Z. Houlton, and R. A. Dahlgren, 2011: Increased forest ecosystem carbon and nitrogen storage from nitrogen rich bedrock. *Nature*, **477**, 78-81.
Mosier, A., C. Kroeze, C. Nevison, O. Oenema, S. Seitzinger, and O. van Cleemput, 1998: Closing the global N2O budget: nitrous oxide emissions through the agricultural nitrogen cycle - OECD/IPCC/IEA phase II development of IPCC guidelines for national greenhouse gas inventory methodology. *Nutrient Cycling in Agroecosystems*, **52**, 225-248.
Mosier, A. R., J. A. Morgan, J. Y. King, D. LeCain, and D. G. Milchunas, 2002: Soil-atmosphere exchange of CH4, CO2, NOx, and N2O in the Colorado shortgrass steppe under elevated CO2. *Plant and Soil*, **240**, 201-211.
Moss, R., et al., 2010: The next generation of scenarios for climate change research and assessment. *Nature*, **463**, 747-756.
Murata, A., Y. Kumamoto, S. Watanabe, and M. Fukasawa, 2007: Decadal increases of anthropogenic CO2 in the South Pacific subtropical ocean along 32 degrees S. *J Geophys Res-Oceans*, **112**.
Murata, A., Y. Kumamoto, K.-i. Sasaki, S. Watanabe, and M. Fukasawa, 2009: Decadal increases of anthropogenic CO(2) along 149 degrees E in the western North Pacific. *J Geophys Res-Oceans*, **114**.
Murata, A., Y. Kumamoto, K. Sasaki, S. Watanabe, and M. Fukasawa, 2010: Decadal increases in anthropogenic CO2 along 20 degrees S in the South Indian Ocean. *J Geophys Res-Oceans*, **115**.
Nabuurs, G. J., et al., 2008: Hotspots of the European forests carbon cycle. *Forest Ecology and Management*, **256**, 194-200.
Naqvi, S. W. A., H. W. Bange, L. Farias, P. M. S. Monteiro, M. I. Scranton, and J. Zhang, 2009: Coastal hypoxia/anoxia as a source of CH4 and N2O. *Biogeosciences Discuss.*, **6**, 9455-9523.
Neef, L., M. van Weele, and P. van Velthoven, 2010: Optimal estimation of the present-day global methane budget. *Global Biogeochemical Cycles*, **24**.
Neftel, A., H. Oeschger, J. Schwander, B. Stauffer, and R. Zumbrunn, 1982: Ice core sample measurements give atmospheric CO2 content during the past 40,000 yr. *Nature*, **295**, 220-223.
Nemani, R. R., et al., 2003: Climate-driven increases in global terrestrial net primary production from 1982 to 1999. *Science*, **300**, 1560-1563.
Nepstad, D. C., I. M. Tohver, D. Ray, P. Moutinho, and G. Cardinot, 2007: Mortality of large trees and lianas following experimental drought in an Amazon forest. *Ecology*, **88**, 2259-2269.
Nepstad, D. C., et al., 2002: The effects of partial throughfall exclusion on canopy processes, aboveground production, and biogeochemistry of an Amazon forest. *J. Geophys. Res.*, **107**, 8085.
Nevison, C., J. H. Butler, and J. W. Elkins, 2003: Global distribution of N2O and the ΔN2O-AOU yield in the subsurface ocean. *Global Biogeochem. Cycles*, **17**, 1119.
Nevison, C. D. D., E. Dutton, G. Elkins, J. W. Fraser, P. Hall, B. Krummel, P. B. Langenfelds, R. L. O'Doherty, S. Prinn, R. G. Steele, L. P. Weiss, R. F., 2011: Exploring causes of interannual variability in the seasonal cycles of tropospheric nitrous oxide. *Atmospheric Chemistry and Physics*, **11**, 3713–3730.

Nevle, R. J., and D. K. Bird, 2008: Effects of syn-pandemic fire reduction and reforestation in the tropical Americas on atmospheric CO2 during European conquest. *Palaeogeography Palaeoclimatology Palaeoecology*, **264**, 25-38.
Nevle, R. J., D. K. Bird, W. F. Ruddiman, and R. A. and Dull, 2011: Neotropical human landscape interactions, fire, and atmospheric CO_2 during European conquest. *The Holocene*.
Nisbet, R. E. R., et al., 2009: Emission of methane from plants. *Proceedings of the Royal Society B-Biological Sciences*, **276**, 1347-1354.
Norby, R. J., J. M. Warren, C. M. Iversen, B. E. Medlyn, and R. E. McMurtrie, 2010: CO2 enhancement of forest productivity constrained by limited nitrogen availability. *Proceedings of the National Academy of Sciences of the United States of America*, **107**, 19368-19373.
Norby, R. J., et al., 2005: Forest response to elevated CO2 is conserved across a broad range of productivity. *Proceedings of the National Academy of Sciences of the United States of America*, **102**, 18052-18056.
Nowak, R. S., D. S. Ellsworth, and S. D. Smith, 2004: Functional responses of plants to elevated atmospheric CO2 - do photosynthetic and productivity data from FACE experiments support early predictions? *New Phytologist*, **162**, 253-280.
O'Connor, F. M., et al., 2010: Possible role of wetlands, permafrost, and methane hydrates in the methane cycle under future climate change: A review. *Reviews of Geophysics*, ARTN RG4005, DOI 10.1029/2010RG000326, -.
Oh, N.-H., and P. A. Raymond, 2006: Contribution of agricultural liming to riverine bicarbonate export and CO2 sequestration in the Ohio River basin. *Global Biogeochemical Cycles*, **20**.
Oleson, K. W., et al., 2010: Technical description of version 4.0 of the Community Land Model (CLM).
Olivier, J., J. Aardenne, F. Dentener, L. Ganzeveld, and J. Peters, 2005: Recent trends in global greenhouse emissions: regional trends 1970-2000 and spatial distribution of key sources in 2000. *Environmental Science*, **2**, 81-99.
Olofsson, J., and T. Hickler, 2008: Effects of human land-use on the global carbon cycle during the last 6,000 years. *Vegetation History and Archaeobotany*, **17**, 605-615.
Olsen, A., et al., 2006: Magnitude and origin of the anthropogenic CO2 increase and C-13 Suess effect in the Nordic seas since 1981. *Global Biogeochemical Cycles*, **20**.
Orr, J., et al., 2001: Estimates of anthropogenic carbon uptake from four three-dimensional global ocean models. *Global Biogeochemical Cycles*, **15**, 43-60.
Orr, J. C., 2011: Future changes in ocean carbonate chemistry. *Ocean Acidification*, J.-P. G. a. L. Hansson, Ed., Oxford University Press.
Orr, J. C., V. J. Fabry, O. Aumont, and *i.* s. e. al., 2005: Anthropogenic ocean acidification over the twenty-first century and its impact on calcifying organisms. *Nature*, **437**, 681-686.
Oschlies, A., 2001: Model-derived estimates of new production: New results point towards lower values. *Deep-Sea Res Pt Ii*, **48**, 2173-2197.
Oschlies, A., K. G. Schulz, U. Riebesell, and A. Schmittner, 2008: Simulated 21st century's increase in oceanic suboxia by CO2-enhanced biotic carbon export. *Global Biogeochem. Cycles*, **22**, GB4008.
Oschlies, A., K. W., W. Rickels, and K. Rehdanz, 2010a: Side effects and accounting aspects of hypothetical large-scale Southern Ocean iron fertilization. *Biogeosciences*, **7**, 4017-4035.
Otto, D., D. Rasse, J. Kaplan, P. Warnant, and L. Francois, 2002: Biospheric carbon stocks reconstructed at the Last Glacial Maximum: comparison between general circulation models using prescribed and computed sea surface temperatures. *Global and Planetary Change*, **33**, 117-138.
Pacala, S. W., et al., 2001: Consistent land- and atmosphere-based US carbon sink estimates. *Science*, **292**, 2316-2320.
Page, S. E., J. O. Rieley, and C. J. Banks, 2010: Global and regional importance of the tropical peatland carbon pool. *Global Change Biology*, **17**, 798-818.
Page, S. E., F. Siegert, J. O. Rieley, H.-D. V. Boehm, A. Jayak, and S. Limin, 2002: The amount of carbon released from peat and forest fires in Indonesia during 1997. *Nature*, **420**, 61-65.
Palmroth, S., et al., 2006: Aboveground sink strength in forests controls the allocation of carbon below ground and its [CO2]-induced enhancement. *PNAS*, **103**, 19362-19367.
Pan, Y. D., et al., 2011: A Large and Persistent Carbon Sink in the World's Forests. *Science*, **333**, 988-993.
Parekh, P., F. Joos, and S. A. Müller, 2008: A modeling assessment of the interplay between aeolian iron fluxes and iron-binding ligands in controlling carbon dioxide fluctuations during Antarctic warm events. *Paleoceanography*, **23**.
Park, G.-H., et al., 2010: Variability of global net air-sea CO2 fluxes over the last three decades using empirical relationships. *Tellus B*, **62**, 352-368.
Park, S., et al., 2012: Trends and seasonal cycles in the isotopic composition of nitrous oxide since 1940. *Nature Geosci*, **5**, 261-265.
Pechony, O., and D. Shindell, 2010: Driving forces of global wildfires over the past millennium and the forthcoming century. *Proceedings of the National Academy of Sciences of the United States of America*, **107**, 19167-19170.
Peng, T. H., R. Wanninkhof, and R. A. Feely, 2003: Increase of anthropogenic CO2 in the Pacific Ocean over the last two decades. *Deep-Sea Res Pt Ii*, **50**, 3065-3082.
Peng, T. H., R. Wanninkhof, J. L. Bullister, R. A. Feely, and T. Takahashi, 1998: Quantification of decadal anthropogenic CO2 uptake in the ocean based on dissolved inorganic carbon measurements. *Nature*, **396**, 560-563.

Peñuelas, J., J. G. Canadell, and R. Ogaya, 2011: Increased water-use-efficiency during the 20th century did not translate into enhanced tree growth. *Global Ecology and Biogeography*, **20**, 597-608.
Perez, F. F., M. Vazquez-Rodriguez, E. Louarn, X. A. Padin, H. Mercier, and A. F. Rios, 2008: Temporal variability of the anthropogenic CO2 storage in the Irminger Sea. *Biogeosciences*, **5**, 1669-1679.
Perrin, A.-S., A. Probst, and J.-L. Probst, 2008: Impact of nitrogenous fertilizers on carbonate dissolution in small agricultural catchments: Implications for weathering CO2 uptake at regional and global scales. *Geochimica Et Cosmochimica Acta*, **72**, 3105-3123.
Pershing, A. J., L. B. Christensen, N. R. Record, G. D. Sherwood, and P. B. Stetson, 2010: The Impact of Whaling on the Ocean Carbon Cycle: Why Bigger Was Better. *Plos One*, **5**.
Peters, G. P., G. Marland, C. Le Quéré, T. Boden, J. G. Canadell, and M. R. Raupach, 2012: Correspondence: Rapid growth in CO_2 emissions after the 2008-2009 global financial crisis. *Nature Climate Change*, **2**, 2-4.
Petit, J. R., et al., 1999: Climate and atmospheric history of the past 420,000 years from the Vostok ice core, Antarctica. *Nature*, **399**, 429-436.
Petrenko, V. V., et al., 2009: (CH4)-C-14 Measurements in Greenland Ice: Investigating Last Glacial Termination CH4 Sources. *Science*, **324**, 506-508.
Peylin, P., et al., 2005: Multiple constraints on regional CO2 flux variations over land and oceans. *Global Biogeochemical Cycles*, ARTN GB1011, DOI 10.1029/2003GB002214, -.
Pfeil, B., et al., subm.: A Uniform, Quality Controlled Surface Ocean CO2 Atlas (SOCAT). *Earth System Science Data*.
Phoenix, G., et al., 2006: Atmospheric nitrogen deposition in world biodiversity hotspots: the need for a greater global perspective in assessing N deposition impacts. *Global Change Biology*, **12**, 470-476.
Piao, S., P. Friedlingstein, P. Ciais, L. Zhou, and A. Chen, 2006: Effect of climate and CO2 changes on the greening of the Northern Hemisphere over the past two decades. *Geophysical Research Letters*, ARTN L23402, DOI 10.1029/2006GL028205, -.
Piao, S., et al., 2011: Contribution of climate change and rising CO_2 to terrestrial carbon balance in East Asia: A multi-model analysis. *Global and Planetary Change*, **75**, 133-142.
Piao, S., et al., subm.: Evaluation of terrestrial carbon cycle models for their sensitivity to climate variability and the observed rise in atmospheric CO_2 abundance. *Global Change Biology*.
Piao, S. L., J. Y. Fang, P. Ciais, P. Peylin, Y. Huang, S. Sitch, and T. Wang, 2009a: The carbon balance of terrestrial ecosystems in China. *Nature*, **458**, 1009-U1082.
Piao, S. L., P. Ciais, P. Friedlingstein, N. de Noblet-Ducoudre, P. Cadule, N. Viovy, and T. Wang, 2009b: Spatiotemporal patterns of terrestrial carbon cycle during the 20th century. *Global Biogeochemical Cycles*, **23**, -.
Pison, I., P. Bousquet, F. Chevallier, S. Szopa, and D. Hauglustaine, 2009: Multi-species inversion of CH4, CO and H-2 emissions from surface measurements. *Atmospheric Chemistry and Physics*, **9**, 5281-5297.
Plattner, G.-K., et al., 2008: Long-term climate commitments projected with climate-carbon cycle models. *Journal of Climate*, DOI 10.1175/2007JCLI1905.1, 2721-2751.
Plattner, G. K., F. Joos, and T. Stocker, 2002: Revision of the global carbon budget due to changing air-sea oxygen fluxes. *Global Biogeochemical Cycles*, **16**, 1096.
Plattner, G. K., F. Joos, T. F. Stocker, and O. Marchal, 2001: Feedback mechanisms and sensitivities of ocean carbon uptake under global warming. *Tellus Series B-Chemical and Physical Meteorology*, **53**, 564-592.
Plug, L. J., and J. J. West, 2009: Thaw lake expansion in a two-dimensional coupled model of heat transfer, thaw subsidence, and mass movement. *Journal of Geophysical Research-Earth Surface*, **114**, -.
Pongratz, J., C. H. Reick, T. Raddatz, and M. Claussen, 2009: Effects of anthropogenic land cover change on the carbon cycle of the last millennium. *Global Biogeochemical Cycles*, **23**.
Pongratz, J., K. Caldeira, C. H. Reick, and M. Claussen, 2011: Coupled climateâ€"carbon simulations indicate minor global effects of wars and epidemics on atmospheric CO2 between AD 800 and 1850. *The Holocene*, 10.1177/0959683610386981.
Poulter, B., et al., 2010: Net biome production of the Amazon Basin in the 21st century. *Global Change Biology*, **16**, 2062-2075.
Power, M. J., et al., 2008: Changes in fire regimes since the Last Glacial Maximum: an assessment based on a global synthesis and analysis of charcoal data. *Climate Dynamics*, **30**, 887-907.
Prentice, I. C., and S. P. Harrison, 2009: Ecosystem effects of CO_2 concentration: evidence from past climates. *Climate of the Past*, **5**, 297-307.
Prentice, I. C., et al., 2001: The Carbon Cycle and Atmospheric Carbon Dioxide. *Climate Change 2001: The Scientific Basis*, J. T. Houghton, et al., Eds., Cambridge University Press.
Prinn, R. G., et al., 2001: Evidence for substantial variations of atmospheric hydroxyl radicals in the past two decades. *Science*, **292**, 1882-1888.
Prinn, R. G., et al., 2005: Evidence for variability of atmospheric hydroxyl radicals over the past quarter century. *Geophysical Research Letters*, **32**.
Prinn, R. G., et al., 2000: A history of chemically and radiatively important gases in air deduced from ALE/GAGE/AGAGE. *Journal of Geophysical Research-Atmospheres*, **105**, 17751-17792.
Quinton, J. N., G. Govers, K. Van Oost, and R. D. Bardgett, 2010: The impact of agricultural soil erosion on biogeochemical cycling. *Nature Geoscience*, **3**, 311 - 314.

Rabalais, N. N., R. J. Diaz, L. A. Levin, R. E. Turner, D. Gilbert, and J. Zhang, 2010: Dynamics and distribution of natural and human-caused hypoxia. *Biogeosciences*, **7**, 585-619.
Raddatz, T., et al., 2007: Will the tropical land biosphere dominate the climate-carbon cycle feedback during the twenty-first century? *Climate Dynamics*, **29**, 565-574.
Rafelski, L. E., S. C. Piper, and R. F. Keeling, 2009: Climate effects on atmospheric carbon dioxide over the last century. *Tellus B*, **61**, 718-731.
Ramankutty, N., and J. A. Foley, 1999: Estimating historical changes in global land cover: Croplands from 1700 to 1992. *Global Biogeochemical Cycles*, **13**, 997-1027.
Ramankutty, N., C. Delire, and P. Snyder, 2006: Feedbacks between agriculture and climate: An illustration of the potential unintended consequences of human land use activities. *Global and Planetary Change*, **54**, 79-93.
Ramaswamy, V., O. Boucher, J. Haigh, D. Hauglustaine, J. Haywood, and G. Myhre, 2001: Radiative Forcing of Climate Change. *Climate Change 2001: The Scientific Basis Contribution of Working Group I to the Third Assessment Report of the Intergovernmental Panel on Climate Change.*, D. Y. Houghton J. T., Griggs D. J., Noguer M., Linden P. Jvd, Dai X., et al., Ed., Cambridge University Press, 351-416.
Randerson, J. T., et al., 2009: Systematic assessment of terrestrial biogeochemistry in coupled climate-carbon models. *Global Change Biology*, **15**, 2462-2484.
Rau, G. H., 2008: Electrochemical Splitting of Calcium Carbonate to Increase Solution Alkalinity: Implications for Mitigation of Carbon Dioxide and Ocean Acidity. *Environ. Sci. Technol.*, **42**, 8935-8940.
Raupach, M. R., J. G. Canadell, and C. Le Quere, 2008: Anthropogenic and biophysical contributions to increasing atmospheric CO2 growth rate and airborne fraction. *Biogeosciences*, **5**, 1601-1613.
Raupach, M. R., et al., subm.: Detection and attribution of trends in CO2 airborne fraction and sink uptake rate. *Nature Climate Change*.
Ravishankara, A. R., J. S. Daniel, and R. W. Portmann, 2009: Nitrous Oxide (N_2O): The Dominant Ozone-Depleting Substance Emitted in the 21st Century. *Science*, **326**, 123-125.
Raymond, P. A., and J. J. Cole, 2003: Increase in the export of alkalinity from North America's largest river. *Science*, **301**, 88-91.
Raymond, P. A., N.-H. Oh, R. E. Turner, and W. Broussard, 2008: Anthropogenically enhanced fluxes of water and carbon from the Mississippi River. *Nature*, **451**, 449-452.
Rayner, P. J., R. M. Law, C. E. Allison, R. J. Francey, C. M. Trudinger, and C. Pickett-Heaps, 2008: Interannual variability of the global carbon cycle (1992–2005) inferred by inversion of atmospheric CO2andδ13CO2measurements. *Global Biogeochemical Cycles*, **22**.
Reagan, M., and G. Moridis, 2007: Oceanic gas hydrate instability and dissociation under climate change scenarios. *Geophysical Research Letters*, **34**, -.
——, 2009: Large-scale simulation of methane hydrate dissociation along the West Spitsbergen Margin. *Geophysical Research Letters*, **36**, -.
Reay, D. S., F. Dentener, P. Smith, J. Grace, and R. A. Feely, 2008: Global nitrogen deposition and carbon sinks. *Nature Geoscience*, **1**, 430-437.
Regalado, A., 2010: BIODIVERSITY Brazil Says Rate of Deforestation in Amazon Continues to Plunge. *Science*, **329**, 1270-1271.
Reich, P. B., et al., 2006: Nitrogen limitation constrains sustainability of ecosystem response to CO2. *Nature*, **440**, 922-925.
Rhee, T. S., A. J. Kettle, and M. O. Andreae, 2009: Methane and nitrous oxide emissions from the ocean: A reassessment using basin-wide observations in the Atlantic. *J. Geophys. Res.*, **114**, D12304.
Ridgwell, A., and R. E. Zeebe, 2005: The role of the global carbonate cycle in the regulation and evolution of the Earth system. *Earth and Planetary Science Letters*, **234**, 299-315.
Ridgwell, A., and J. C. Hargreaves, 2007: Regulation of atmospheric CO2 by deep-sea sediments in an Earth system model. *Global Biogeochemical Cycles*, **21**.
Ridgwell, A. J., 2001: Glacial-interglacial perturbations in the global carbon cycle, University of East Anglia, Norwich, UK., 134 pp.
Ridgwell, A. J., A. J. Watson, M. A. Maslin, and J. O. Kaplan, 2003: Implications of coral reef buildup for the controls on atmospheric CO2 since the Last Glacial Maximum. *Paleoceanography*, **18**, doi:10.1029/2003PA000893.
Riebesell, U., A. Kortzinger, and A. Oschlies, 2009: Sensitivities of marine carbon fluxes to ocean change. *Proceedings of the National Academy of Sciences of the United States of America*, **106**, 20602-20609.
Riebesell, U., K. G. Schulz, R. G. J. Bellerby, M. Botros, P. Fritsche, M. Meyerhofer, and C. Neill, 2007: Enhanced biological carbon consumption in a high CO_2 ocean. *Nature*, **450**, 545-548.
Rigby, M., et al., 2008: Renewed growth of atmospheric methane. *Geophysical Research Letters*, **35**.
Riley, W., et al., 2011: Barriers to predicting changes in global terrestrial methane fluxes: analyses using CLM4Me, a methane biogeochemistry model integrated in CESM. *Biogeosciences*, **8**, 1925-1953.
Ringeval, B., P. Friedlingstein, C. Koven, P. Ciais, N. de Noblet-Ducoudre, B. Decharme, and P. Cadule, 2011: Climate-CH4 feedback from wetlands and its interaction with the climate-CO2 feedback. *Biogeosciences*, **8**, 2137-2157.
Rodenbeck, C., S. Houweling, and M. H. Gloor, M., 2003: CO2 flux history 1982–2001 inferred from atmospheric data using a global inversion of atmospheric transport. *Atmos Chem Phys Discuss*, **3**, 2575-2659.

Roderick, M. L., G. D. Farquhar, S. L. Berry, and I. R. Noble, 2001: On the direct effect of clouds and atmospheric particles on the productivity and structure of vegetation. *Oecologia*, **129**, 21–30.
Rogelj, J., et al., 2011: Emission pathways consistent with a 2 °C global temperature limit. *Nature Climate Change*, **1**, 413-418.
Romanou, A., B. Liepert, G. A. Schmidt, W. B. Rossow, R. A. Rued, and Y. Zhang, 2007: 20th century changes in surface solar irradiance in simulations and observations. *Geophysical Research Letters*, **34**.
Roth, R., and F. Joos, 2012: Model limits on the role of volcanic carbon emissions in regulating glacial-interglacial CO2 variations. *Earth and Planetary Science Letters*, **329**, 141-149.
Rothlisberger, R., M. Bigler, E. W. Wolff, F. Joos, E. Monnin, and M. A. Hutterli, 2004: Ice core evidence for the extent of past atmospheric CO2 change due to iron fertilisation. *Geophysical Research Letters*, **31**.
Rotty, R. M., 1983: Distribution of and changes in industrial carbon-cycle production. *Journal of Geophysical Research - Ocean and Atmosphere*, **88**, 1301-1308.
Roy, T., et al., 2011: Regional Impacts of Climate Change and Atmospheric CO2 on Future Ocean Carbon Uptake: A Multimodel Linear Feedback Analysis. *Journal of Climate*, **24**, 2300-2318.
Rubasinghege, G., S. N. Spak, C. O. Stanier, G. R. Carmichael, and V. H. Grassian, 2011: Abiotic Mechanism for the Formation of Atmospheric Nitrous Oxide from Ammonium Nitrate. *Environ. Sci. Technol.*, **45**, 2691-2697.
Ruddiman, W. F., 2003: The anthropogenic greenhouse era began thousands of years ago. *Climatic Change*, **61**, 261-293.
——, 2007: The early anthropogenic hypothesis: Challenges and responses. *Reviews of Geophysics*, **45**.
Rustad, L. E., et al., 2001: A meta-analysis of the response of soil respiration, net nitrogen mineralization, and aboveground plant growth to experimental ecosystem warming. *Oecologia*, **126**, 543-562.
Sabine, C. L., R. A. Feely, F. J. Millero, A. G. Dickson, C. Langdon, S. Mecking, and D. Greeley, 2008: Decadal changes in Pacific carbon. *J Geophys Res-Oceans*, **113**.
Sabine, C. L., et al., 2004: The oceanic sink for anthropogenic CO2. *Science*, 367-371.
Salisbury, J., M. Green, C. Hunt, and J. Campbell, 2008: Coastal Acidification by Rivers:A Threat to Shellfish? *Eos Trans. AGU*, **89**.
Sallée, J.-B., R. J. Matear, S. R. Rintoul, and A. Lenton, 2012: Localized subduction of anthropogenic carbon dioxide in the Southern Hemisphere oceans. *Nature Geoscience*, **5**, 579-584.
Samanta, A., M. H. Costa, E. L. Nunes, S. A. Viera, L. Xu, and R. B. Myneni, 2011: Comment on "Drought-induced reductions in global terrestrial net primary production from 2000 through 2009". *Science*, **333**, 1093-c.
Sanderson, M. G., 1996: Biomass of termites and their emissions of methane and carbon dioxide: A global database. *Global Biogeochem. Cycles*, **10**, 543-557.
Sarmiento, J. L., and N. Gruber, 2006: *Ocean Biogeochemical Dynamics.* Princeton University.
Sarmiento, J. L., T. M. C. Hughes, R. J. Stouffer, and S. Manabe, 1998: Simulated response of the ocean carbon cycle to anthropogenic climate warming. *Nature*, **393**, 245-249.
Sarmiento, J. L., P. Monfray, E. Maier-Reimer, O. Aumont, R. Murnane, and J. Orr, 2000: Air-sea CO2 Fluxes and carbon transport: a comparison of three ocean general circulation models. *Global Biogeochemical Cycles*, **14**, 1267-1281.
Sarmiento, J. L., et al., 2010: Trends and regional distributions of land and ocean carbon sinks. *Biogeosciences*, **7**, 2351-2367.
Savolainen, I., S. Monni, and S. Syri, 2009: The mitigation of methane emissions from the industrialised countries can explain the atmospheric concentration level-off. *International Journal of Energy for a Clean Environment*, **10**, 193-201.
Schaefer, K., T. Zhang, L. Bruhwiler, and A. P. Barrett, 2011: Amount and timing of permafrost carbon release in response to climate warming. *Tellus B*, **63**, 165-180.
Scheffer, M., V. Brovkin, and P. M. Cox, 2006: Positive feedback between global warming and atmospheric CO2 concentration inferred from past climate change. *Geophysical Research Letters*, **33**.
Schilt, A., M. Baumgartner, T. Blunier, J. Schwander, R. Spahni, H. Fischer, and T. F. Stocker, 2010a: Glacial-interglacial and millennial-scale variations in the atmospheric nitrous oxide concentration during the last 800,000 years. *Quaternary Science Reviews*, **29**, 182-192.
Schilt, A., et al., 2010b: Atmospheric nitrous oxide during the last 140,000 years. *Earth and Planetary Science Letters*, **300**, 33-43.
Schmitt, J., et al., 2012: Carbon isotope constraints on the deglacial CO_2 rise from ice cores. *Science*, **336**, 711-714.
Schmittner, A., and E. D. Galbraith, 2008: Glacial greenhouse-gas fluctuations controlled by ocean circulation changes. *Nature*, **456**, 373-376.
Schmittner, A., A. Oschlies, H. D. Matthews, and E. D. Galbraith, 2008: Future changes in climate, ocean circulation, ecosystems, and biogeochemical cycling simulated for a business-as-usual CO_2 emission scenario until year 4000 AD. *Global Biogeochemical Cycles*, **22**.
Schmittner, A., N. M. Urban, K. Keller, and D. Matthews, 2009: Using tracer observations to reduce the uncertainty of ocean diapycnal mixing and climate-carbon cycle projections. *Global Biogeochemical Cycles*, **23**.
Scholze, M., W. Knorr, N. Arnell, and I. Prentice, 2006: A climate-change risk analysis for world ecosystems. *Proceedings of the National Academy of Sciences of the United States of America*, **103**, 13116-13120.

Schuiling, R. D., and P. Krijgsman, 2006: Enhanced weathering: An effective and cheap tool to sequester CO2. *Climatic Change*, **74**, 349-354.
Schultz, M. G., et al.: Emission data sets and methodologies for estimating emissions
Schulze, E. D., S. Luyssaert, P. Ciais, A. Freibauer, I. A. Janssens, and e. al., 2009: Importance of methane and nitrous oxide for Europe's terrestrial greenhouse-gas balance. *Nature Geoscience*, **2**, 842-850.
Schulze, E. D., et al., 2010: The European carbon balance. Part 4: integration of carbon and other trace-gas fluxes. *Global Change Biology*, **16**, 1451-1469.
Schurgers, G., U. Mikolajewicz, M. Groger, E. Maier-Reimer, M. Vizcaino, and A. Winguth, 2006: Dynamics of the terrestrial biosphere, climate and atmospheric CO2 concentration during interglacials: a comparison between Eemian and Holocene. *Climate of the Past*, **2**, 205-220.
Schuster, U., and A. J. Watson, 2007: A variable and decreasing sink for atmospheric CO2 in the North Atlantic. *J Geophys Res-Oceans*, **112**.
Schuster, U., et al., 2009: Trends in North Atlantic sea-surface fCO(2) from 1990 to 2006. *Deep-Sea Res Pt Ii*, **56**, 620-629.
Schuster, U., et al., subm.: Atlantic and Arctic Air-Sea CO2 Fluxes, 1990-2009. *Biogeosciences Discussions*.
Schwalm, C. R., et al., 2010: A model-data intercomparison of CO_2 exchange across North America: Results from the North American Carbon Program site synthesis. *Journal of Geophysical Research*, **115**, G00H05.
Seitzinger, S. P., and C. Kroeze, 1998: Global distribution of nitrous oxide production and N inputs in freshwater and coastal marine ecosystems. *Global Biogeochem. Cycles*, **12**, 93-113.
Seitzinger, S. P., J. A. Harrison, E. Dumont, A. H. W. Beusen, and A. F. Bouwman, 2005: Sources and delivery of carbon, nitrogen, and phosphorus to the coastal zone: An overview of Global Nutrient Export from Watersheds (NEWS) models and their application. *Global Biogeochemical Cycles*, **19**.
Seitzinger, S. P., et al., 2010: Global river nutrient export: A scenario analysis of past and future trends. *Global Biogeochemical Cycles*, **24**, GB0A08.
Shackleton, N. J., 2000: The 100,000-year ice-age cycle identified and found to lag temperature, carbon dioxide, and orbital eccentricity. *Science*, **289(5486)**, 1897-1902.
Shaffer, G., 2010: Long-term effectiveness and consequences of carbon dioxide sequestration. *Nature Geoscience*, **3**, 464-467.
Shaffer, G., S. M. Olsen, and J. O. P. Pedersen, 2009: Long-term ocean oxygen depletion in response to carbon dioxide emission from fossil fuels. *Nature Geoscience*, **2**, 105-109.
Shakhova, N., I. Semiletov, A. Salyuk, V. Yusupov, D. Kosmach, and O. Gustafsson, 2010: Extensive Methane Venting to the Atmosphere from Sediments of the East Siberian Arctic Shelf. *Science*, **327**, 1246-1250.
Shallcross, D. E., M. A. K. Khalil, and C. L. Butenhoff, 2007: The atmospheric methane sink. *Greenhouse Gas Sinks*, D. Reay, Ed., CABI Publishing.
Shevliakova, E., et al., 2009a: Carbon cycling under 300 years of land use change: Importance of the secondary vegetation sink. *Global Biogeochemical Cycles*, **23**, 1-16.
Shevliakova, E., et al., 2009b: Carbon cycling under 300 years of land use change: Importance of the secondary vegetation sink. *Global Biogeochemical Cycles*, **23**, -.
Shevliakova, E., et al., subm: Land carbon sink mitigated 20th century climate warming. *Nature Climate Change*, (submitted).
Shindell, D., B. Walter, and G. Faluvegi, 2004: Impacts of climate change on methane emissions from wetlands. *Geophysical Research Letters*, **31**.
Siegenthaler, U., et al., 2005a: Supporting evidence from the EPICA Dronning Maud Land ice core for atmospheric CO2 changes during the past millennium. *Tellus Series B-Chemical and Physical Meteorology*, **57**, 51-57.
Siegenthaler, U., et al., 2005b: Stable carbon cycle-climate relationship during the late Pleistocene. *Science*, **310**, 1313-1317.
Sigman, D., M. Hain, and G. Haug, 2010: The polar ocean and glacial cycles in atmospheric CO2 concentration. *Nature*, **466**, 47-55.
Singarayer, J. S., P. J. Valdes, P. Friedlingstein, S. Nelson, and D. J. Beerling, 2011: Late Holocene methane rise caused by orbitally controlled increase in tropical sources. *Nature*, **470**, 82-U91.
Singh, B. K., R. D. Bartgett, P. Smith, and D. S. Peay, 2010: Microorganisms and climate change: terrestrial feedbacks and mitigation options. *Nature Microbiology*, **8**, 779-790.
Sitch, S., P. M. Cox, W. J. Collins, and C. Huntingford, 2007: Indirect radiative forcing of climate change through ozone effects on the land-carbon sink. *Nature*, **448**, 791-U794.
Sitch, S., P. Friedlingstein, N. Gruber, and S. Jones, subm: Trends and drivers of regional sources and sinks of carbon dioxide over the past two decades. *Biogeosciences*.
Sitch, S., V. Brovkin, W. von Bloh, D. van Vuuren, B. Assessment, and A. Ganopolski, 2005: Impacts of future land cover changes on atmospheric CO2 and climate. *Global Biogeochemical Cycles*, **19**.
Sitch, S., et al., 2003: Evaluation of ecosystem dynamics, plant geography and terrestrial carbon cycling in the LPJ dynamic global vegetation model. *Global Change Biology*, **9**, 161-185.
Sitch, S., et al., 2008: Evaluation of the terrestrial carbon cycle, future plant geography and climate-carbon cycle feedbacks using five Dynamic Global Vegetation Models (DGVMs). *Global Change Biology*, **14**, 2015-2039.

Smith, B., I. C. Prentice, and M. T. Sykes, 2001a: Representation of vegetation dynamics in the modelling of terrestrial ecosystems: comparing two contrasting approaches within European climate space. *Global Ecology and Biogeography*, **10**, 621-637.
Smith, L. C., Y. Sheng, G. M. MacDonald, and L. D. Hinzman, 2005: Disappearing Arctic lakes. *Science*, **308**, 1429-1429.
Smith, S. V., W. H. Renwick, R. W. Buddemeier, and C. J. Crossland, 2001b: Budgets of soil erosion and deposition for sediments and sedimentary organic carbon across the conterminous United States. *Global Biogeochemical Cycles*, **15**, 697-707.
Smith, T. M., and H. H. Shugart, 1993: The transient-response of terrestrial carbon storage to a perturbed climate. *Nature*, **361**, 523-526.
SOCCR, 2007: The First State of the Carbon Cycle Report (SOCCR): The North American Carbon Budget and Implications for the Global Carbon Cycle.
Sokolov, A. P., D. W. Kicklighter, J. M. Melillo, B. S. Felzer, C. A. Schlosser, and T. W. Cronin, 2008: Consequences of considering carbon-nitrogen interactions on the feedbacks between climate and the terrestrial carbon cycle. *Journal of Climate*, **21**, 3776-3796.
Sowers, T., 2006: Late quaternary atmospheric CH4 isotope record suggests marine clathrates are stable. *Science*, **311**, 838-840.
Sowers, T., R. B. Alley, and J. Jubenville, 2003: Ice core records of atmospheric N2O covering the last 106,000 years. *Science*, **301**, 945-948.
Spahni, R., et al., 2011: Constraining global methane emissions and uptake by ecosystems. *Biogeosciences*, **8**, 1643-1665.
Spracklen, D., L. Mickley, J. Logan, R. Hudman, R. Yevich, M. Flannigan, and A. Westerling, 2009: Impacts of climate change from 2000 to 2050 on wildfire activity and carbonaceous aerosol concentrations in the western United States. *Journal of Geophysical Research-Atmospheres*, **114**, -.
Stallard, R. F., 1998: Terrestrial sedimentation and the carbon cycle: Coupling weathering and erosion to carbon burial. *Global Biogeochemical Cycles*, **12**, 231-257.
Stanhill, G., and S. Cohen, 2001: Global dimming: a review of the evidence for a widespread and significant reduction in global radiation with discussion of its probable causes and possible agricultural consequences. *Agricultural And Forest Meteorology*, **107**, 255-278.
Steinacher, M., F. Joos, T. L. Frolicher, G. K. Plattner, and S. C. Doney, 2009: Imminent ocean acidification in the Arctic projected with the NCAR global coupled carbon cycle-climate model. *Biogeosciences*, **6**, 515-533.
Steinacher, M., et al., 2010: Projected 21st century decrease in marine productivity: a multi-model analysis. *Biogeosciences*, **7**, 979-1005.
Stephens, B. B., and R. F. Keeling, 2000: The influence of Antarctic sea ice on glacial-interglacial CO2 variations. *Nature*, **404**, 171-174.
Stephens, B. B., et al., 2007: Weak Northern and Strong Tropical Land Carbon Uptake from Vertical Profiles of Atmospheric CO2. *Science*, **316**, 1732-1735.
Stocker, B. D., K. Strassmann, and F. Joos, 2011: Sensitivity of Holocene atmospheric CO2 and the modern carbon budget to early human land use: analyses with a process-based model. *Biogeosciences*, **8**, 69-88.
Stocker, B. D., et al., subm.: Multiple greenhouse gas feedbacks from the land biosphere under future climate change scenarious. *Nature Climate Change*.
Stockli, R., et al., 2008: Use of FLUXNET in the community land model development. *Journal of Geophysical Research-Biogeosciences*, **113**, -.
Stramma, L., A. Oschlies, and S. Schmidtko, 2012: Anticorrelated observed and modeled trends in dissolved oceanic oxygen over the last 50 years. *Biogeosciences Discuss.*, **9**, 4595-4626.
Strassmann, K. M., F. Joos, and G. Fischer, 2008: Simulating effects of land use changes on carbon fluxes: past contributions to atmospheric CO2 increases and future commitments due to losses of terrestrial sink capacity. *Tellus Series B-Chemical and Physical Meteorology*, **60**, 583-603.
Stuiver, M., and P. D. Quay, 1981: Atmospheric C-14 changes resulting from fossil-fuel CO2 release and cosmic-ray flux variability. *Earth and Planetary Science Letters*, **53**, 349-362.
Suchet, P. A., and J. L. Probst, 1995: A Global model for present-day atmospheric soil CO2 consumption by chemical erosion of continental rocks (GEM-CO2). *Tellus B, Chemical and Physical Meteorology*, **85**, 1563-1568.
Sugimoto, A., T. Inoue, N. Kirtibutr, and T. Abe, 1998: Methane oxidation by termite mounds estimated by the carbon isotopic composition of methane. *Global Biogeochem. Cycles*, **12**, 595-605.
Sundquist, E. T., 1986: Geologic analogs: Their value and limitations in carbon dioxide research. *The Changing Carbon Cycle*, J. R. a. R. Trabalka, D. E., Ed., 371-402.
——, 1990: Influence of Deep-Sea Benthic Processes on Atmospheric Co2. *Philos T Roy Soc A*, **331**, 155-165.
Suntharalingam, P., et al., 2012: Quantifying the impact of anthropogenic nitrogen deposition on oceanic nitrous oxide. *Geophys. Res. Lett.*, **39**, L07605.
Sussmann, R., F. Forster, M. Rettinger, and P. Bousquet, 2012: Renewed methane increase for five years (2007–2011) observed by solar FTIR spectrometry. *Atmos. Chem. Phys. Discuss.*, **11**, 30757-30772.

Sutka, R. L., N. E. Ostrom, O. P. H., J. A. Breznak, H. Gandhi, A. J. Pitt, and F. Li, 2006: Distinguishing nitrous oxide production from nitrification and denitrification on the basis of isotopomer abundances. *Applied and Environmental Microbiology*, **72**, 638- 644.
Sutton, M. A., et al., 2007: Challenges in quantifying biosphere-atmosphere exchange of nitrogen species. *Environmental Pollution*, **150**, 125-139.
Syakila, A., and C. Kroeze, 2011: The Global N_2O Budget Revisited. *Greenhouse Gas Measurement and Mitigation*, **1**, 17-26.
Syakila, A., C. Kroeze, and C. P. Slomp, 2010: Neglecting sinks for N_2O at the earth's surface: does it matter? *Journal of Integrative Environmental Sciences*, **7**, 79-87.
Syvitski, J. P. M., C. J. Vorosmarty, A. J. Kettner, and P. Green, 2005: Impact of humans on the flux of terrestrial sediment to the global coastal ocean. *Science*, **308**, 376-380.
Tagaris, E., K. Liao, K. Manomaiphiboon, J. Woo, S. He, P. Amar, and A. Russell, 2008: Impacts of future climate change and emissions reductions on nitrogen and sulfur deposition over the United States. *Geophysical Research Letters*, **35**, -.
Tagliabue, A., L. Bopp, and O. Aumont, 2008: Ocean biogeochemistry exhibits contrasting responses to a large scale reduction in dust deposition. *Biogeosciences*, **5**, 11-24.
Tagliabue, A., L. Bopp, and M. Gehlen, 2011: The response of marine carbon and nutrient cycles to ocean acidification: Large uncertainties related to phytoplankton physiological assumptions. *Global Biogeochemical Cycles*, **25**, -.
Takahashi, T., S. C. Sutherland, R. A. Feely, and R. Wanninkhof, 2006: Decadal change of the surface water pCO(2) in the North Pacific: A synthesis of 35 years of observations. *J Geophys Res-Oceans*, **111**, -.
Takahashi, T., J. Olafsson, J. G. Goddard, D. W. Chipman, and S. C. Sutherland, 1993: Seasonal-Variation of Co2 and Nutrients in the High-Latitude Surface Oceans - a Comparative-Study. *Global Biogeochemical Cycles*, **7**, 843-878.
Takahashi, T., et al., 2009: Climatological mean and decadal change in surface ocean pCO(2), and net sea-air CO2 flux over the global oceans. *Deep-Sea Res Pt Ii*, **56**, 554-577.
Tan, K., et al., 2010: Application of the ORCHIDEE global vegetation model to evaluate biomass and soil carbon stocks of Qinghai-Tibetan grasslands. *Global Biogeochemical Cycles*, **24**.
Tanhua, T., A. Kortzinger, K. Friis, D. W. Waugh, and D. W. R. Wallace, 2007: An estimate of anthropogenic CO2 inventory from decadal changes in oceanic carbon content. *Proceedings of the National Academy of Sciences of the United States of America*, **104**, 3037-3042.
Tans, P., T. Conway, and T. Nakazawa, 1989: Latitudinal distribution of the sources and sinks of atmospheric carbon-dioxide derived from surface observations and an atmospheric transport model. *Journal of Geophysical Research-Atmospheres*, **94**, 5151-5172.
Tarnocai, C., J. G. Canadell, E. A. G. Schuur, P. Kuhry, G. Mazhitova, and S. Zimov, 2009: Soil organic carbon pools in the northern circumpolar permafrost region. *Global Biogeochemical Cycles*, **23**.
Taucher, J., and A. Oschlies, 2011: Can we predict the direction of marine primary production change under global warming? *Geophysical Research Letters*, **38**.
Tegen, I., M. Werner, S. P. Harrison, and K. E. Kohfeld, 2004: Relative importance of climate and land use in determining present and future global soil dust emission. *Geophysical Research Letters*, **31**.
Terazawa, K., S. Ishizuka, T. Sakata, K. Yamada, and M. Takahashi, 2007: Methane emissions from stems of Fraxinus mandshurica var. japonica trees in a floodplain forest. *Soil Biology and Biochemistry*, **39**, 2689–2692.
Thomas, H., et al., 2007: Rapid decline of the CO2 buffering capacity in the North Sea and implications for the North Atlantic Ocean. *Global Biogeochemical Cycles*, **21**, -.
Thompson, D., and S. Solomon, 2002: Interpretation of recent Southern Hemisphere climate change. *Science*, **296**, 895-899.
Thompson, R. L., et al., subm.: Importance of tropical regions to global N2O emissions. *Letters to Nature*.
Thomson, A. M., et al., 2010: Climate mitigation and the future of tropical landscapes. *PNAS*, **107**, 19633-19638.
Thornton, P. E., J. F. Lamarque, N. A. Rosenbloom, and N. M. Mahowald, 2007: Influence of carbon-nitrogen cycle coupling on land model response to CO2 fertilization and climate variability. *Global Biogeochemical Cycles*, **21**.
Thornton, P. E., et al., 2009: Carbon-nitrogen interactions regulate climate-carbon cycle feedbacks: results from an atmosphere-ocean general circulation model. *Biogeosciences*, **6**, 2099-2120.
Tian, H., X. Xu, M. Liu, W. Ren, C. Zhang, G. Chen, and C. Lu, 2010: Spatial and temporal patterns of CH4 and N2O fluxes in terrestrial ecosystems of North America during 1979-2008: application of a global biogeochemistry model. *Biogeosciences*, **7**, 2673-2694.
Tilman, D., C. Balzer, J. Hill, and B. Befort, 2011: Global food demand and the sustainable intensification of agriculture. *Proceedings of the National Academy of Sciences of the United States of America*, **108**, 20260-20264.
Tjiputra, J., A. Olsen, K. Assmann, B. Pfeil, and C. Heinze, 2012: A model study of the seasonal and long-term North Atlantic surface pCO2 variability. *Biogeosciences*, **9**, 907-923.
Toggweiler, J., J. L. Russell, and S. R. Carson, 2006: Midlatitude westerlies, atmospheric CO_2, and climate change during the ice ages. *Paleoceanography*, **21**.
Toggweiler, J. R., 1999: Variation of atmospheric CO2 by ventilation of the ocean's deepest water. *Paleoceanography*, **14**, 571-588.

Trudinger, C. M., I. G. Enting, P. J. Rayner, and R. J. Francey, 2002: Kalman filter analysis of ice core data - 2. Double deconvolution of CO2 and delta C-13 measurements. *Journal of Geophysical Research-Atmospheres*, **107**.
Turetsky, M., C. Treat, M. Waldrop, J. Waddington, J. Harden, and A. McGuire, 2008: Short-term response of methane fluxes and methanogen activity to water table and soil warming manipulations in an Alaskan peatland. *Journal of Geophysical Research-Biogeosciences*, **113**, -.
Turetsky, M., E. Kane, J. Harden, R. Ottmar, K. Manies, E. Hoy, and E. Kasischke, 2011: Recent acceleration of biomass burning and carbon losses in Alaskan forests and peatlands. *Nature Geoscience*, **4**, 27-31.
Tymstra, C., M. Flannigan, O. Armitage, and K. Logan, 2007: Impact of climate change on area burned in Alberta's boreal forest. *International Journal of Wildland Fire*, **16**, 153-160.
Tyrrell, T., J. G. Shepherd, and S. Castle, 2007: The long-term legacy of fossil fuels. *Tellus Series B-Chemical and Physical Meteorology*, **59**, 664-672.
Ullman, D. J., G. A. McKinley, V. Bennington, and S. Dutkiewicz, 2009: Trends in the North Atlantic carbon sink: 1992-2006. *Global Biogeochemical Cycles*, **23**, -.
UNEP, 2011: Integrated Assessment of Black Carbon and Tropospheric Ozone: Summary for Decision Makers. UNEP, WMO, 36 pp.
Valdes, P. J., D. J. Beerling, and C. E. Johnson, 2005: The ice age methane budget. *Geophysical Research Letters*, **32**.
Valsala, V., S. Maksyutov, M. Telszewski, S. Nakaoka, Y. Nojiri, M. Ikeda, and R. Murtugudde, 2012: Climate impacts on the structures of the North Pacific air-sea CO2 flux variability. *Biogeosciences*, **9**, 477-492.
van-der-Werf, G. R., and R. S. Defries, subm.: Comment on "Baseline Map of Carbon Emissions from Deforestation in Tropical Regions". *Science*.
van der Werf, G. R., et al., 2004: Continental-scale partitioning of fire emissions during the 1997 to 2001 El Nino/La Nina period. *Science*, **303**, 73-76.
van der Werf, G. R., et al., 2009: CO2 emissions from forest loss. *Nature Geoscience*, **2**.
van der Werf, G. R., et al., 2010: Global fire emissions and the contribution of deforestation, savanna, forest, agricultural, and peat fires (1997-2009). *Atmospheric Chemistry and Physics*, **10**, 11707-11735.
van Huissteden, J., C. Berrittella, F. J. W. Parmentier, Y. Mi, T. C. Maximov, and A. J. Dolman, 2011: Methane emissions from permafrost thaw lakes limited by lake drainage. *Nature Climate Change*, **1**, 119-123.
Van Oost, K., et al., 2007: The impact of agricultural soil erosion on the global carbon cycle. *Science*, **318**, 626-629.
van Vuuren, D. P., L. F. Bouwman, S. J. Smith, and F. Dentener, 2011: Global projections for anthropogenic reactive nitrogen emissions to the atmosphere: an assessment of scenarios in the scientific literature. *Current Options in Environmental Sustainability*, **3**, 359-369.
vanDingenen, R., F. Dentener, F. Raes, M. Krol, L. Emberson, and J. Cofala, 2009: The global impact of ozone on agricultural crop yields under current and future air quality legislation. *Atmospheric Environment*, **43**, 604-618.
vanGroenigen, K. J., C. Osenberg, and B. Hungate, 2011: Increased soil emissions of potent greenhouse gases under increased atmospheric CO2. *Nature*, **475**, 214-216.
vanMinnen, J. G., K. K. Goldewijk, E. Stehfest, B. Eickhout, G. van Drecht, and R. Leemans, 2009: The importance of three centuries of land-use change for the global and regional terrestrial carbon cycle. *Climatic Change*, **97**, 123-144.
Verdy, A., S. Dutkiewicz, M. J. Follows, J. Marshall, and A. Czaja, 2007: Carbon dioxide and oxygen fluxes in the Southern Ocean: Mechanisms of interannual variability. *Global Biogeochemical Cycles*, **21**, -.
Vigano, I., H. van Weelden, R. Holzinger, F. Keppler, A. McLeod, and T. Rockmann, 2008: Effect of UV radiation and temperature on the emission of methane from plant biomass and structural components. *Biogeosciences*, **5**, 937-947.
Vitousek, P. M., S. Porder, B. Z. Houlton, and O. A. Chadwick, 2010: Terrestrial phosphorus limitation: mechanisms, implications, and nitrogen-phosphorus interactions. *Ecol. Appl.*, **20**, 5-15.
Vitousek, P. M., D. N. L. Menge, S. C. Reed, and C. C. Cleveland, subm.: Biological nitrogen fixation: rates, patterns, and ecological controls in terrestrial ecosystems. *Philisophical Transactions B*.
Volodin, E. M., 2008: Methane cycle in the INM RAS climate model. *Izvestiya Atmospheric and Oceanic Physics*, **44**, 153-159.
von Deimling, T., M. Meinshausen, A. Levermann, V. Huber, K. Frieler, D. Lawrence, and V. Brovkin, 2012: Estimating the near-surface permafrost-carbon feedback on global warming. *Biogeosciences*, **9**, 649-665.
Waelbroeck, C., et al., 2009: Constraints on the magnitude and patterns of ocean cooling at the Last Glacial Maximum. *Nature Geoscience*, **2**, 127-132.
Wahlen, M., et al., 1989: C-14 in Methane Sources and in Atmospheric Methane - the Contribution From Fossil Carbon. *Science*, **245**, 286-290.
Wakita, M., S. Watanabe, A. Murata, N. Tsurushima, and M. Honda, 2010: Decadal change of dissolved inorganic carbon in the subarctic western North Pacific Ocean. *Tellus Series B-Chemical and Physical Meteorology*, **62**, 608-620.
Walker, J. C. G., and J. F. Kasting, 1992: Effects of fuel and forest conservation on future levels of atmospheric carbon dioxide. *Palaeogeography Palaeoclimatology Palaeoecology*, **97**, 151-189.
Walter, K. M., L. C. Smith, and F. Stuart Chapin, 2007: Methane bubbling from northern lakes: present and future contributions to the global methane budget. *Philosophical Transactions of the Royal Society A: Mathematical, Physical and Engineering Sciences*, **365**, 1657-1676.

Walter, K. M., S. A. Zimov, J. P. Chanton, D. Verbyla, and F. S. Chapin, 2006: Methane bubbling from Siberian thaw lakes as a positive feedback to climate warming. *Nature*, **443**, 71-75.
Wang, D., S. A. Heckathorn, X. Wang, and S. M. Philpott, 2012: A meta-analysis of plant physiological and growth responses to temperature and elevated CO2. *Oecologia*, **169**, 1–13.
Wang, W. L., et al., subm.: Variations in Atmospheric CO2 Growth Rates Controlled by Tropical Temperature. *Nature Geoscience*.
Wang, Y. P., and B. Z. Houlton, 2009: Nitrogen constraints on terrestrial carbon uptake: Implications for the global carbon-climate feedback. *Geophysical Research Letters*, **36**, -.
Wang, Y. P., R. M. Law, and B. Pak, 2010a: A global model of carbon, nitrogen and phosphorus cycles for the terrestrial biosphere. *Biogeosciences*, **7**, 2261-2282.
Wang, Z., J. Chappellaz, K. Park, and J. E. Mak, 2010b: Large Variations in Southern Hemisphere Biomass Burning During the Last 650 Years. *Science*, **330**, 1663-1666.
Wang, Z. P., X. G. Han, G. G. Wang, Y. Song, and J. Gulledge, 2008: Aerobic methane emission from plants in the Inner Mongolia steppe. *Environ. Sci. Technol.*, **42**, 62-68.
Wania, R., 2007: Modelling northern peatland land surface processes, vegetation dynamics and methane emissions, Bristol, UK.
Wanninkhof, R., S. C. Doney, J. L. Bullister, N. M. Levine, M. Warner, and N. Gruber, 2010: Detecting anthropogenic CO2 changes in the interior Atlantic Ocean between 1989 and 2005. *J Geophys Res-Oceans*, **115**.
Wanninkhof, R., et al., subm.: Global Ocean Carbon Uptake: Magnitude, Variability and Trends. *Biogeosciences Discussions*.
Watanabe, S., et al., 2011: MIROC-ESM 2010: model description and basic results of CMIP5-20c3m experiments. *Geoscientific Model Development*, **4**, 845-872.
Watson, A., et al., 2009: Tracking the Variable North Atlantic Sink for Atmospheric CO2. *Science*, **326**, 1391-1393.
Watson, A. J., and A. C. N. Garabato, 2006: The role of southern Ocean mixing and upwelling in glacial-interglacial atmospheric CO_2 change. *Tellus, Ser. B*, **58**, 73-87.
Watson, A. J., D. C. E. Bakker, A. J. Ridgwell, P. W. Boyd, and C. S. Law, 2000: Effect of iron supply on Southern Ocean CO2 uptake and implications for glacial atmospheric CO2. *Nature*, **407**, 730-733.
Waugh, D. W., T. M. Hall, B. I. McNeil, R. Key, and R. J. Matear, 2006: Anthropogenic CO2 in the oceans estimated using transit time distributions. *Tellus Series B-Chemical and Physical Meteorology*, **58**, 376-389.
Westbrook, G., et al., 2009: Escape of methane gas from the seabed along the West Spitsbergen continental margin. *Geophysical Research Letters*, **36**, -.
Westerling, A., M. Turner, E. Smithwick, W. Romme, and M. Ryan, 2011: Continued warming could transform Greater Yellowstone fire regimes by mid-21st century. *Proceedings of the National Academy of Sciences of the United States of America*, **108**, 13165-13170.
Wiedinmyer, C., S. K. Akagi, R. J. Yokelson, L. K. Emmons, J. A. Al-Saadi, J. J. Orlando, and A. J. Soja, 2011: The Fire INventory from NCAR (FINN): a high resolution global model to estimate the emissions from open burning. *Geoscientific Model Development*, **4**, 625-641.
Williams, C. A., G. J. Collatz, J. Masek, and S. N. Goward, 2011: Carbon consequences of forest disturbance and recovery across the conterminous United States. *Global Biogeochemical Cycles*, **in press**.
——, 2012a: Carbon consequences of forest disturbance and recovery across the conterminous United States. *Global Biogeochemical Cycles*, **26**.
Williams, J., and P. J. Crutzen, 2010: Nitrous oxide from aquaculture. *Nature Geosci*, **3**, 143-143.
Williams, J. E., A. Strunk, V. Huijnen, and M. van Weele, 2012b: The application of the Modified Band Approach for the calculation of on-line photodissociation rate constants in TM5: implications for oxidative capacity. *Geoscientific Model Development*, **5**, 15-35.
Winiwarter, W., J. W. Erisman, J. N. Galloway, Z. Klimont, and M. Sutton, subm.: Estimating environmental loads of reactive nitrogen in the 21st century. *Climatic Change*.
Wise, M., et al., 2009: Implications of Limiting CO2 Concentrations for Land Use and Energy. *Science*, **324**, 1183-1186.
Woodward, F. I., and M. R. Lomas, 2004: Simulating vegetation processes along the Kalahari transect. *Global Change Biology*, **10**, 383-392.
Woolf, D., J. E. Amonette, F. A. Street-Perrott, J. Lehmann, and S. Joseph, 2010: Sustainable biochar to mitigate global climate change. *Nature Communications*, **1**.
Worrall, F., T. Burt, and R. Shedden, 2003: Long term records of riverine dissolved organic matter. *Biogeochemistry*, **64**, 165-178.
Wotton, B., C. Nock, and M. Flannigan, 2010: Forest fire occurrence and climate change in Canada. *International Journal of Wildland Fire*, **19**, 253-271.
Wu, T., et al., subm.: Global Carbon budgets simulated by the Beijing Climate Center Climate System Model for the last Century. *Journal of Climate*.
Yamamoto-Kawai, M., F. A. McLaughlin, E. C. Carmack, S. Nishino, and K. Shimada, 2009: Aragonite Undersaturation in the Arctic Ocean: Effects of Ocean Acidification and Sea Ice Melt. *Science*, **326**, 1098-1100.
Yamamoto, A., M. Kawamiya, A. Ishida, Y. Yamanaka, and S. Watanabe, 2012: Impact of rapid sea-ice reduction in the Arctic Ocean on the rate of ocean acidification. *Biogeosciences*, **9**, 2365-2375.

Yan, X., H. Akiyama, K. Yagi, and H. Akimoto, 2009: Global estimations of the inventory and mitigation potential of methane emissions from rice cultivation conducted using the 2006 Intergovernmental Panel on Climate Change Guidelines. *Global Biogeochemical Cycles*, **23**.

Yang, X., and W. M. Post, 2011: Phosphorus transformations as a function of pedogenesis: A synthesis of soil phosphorus data using Hedley fractionation method. *Biogeosciences*, **8**, 2907-2916.

Yevich, R., and J. A. Logan, 2003: An assessment of biofuel use and burning of agricultural waste in the developing world. *Global Biogeochemical Cycles*, **17**.

Yoshikawa, C., M. Kawamiya, T. Kato, Y. Yamanaka, and T. Matsuno, 2008: Geographical distribution of the feedback between future climate change and the carbon cycle. *Journal of Geophysical Research-Biogeosciences*, **113**.

Yu, J. M., W. S. Broecker, H. Elderfield, Z. D. Jin, J. McManus, and F. Zhang, 2010: Loss of Carbon from the Deep Sea Since the Last Glacial Maximum. *Science*, **330**, 1084-1087.

Yu, Z., 2011: Holocene carbon flux histories of the worldâ€™s peatlands: Global carbon-cycle implications. *The Holocene*, 10.1177/0959683610386982.

Zaehle, S., subm.: Terrestrial Nitrogen-Carbon cycle interactions at the global scale.

Zaehle, S., and A. Friend, 2010: Carbon and nitrogen cycle dynamics in the O-CN land surface model: 1. Model description, site-scale evaluation, and sensitivity to parameter estimates. *Global Biogeochemical Cycles*, **24**, -.

Zaehle, S., and D. Dalmonech, 2011: Carbon-nitrogen interactions on land at global scales: Current understanding in modelling climate biosphere feedbacks. *Current Opinions in Environmental Sustainability*, **3**, 311-320.

Zaehle, S., P. Friedlingstein, and A. D. Friend, 2010a: Terrestrial nitrogen feedbacks may accelerate future climate change. *Geophysical Research Letters*, **37**, -.

Zaehle, S., P. Ciais, A. D. Friend, and V. Prieur, 2011: Carbon benefits of anthropogenic reactive nitrogen offset by nitrous oxide emissions. *Nature Geosci*, **4**, 601-605.

Zaehle, S., A. D. Friend, P. Friedlingstein, F. Dentener, P. Peylin, and M. Schulz, 2010b: Carbon and nitrogen cycle dynamics in the O-CN land surface model: 2. Role of the nitrogen cycle in the historical terrestrial carbon balance. *Global Biogeochemical Cycles*, **24**.

Zak, D. R., K. S. Pregitzer, M. E. Kubiske, and A. J. Burton, 2011: Forest productivity under elevated CO2 and O3: positive feedbacks to soil N cycling sustain decade-long net primary productivity enhancement by CO2. *Ecology Letters*, **14**, 1220-1226.

Zeebe, R. E., and D. Wolf-Gladrow, 2001: *CO2 in Seawater: Equilibrium, Kinetics, Isotopes.*

Zeebe, R. E., and D. Archer, 2005: Feasibility of ocean fertilization and its impact on future atmospheric CO2 levels. *Geophysical Research Letters*, **32**.

Zeng, N., 2003: Glacial-interglacial atmospheric CO2 change —The glacial burial hypothesis. *Advances In Atmospheric Sciences*, **20**, 677-693.

Zhao, M., and S. W. Running, 2010: Drought-Induced Reduction in Global Terrestrial Net Primary Production from 2000 Through 2009. *Science*, **329**, 940-943.

Zhao, M. S., and S. W. Running, 2011: Response to Comments on Comment on "Drought-induced reductions in global terrestrial net primary production from 2000 through 2009". *Science*, **333**, 1093-e.

Zhou, L. M., C. J. Tucker, R. K. Kaufmann, D. Stayback, N. V. Shabanov, and R. B. Myneni, 2001: Variations in northern vegetation activity inferred from satellite data of vegetation index during 1981 to 1999. *Journal of Geophysical Research - Atmospheres*, **106**, 20069-20083.

Zhou, S., and P. C. Flynn, 2005: Geoengineering downwelling ocean currents: A cost assessment. *Climatic Change*, **71**, 203-220.

Zhuang, Q., et al., 2006: CO2 and CH4 exchanges between land ecosystems and the atmosphere in northern high latitudes over the 21st century. *Geophysical Research Letters*, **33**, -.

Zickfeld, K., M. Eby, H. D. Matthews, A. Schmittner, and A. J. Weaver, 2011: Nonlinearity of Carbon Cycle Feedbacks. *Journal of Climate*, **24**, 4255-4275.

Tables

Table 6.7: Global CH_4 budget for the past three decades (in $Tg(CH_4)\ yr^{-1}$). T-D stands for Top-Down inversions and B-U for Bottom-Up approaches. Full references are given at the end of the chapter. Ranges represent minimum and maximum values from the cited references. The sum of sources and sinks from B-U approaches does not automatically balance the atmospheric changes. Only studies covering at least five years of each decade have been used. For B-U studies, individual source types are also presented. For T-D inversions, the 1980s decade starts in 1984. As some atmospheric inversions did not reference their global sink, balance with the atmosphere and the sum of the sources has been assumed. One biomass burning estimate[22] excludes biofuels (a). Stratospheric loss for B-U is the sum of the loss by OH radicals, a 10 Tg yr^{-1} loss due to O^1D radicals (Neef et al., 2010) and a 20–35% contribution due to Cl radicals[24].

$Tg(CH_4)\ yr^{-1}$	1980–1989		1990–1999		2000–2009	
	Top-Down	**Bottom-Up**	**Top-Down**	**Bottom-Up**	**Top-Down**	**Bottom-Up**
Natural Sources	**203 [150–267]**	**355 [229–451]**	**182 [167–197]**	**336 [215–450]**	**218 [179–273]**	**347 [223–469]**
Natural Wetlands	**167 [115–231]** [1,2,3]	**225 [183–266]** [4,5]	**150 [144–160]** [1,28,29]	**206 [169–265]** [4,5,27]	**175 [142–208]** [1,29,33,34,35,36]	**217 [177–284]** [4,5,27]
Other Sources	**36 [35-36]** [1,2]	**130 [46-185]**	**32 [23-37]** [1, 28,29]	**130 [46-185]**	**43 [37-65]** [1,29,33,34,35,36]	**130 [46-185]**
Freshwater (Lakes & Rivers)		40 [8–73] [6,7,8]		40 [8–73] [6,7,8]		40 [8–73] [6,7,8]
Wild Animals		15 [-] [9]		15 [-] [9]		15 [-] [9]
Wildfires		3 [1–5] [9,10,11,12,13]		3 [1–5] [9,10,11,12,13]		3 [1–5] [9,10,11,12,13]
Termites		11 [2–22] [9,10,14,15,x]		11 [2–22] [9,10,14,15,x]		11 [2–22] [9,10,14,15,x]
Geological (Incl. Oceans)		54 [33–75] [10,16,17]		54 [33–75] [10,16,17]		54 [33–75] [10,16,17]
Hydrates		6 [2-9] [9,18,19]		6 [2-9] [9,18,19]		6 [2-9] [9,18,19]
Permafrost (Excl. lakes & wetlands)		1 [0-1] [10]		1 [0-1] [10]		1 [0-1] [10]
Anthropogenic Sources	**349 [305–383]**	**307 [304-310]**	**372 [290–453]**	**300 [267–330]**	**331 [273–409]**	**318 [289–353]**
Agriculture & Waste	**208 [187-220]** [1,2,3]	**185 [178-197]** [20]	**239 [180-301]** [1, 28,29]	**187 [180-193]** [20,30,31]	**209 [180-241]** [1,29,33,34,35,36]	**200 [188-217]** [20,30,31]
Rice		43 [41-47] [20]		37 [32-44] [20,27,30,31]		38 [32-44] [20,27,30,31]
Ruminants		85 [81-90] [20]		86 [82-92] [20,30,31]		89 [87-97] [20,30,31]
Landfills & Waste		56 [50-60] [20]		65 [61-68] [20,30,31]		75 [65-90] [20,30,31]
Biomass Burning (Incl. Biofuels)	**47 [43-55]** [1,2,3]	**20 [17-23]** [21,22a]	**38 [26-45]** [1, 28,29]	**25 [21-28]** [13,21,22a,32]	**26 [16-45]** [1,29,33,34,35,36]	**18 [16-20]** [13,21,32,37]
Fossil Fuels	**94 [75-108]** [1,2,3]	**102 [-]** [20]	**95 [84-107]** [1, 28,29]	**88 [66-109]** [20,30,31]	**96 [77-123]** [1,29,33,34,35,36]	**100 [85-116]** [20,30,31]
Sinks						
Total Chemical Loss	**490 [450–533]** [1,2,3]	**539 [411–671]** [23,24,25,26]	**525 [491–554]** [1,28,29]	**571 [546–646]** [23,24,25,26]	**518 [510–538]** [1,29,33,34,36]	**604 [509–764]** [23,24,25,2
Tropospheric OH		468 [382–567] [26]		479 [457–501] [26]		528 [454–617] [25,26]
Stratospheric OH		46 [16–67] [23,25,26]		67 [51–83] [23,25,26]		51 [16–84] [23,25,26]
Tropospheric Cl		25 [13-37] [24]		25 [13-37] [24]		25 [13-37] [24]
Soils	21 [10–27] [1,2,3]	25 [-] [27]	27 [-] [1]	25 [-] [27]	33 [26-42] [1,33,34,35,36]	26 [-] [27]

Global						
Sum of Sources	**552 [500–592]**	**662**	**554 [529–596]**	**636**	**549 [526–569]**	**665**
Sum of Sinks	**511 [460–559]**	**539 [411-671]**	**542 [518–579]**	**596 [546–646]**	**540 [514–560]**	**630 [509–764]**
Imbalance (Sources-Sinks)	**30 [16–40]**		**12 [7–17]**		**9 [-4–19]**	
Atmospheric Growth Rate	**34**		**17**		**6**	

[1] Bousquet et al. (2011)
[2] Fung et al. (1991)
[3] Hein et al. (1997)
[4] Hodson et al. (2011)
[5] Ringeval et al. (2011)
[6] Bastviken et al. (2004)
[7] Bastviken et al. (2011)
[8] Walter et al. (2007)
[9] Denman et al. (2007)
[10] EPA (2010)
[11] Hoelzemann et al. (2004)
[12] Ito and Penner (2004)
[13] van der Werf et al. (2010)
[14] Sanderson (1996)
[15] Sugimoto et al. (1998)
[16] Etiope et al. (2008)
[17] Rhee et al. (2009)
[18] Dickens (2003)
[19] Shakhova et al. (2010)
[20] EDGAR4-database (2009)
[21] Mieville et al. (2010)
[22] Schultz et al. (2007) (a excluding biofuels)
[23] Neef et al. (2010)
[24] Allan et al. (2007)
[25] Williams et al. (2012b)
[26] Kirschke et al. (subm.)
[27] Spahni et al. (2011)
[28] Chen and Prinn (2006)
[29] Pison et al. (2009)
[30] Dentener et al. (2005)
[31] EPA (2011)
[32] van der Werf (2004)
[33] Bergamaschi et al. (2009)
[34], [35], [36] Kirschke et al. (subm.)
[37] Wiedinmyer et al. (2011)

Table 6.8: Section 1 gives the Global N budget (TgN yr^{-1}): a) creation of reactive N, b) emissions of NO_x, NH_3 in 2000s to atmosphere, c) deposition of N to land and oceans and d) discharge of total N to coastal ocean. Section 2 gives the N_2O budget for the year 2005, and for the 1990s compared to AR4. Unit: Tg(N_2O-N) yr^{-1}.

SECTION 1 (NOy and NHx)			
a. Conversion of N_2 to Nr	**2005**		**References**
Anthropogenic sources			
Fossil Fuel Combustion	24.5		Galloway et al. (2008)
Haber-Bosch Process			
Fertilizer	100		Galloway et al. (2008)
Industrial Feedstock	24		Galloway et al. (2008)
BNF	70 (60–80)		Herridge et al. (2008)
Anthropogenic total	**219**		
Natural sources			
BNF, terrestrial	100 (90–120)		Galloway et al. (2004)
BNF, marine	100 (60–200)		Duce et al. (2008)
Lightning	4 (3–5)		AR4
Natural total	**204**		
Total Conversion of N_2 to reactive N	**423**		
b. Emissions to atmosphere			
	NO_x	**NH_3**	
Fossil Fuel Combustion & industrial processes	28.3	0.5	Dentener et al. (2006)
Agriculture	3.7	30.4	Dentener et al. (2006)
Biomass and biofuel burning	5.5	9.2	Dentener et al. (2006)
Anthropogenic total	**37.5**	**40.1**	
Natural Sources			
Soils under natural vegetation	7.3 (5–8)	2.4 (1–10)	AR4
Oceans	-	8.2 (3.6)	AR4
Lightning	4 (3–5)	-	AR4
Natural total	**11.3**	**10.6**	AR4
Total Sources	**48.8**	**50.7**	
c. Deposition from the atmosphere			
	NO_y	**NH_x**	
Continents	27.1	36.1	Lamarque et al. (2010)
Oceans	19.8	17.0	Lamarque et al. (2010)
Total	46.9	53.1	
d. Discharge to coastal ocean			
Surface water N flux	45		Mayorga et al. (2010)

SECTION 2 (N_2O)			
	AR5 (2006)	**AR5 (mid-1990s)**	**AR4 (1990s)**
Anthropogenic sources			
Fossil fuel combustion & industrial processes	0.7 (0.2–1.8)[a]	0.7 (0.2–1.8)[a]	0.7 (0.2–1.8)
Agriculture	4.1 (1.7–4.8) [b]	3.7 (1.7–4.8) [b]	2.8(1.7–4.8)
Biomass and biofuel burning	0.7(0.2–1.0)[a]	0.7(0.2–1.0)[a]	0.7(0.2–1.0)
Human excreta	0.3 (0.1–0.4)[a]	0.3 (0.1–0.4)[a]	0.2 (0.1–0.3)
Rivers, estuaries, coastal zones	0.6 (0.1–2.9)[c]	0.6 (0.1–2.9)[c]	1.7(0.5–2.9)
Atmospheric deposition on land	0.4 (0.3–0.9)[d]	0.4 (0.3–0.9)[d]	0.6 (0.3–0.9)
Atmospheric deposition on ocean	0.2 (0.1–0.4)[e]	0.9 (0.5–1.4)[e]	-
Surface sink	–0.01 (0–1)[f]	–0.01 (0-1)[f]	-

Anthropogenic total	**6.9**	**6.5**	**6.7**
Natural sources[a]			
Soils under natural vegetation	6.6 (3.3–9.0)	6.6 (3.3–9.0)	6.6 (3.3–9.0)
Oceans	3.8(1.8–5.8)	3.8(1.8–5.8)	3.8(1.8–5.8)
Lightning	–	–	–
Atmospheric chemistry	0.6 (0.3–1.2)	0.6 (0.3–1.2)	0.6 (0.3–1.2)
Natural total	**10.8**	**10.8**	**11.0**
Total sources	**17.8 (8.5–27.7)**	**17.4 (8.5–27.7)**	**17.7 (8.5–27.7)**

Notes:
(a) As in AR4 (not based on 2006 IPCC Guidelines); lower end of range in the natural ocean from Rhee et al. (2009).
(b) Direct soil emissions and emissions from animal production; calculated following 2006 IPCC Guidelines (Syakila and Kroeze, 2011); Range from AR4.
(c) Following 2006 IPCC Guidelines (Kroeze et al., 2010; Syakila and Kroeze, 2011); Higher end of range from AR4; lower end of range from 1996 IPCC Guidelines (Mosier et al., 1998). Note that a recent studies indicates that IPCC may underestimate emissions from rivers (Beaulieu et al., 2011a).
(d) Following 2006 IPCC Guidelines (Syakila and Kroeze, 2011).
(e) Suntharalingam et al. (2012).
(f) Syakila et al. (2010).

Table 6.9: Comparison of the magnitude of changes in carbon storage (PgC) by land and ocean over different timescales. These changes are shown as approximate numbers to allow a comparison across timescales. For more details see the indicated chapter section. An indication, where known, of what causes these changes (climate, CO_2, land-use change) is also given with an indication of the sign: '+' means that an increase in CO_2 or global-mean temperature is associated with an increase in carbon storage (positive β or γ), and a '–' means an increase in CO_2 or global-mean temperature is associated with a decrease in carbon storage (negative β or γ). The processes which operate to drive these changes can vary markedly from seasonal phenology of vegetation to long-term changes in ice sheet cover or ocean circulation. Some of these processes are 'reversible' in the context that they can increase and decrease cyclically, whereas some are 'irreversible' in the context that changes in one sense might be much longer than in the opposite direction.

Time Period	Duration	Land			Ocean		Section
		Climate	CO_2	Land Use	Climate	CO_2	
Seasonal Cycle	Weeks-Months	3–8 [a]			2	1	6.3.2.5.1
		+				+	
Interannual Variability	Months-Years	2–4 [b]			1	0.2	6.3.2.5.4
		–			+	+	
Historical (1750–Present)	Decades-Centuries	150 [c]		–180	2	155	6.3.2.5.3, Table 6.1
		–	+		?	+	
21st Century	Decades-Centuries	100–400 [d]		–100 to +100 [e]	100–600 [d]		6.4.3
		–	+		–	+	
Little Ice Age (LIA) [f]	Century	+5		+2 to +30			6.2.3
		–	+				
Holocene	10 kyr	+300		–50 to –150	+270 to –220 [g]		6.2.2
		+	+				
LGM / Glacial Cycles	>10 kyr	+300 to +1000 [h]			–500 to –1200 [h]		6.2.1
		+	+		–	+	
Pulse [i], 100 PgC	1 kyr	+0 to +35		n/a	+48 to +75		6.2.2
			+		–	+	

Notes:
(a) Dominated by northern mid- to high-latitudes.
(b) Dominated by the tropics.
(c) 'Residual terrestrial sink', Table 6.1.
(d Varies widely according to scenario. Climate effect estimated separately for RCP4.5 as –157 PgC (combined land and ocean), but not for other scenarios.
(e) Future scenarios may increase or decrease area of anthropogenic land use.
(f) Little Ice Age, 1500–1750.
(g) Shown here are two competing drivers of Holocene ocean carbon changes: carbonate accumulation on shelves (coral growth) and carbonate compensation to pre-Holocene changes. These are discussed in Section 6.2.2.
(h) Defined as positive if increasing from LGM to present, negative if decreasing.
(i) Idealised simulations with models to assess the response of the global carbon cycle to a sudden release of 100 PgC.

Table 6.10: CMIP5 model descriptions in terms of carbon cycle attributes and processes.

Model	Modelling Centre	Atmos Resolution	Ocean Resolution	Land-Carbon						Ocean Carbon			Reference
				Model Name	Dynamic Vegetation Cover?	#PFTs	Incl. LUC?	N-cycle	Fire	Model Name	#Plankton Types	Micro-nutrients?	
BCC-CSM1.1	BCC	≈2.8°, L26	0.3–1°, L40	BCC_AVIM1.0	N	15		N	N	OCMIP2	n/a	n/a	Wu et al. (subm.)
CanESM2	CCCma	T63, L35	1.41° × 0.94°, L40	CTEM	N	9	Y	N	N	CMOC	1	N	Arora et al. (2011)
CESM1-BGC	NSF-DOE-NCAR	FV 0.9 x 1.25	1°	CLM4	N	15	Y	Y	Y	BEC	4	Y	Lindsay et al. (subm.)
GFDL-ESM2G	NOAA GFDL	2x2.5°, L24	1°, tri-polar, 1/3° at equator, L63.	LM3	Y	5	Y	N	Y	TOPAZ2	6	y	Dunne et al. (2012); Dunne et al. (subm.)
GFDL-ESM2M	NOAA GFDL	2x2.5°, L24	1°, tri-polar, 1/3° at equator, L50.	LM3	Y	5	Y	N	Y	TOPAZ2	6	y	Dunne et al. (2012); Dunne et al. (subm.)
HadGEM2-ES	MOHC	N96 (ca. 1.6°), L38	1°, 1/3 ° at equator, L40	JULES	Y	5	Y	N	N	Diat-HadOCC	3	Y	Collins et al. (2011); Jones et al. (2011)
INMCM4	INM												
IPSL-CM5A-LR	IPSL	3.75x1.9 , L39	Zonal 2°, Meridional 2°–0.5° L31	ORCHIDEE	N	13	Y	N	Y	PISCES	2	Y	Dufresne et al. (subm.)
MIROC-ESM	MIROC	T42, L80	Zonal: 1.4°, Meridional: 0.5–1.7°, Vertical: L43+BBL1	SEIB-DGVM	Y	13	Y	N	N	NPZD (Oschlies, 2001)	2 (Phyoto-plankton and Zoolo-plankton)	N	Watanabe et al. (2011)
MPI-ESM-LR	MPI-M	T63 (ca. 1.9°), L47	ca.1.5°, L47	JSBACH	Y	12 (8 natural)	Y	N	Y	HAMOCC	2	Y	Raddatz et al. (2007), Brovkin et al. (2009), Maier-Reimer et al. (2005)
NorESM-ME	NCC	1.9x2.5°, L26	1°, L53	CLM4	N	16	Y	Y	Y	HAMOCC	2	N	Bentsen et al. (subm.), Iversen et al. (subm.)

Table 6.16: Characteristics of some CDR methods which have peer-reviewed literature. It should be noted that a variety of economic, environmental, and other constraints could also limit deployment.

Carbon Dioxide Removal Method	Means of Removing CO_2 from Atmosphere	Carbon Storage /Form	Time Scale of Carbon Storage	Physical Potential of CO_2 Removed in a Century*	Reference	Unintended Side Effects
Afforestation and reforestation	Biological	Land /Organic	Decades to centuries	80–140 PgC[a], 48 PgC[b]	[a]Canadell and Raupach (2008) [b]Sitch et al. (2005)	Alters surface energy budget; depending on location, climate change is increased or decreased
Biomass energy with carbon capture and storage	Biological	Geological or ocean /Inorganic	Effectively permanent for geologic, centuries for ocean	100 PgC	[≠]See the footnote	Same as above
Biochar	Biological	Land /Organic	Decades to centuries	130 PgC	Woolf et al. (2010)	Same as above
Ocean fertilisation	Biological	Ocean /Inorganic	Centuries to millennia	30–66 PgC[c] 200Pg C[d]	[c]Aumont and Bopp (2006), Zeebe and Archer (2005) [d]Cao and Caldeira (2010a)	Expanded regions with low oxygen concentration; Altered production of DMS and non-CO_2 greenhouse gases; possible disruptions to marine ecosystems and regional carbon cycles
Accelerated weathering over land	Geo-chemical	Ocean (and some soils) /Inorganic	Centuries to millennia for carbonates, permanent for silicate weathering	[e]No determined limit [f]100 PgC	[e]Kelemen and Matter (2008), Schuiling and Krijgsman (2006) [f]Köhler et al. (2010)	pH of soils and rivers could be increased locally causing disturbance to existing ecosystems
Ocean-based weathering	Geo-chemical	Ocean /Inorganic	Centuries to millennia for carbonates, permanent for silicate weathering	No determined limit	Rau (2008), Kheshgi (1995)	Increased alkalinity could disturb existing marine ecosystems
Direct air capture	Chemical	Geological or ocean /Inorganic	Effectively permanent for geologic, centuries for ocean	No determined limit	Keith et al. (2006), Shaffer (2010)	Not known
Modification of upwelling/ down welling	Biological/ chemical	Ocean /Inorganic	Centuries to millennia	[g]90 PgC [h]1–2 PgC	[g] Oschlies et al. (2010a); [h] Lenton and Vaughan (2009), Zhou and Flynn (2005)	Likely to cause changes to regional carbon cycle

Notes:
* Physical potential does not account for economic or environmental constraints of CDR methods, for example the value of the physical constraint for afforestation and reforestation does not consider the conflicts with land needed for agricultural production. Potentials for BECCS and biochar are highly speculative.
[≠] If 2.5 tC per year per hectare can be harvested on a sustainable basis Kraxner et al. (2003) on ~4% (~500 million hectares, about one tenth of global agricultural land area) of global land (13.4 billion hectares) for BECCS, approximately 1.25 PgC per year could be removed or about 125 PgC in this century.

Chapter 6: Carbon and Other Biogeochemical Cycles

Coordinating Lead Authors: Philippe Ciais (France), Christopher Sabine (USA)

Lead Authors: Govindsamy Bala (India), Laurent Bopp (France), Victor Brovkin (Germany), Josep Canadell (Australia), Abha Chhabra (India), Ruth DeFries (USA), James Galloway (USA), Martin Heimann (Germany), Christopher Jones (UK), Corinne Le Quéré (UK), Ranga Myneni (USA), Shilong Piao (China), Peter Thornton (USA)

Contributing Authors: Ayako Abe-Ouchi (Japan), Anders Ahlström (Sweden), Oliver Andrews (UK), David Archer (USA), Vivek Arora (Canada), Gordon Bonan (USA), Alberto Borges (Belgium), Philippe Bousquet (France), Lori Bruhwiler (USA), Kenneth Caldeira (USA), Long Cao (China), Jerome Chappellaz (France), F. Chevallier (France), Cory Cleveland (USA), Peter Cox (UK), Frank J. Dentener (Italy), Scott Doney (USA), Jan Willem Erisman (The Netherlands), Eugenie Euskirchen (USA), Pierre Friedlingstein (UK), S. Gourdji (USA), Nicolas Gruber (Switzerland), Guido van der Werf (Netherlands), K. Gurney (USA), Paul Hanson (USA), Elizabeth Holland (USA), Richard A. Houghton (USA), Jo House (UK), Sander Houweling (TN), Stephen Hunter (UK), George Hurtt (US), A. Jacobson (USA), Atul Jain (USA), Fortunat Joos (Switzerland), Johann Jungclaus (Germany), Jed Kaplan (Switzerland), Etsushi Kato (Japan), Ralph Keeling (USA), Samar Khatiwala (USA), Stefanie Kirschke (France), Kees Klein Goldewijk (Netherlands), Silvia Kloster (Germany), Charlie Koven (USA), Carolien Kroeze (Netherlands), Jean-François Lamarque (USA), Keith Lassey (New Zealand), R. Law (Australia), Andrew Lenton (Australia), Spencer Liddicoat (UK), Mark R. Lomas (UK), Yiqi Luo (USA), Takashi Maki (Japan), Gregg Marland (USA), Damon Matthews (Canada), David McGuire (USA), Joe Melton (Switzerland), Nicolas Metzl (France), Vaishali Naik (USA), Y. Niwa (Japan), Richard Norby (USA), James Orr (France), Geun-Ha Park (USA), Prabir Patra (Japan), W. Peters (The Netherlands), Philippe Peylin (France), Stephen Piper (USA), Julia Pongratz (USA), Ben Poulter (France), Peter A. Raymond (USA), P. Rayner (Australia), Andy Ridgwell (UK), Bruno Ringeval (France), C. Roedenbeck (Germany), Marielle Saunois (France), Andreas Schmittner (USA), Edward Schuur (USA), Elena Shevliakova (USA), Stephen Sitch (UK), Renato Spahni (Switzerland), Benjamin Stocker (Switzerland), Taro Takahashi (USA), Rona Thompson (France), Jerry Tjiputra (Norway), Detlef van Vuuren (Netherlands), Apostolos Voulgarakis (USA), Rita Wania (Canada), Soenke Zaehle (Germany), Ning Zeng (USA)

Review Editors: Christoph Heinze (Norway), Pieter Tans (USA), Timo Vesala (Finland)

Date of Draft: 5 October 2012

Notes: TSU Compiled Version

Figures

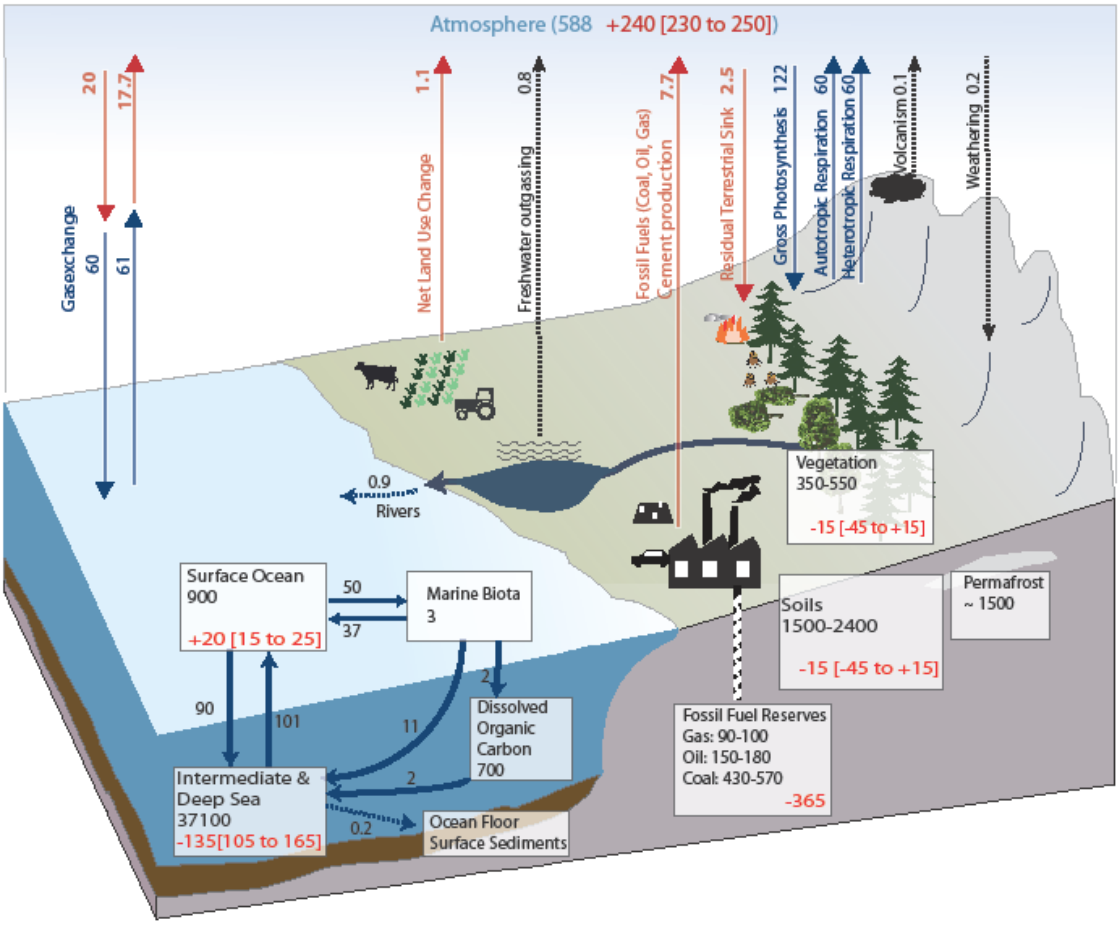

Figure 6.1: Simplified schematic of the global carbon cycle. Numbers represent reservoir sizes (in PgC), and carbon exchange fluxes (in PgC yr^{-1}). Dotted arrow lines denote carbon fluxes between the fast and the slow carbon cycle domain (see text). Darkblue numbers and arrows indicate reservoir sizes and natural exchange fluxes estimated for the time prior to the Industrial Era. Red arrows and numbers indicate fluxes averaged over 2000–2009 time period resulting from the emissions of CO_2 from fossil fuel combustion, cement production , and changes in land use, and their partitioning among atmosphere, ocean and terrestrial reservoirs (see Section 6.3). Red numbers in the reservoirs denote cumulative changes over the Industrial Period 1750–2011.

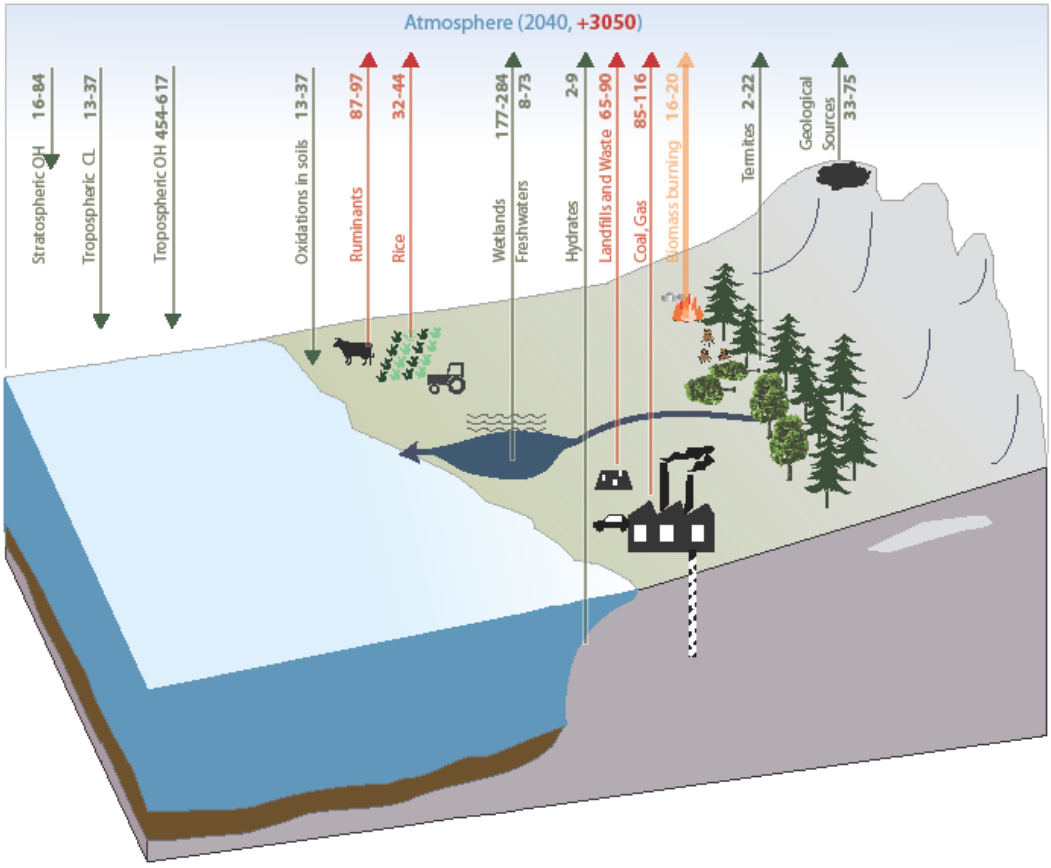

Figure 6.2: Schematic of the global cycle of CH_4. Numbers represent fluxes in Tg (CH_4) yr^{-1} estimated for the time period 2000–2009 (see Section 6.3). Green arrows denote natural fluxes, red arrows anthropogenic fluxes, and orange arrow denotes a combined natural+anthropogenic flux.

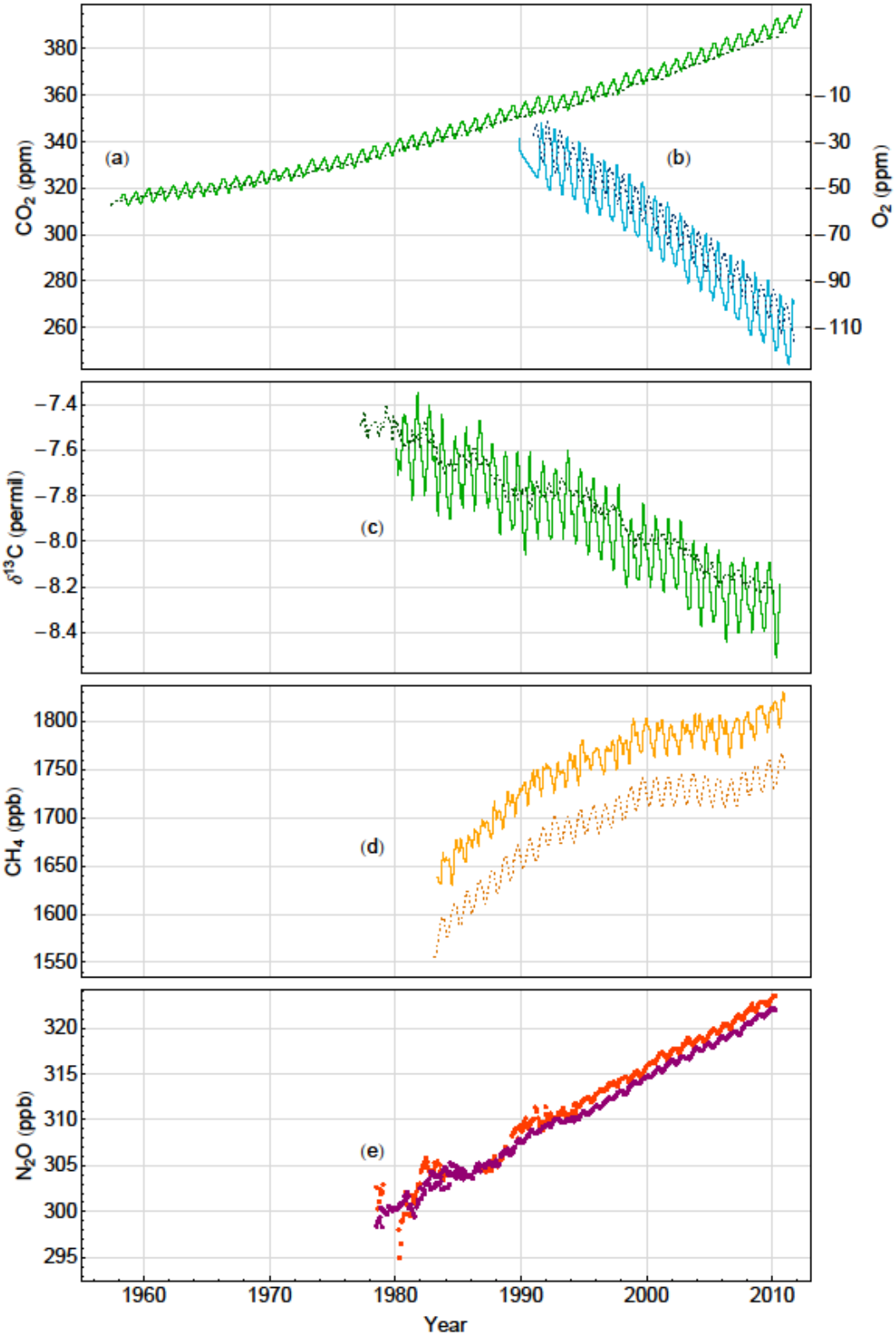

Figure 6.3: Atmospheric concentration of CO_2, oxygen, $^{13}C/^{12}C$ stable isotope ratio in CO_2, CH_4 and N_2O recorded over the last decades at representative stations in the northern (solid lines) and the southern (dashed lines) hemisphere. (**a:** CO_2 from Mauna Loa and South Pole atmospheric stations (Keeling et al., 2005), O_2 from Alert and Cape Grim stations (http://scrippso2.ucsd.edu/ right axes), **b:** $^{13}C/^{12}C$: Mauna Loa, South Pole (Keeling et al., 2005), **c:** CH_4 from Mauna Loa and South Pole stations (Dlugokencky et al., 2010), **d:** N_2O from Adrigole and Cape Grim stations (Prinn et al., 2000).

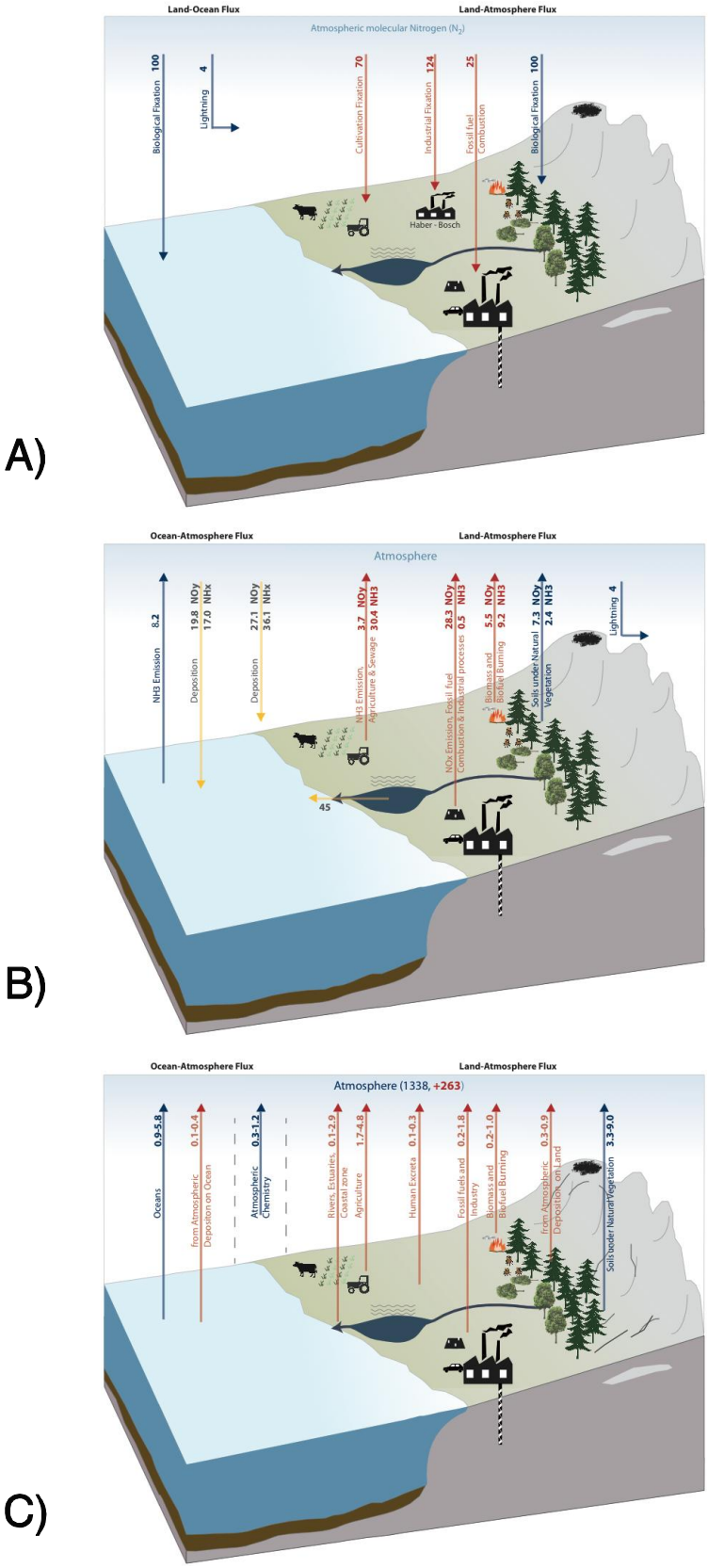

Figure 6.4: Global nitrogen cycle. The upper panel (A) shows natural and anthropogenic process that create reactive nitrogen Nr. The middle panel (B) shows the flows of reactive Nitrogen species. The bottom panel (C) shows a schematic of the global cycle of N_2O. Blue arrows are natural, red arrows anthropogenic fluxes, and yellow arrows represent fluxes with an anthropogenic and natural component. Units: TgN yr^{-1}.

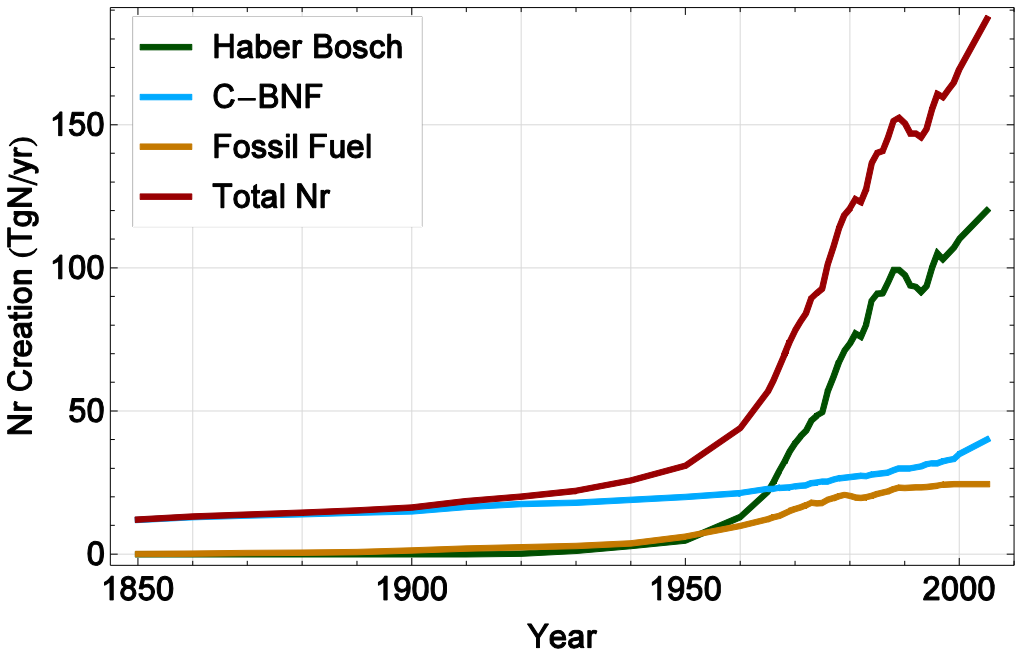

Box 6.1, Figure 1: Reactive nitrogen (Nr) creation fluxes (in TgN yr^{-1}) from fossil fuel burning (green line), cultivation-induced BNF, C-BNF (red line), Haber-Bosch process (blue line), and total creation (purple line). Source: Galloway et al. (2003), Galloway et al. (2008).

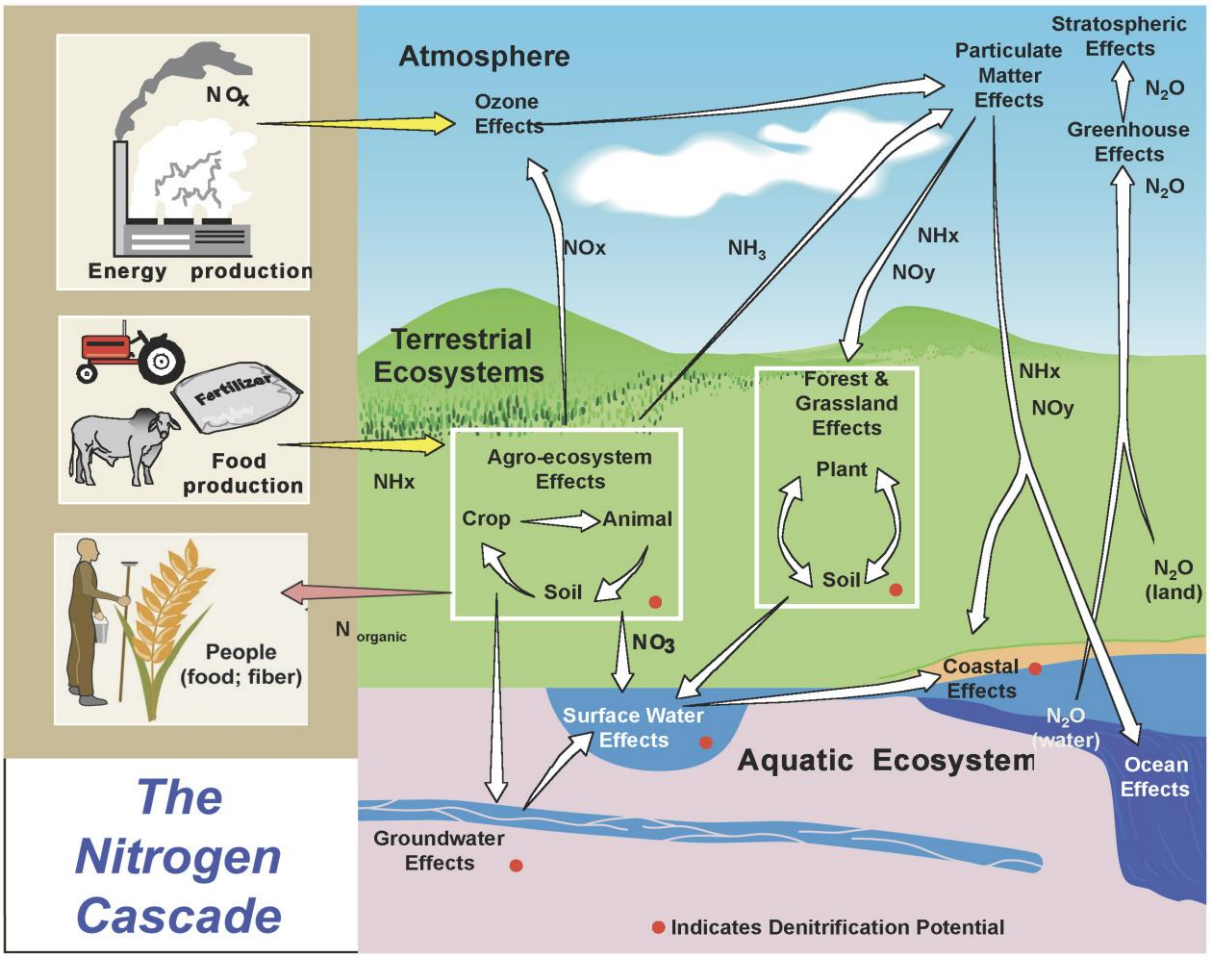

Box 6.1, Figure 2: Illustration of the nitrogen cascade showing the sequential effects that a single atom of N can have in various reservoirs after it has been converted from nonreactive N_2 to a reactive form (yellow arrows). Abbreviations: NH_3, ammonia; NH_x, ammonia plus ammonium; NO_3^-, nitrate; NO_x, nitrogen oxides; NO_y, NO_x and other combinations of N and O (except N O); N_2O, nitrous oxide (after Galloway et al.; 2003).

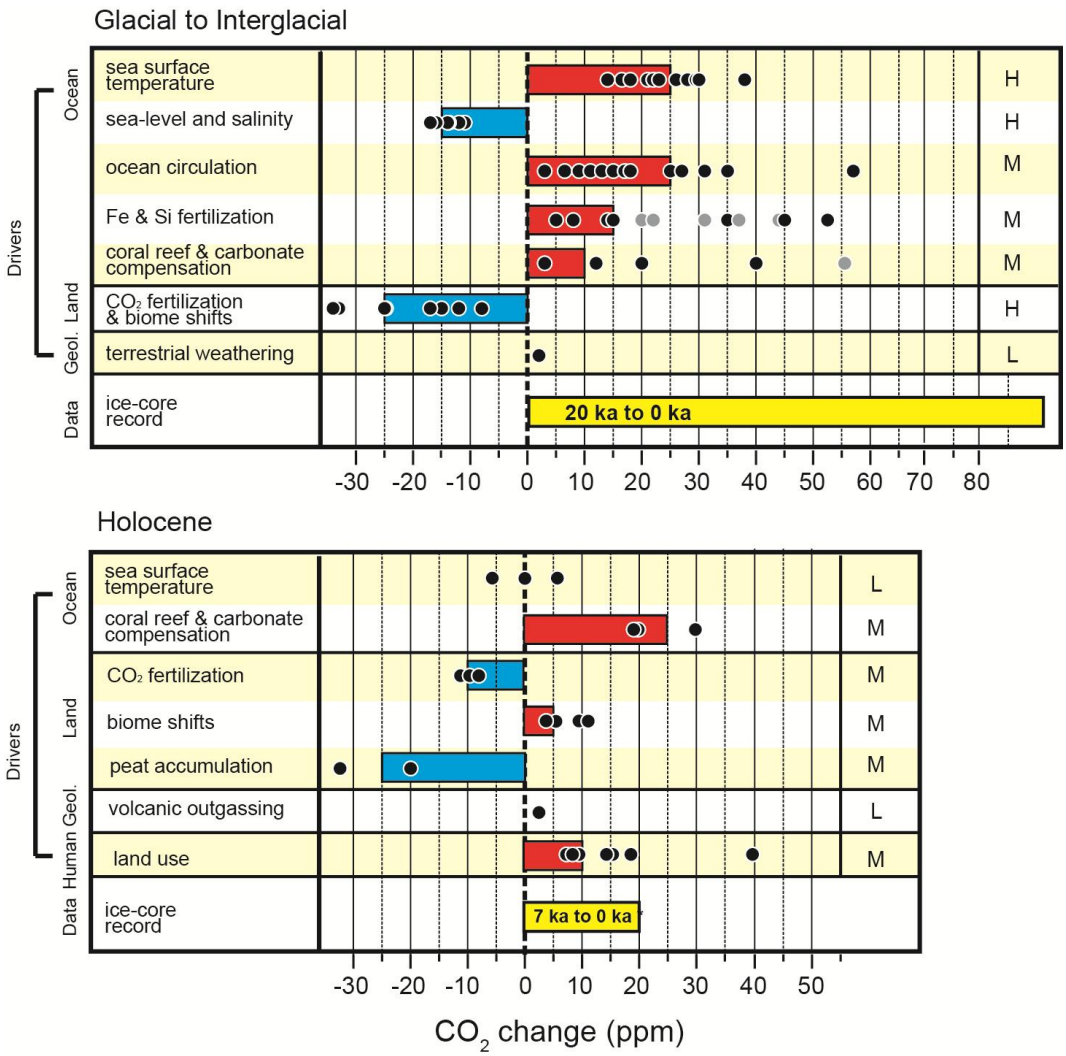

Figure 6.5: Carbon dioxide concentrations changes from LGM to late Holocene (top) and from early/mid Holocene (7 ka) to late Holocene (bottom). Filled black circles represent individual model-based estimates for individual ocean, land, geological or human drivers. Solid color bars represent expert judgment (to the nearest 5 ppm) rather than a formal statistical average. References for the different model assessment used for the glacial drivers are as per Kohfeld and Ridgwell (2009) with excluded model projections in grey. References for the different model assessment used for the Holocene drivers are Joos et al. (2004), Brovkin et al. (2008), Kleinen et al. (2010), Broecker et al. (1999), Ridgwell et al. (2003), Brovkin et al. (2002), Schurgers et al. (2006), Yu (2011), Kleinen et al. (2011), Ruddiman (2003, 2007), Strassmann et al. (2008), Olofsson and Hickler (2008), Pongratz et al. (2009), Kaplan et al. (2011), Lemmen (2009), Stocker et al. (2011) and Roth and Joos (2012).

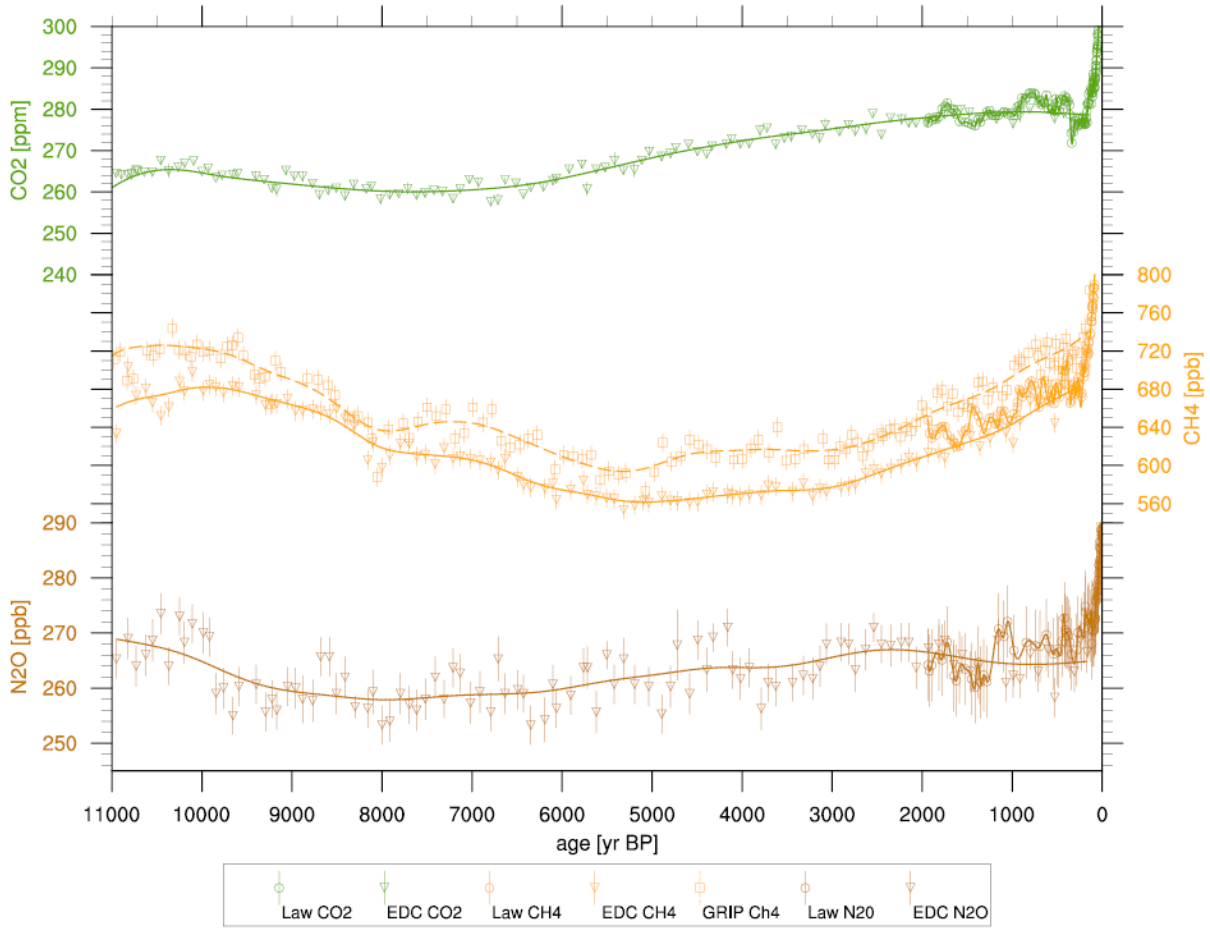

Figure 6.6: Variations of CO_2, CH_4, and N_2O concentrations during the Holocene. The data are for Antarctic ice cores: EPICA Dome C (Fluckiger et al., 2002; Monnin et al., 2004), triangles; Law Dome (MacFarling-Meure et al., 2006), circles, and for Greenland ice core GRIP (Blunier et al., 1995), squares. Lines are for spline fits.

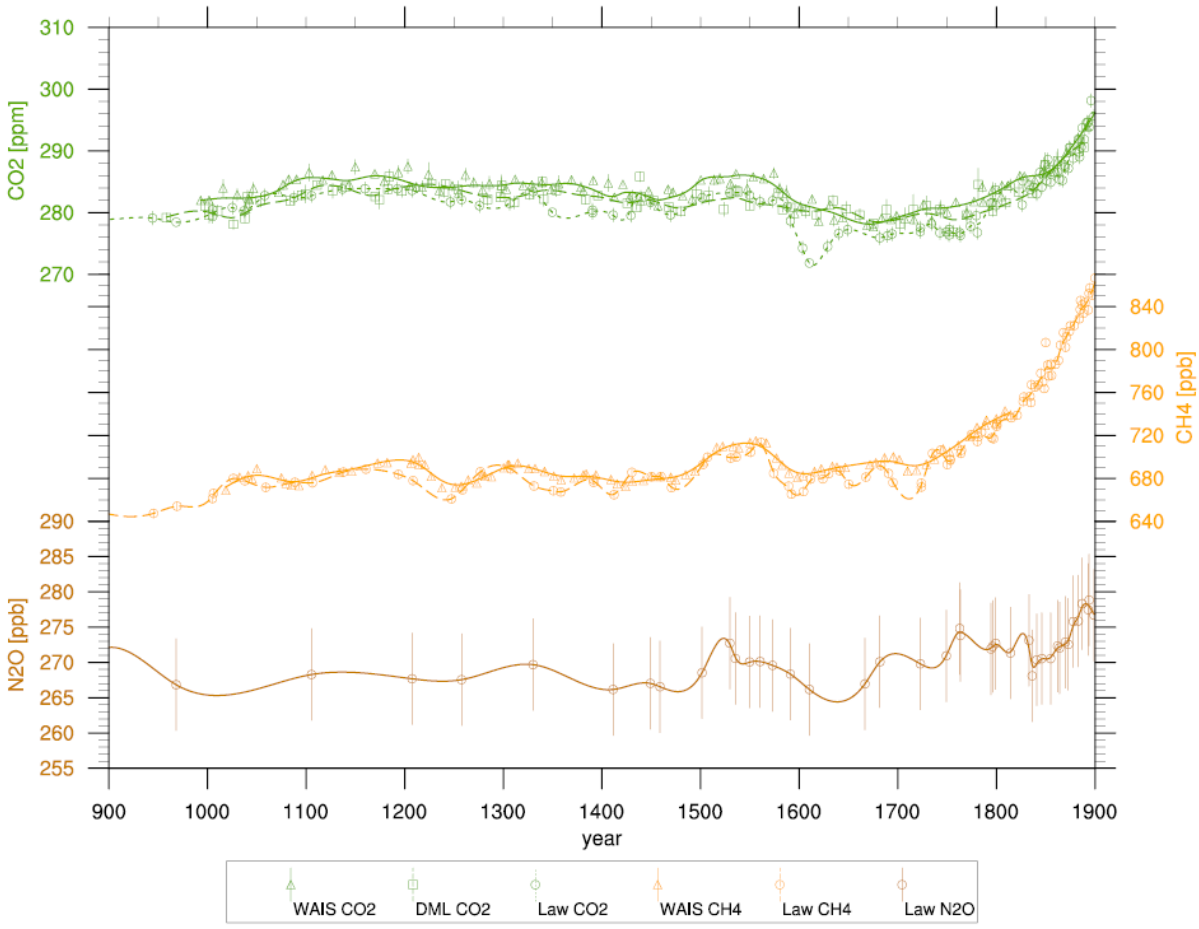

Figure 6.7: Variations of CO_2, CH_4, and N_2O during 900–1900 AD from ice cores. The data are for Antarctic ice cores: Law Dome (Etheridge et al., 1996; MacFarling-Meure et al., 2006), circles; West Antarctic Ice Sheet (Ahn et al., 2012; Mitchell et al., 2011), triangles; Dronning Maud Land (Siegenthaler et al., 2005a), squares. Lines are spline fits to individual measurements.

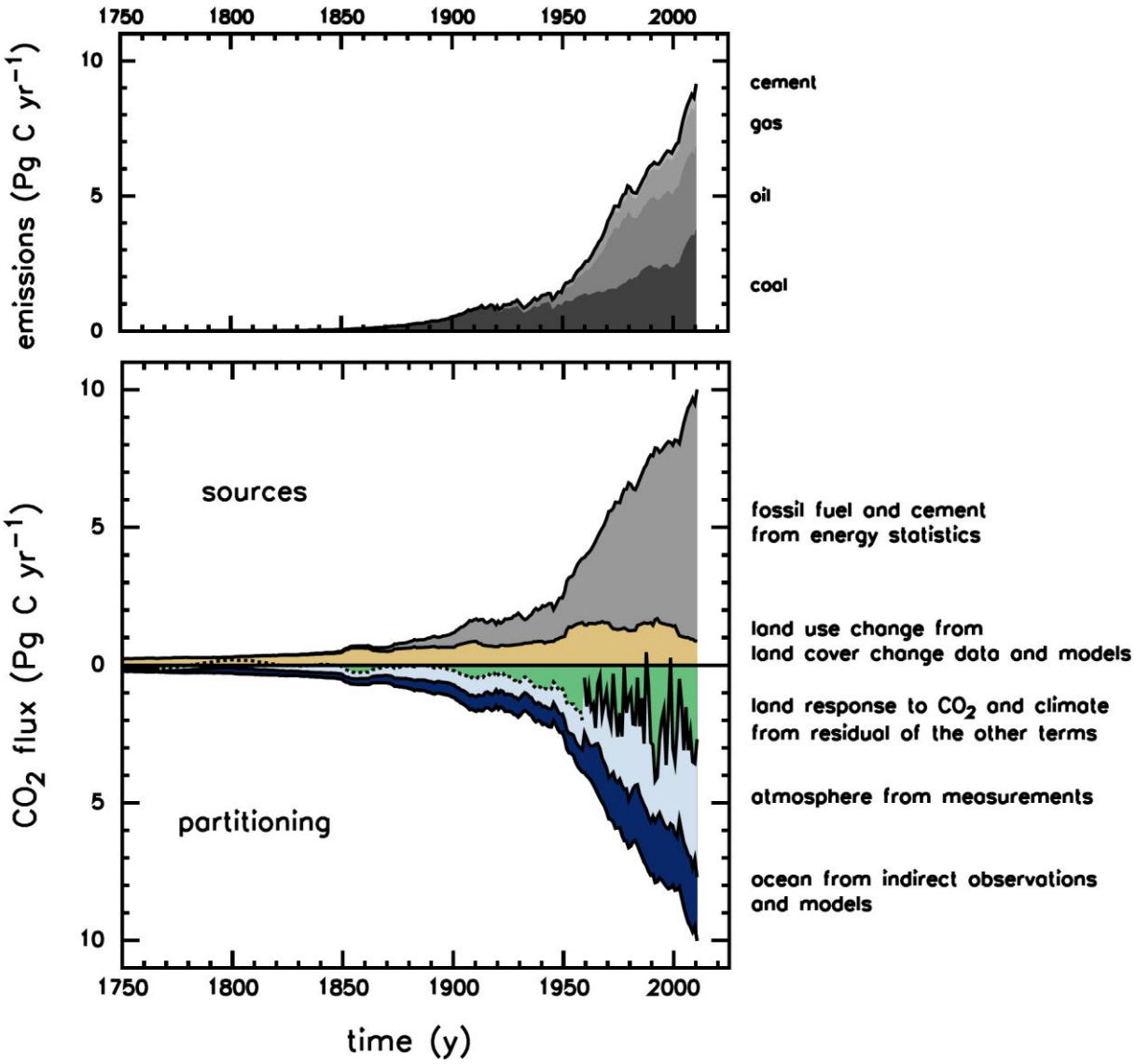

Figure 6.8: Sources and sinks fluxes (PgC yr^{-1}) for the component of the global anthropogenic CO_2 budget from 1750 to 2010. (Top) Fossil fuel and cement CO_2 emissions by category, estimated by the Carbon Dioxide Information Analysis Center (CDIAC) based on UN energy statistics for fossil fuel combustion and US Geological Survey for cement production (Boden et al., 2011). (Bottom) Fossil fuel and cement CO_2 emissions as above. CO_2 emissions from net land use change, mainly deforestation for 1750–1850 are from the average of estimates (Pongratz et al., 2009; Shevliakova et al., 2009b; vanMinnen et al., 2009; Zaehle et al., 2011) and from Houghton et al. (2012) after 1850. The atmospheric CO_2 growth rate prior to 1960 is based on a spline fit to ice core observations (Etheridge et al., 1996; Friedli et al., 1986; Neftel et al., 1982) and a synthesis of atmospheric observations from 1960 (Conway and Tans, 2011). The fit to ice core observations does not capture the large interannual variability in atmospheric CO_2 and is represented with a dashed line on the figure. The ocean CO_2 sink prior to 1960 is from Khatiwala et al. (2009) and from a combination of model and observations from 1960 updated from (LeQuere et al., 2009). The residual land sink is computed from the residual of the other terms. The sources and sinks only include the fluxes that have changed since 1750, and not the natural CO_2 fluxes (e.g., atmospheric CO_2 uptake from weathering, natural river transport of carbon from land to ocean, and compensatory CO_2 outgassing by the ocean) between the atmosphere, and ocean reservoirs that existed before that date and still exist today. The uncertainties in the various terms are discussed in the text and reported in Table 6.1.

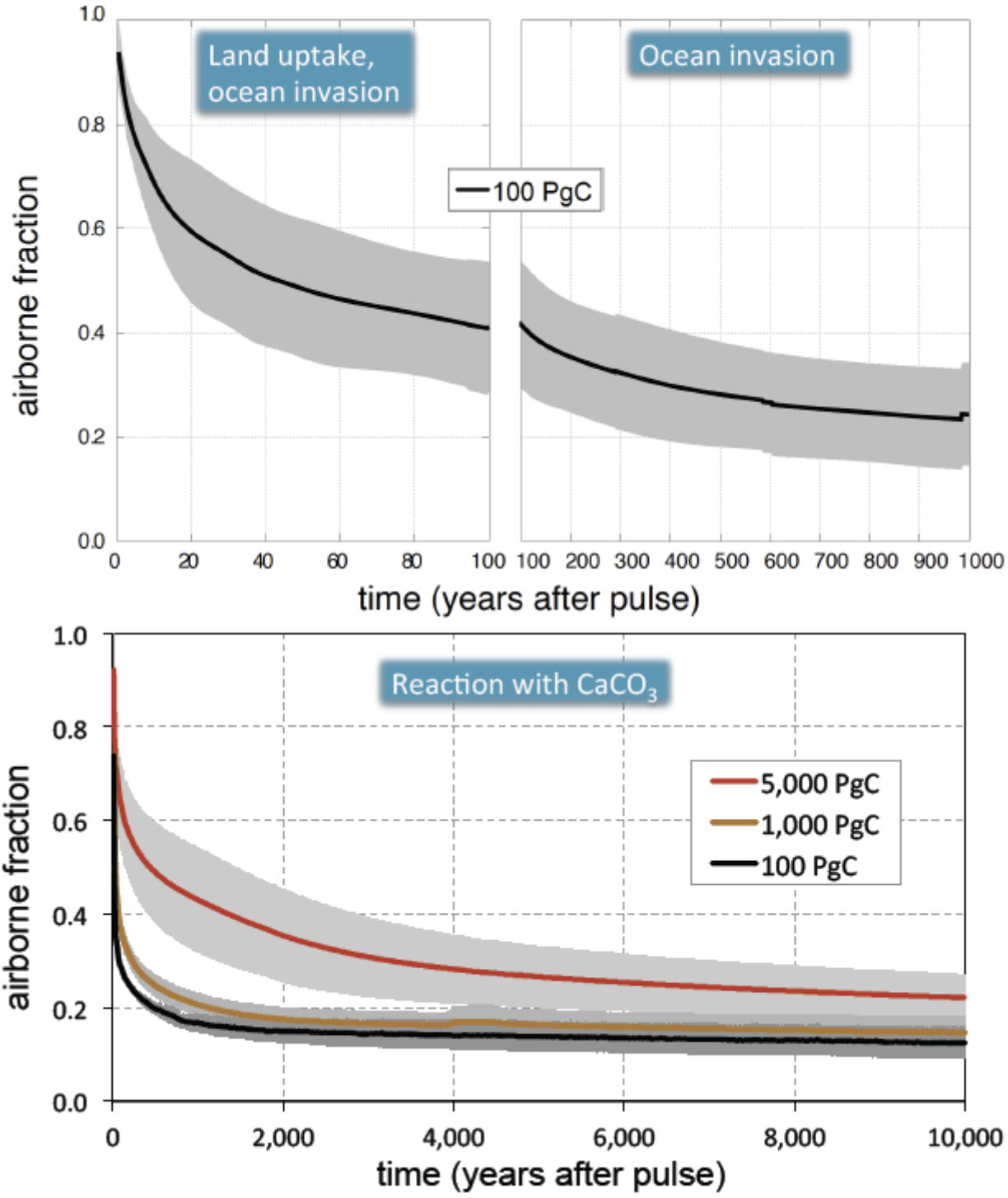

Box 6.2, Figure 1: A fraction of a given amount of CO_2 emitted to the atmosphere remaining in the atmosphere in response to an idealized instantaneous CO_2 pulse in year 0 as calculated by a range of coupled climate-carbon cycle models. (Top) Multi-model mean (black line) and the uncertainty interval (±2 standard deviations, grey shading) simulated during 1,000 years following the instantaneous pulse of 100 PgC (Joos et al., submitted). (Bottom) A mean of models with oceanic and terrestrial carbon components (solid lines) and a maximum range of these models (grey shading) for instantaneous CO_2 pulse in year 0 of 100 PgC (black), 1,000 PgC (brown) and 5,000 PgC (red line) on a time interval up to ten thousand years (Archer et al., 2009b). (Blue boxes) the dominant processes that remove the excess of CO_2 emitted in the atmosphere on the sucessive timescales. Note that higher pulse of CO_2 emissions leads to higher airborne CO_2 fraction (Section 6.3.2.4) due to reduced carbonate buffer capacity of the ocean and positive climate-carbon cycle feedback (Section 6.3.2.6.6).

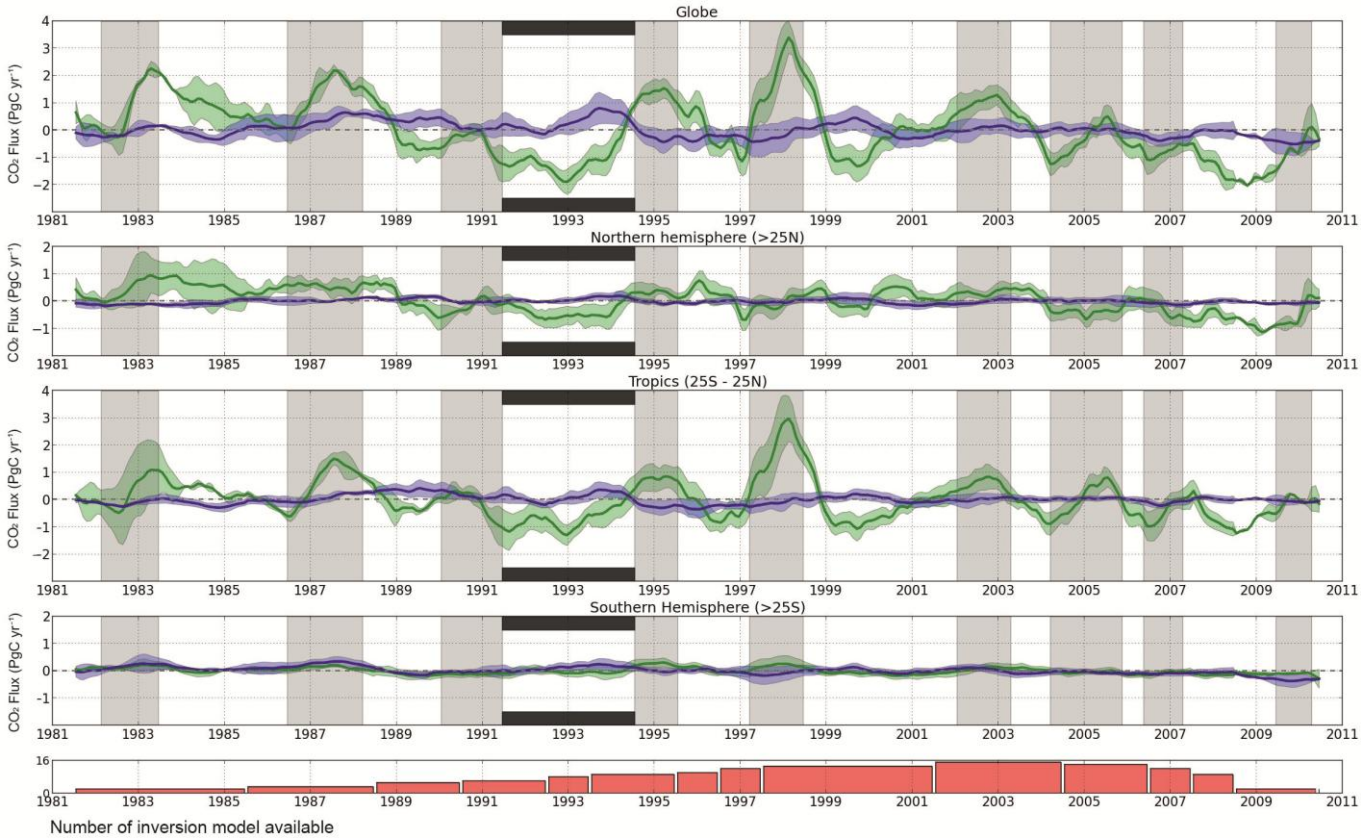

Figure 6.9: The interannual variability of surface CO_2 fluxes from inversions of the TRANSCOM project for the period of 1981–2010. The ensemble of inversion results contains up to 17 atmospheric inversion models. The orange bars at the bottom panel indicates the number of available inversion models for each time period. The ensemble mean is bounded by the 1 sigma inter-model spread in ocean-atmosphere (blue) and land-atmosphere (green) CO_2 fluxes (PgC yr^{-1}) grouped into large latitude bands, and the global. For each flux and each region, the CO_2 flux anomalies were obtained by subtracting the long term mean flux from each inversion and removing the seasonal signal. Grey shaded regions indicate El Niño episodes, and the back bars indicate the cooling period following the Mt. Pinatubo eruption. A positive flux means a larger than normal source of CO_2 to the atmosphere (or a smaller CO_2 sink).

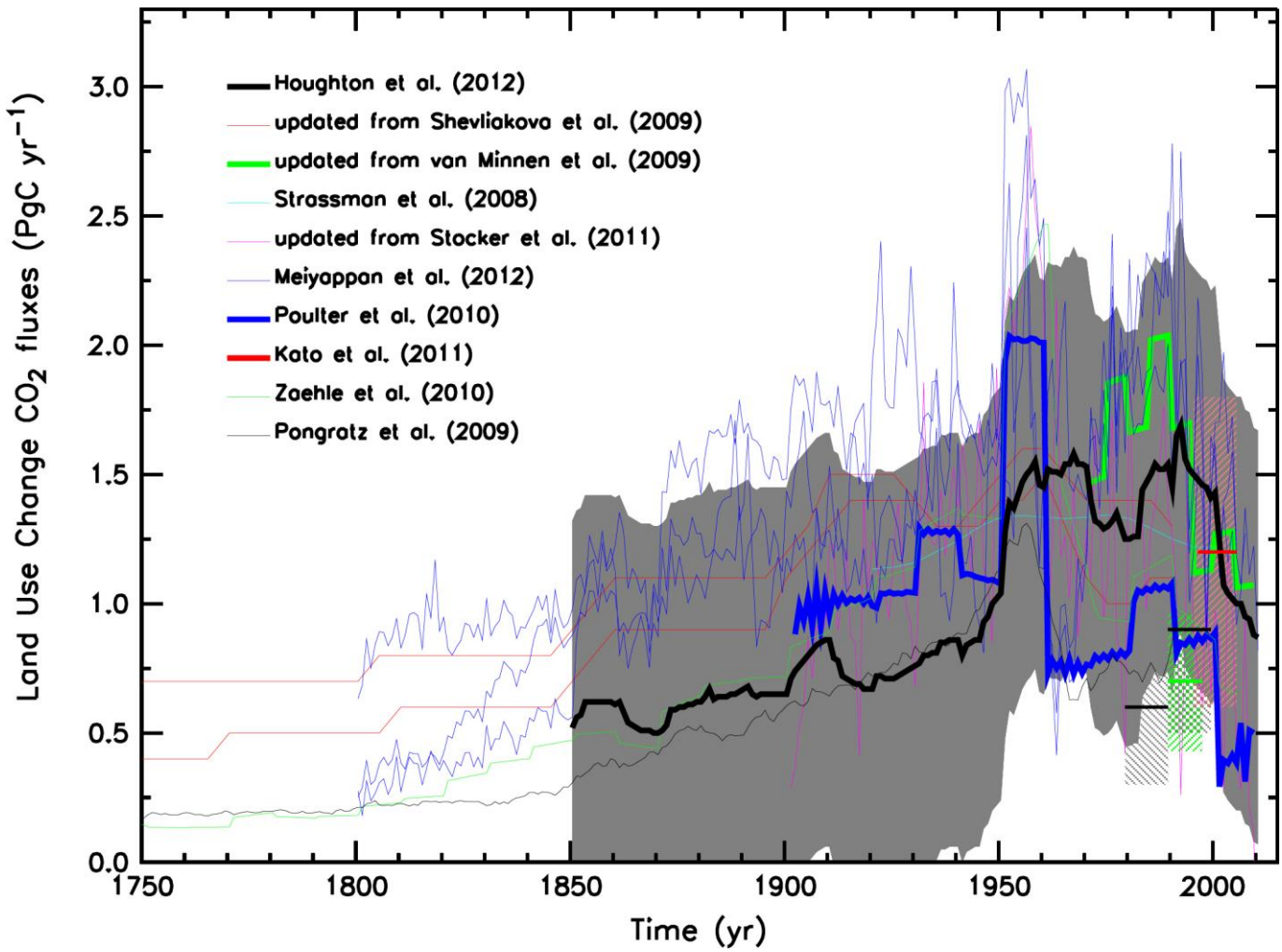

Figure 6.10: CO_2 emissions from land use change from a range of methods (PgC yr^{-1}). The estimate from Houghton et al. (2012) (thick black) is used in Table 6.1. The sources for the other estimates are shown in the legend and described in Table 6.2.

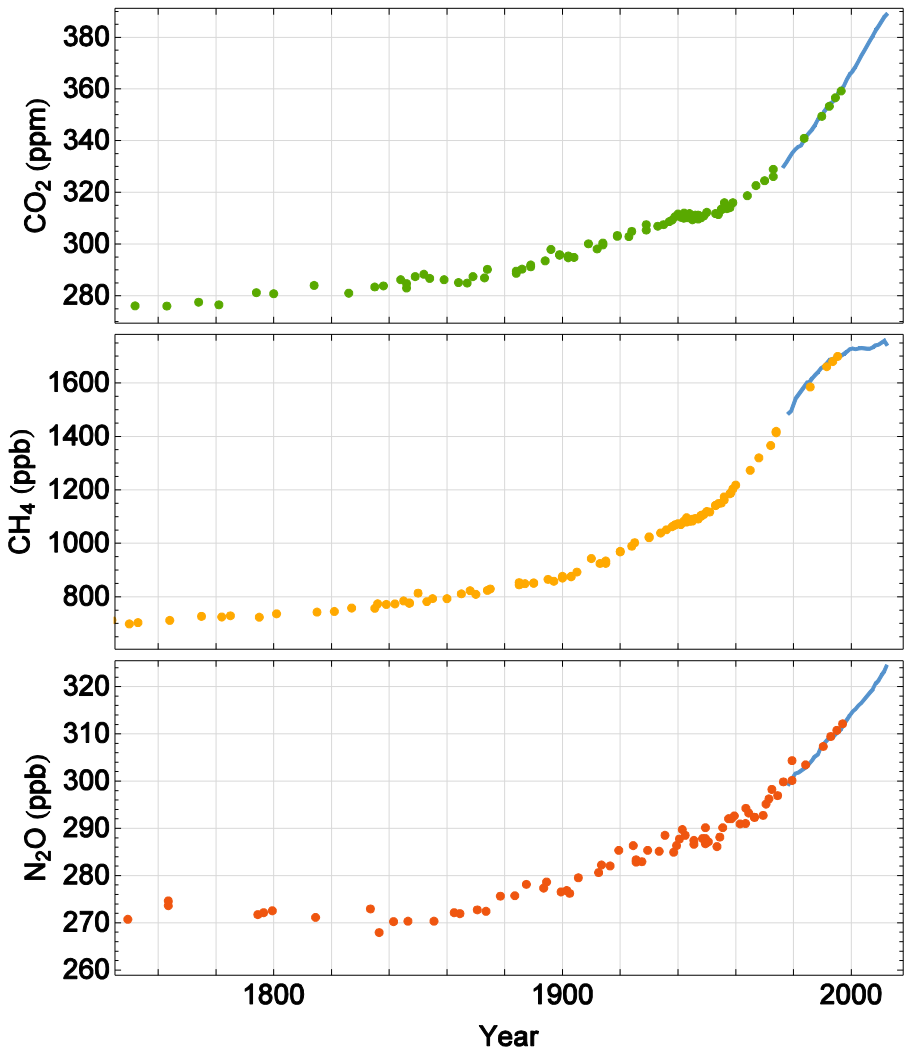

Figure 6.11: Atmospheric CO_2, CH_4, and N_2O concentrations history over the last 260 years determined from air enclosed in ice cores and firn air (color symbols) and from direct atmospheric measurements (blue lines, measurements from the Cape Grim observatory) (MacFarling-Meure et al., 2006).

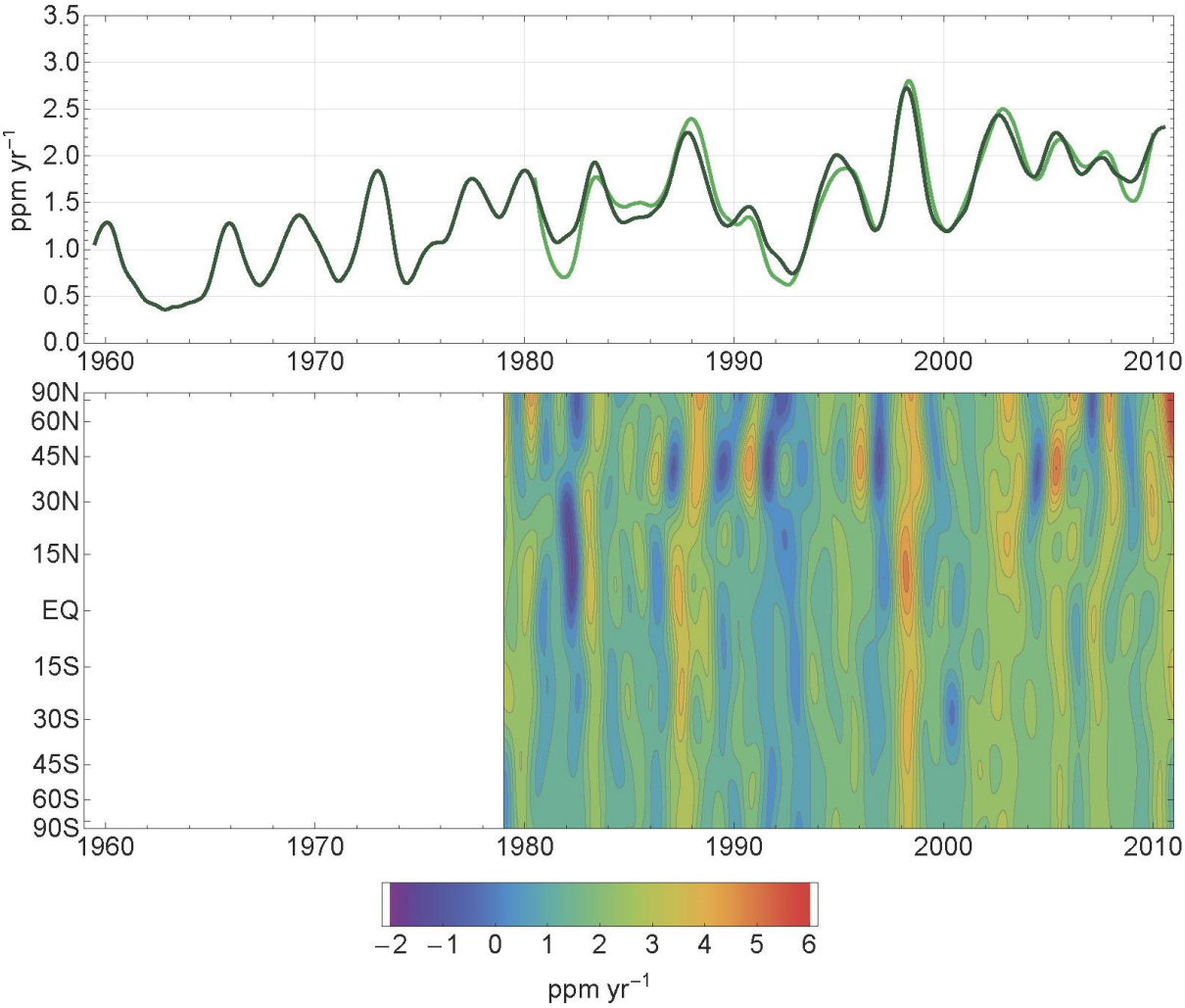

Figure 6.12: (Top) Global average atmospheric CO_2 growth rate, computed from the observations of the SIO network (dark green curve; Keeling et al., 2005) and from the marine boundary layer air reference measurements of the NOAA-GMD network (Conway et al., 1994; Keeling et al., 2005). (Bottom) Atmospheric growth rate of CO_2 as a function of latitude determined from the GLOBALVIEW data product, representative of stations located in the marine boundary layer at each given latitude (Masarie and Tans, 1995). Sufficient observations are available only since 1979.

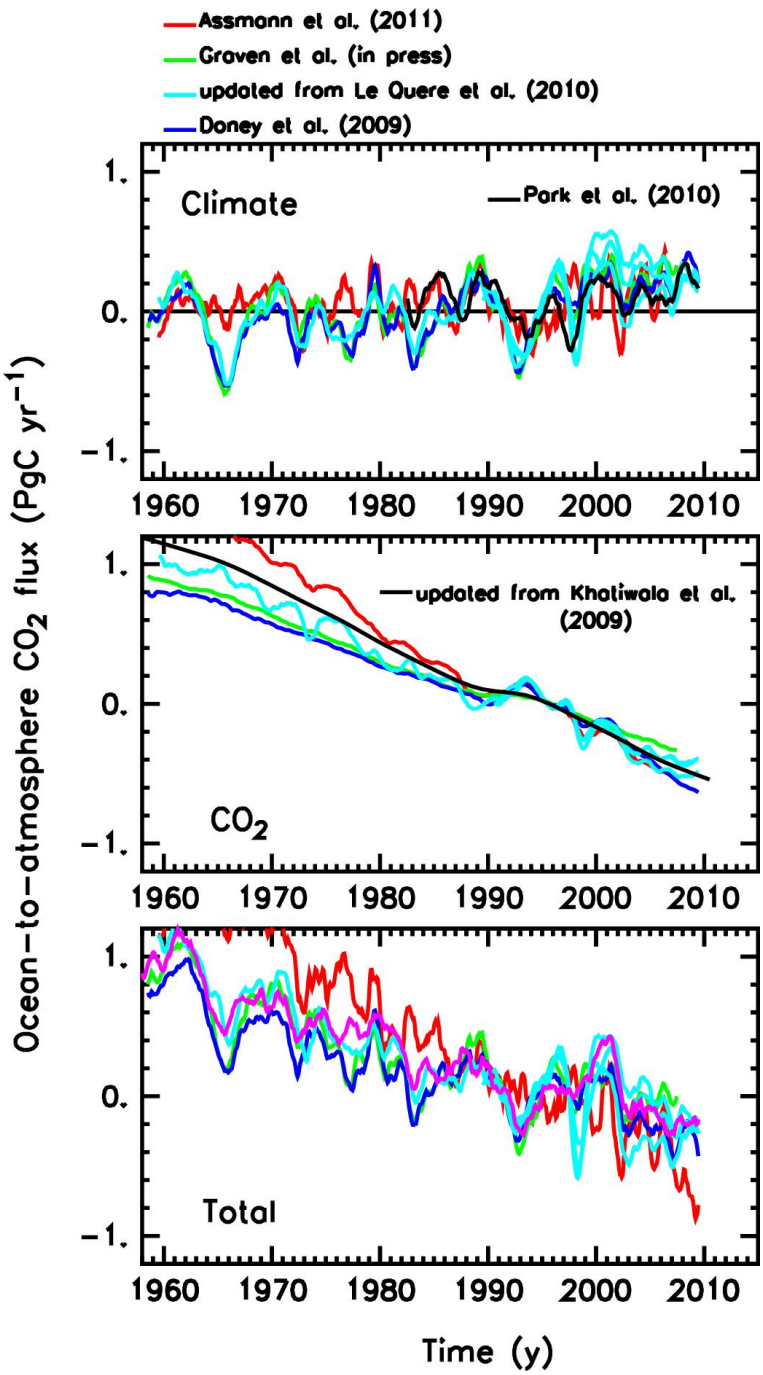

Figure 6.13: Trends in the ocean-to-atmosphere flux of CO_2 in response to: (Top) variability and trends in surface climate, (middle) increasing atmospheric CO_2, and (Bottom) the sum of both effects (PgC yr^{-1}). All estimates are normalized to zero during 1990–2000 to highlight the trends. Estimates are updates from ocean models (in colours) and from indirect methods based on observations (Khatiwala et al., 2009; Park et al., 2010).

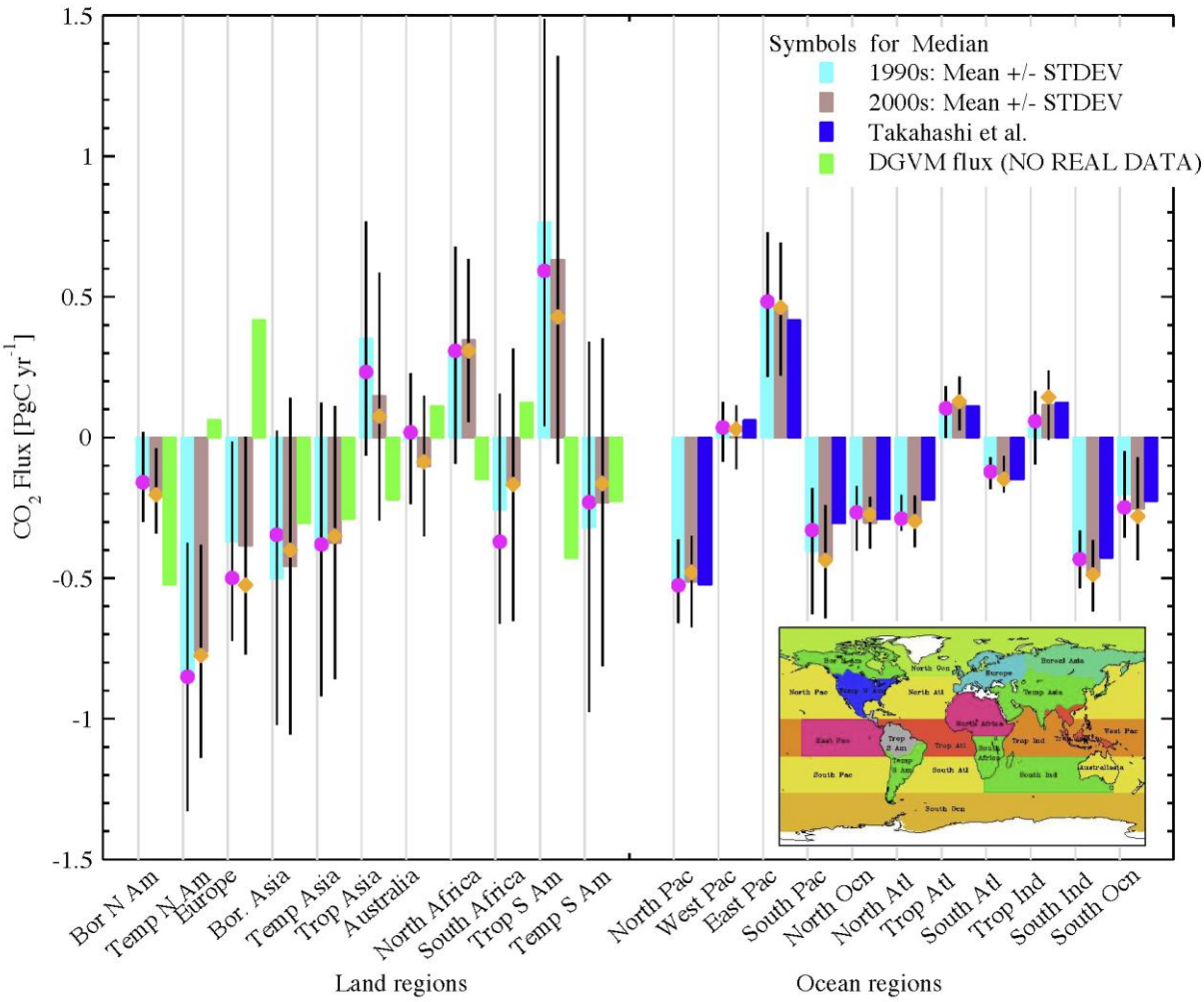

Figure 6.14: Decadal average CO_2 fluxes for 22 partitions of the globe for (1) the 1990s (cyan) and 2000s (brown) as estimated by atmospheric CO_2 inversions, (2) the dynamic vegetation models (DGVMs), and (3) pCO_2 measurements based air-sea exchange climatology. The regional partitions are depicted as an inset and shaded by CO_2 flux density (blue-green-brown: -ve flux, red-grey: +ve flux). The mean values are calculated from monthly-mean fluxes from 17 inverse models for the period of 1990–2008, and standard deviations shown as error bars are for model-to-model differences within each decade. The DGVM fluxes are calculated using 14 climate-carbon model simulations (not true values).

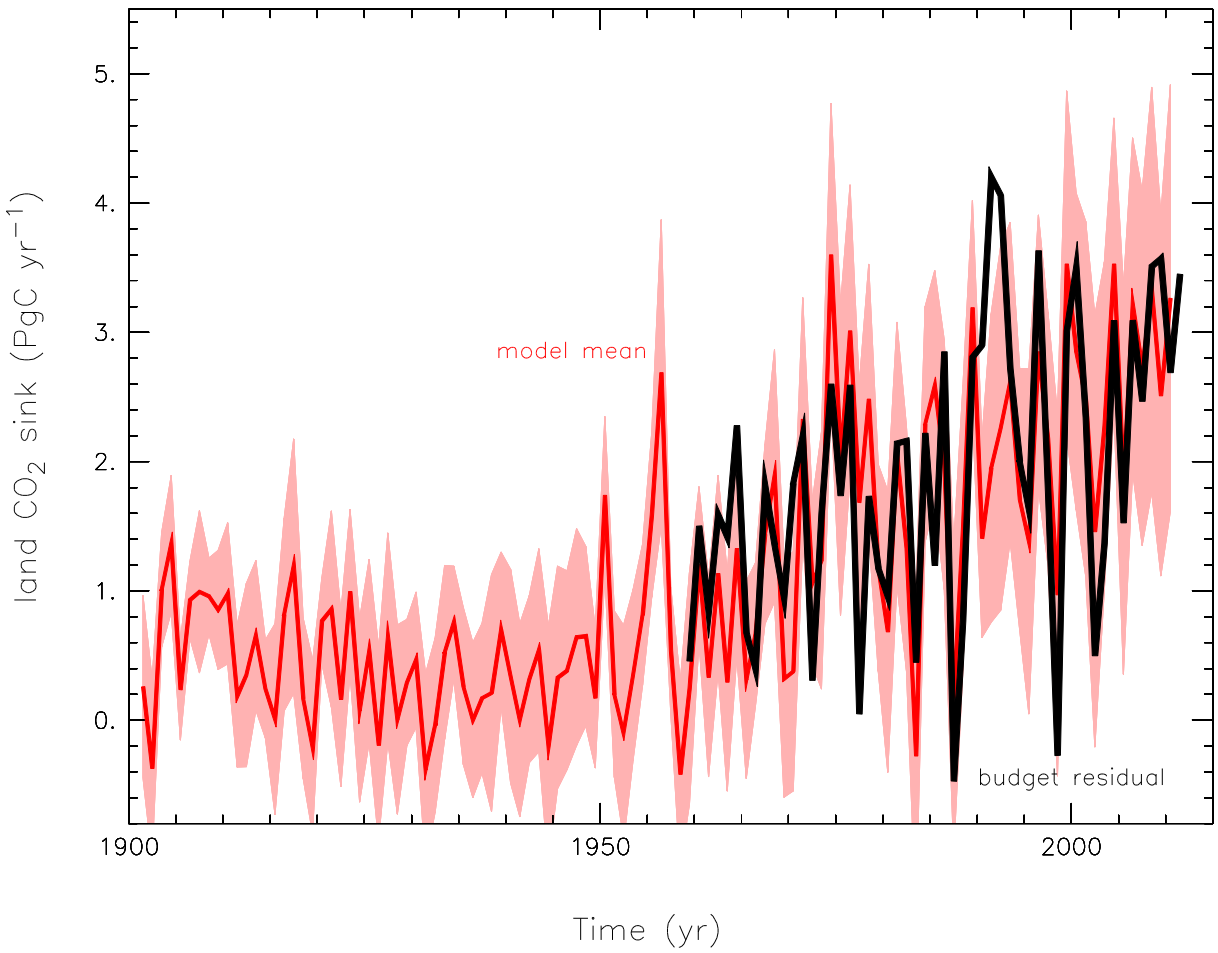

Figure 6.15: Time series for the land CO_2 sink showing the residual land sink deduced (1) from the global budget (Figure 6.8) with the black line being obtained as the difference between emissions from fossil fuel and land use change, minus the atmospheric growth rate and the ocean sink, and (2) from global process-based terrestrial ecosystem models (Table 6.6 for references) shown as red lines. The red shading shows one standard deviation from the model mean.

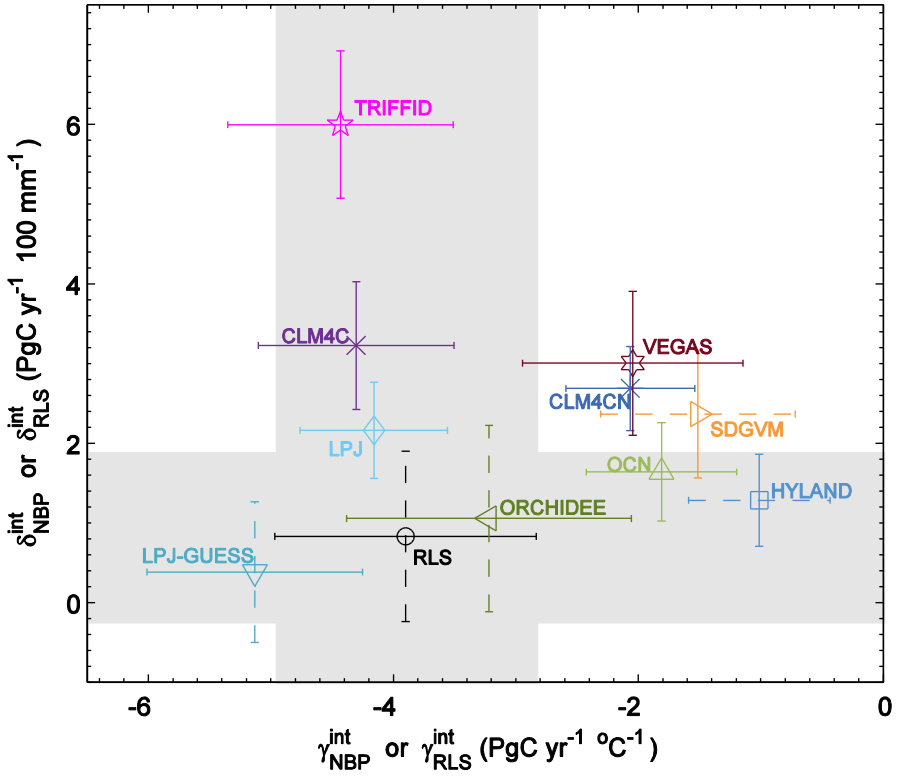

Figure 6.16: The sensitivity of Net Ecosystem Production (NEP) to interannual variation in temperature and interannual variation in precipitation at the global and regional scales. The gloal residual land sink is estimated as the sum of fossil fuel and cement emissions and land use change emissions minus the sum of CO_2 growth rate and modelled ocean sink (Friedlingstein and Prentice, 2010; Le Quere et al., 2009). The sensitivities of NEP to interannual variation of temperature and precipitation are estimated by a multiple linear regression approach using detrended NEP as dependent variable and detrended annual temperature and annual precipitation as independent variables (Piao et al., subm.). 10 carbon cycle models are Community Land Model 4C (CLM4C), Community Land Model 4CN (CLM4CN), Hyland (HYL), Lund-Potsdam-Jena (LPJ), LPJ_GUESS, ORCHIDEE-CN (OCN), ORCHIDEE (ORC), Sheffield-DGVM (SDGVM), TRIFFID (TRI), and VEGAS. Negative value indicates decrease in carbon sink.

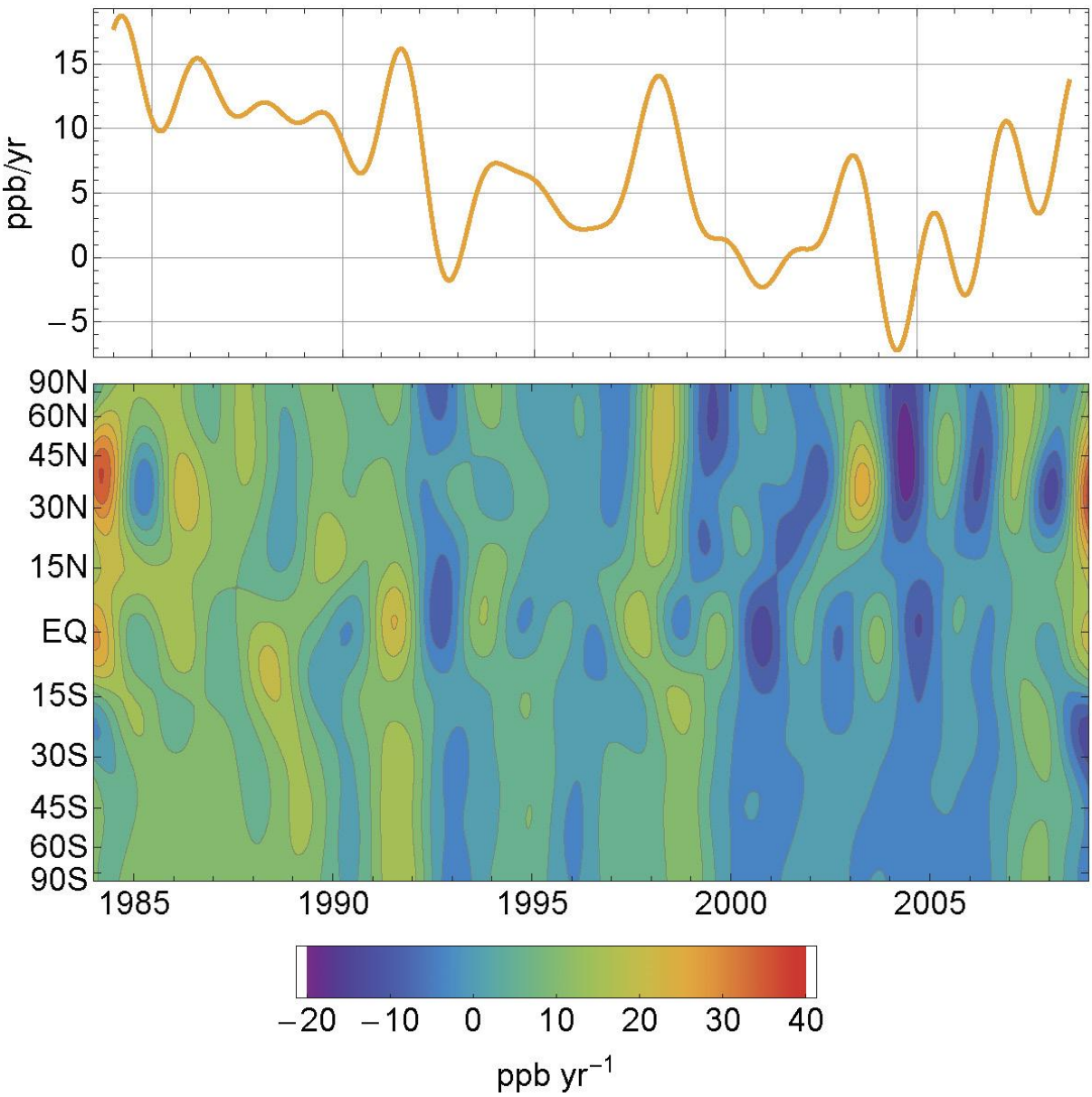

Figure 6.17: Upper panel: Globally averaged growth rate of atmospheric CH_4 in ppb yr^{-1} determined from the GLOBALVIEW data product, representative for the marine boundary layer (Masarie and Tans, 1995). Lower panel: Atmospheric growth rate of CH_4 as a function of latitude determined from the GLOBALVIEW data product.

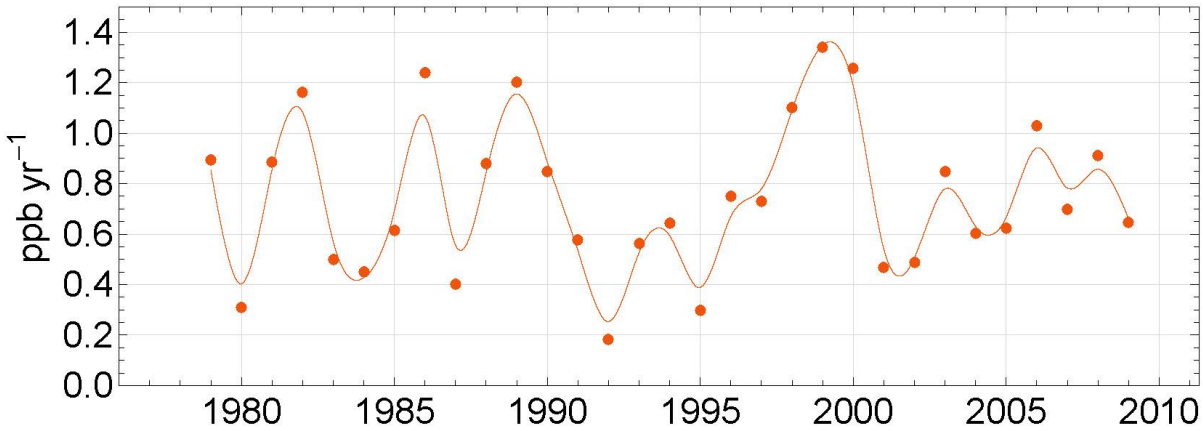

Figure 6.18: Globally averaged growth rate of N_2O in ppb yr^{-1} determined from the observations of the NOAA/ESRL halocarbons program. Brown dots indicate annual values augmented by a smoothed line to guide the eye.

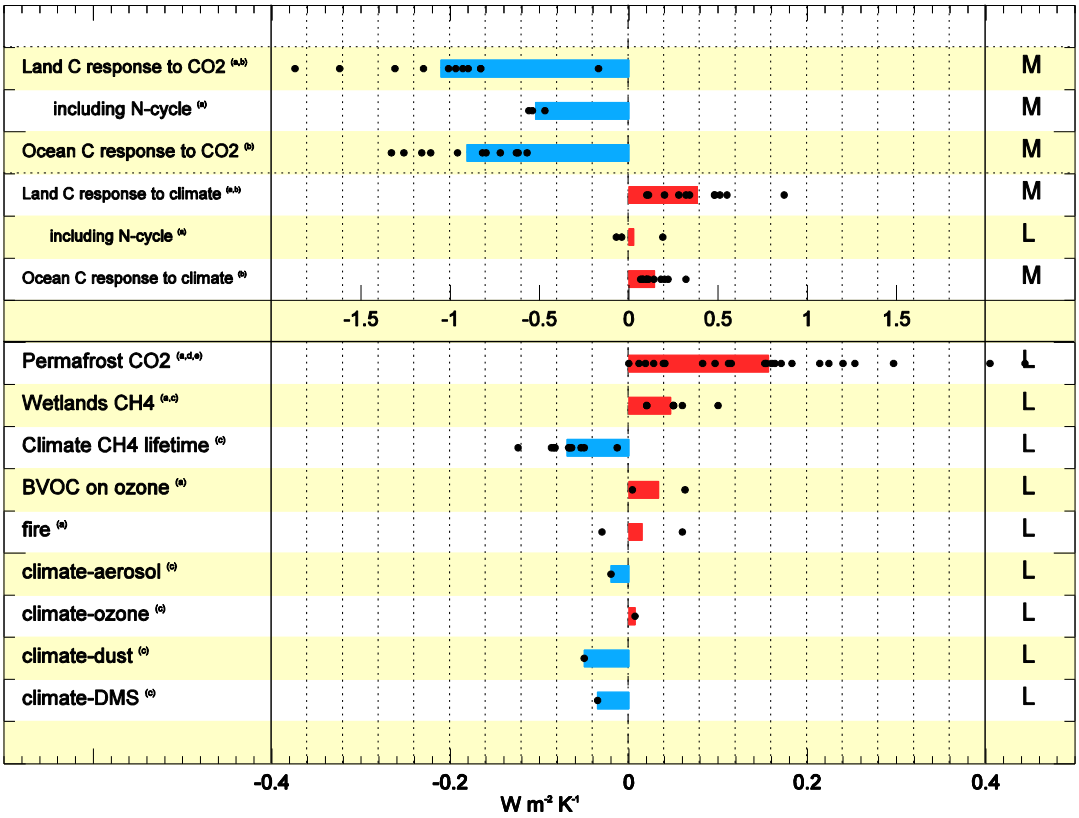

Figure 6.19: A summary of the magnitude of biogeochemical feedbacks. Gregory et al. (2009) proposed a framework for expressing non-climate feedbacks in common units (W m^{-2} K^{-1}) with physical feedbacks, and Arneth et al. (2010) extended this beyond carbon cycle feedbacks to other terrestrial biogeochemical feedbacks. The figure shows the results compiled by Arneth et al. (2010), with ocean carbon feedbacks from the C4MIP coupled climate-carbon models used for AR4 also added. Some further biogeochemical feedbacks from the HadGEM2-ES Earth System model (Collins et al., 2011) are also shown. Black dots represent single estimates, and coloured bars denote the simple mean of the dots with no weighting or assessment being made to likelihood of any single estimate. An indication of the confidence in the magnitude of these estimates is shown in the right hand column and is low for feedbacks with only one, or few, dots. The role of nitrogen limitation on terrestrial carbon sinks is also shown – this is not a separate feedback, but rather a modulation to the climate-carbon and concentration-carbon feedbacks. This list is not exhaustive. These feedback metrics are also likely to be state or scenario dependent and so cannot always be compared like-for-like (see Section 6.4.2.2). Results have been compiled from (a) Arneth et al. (2010), (b) Friedlingstein et al. (2006), (c) HadGEM2-ES (Collins et al., 2011) simulations, (d) Burke et al. (subm.), (e) von Deimling et al. (2012). Note the expanded x-axis scale for the lower portion of the figure.

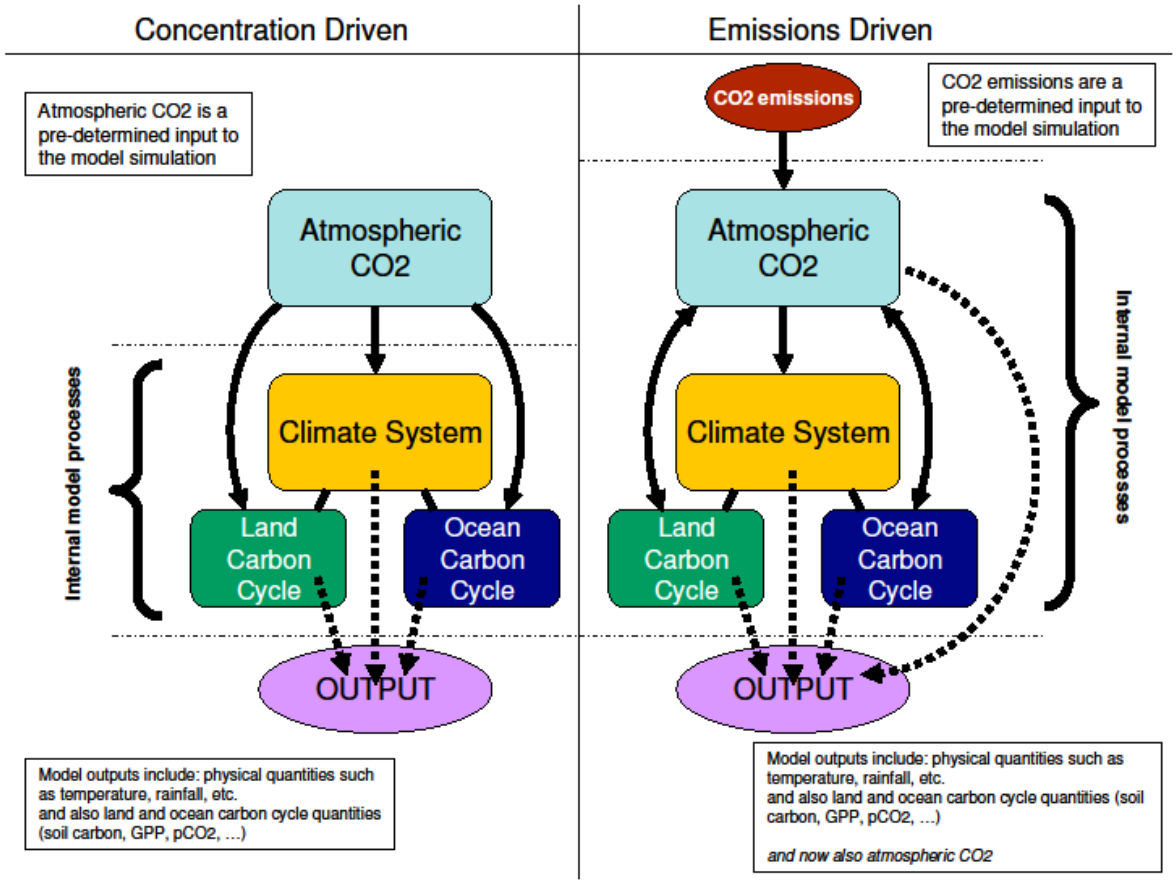

Box 6.4, Figure 1: Schematic representation of carbon cycle numerical experimental design. Concentration-driven (left hand side) and emissions-driven (right hand side) simulation experiments make use of the same ESM models, but configured differently. Concentration-driven simulations prescribe atmospheric CO_2 as a pre-defined input to the climate and carbon cycle model components, but their output does not affect the CO_2. Emissions-driven simulations prescribe CO_2 emissions as the input and atmospheric CO_2 is now an internally calculated element of the earth system model.

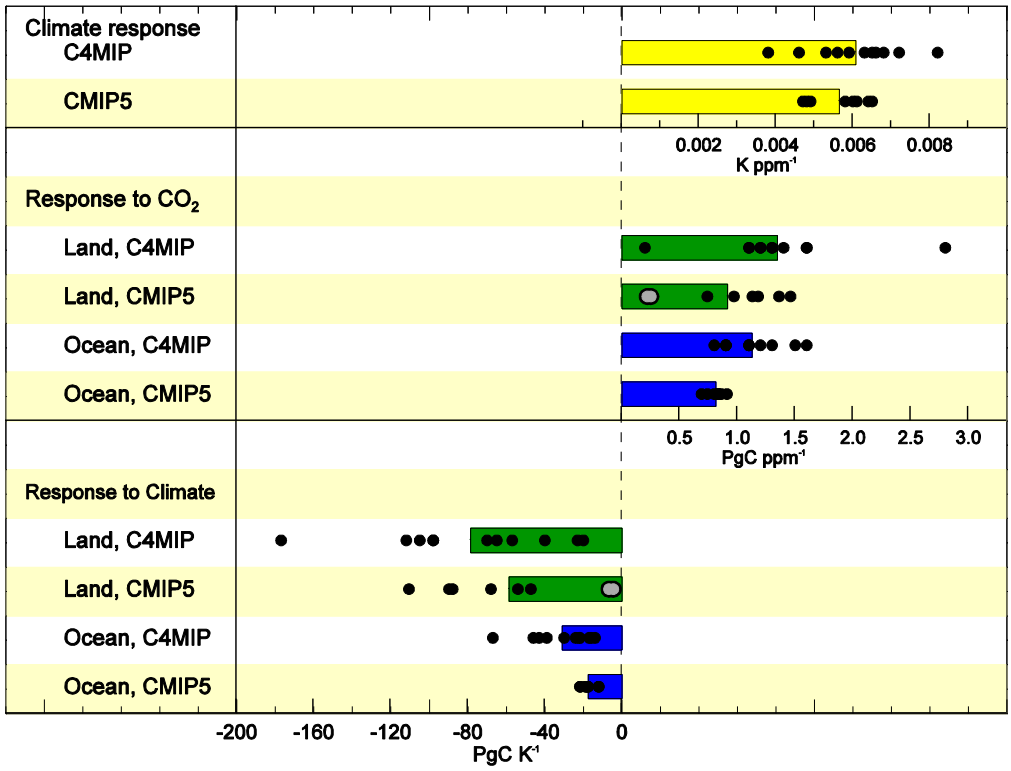

Figure 6.20: Comparison of carbon cycle feedback metrics between the C4MIP ensemble of 7 GCMs and 4 EMICs under the SRES-A2 scenario (Friedlingstein et al., 2006) and 8 CMIP5 models (Arora et al., subm.) under the 1% increase per year CO_2 scenario. Black dots represent a single model simulation and coloured bars the mean of the multi-model results, grey dots are used for models with a coupled terrestrial nitrogen cycle. The comparison with C4MIP is for context, but these metrics are known to be variable across different scenarios and rates of change (see Section 6.4.2.2). Some of the CMIP5 models are derived from models that contributed to C4MIP and some are new to this analysis. Table 6.10 lists the main attributes of each CMIP5 model used in this analysis. The SRES A2 scenario is closer in rate of change to a 0.5% yr^{-1} scenario and as such it should be expected that the CMIP5 gamma terms are comparable, but the beta terms are likely to be around 20% smaller for CMIP5 than for C4MIP. This high dependence on scenario (Section 6.4.2.2) reduces confidence in any quantitative statements of how CMIP5 carbon cycle feedbacks differ from C4MIP. Models used: MPI-ESM-LR, BCC-CSM1, HadGEM2-ES, IPSL-CM5A-LR, CanESM2, NorESM-ME, CESM1-BGC, MIROC-ESM.

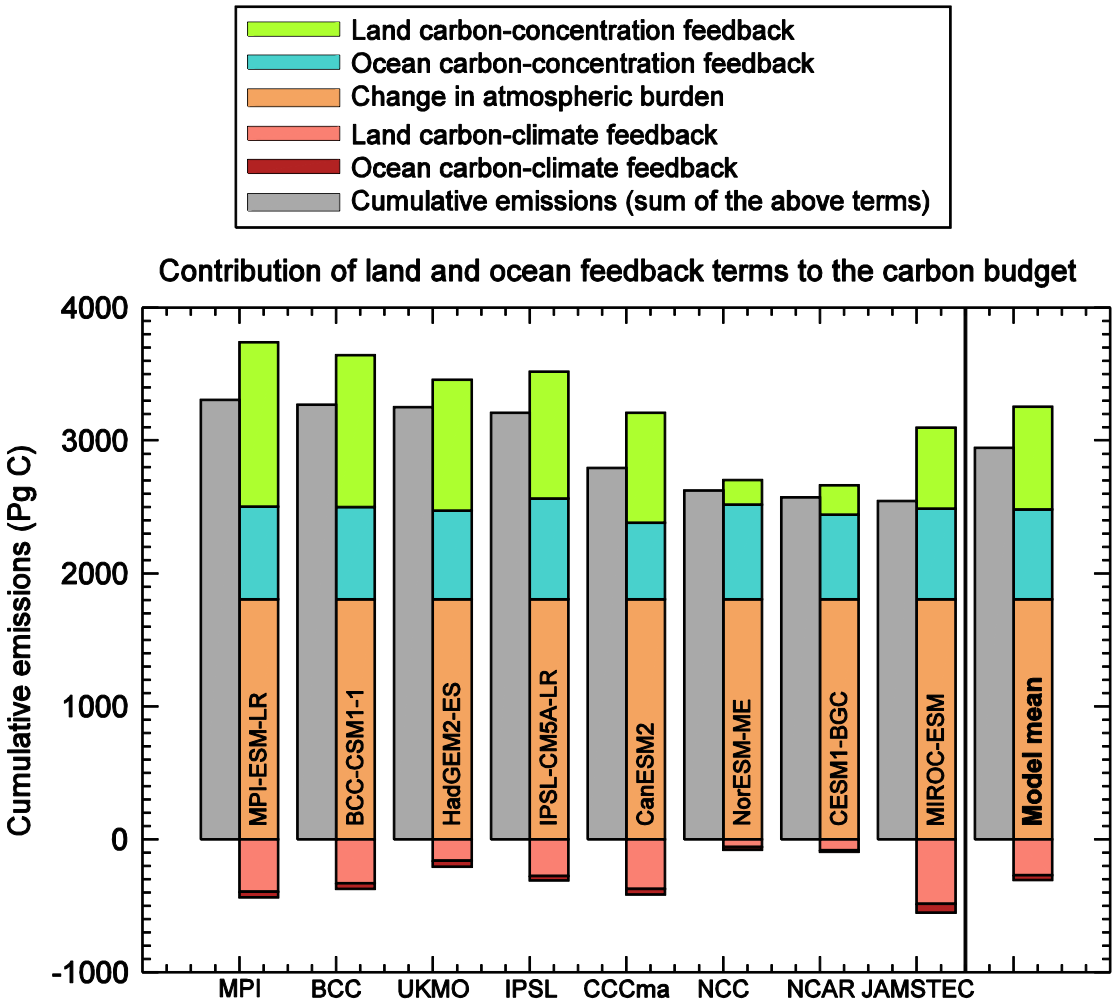

Figure 6.21: Cumulative emissions across CMIP5 models broken down into the contributions of land and ocean response to CO_2 and climate. The contribution of the carbon-concentration feedback is larger than the climate-carbon feedback for all models and the land and ocean contributions to this are typically comparable. The exception is for NorESM-ME and CESM1-BGC which include nitrogen interactions in the terrestrial carbon cycle – these models with nitrogen included in the terrestrial carbon cycle model component simulate a smaller response to both climate and carbon than the other models, but still of the same sign as the other models. The contribution of the ocean to the climate-carbon response is small for all models. Models used: MPI-ESM-LR, BCC-CSM1, HadGEM2-ES, IPSL-CM5A-LR, CanESM2, NorESM-ME, CESM1-BGC, MIROC-ESM.

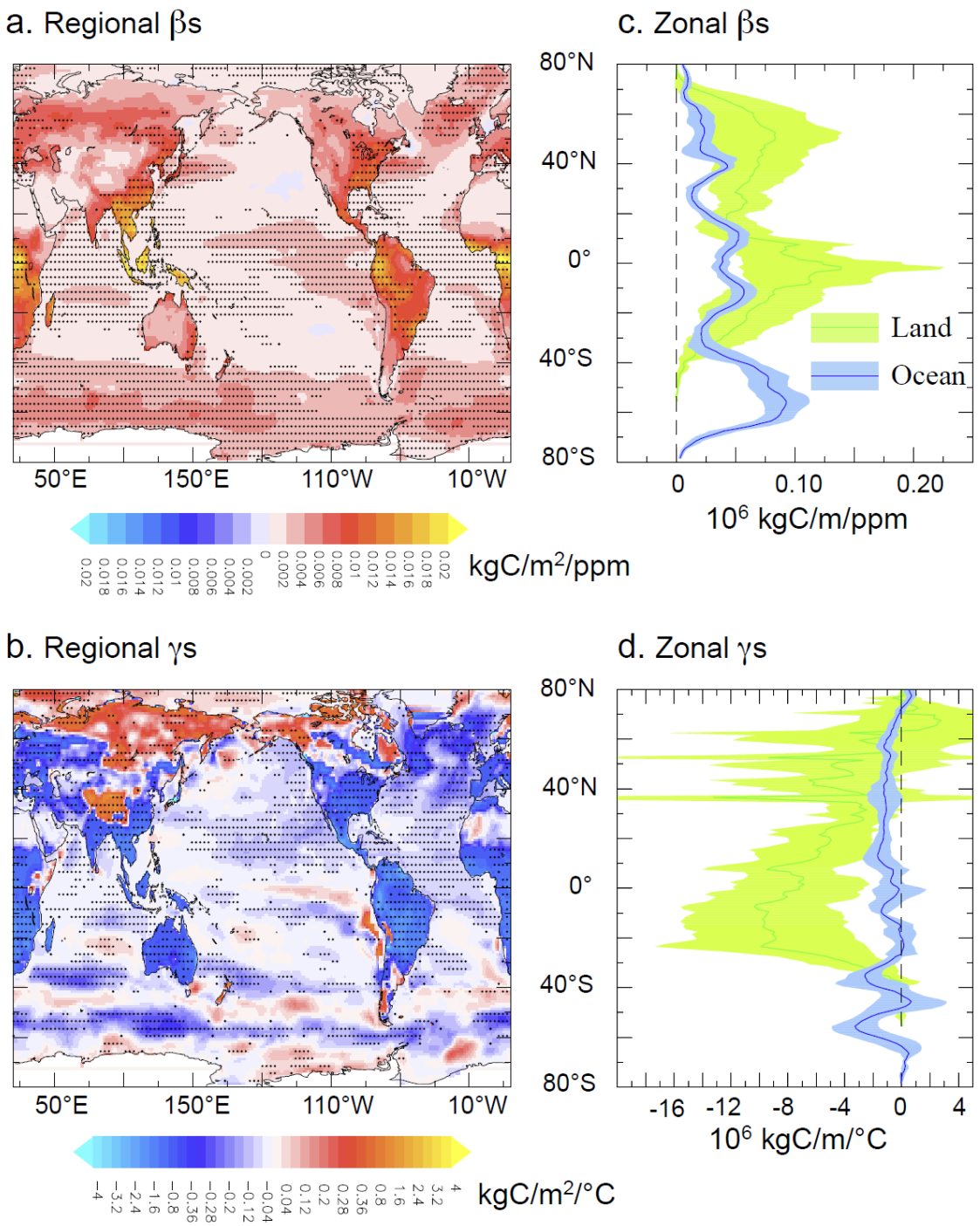

Figure 6.22: The spatial distributions of multi model-mean land and ocean β and γs for 7 CMIP5 models using the *concentration-driven* idealised 1% per year CO_2 simulations. For land and ocean, β and γ are defined from changes in terrestrial carbon storage and changes in air-sea accumulated fluxes respectively, from the beginning to the end of the 1% simulation relative to global (not local) CO_2 and temperature change. Stippling denotes areas where the magnitude of the multi-model ensemble mean exceeds the 90% confidence level interval for β, and where at least 80% models agree on the sign of change for γ. The solid lines show the multi-model mean and shaded areas denote ±1 standard deviation. Models used are: CanESM2, GFDL-ESM2M, HadGEM2-ES, IPSL-CM5A-LR, MPI-ESM-LR, NorESM1-ME for all, CESM1-BGC for land β, and bcc-csm1-1 for ocean β and γ.

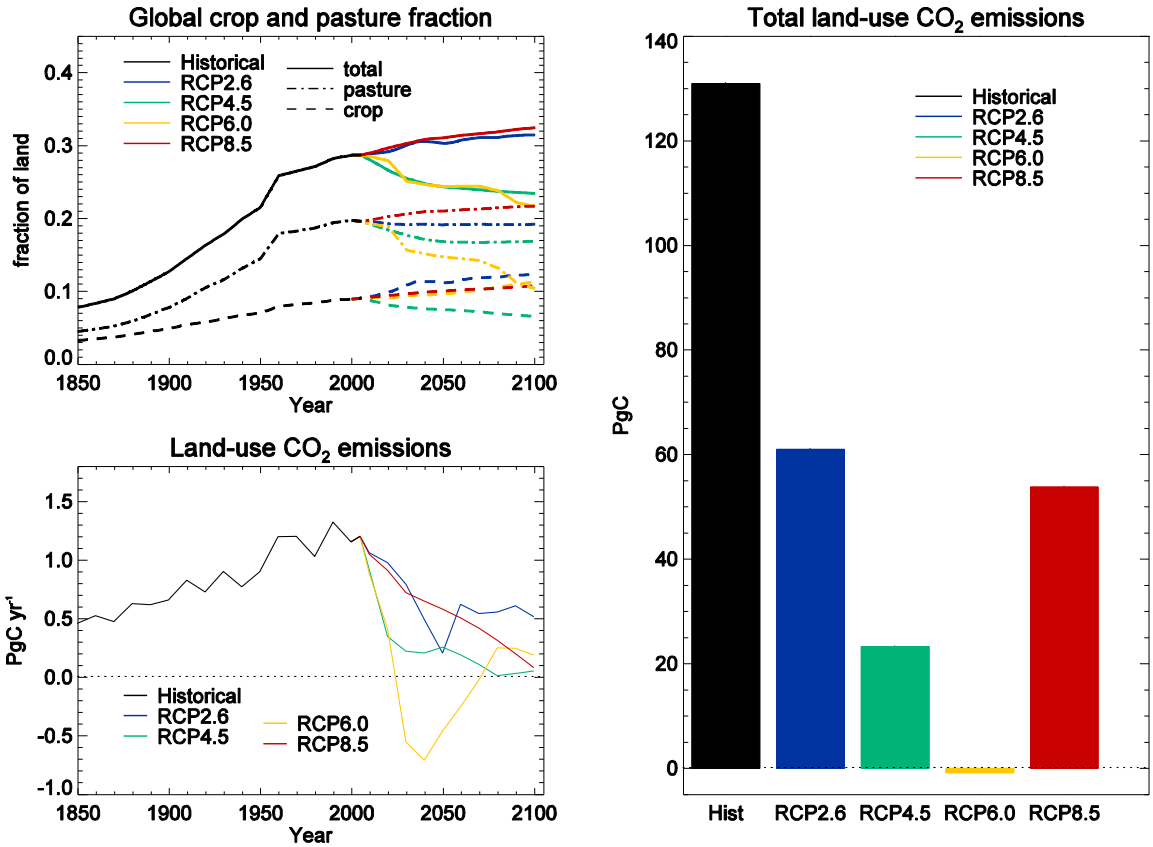

Figure 6.23: Land use trends and emissions according to the four different integrated assessment models (IAM) used to define the RCP scenarios. Global changes in croplands and pasture from the historical record and the RCP scenarios (top left), and associated annual land use emissions of CO_2 (bottom left). Bars (right panel) show cumulative land use emissions for the historical period (defined here as 1850–2005) and the 4 RCP scenarios from 2006 to 2100.

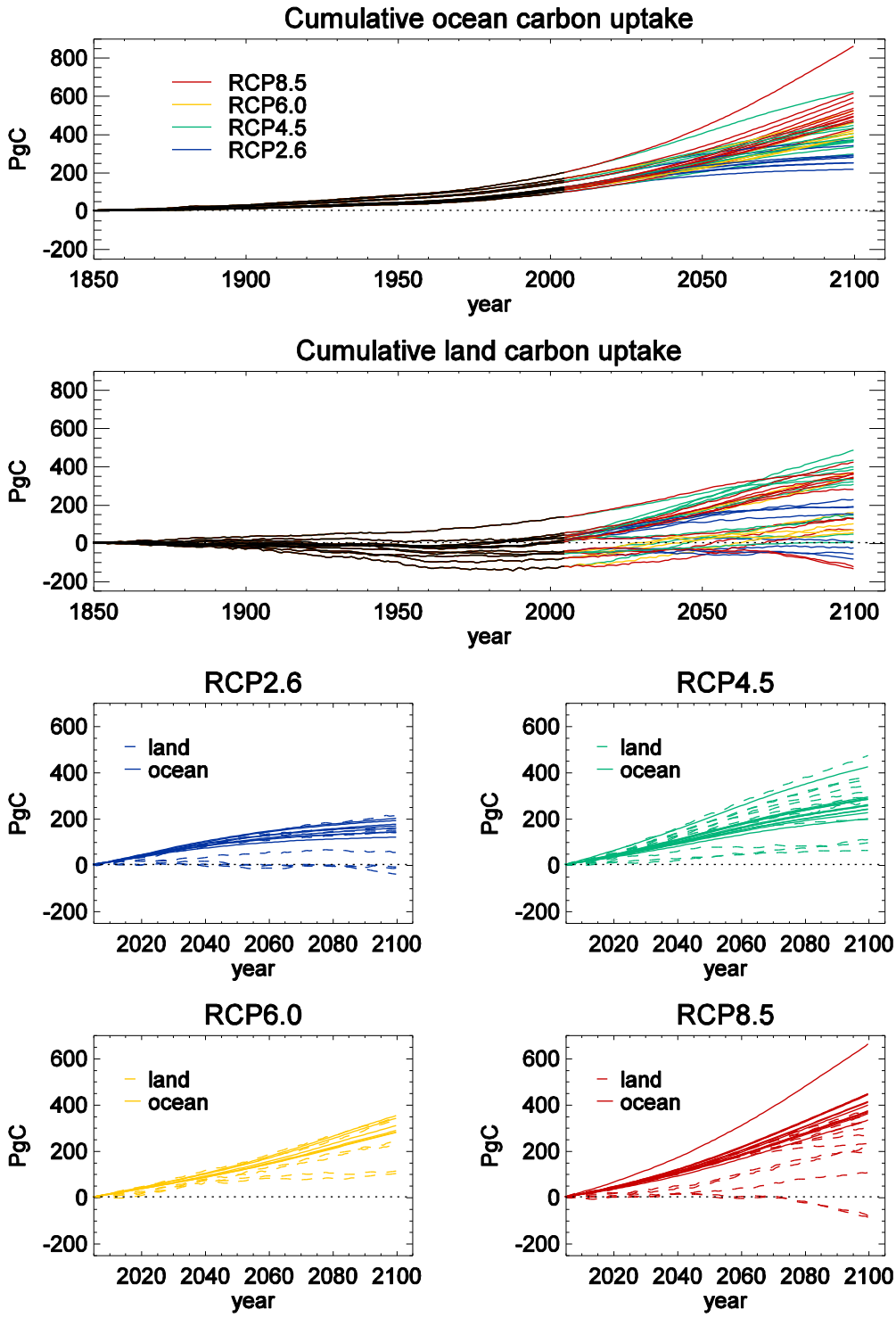

Figure 6.24: Changes in land and ocean carbon uptake simulated for the four RCP scenarios. Total ocean and land reservoirs cumulative changes in carbon content are shown in the top two panels respectively for the whole period from 1850 to 2100. The lower four panels show the 21st century changes in carbon uptake for land (dashed) and ocean (solid) separately for each scenario. Models used: CanESM2, GFDL-ESM2G, GFDL-ESM2M, HadGEM2-CC, HadGEM2-ES, IPSL-CM5A-LR, IPSL-CM5A-MR, IPSL-CM5B-LR, MIROC-ESM-CHEM, MIROC-ESM, MPI-ESM-LR, NorESM1-ME, inmcm4, CESM1-BGC.

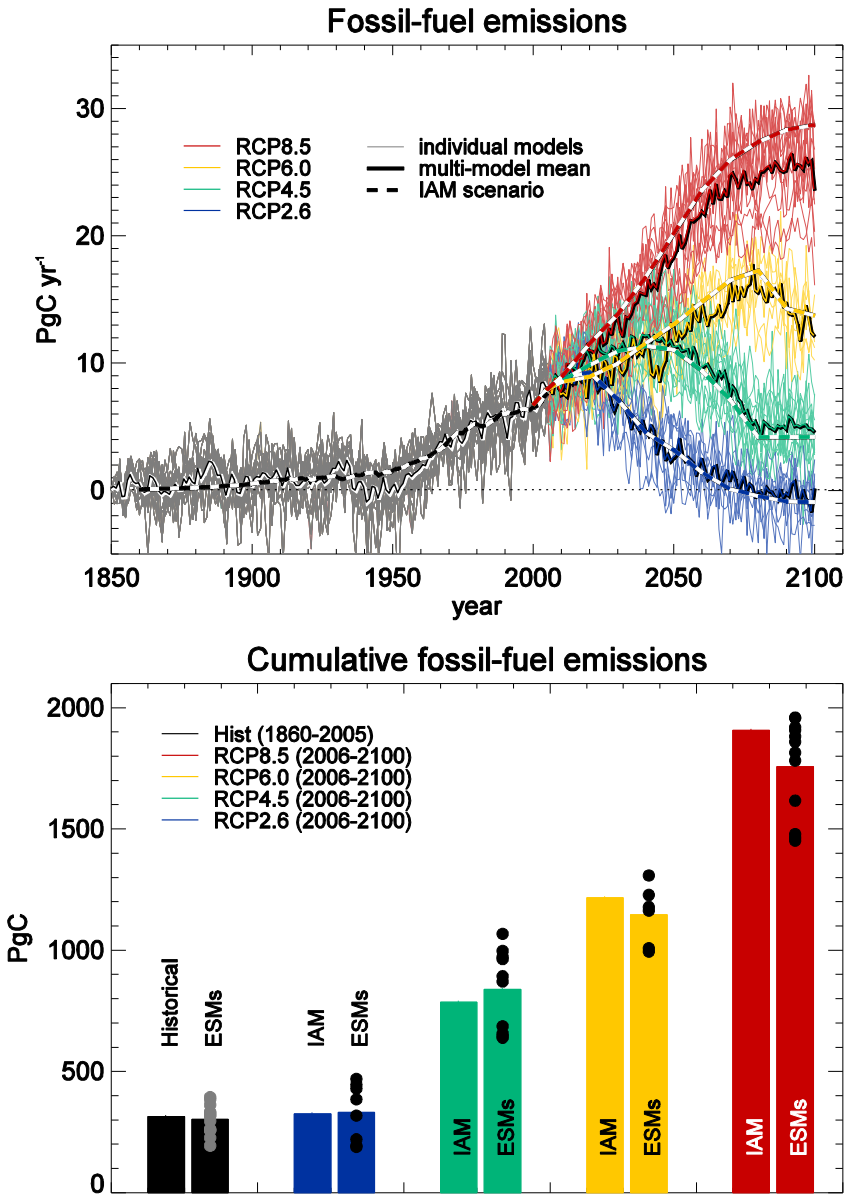

Figure 6.25: Compatible fossil fuel emissions simulated by the CMIP5 models for the 4 RCP scenarios. Top: timeseries of instantaneous emission rate. Thick lines represent the historical estimates and emissions calculated by the integrated assessment models (IAM) used to define the RCP scenarios, thin lines show results from CMIP5 ESMs. Bottom: cumulative emissions for the historical period (1860–2005) and 21st century (defined in CMIP5 as 2006–2100) for historical estimates and RCP scenarios (bars) and ESMs (symbols). In the CMIP5 model results, total carbon in the land-atmosphere-ocean system can be tracked and changes in this total must equal fossil fuel emissions to the system (see also Table 6.13). Other sources and sinks of CO_2 such as from volcanism, sedimentation or rock weathering, which are very small on centennial time scales are not considered here. Hence the compatible emissions are given by cumulative-Emissions = $\Delta C_A + \Delta C_L + \Delta C_O$ or emission rate = d/dt $[C_A + C_L + C_O]$, where C_A, C_L, C_O are carbon stored in atmosphere, land and ocean respectively. Models used: CanESM2, GFDL-ESM2G, GFDL-ESM2M, HadGEM2-CC, HadGEM2-ES, IPSL-CM5A-LR, IPSL-CM5A-MR, IPSL-CM5B-LR, MIROC-ESM-CHEM, MIROC-ESM, MPI-ESM-LR, NorESM1-ME, inmcm4, CESM1-BGC.

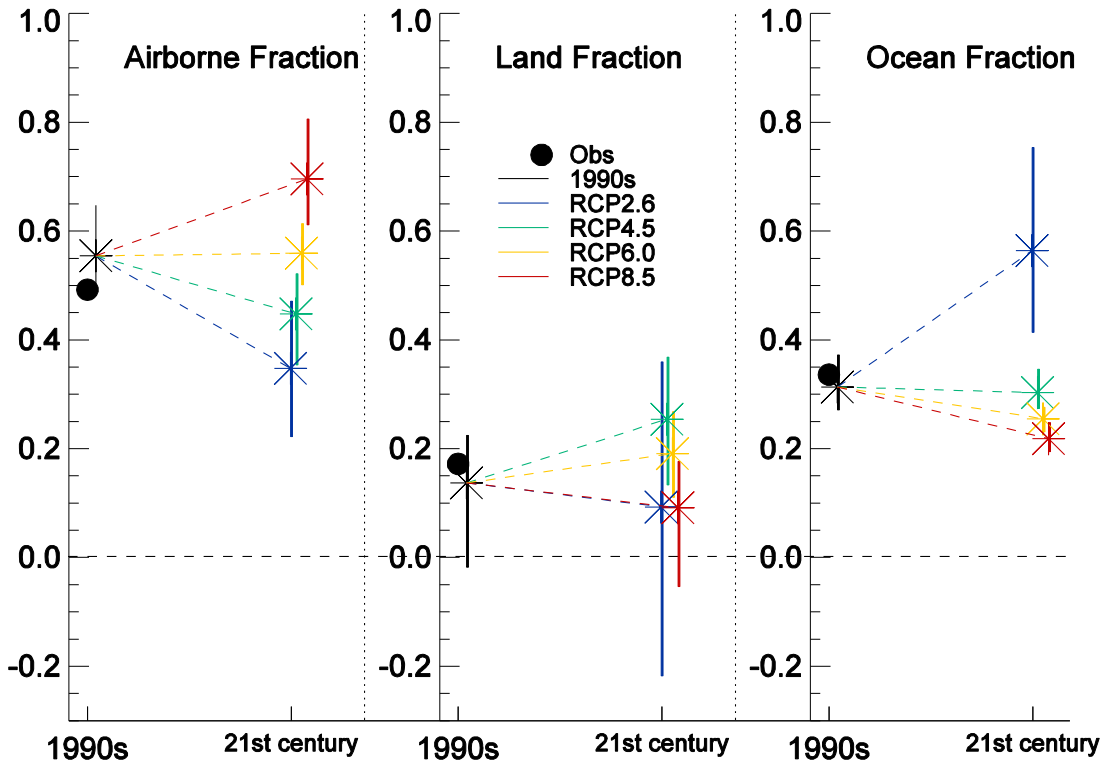

Figure 6.26: changes in airborne, land and ocean fraction of fossil fuel carbon emissions. The fractions are defined as the changes in storage in each component (atmosphere, land, ocean) divided by the compatible fossil fuel emissions derived from each CMIP5 simulation for the 4 RCP scenarios. Solid circles show the observed estimate based on Table 6.11 for the 1990s. The coloured lines and symbols denote the change in uptake fractions under the different RCP scenarios for each model, calculated using the cumulative change in carbon from 2005 to 2100. Multi-model mean values are shown as star symbols and the multi-model range (min-to-max) is shown by the vertical coloured lines. Due to the difficulty of estimating fossil and land use emissions from the ESMs this figure uses a fossil fuel definition of airborne fraction, rather than the preferred definition of fossil + land use emissions discussed in Section 6.3. 21st century cumulative airborne, land and ocean fractions are shown here in preference to the more commonly shown instantaneous fractions because for RCP2.6 emissions reach and cross zero and so an instantaneous definition of AF becomes singular at that point. Models used: CanESM2, GFDL-ESM2G, GFDL-ESM2M, HadGEM2-CC, HadGEM2-ES, IPSL-CM5A-LR, IPSL-CM5A-MR, IPSL-CM5B-LR, MIROC-ESM-CHEM, MIROC-ESM, MPI-ESM-LR, NorESM1-ME, inmcm4, CESM1-BGC.

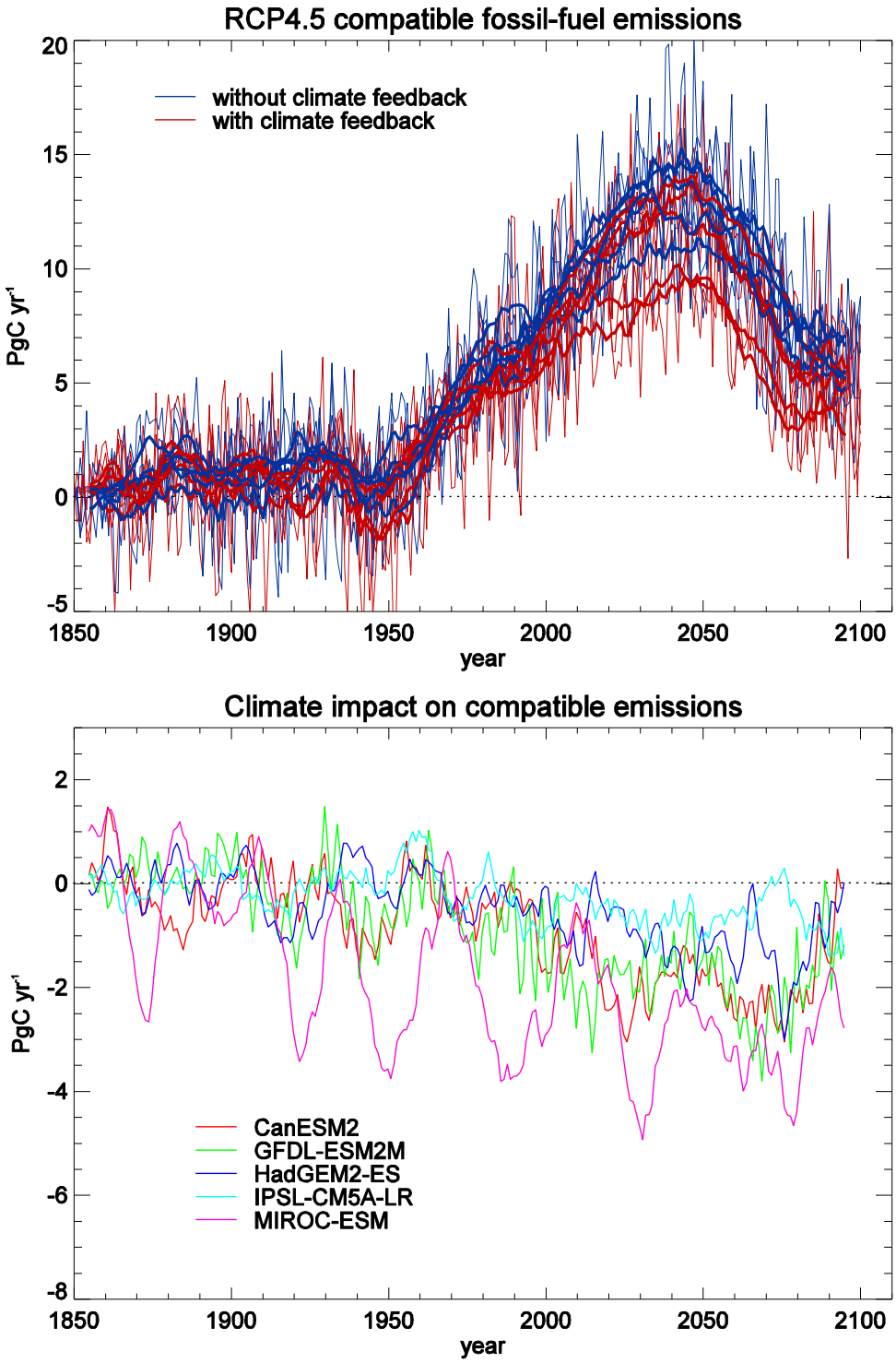

Figure 6.27: Diagnosed compatible fossil fuel emissions (top panel) in the presence (red lines) and absence (blue lines) of the climate impact on the carbon cycle for the RCP4.5 scenario, and the difference between them (bottom panel). Thin lines show annual values and thick lines 10-year smoothed values. This shows the impact of climate change on the compatible fossil fuel CO_2 emissions to achieve the RCP4.5 CO_2 concentration pathway. Models used: CanESM2, GFDL-ESM2M, HadGEM2-ES, IPSL-CM5A-LR and MIROC-ESM.

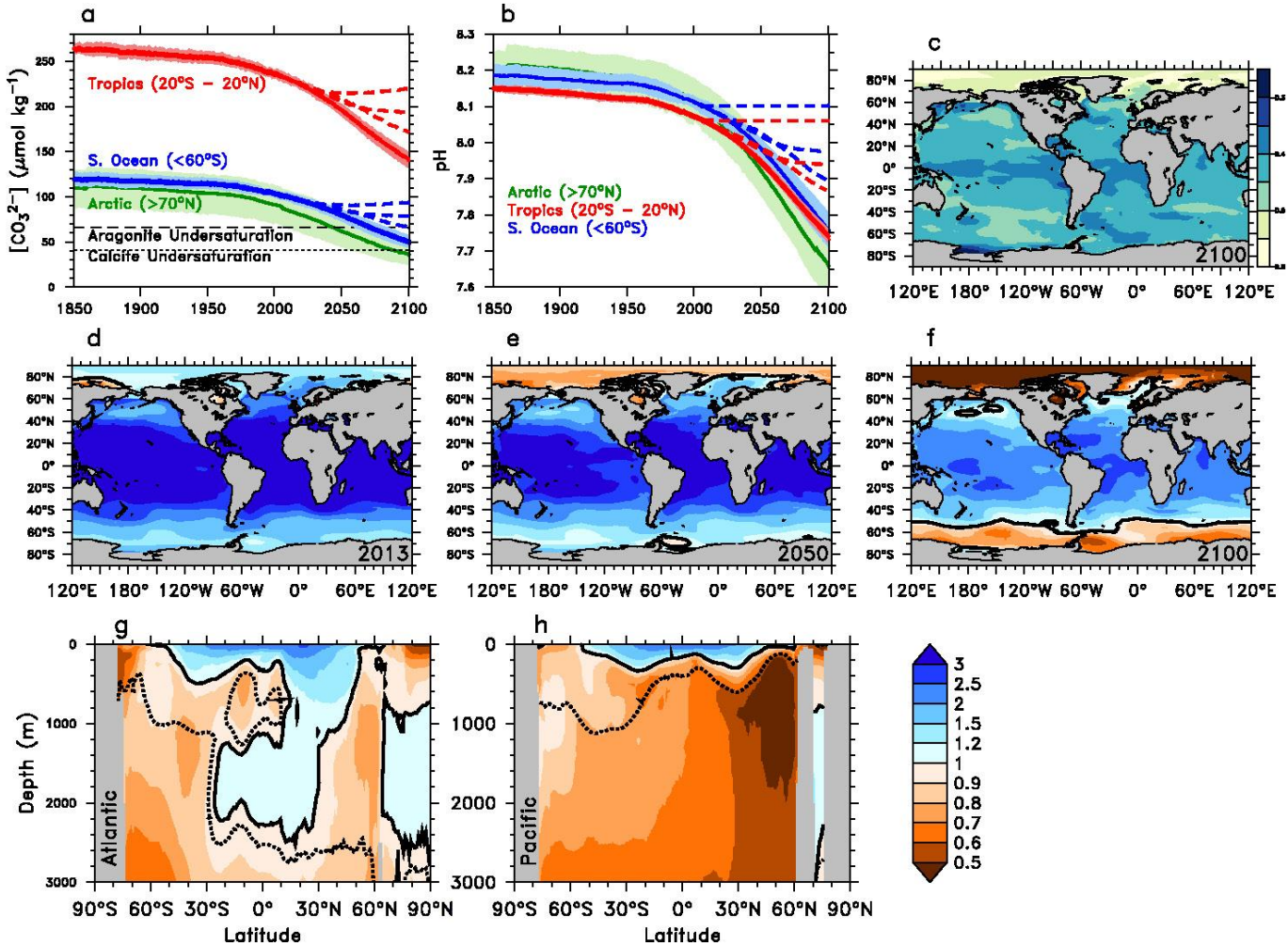

Figure 6.28: Projected ocean acidification from 12 CMIP5 earth system models under the RCP8.5 scenario: time series of surface **(a)** carbonate ion concentration and **(b)** pH shown as the mean (solid line) and range of models (filled), given as area-weighted averages over the Arctic Ocean (green), the tropical oceans (red), and the Southern Ocean (blue); maps of the median model's **(c)** change in surface pH from 1850 to 2100 and its surface Ω_A in **(d)** 2013, **(e)** 2050, and **(f)** 2100; and zonal mean sections (latitude vs. depth) of Ω_A in 2100 over the (g) Atlantic and (h) Pacific, while the ASH is shown in 2013 (dotted line) as well as 2100 (solid line). Panels (a) and (b) also include mean model results from three other scenarios: RCP2.6, RCP4.5, and RCP6.0 (dashed lines). Over most of the ocean, gridded data products of carbonate system variables (Key et al., 2004) are used to correct each model for its present-day bias by subtracting the model-data difference at each grid cell following (Orr et al., 2005). Where gridded data products are unavailable (Arctic Ocean, all marginal seas, and the ocean near Indonesia), results are shown without bias correction. The bias correction reduces the range of model projections by up to a factor of 4, e.g., in panels (a) and (b) compare the large range of model projections for the Arctic (without bias correction) to the smaller range in the Southern Ocean (with bias correction).

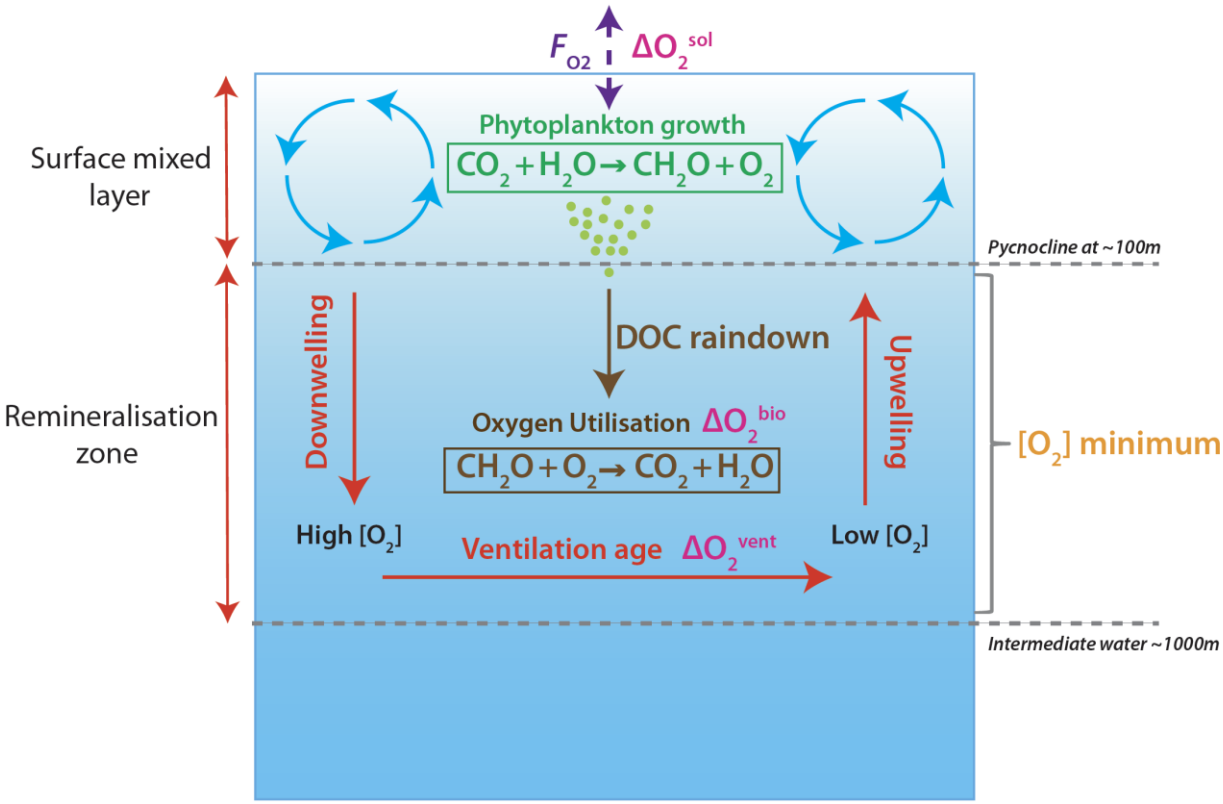

Box 6.5, Figure 1: *The ocean O_2 cycle*. The oceanic reservoir of oxygen communicates with the atmosphere via air-sea gas exchange (F_{O2}). In the ocean interior, a change in dissolved O_2 concentration over time can be driven by changes in: (1) surface ocean O_2 solubility ΔO_2^{sol}, (2) the ventilation age of a water parcel advected into the subsurface (ΔO_2^{vent}) (3) biological utilisation of oxygen in remineralization of Dissolved Organic Carbon (DOC; ΔO_2^{bio}).

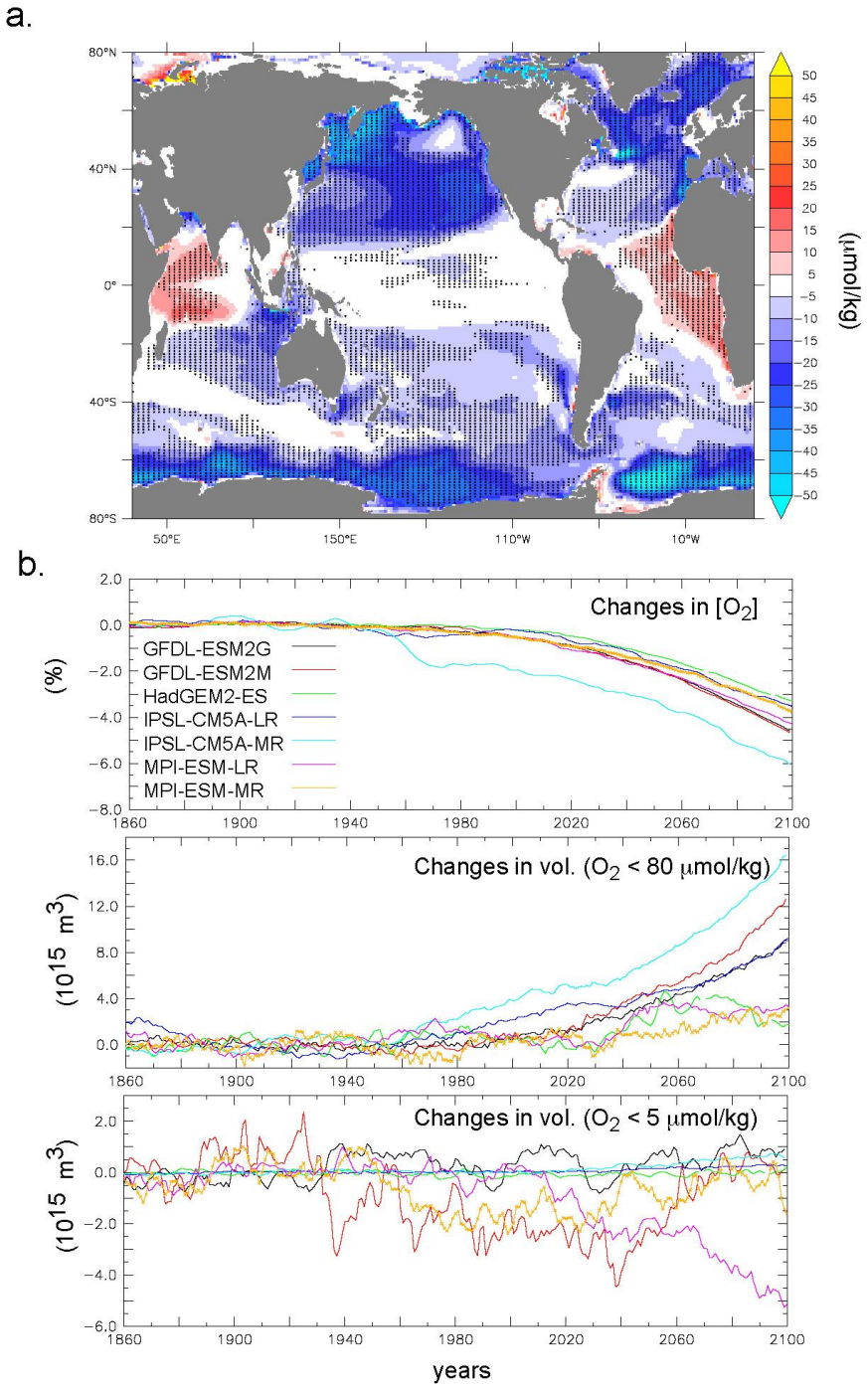

Figure 6.29: (a) Multi-model mean projected changes in dissolved O_2 (μmol kg^{-1} in the main thermocline (100–600 m depth average) from 1995–2005 to 2090–2100 under the RCP8.5 scenario. To indicate consistency in the sign of change, regions are stippled where at least 80% of models agree on the sign of the mean change. (b) Modelled evolution from 1850 to 2100 (under RCP8.5 scenario) of the relative change in global mean O_2 concentration, as well as of volume anomalies of hypoxic (O_2 <80 μmol kg^{-1}) and suboxic (O_2 <5 μmol kg^{-1}) waters. These diagnostics are detailed in Cocco et al. (subm.) in a previous model intercomparison using the SRES-A2 scenario and have been applied to CMIP5 models under RCP8.5 here. Models used: GFDL-ESM2G, GFDL-ESM2M, HadGEM2-ES, IPSL-CM5A-LR, IPSL-CM5A-MR, MPI-ESM-LR, MPI-ESM-MR.

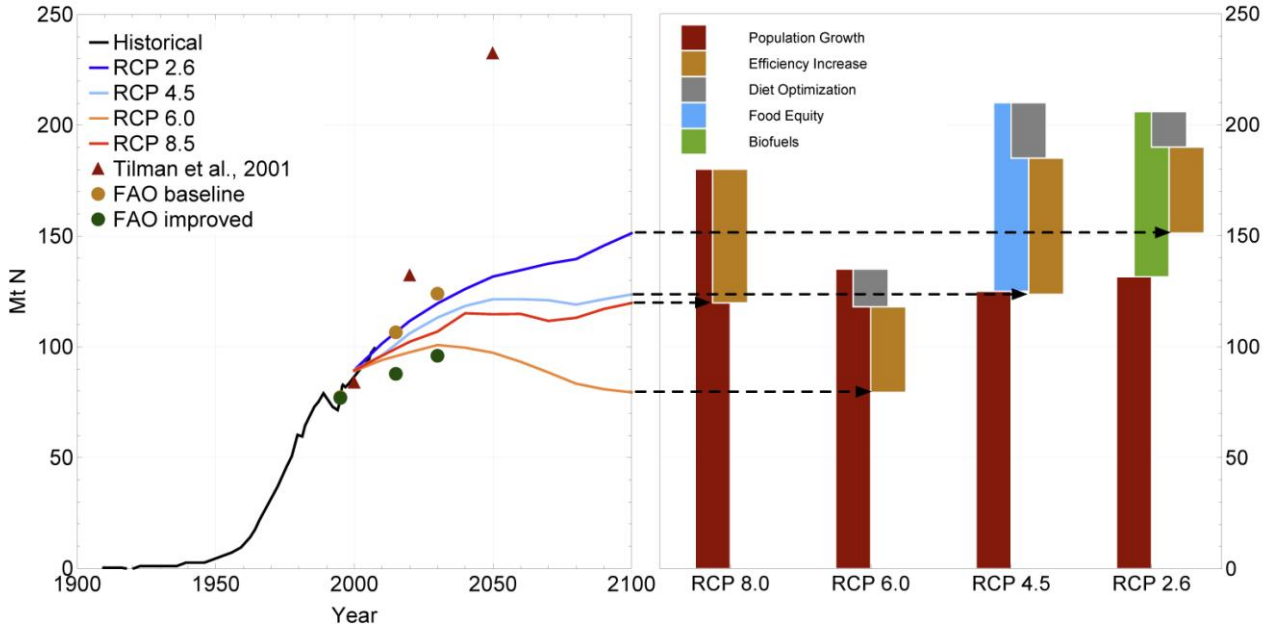

Figure 6.30: Global fertilizer Nr fixation (TgN yr^{-1}) derived as fertilizer demand, projected till 2100. Lines in the left panel reflect trends based on drivers from the RCP scenarios, dots different independent assessment. The asterisks report the ranges of two different interpretations of the SRES scenarios, with Erisman et al. (2008) using a methodology very similar to the one used for RCPs (Winiwarter et al., subm.).

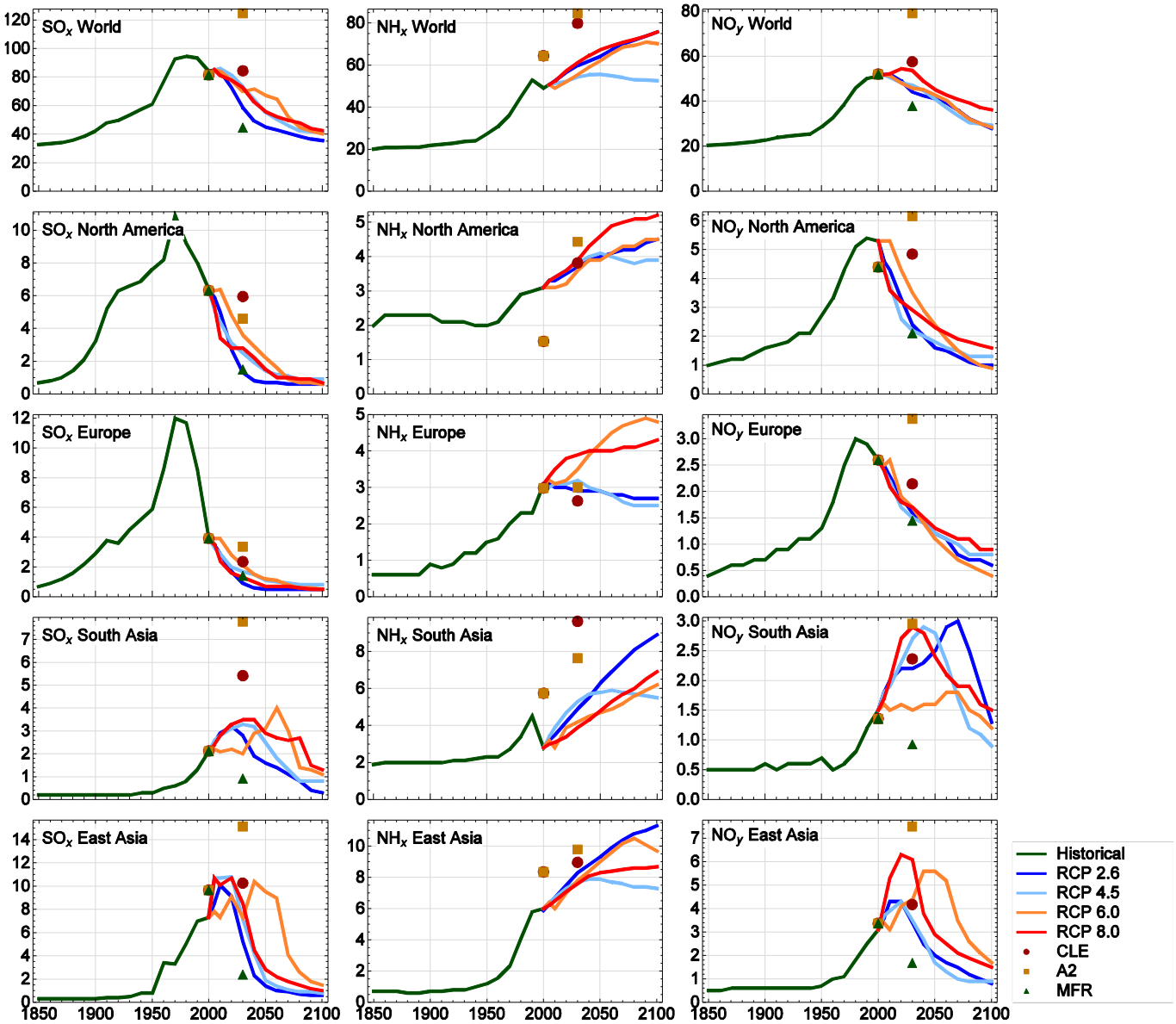

Figure 6.31: Deposition of SO_x (left panel, TgS yr^{-1}), NH_x (middle panel, TgN yr^{-1}) and NO_y (right panel, TgN yr^{-1}) from 1850 to 2000 and projections of deposition to 2100 under the four RCP emission scenarios (Lamarque et al., 2011; van Vuuren et al., 2011). Also shown are the 2030 scenarios using the SRES B1/A2 energy scenario with assumed current legislation and maximum technically feasible air pollutant reduction controls (Dentener et al., 2006).

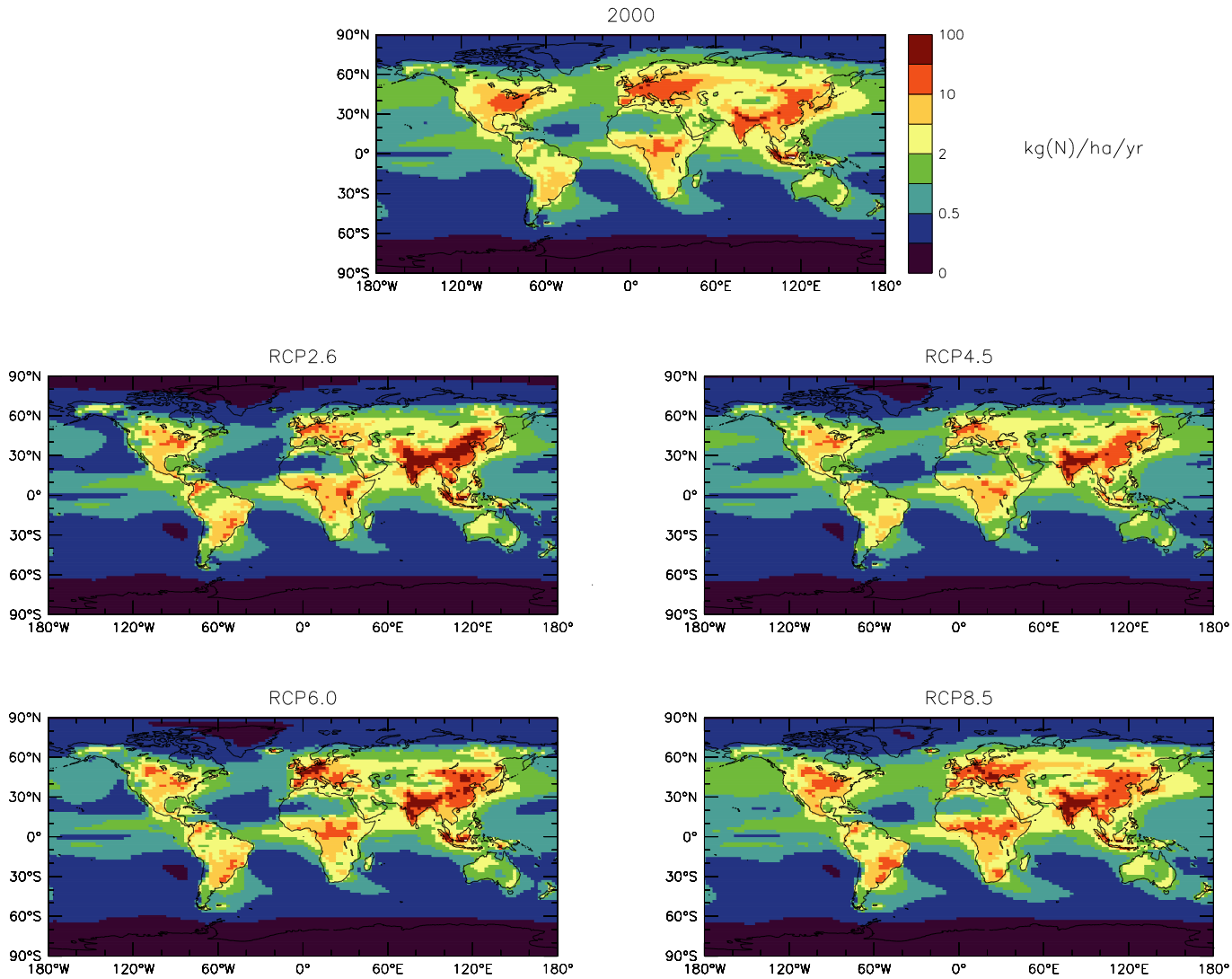

Figure 6.32: Spatial variability of N deposition in 2000 with projections for 2100, using the 2.6, 4.5, 6.0 and 8.5 RCP scenarios, kg N ha^{-1} yr^{-1} adapted from (Lamarque et al., 2011).

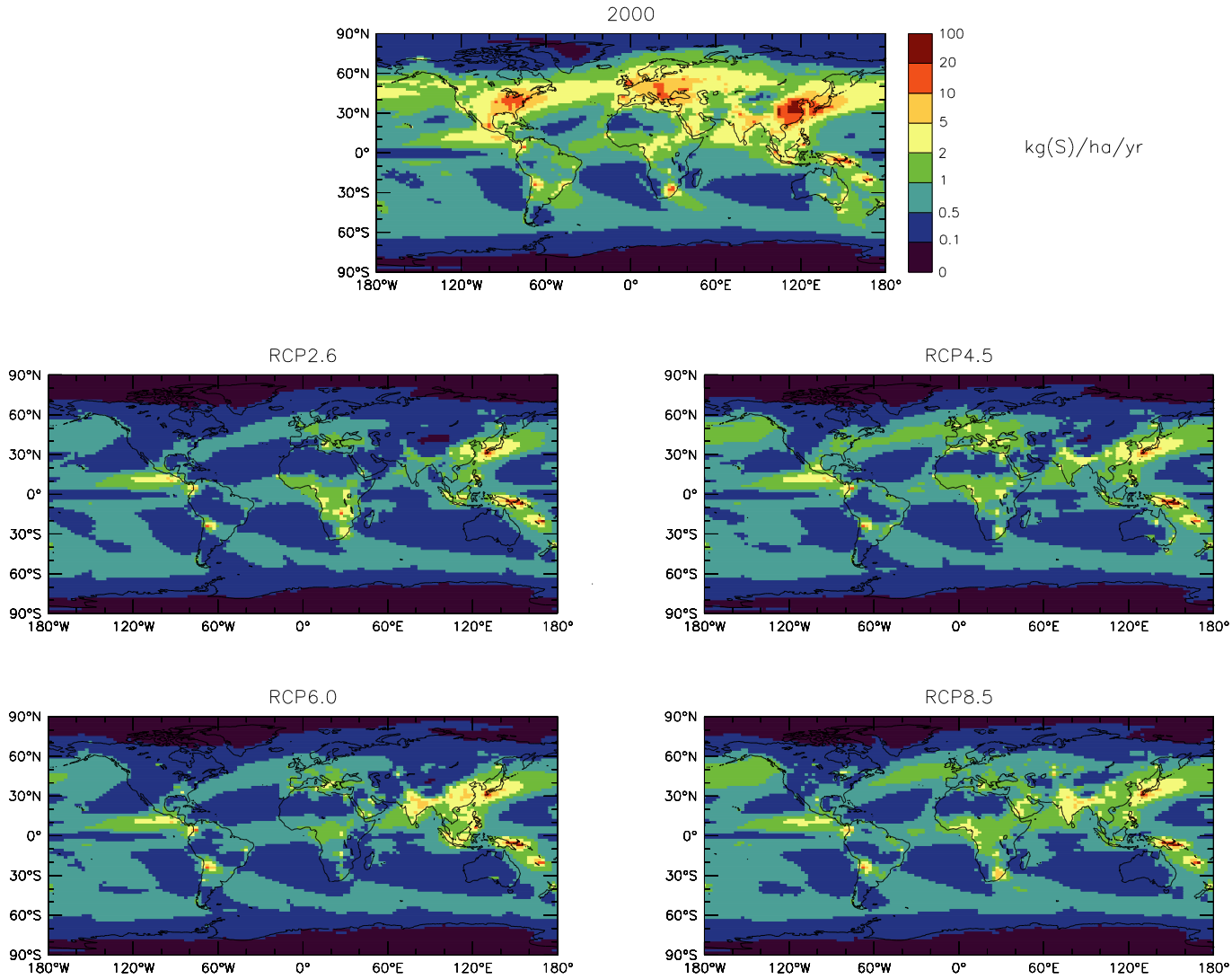

Figure 6.33: Spatial variability of S deposition in 2000 with projections for 2100, using the 2.6, 4.5, 6.0 and 8.5 RCP scenarios, kg S ha^{-1} yr^{-1}(Lamarque et al., 2011).

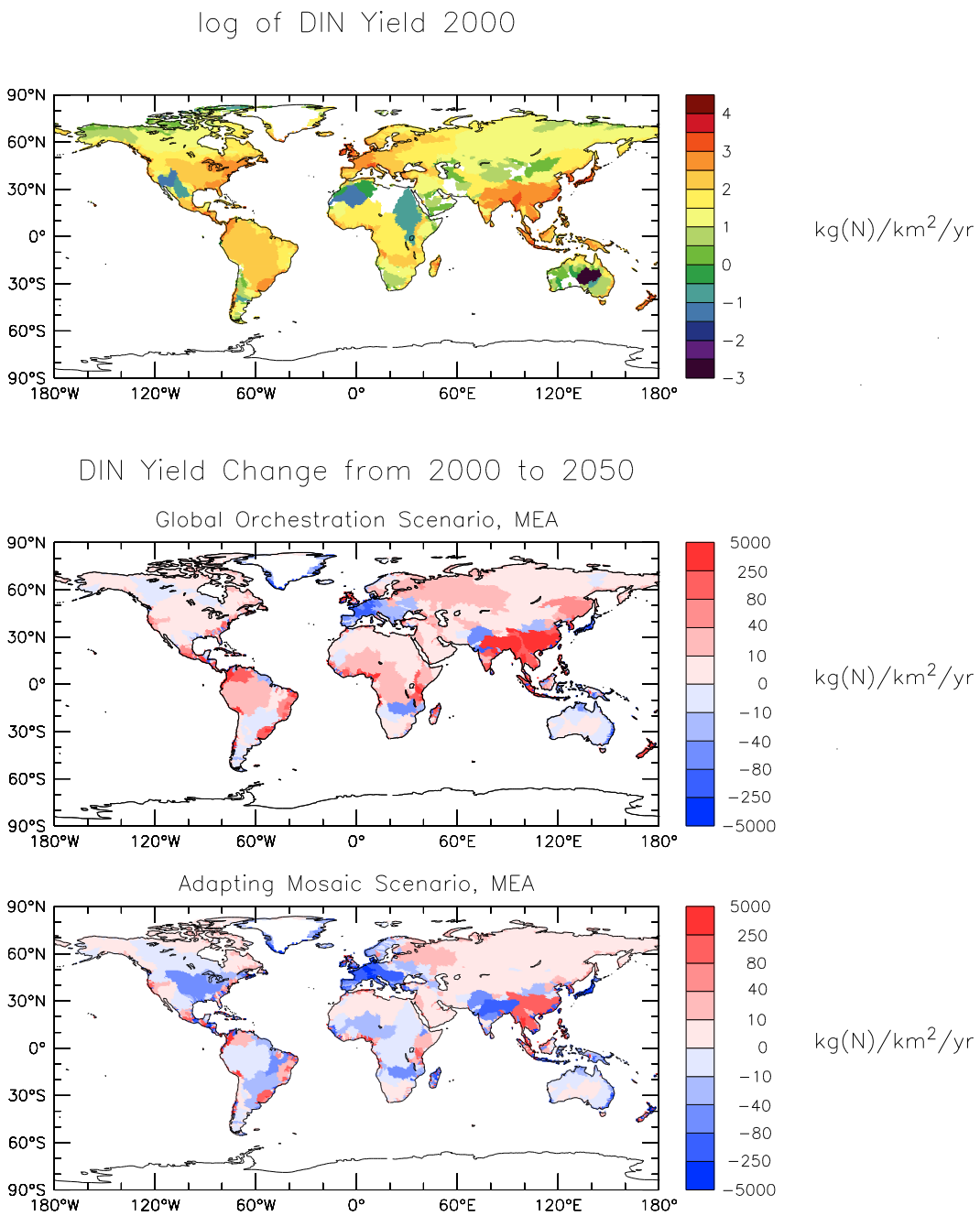

Figure 6.34: (a) Dissolved inorganic nitrogen river discharge to coastal zone (mouth of rivers) in 2000, based up on Global NEWS 2 model, (b) change in DIN discharge from 2000 to 2050, based upon Global Orchestration and the Adapting Mosaic scenarios, Millennium Ecosystem Assessment (Mayorga et al., 2010; Seitzinger et al., 2010). Units are kg N per km^2 watershed per year, as an average for each watershed.

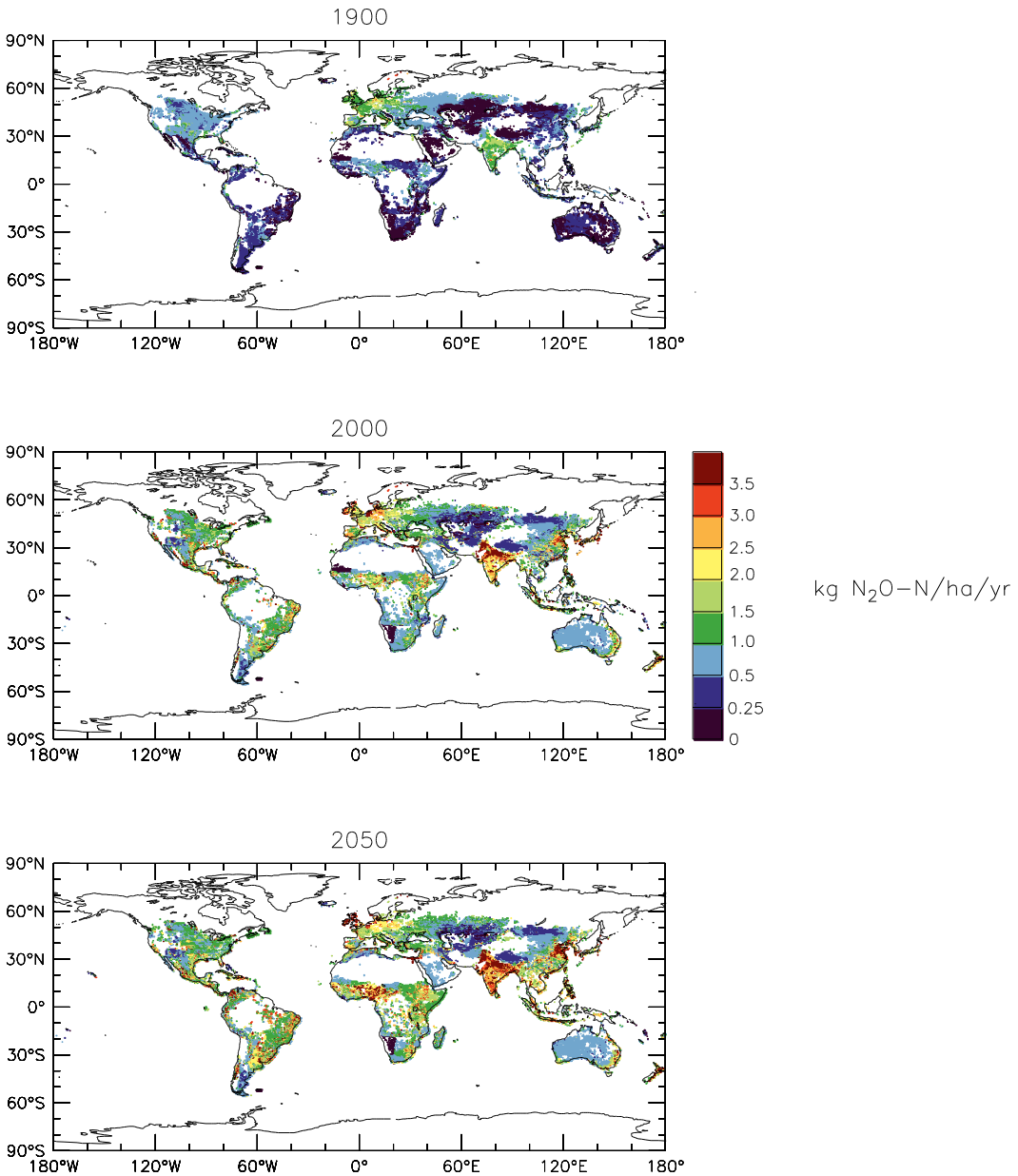

Figure 6.35: N_2O emissions in 1900, 2000 and projected to 2050 (Bouwman et al., 2011a).

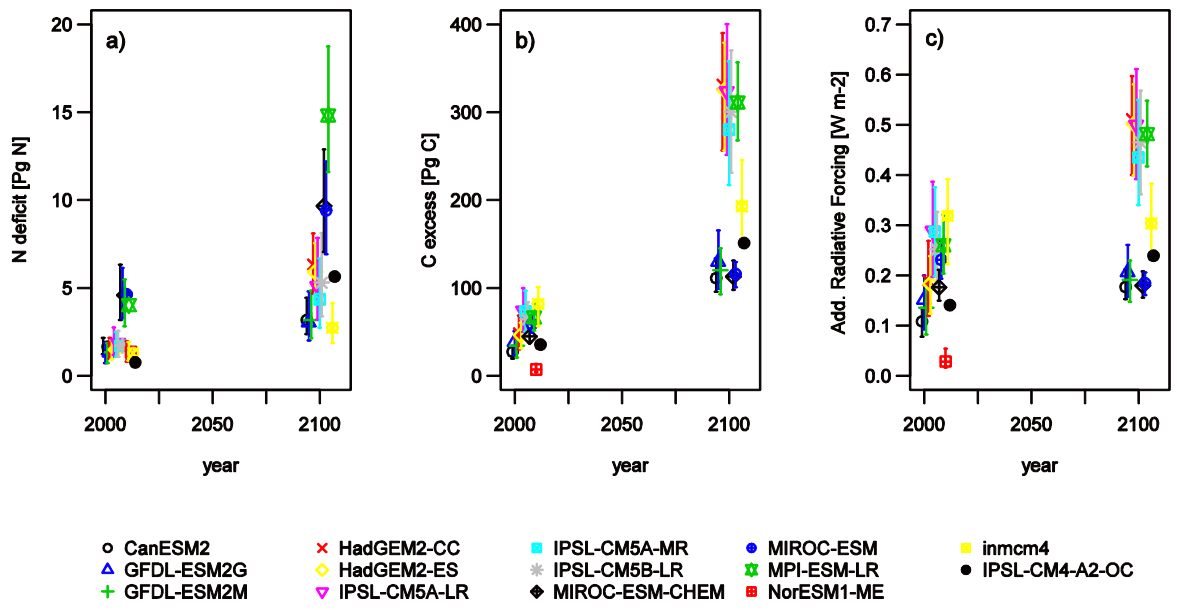

Figure 6.36: (a) Implied global terrestrial nitrogen deficit of the RCP8.5 carbon sequestration projections; (b) implied overestimation of terrestrial C sequestration due to neglecting N limitations; (c) Additional radiative forcing resulting from the nitrogen limitation of terrestrial C sequestration. The N deficit was calculated as follows: The simulated increase in terrestrial C stocks were converted into N requirements as described by Wang and Houlton (2009). The yearly evolution of the nitrogen requirements were compared on a model grid-cell bases against the newly available nitrogen due to changes in biological nitrogen fixation and atmospheric deposition. The error bars represent the range of results obtained using alternative assumption about terrestrial C:N stoichimetry, N retention from N deposition and changes in fixation. Values are presented for the year 2005 and 2100 and displaced in time for clearer visibility. Radiative forcing was calculated using the formulation of Ramaswamy et al. (2001), assuming an air-borne fraction of 0.6, and are evaluated as change in atmospheric CO_2 burden against the RCP8.5 scenario abundances in 2005 (377 ppm) and 2100 (935 ppm). The panels also show simulations of the IPSL-CM4-A2-OC model (Zaehle et al., 2010a), driven with the SRES-A2 scenario projections of the IPSL-CM4 model for which both a C-cycle only and dynamically coupled C-N cycle simulation are available, and for which the N deficit of the C-cycle model can therefore be determined explicitly.

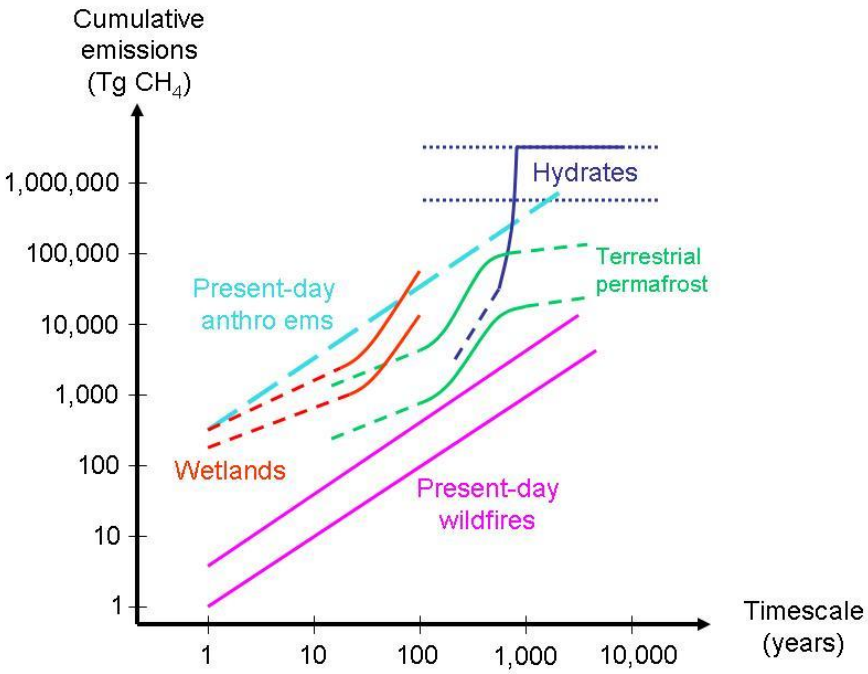

Figure 6.37: Summary of the sizes and time scales associated with future CH_4 emissions (adapted from O'Connor et al., 2010). Uncertainty in these future changes is large, and so this figure demonstrates the relative magnitude of possible future changes. Anthropogenic emissions continuing at a present day level of 300 Tg(CH_4) yr^{-1} (consistent with Table 6.7) are shown for reference. Wetland emissions are taken as 140–280 Tg(CH_4) yr^{-1} present day values (Table 6.7) and increasing by between 0–100% (Section 6.4.7.1; Figure 6.38). Permafrost emissions may become important during the 21st century. Large CH_4 hydrate release to the atmosphere is not expected during the 21st century. No quantitative estimates of future changes in CH_4 emissions from wildfires exist, so plotted here are continued present day emissions of 1–4 Tg(CH_4) yr^{-1} (Table 6.7).

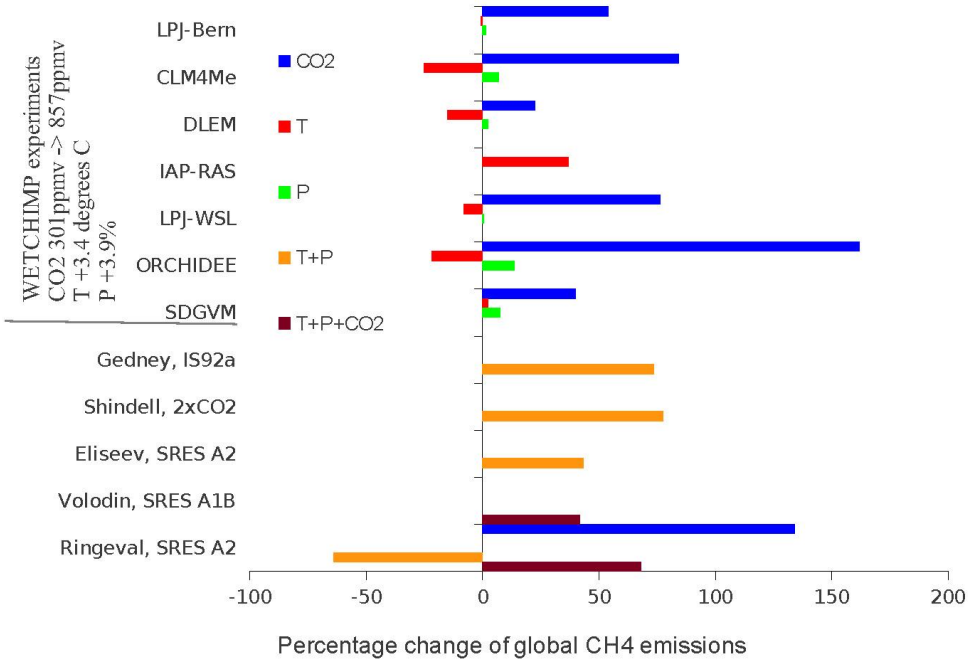

Figure 6.38: Relative changes of global CH_4 emissions from either pre-industrial or present day conditions and environmental changes that reflect potential conditions in 2100. The first seven models took part in the WETCHIMP intercomparison project and were run under a common protocol (Melton et al., subm.) . Other studies used different future conditions as listed in the figure: Eliseev et al. (2008), Gedney et al. (2004), Ringeval et al. (2011), Shindell et al. (2004), Volodin (2008).

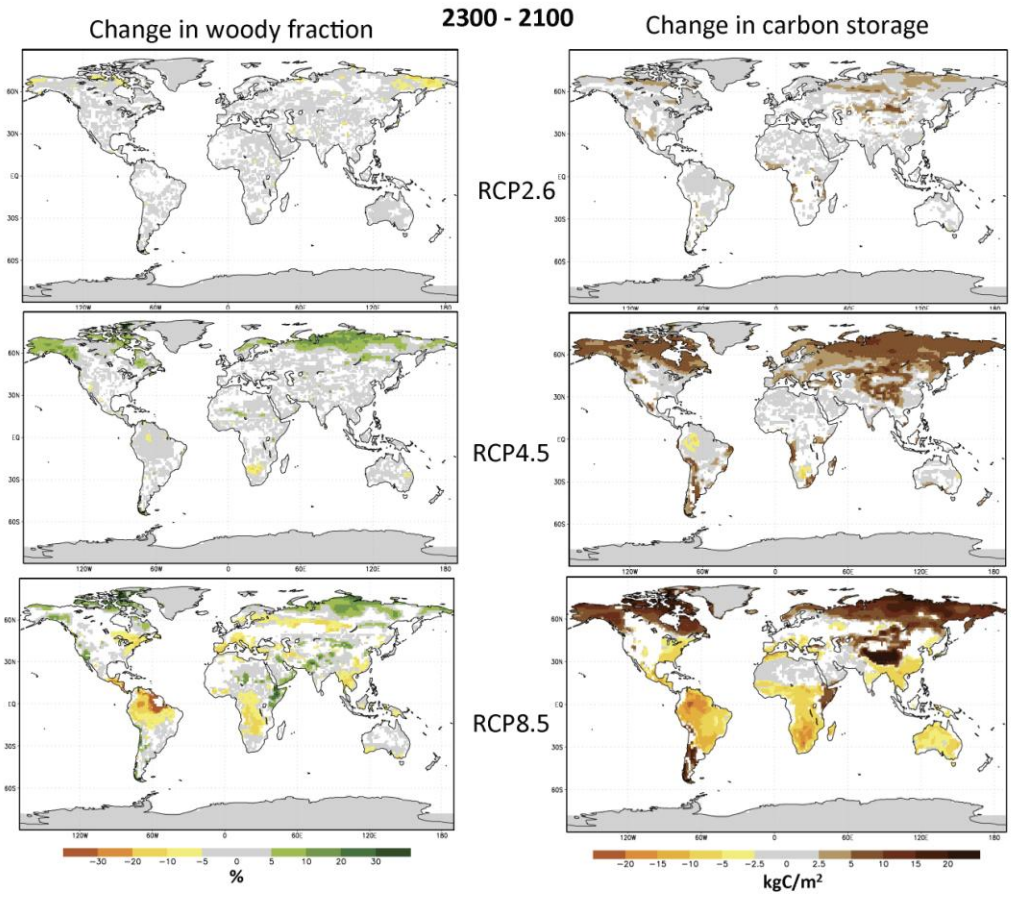

Figure 6.39: Maps of changes in woody cover fraction, %, (left) and terrestrial carbon storage, kg C m^{-2}, (right) for three RCP extension scenarios 2.6 (top), 4.5 (middle), and 8.5 (bottom) between years 2100 and 2300 averaged for two models, HadGEM2-ES and MPI-ESM, which simulate vegetation dynamics. Model results were interpolated on 1° x 1° grid; white colour indicate areas where models disagree in sign of changes. Note the RCP6.0 extension was not a CMIP5 required simulation. Anthropogenic land use in these extension scenarios is kept constant at 2100 levels, so these results show the response of natural ecosystems to the climate change.

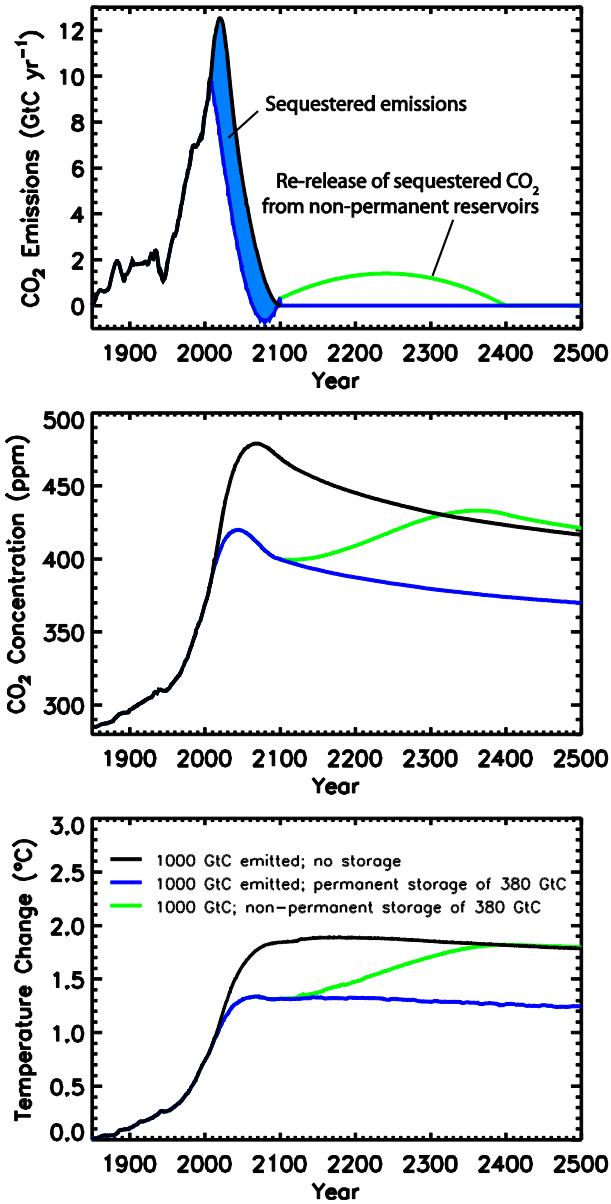

Figure 6.40: Idealized model simulations (Matthews, 2010) to illustrate the effects of CDR methods associated respectively with either permanent or non-permanent carbon sequestration after $CO_2$is removed from the atmosphere. There is an emission of 1000 PgC in the reference case (black line) between 1800 and 2100. Permanent sequestration of the additional emitted CO_2 of 380 PgC, assuming no leakage of sequestered carbon, has the potential to reduce the radiative forcing of $CO_2$and to mitigate climate change (blue line, compared to black line). By contrast, the green line shows an idealized case of a non permanent sequestration CDR method where, after CO_2 removal from the atmosphere, carbon will be sequestered in a non-permanent reservoir, in such a manner that all of the sequestered carbon will get returned as CO_2 back to the atmosphere over three centuries. In this non-permanent sequestration case, climate change would only be only delayed whereas the eventual magnitude of climate change will be equivalent to the no-sequestration case (green line, compared to black). Figure adapted from Figure 5 of Matthews (2010).

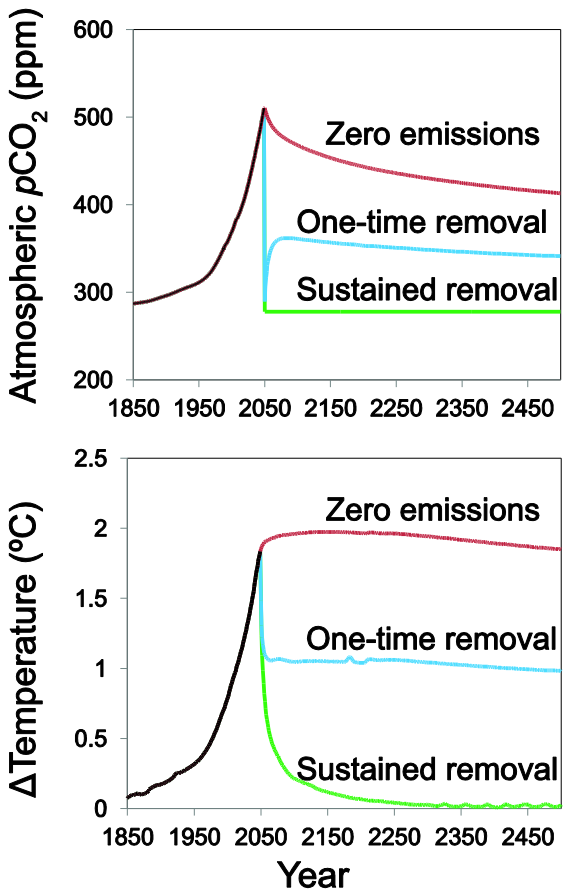

Figure 6.41: Idealized simulations with a simple global carbon cycle model (Cao and Caldeira, 2010b) to illustrate the 'rebound effect'. Effects of an instantaneous cessation of CO_2 emissions (amber line), one-time removal of excess atmospheric CO_2 (blue line) and removal of excess atmospheric CO_2 followed by continued removal of CO_2 that degasses from the atmosphere and ocean (green line). To a first approximation, a cessation of emissions prevents further warming but does not lead to significant cooling on the century time scale. A one-time removal of excess atmospheric CO_2 eliminates approximately half of the warming experienced at the time of the removal. To cool the planet back to pre-industrial levels would require the removal of all previously emitted CO_2, i.e., an amount equivalent to approximately twice the amount of excess CO_2 in the atmosphere above pre-industrial level. Simulations were started in 1800 but results are shown from 1850. Figure adapted from Cao and Caldeira (2010b).

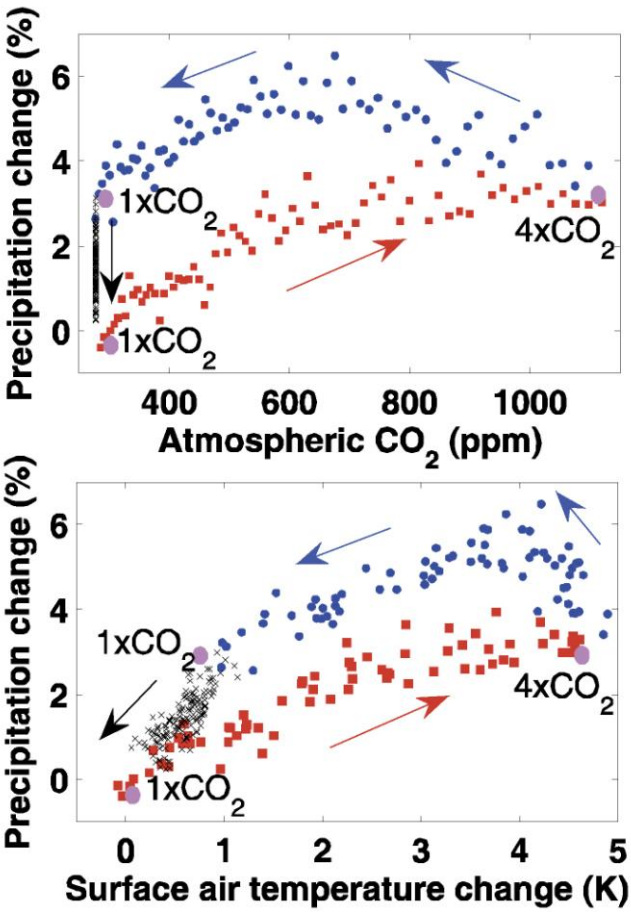

Figure 6.42: HadCM3L results from an idealized simulation (Cao et al., 2011) with 2% annual change in atmospheric CO_2: (a) global and annual mean changes in precipitation as a function of atmospheric CO_2; (b) global and annual mean changes in precipitation as a function of global and annual mean changes in surface temperature. Red dots represent the first 70-year simulation phase with 2% annual CO_2 increase (ramp_up) and time moves forward from the lower left to the upper right. Blue dots represent the subsequent 70-year period with 2% annual CO_2 decrease (ramp_down) and time moves forward from the upper right to the lower left. Black dots represent the following 150-years with the constant control CO_2 concentration and time moves forward from the upper right to the lower left. The simulation states when atmospheric CO_2 reaches $1 \times CO_2$ and $4 \times CO_2$ concentrations are marked with pink circles. Due to the ocean thermal inertia one atmospheric CO_2 state corresponds to two different states of temperature and precipitation, and due to the precipitation sensitivity to atmospheric CO_2 content changes (Bala et al., 2009), one temperature state corresponds to two different precipitation states. Figure adopted from Cao et al. (2011).

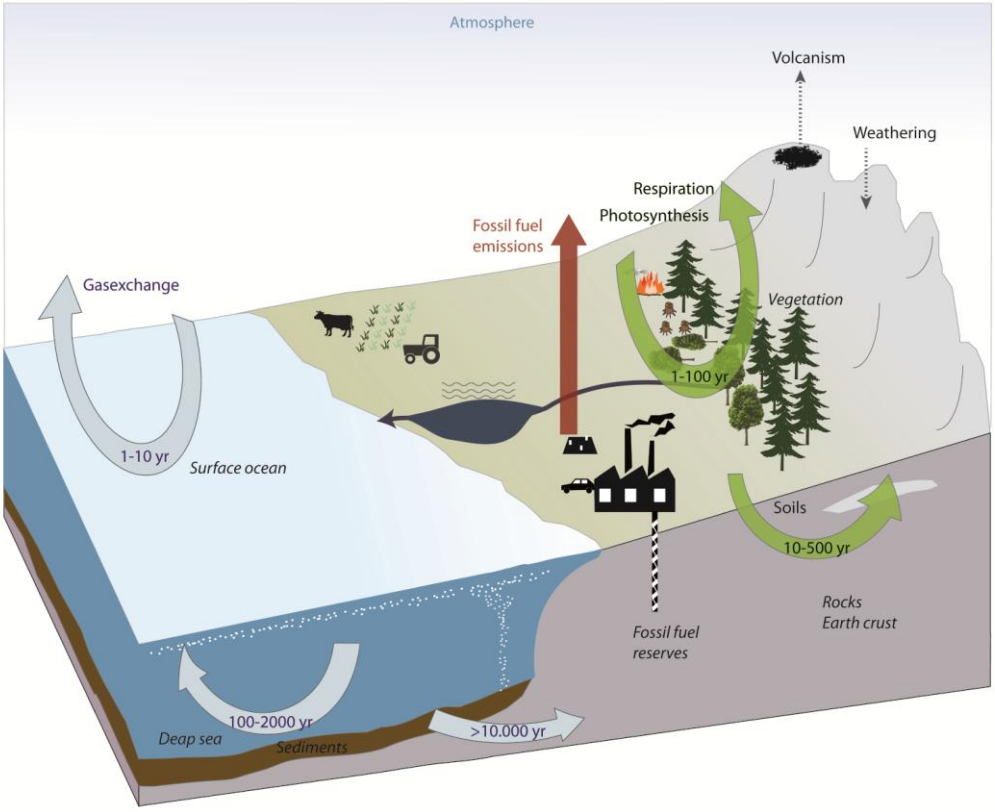

FAQ 6.1, Figure 1: Simplified schematic of the global carbon cycle showing the typical turnover time scales for carbon transfers through the major reservoirs.

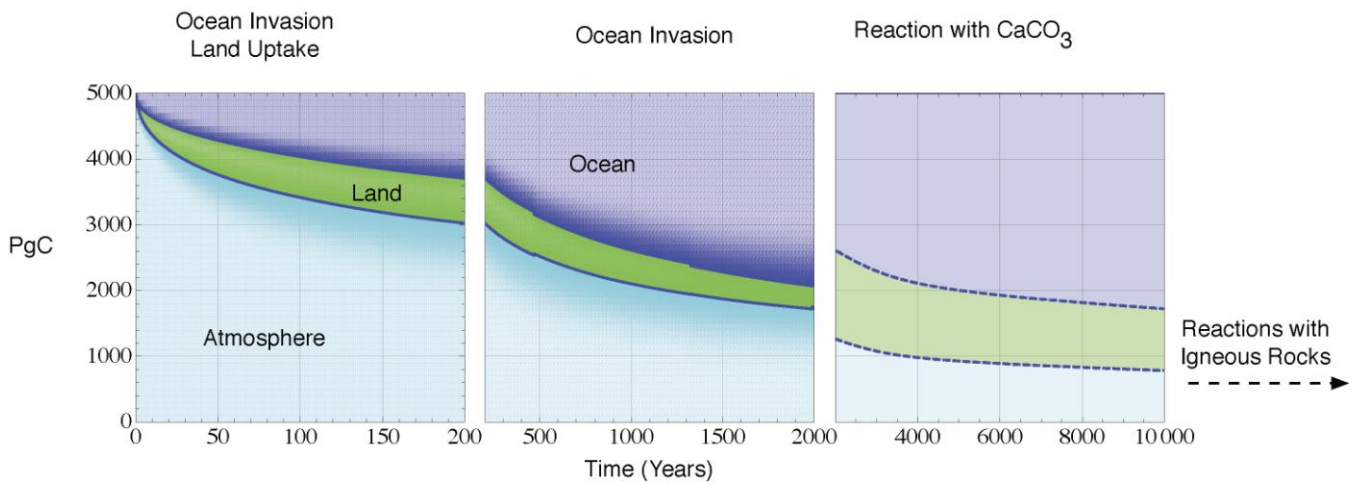

FAQ 6.1, Figure 2: Decay of a CO_2 excess amount of 5000 PgC emitted at time zero into the atmosphere, and its subsequent redistribution into land and ocean as a function of time, computed by coupled carbon–cycle climate models. The size of the colour bands indicate the carbon uptake by the respective reservoir. The first two panels show the multi-model mean from a model intercomparison project (Joos et al., submitted). The last panel shows the longer term redistribution including ocean dissolution of carbonaceous sediments as computed by the CLIMBER-2 model (after Archer et al, 2009b).

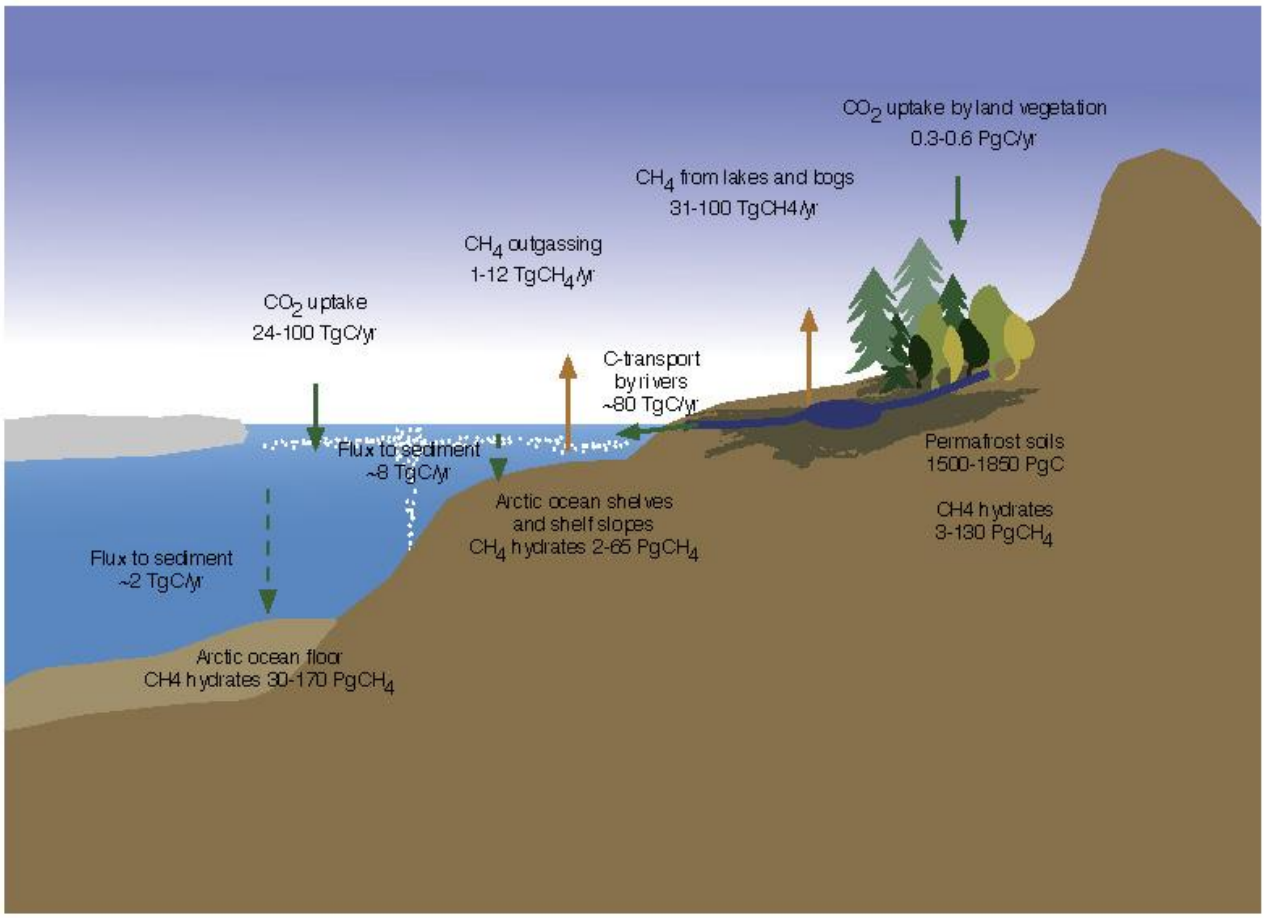

FAQ 6.2, Figure 1: A simplified graph of current major carbon pools and flows in the Arctic domain, including permafrost on land, continental shelves and ocean (adapted from McGuire et al. (2009) and Tarnocai et al. (2009)). TgC = 10^{12} gC, and PgC = 10^{15} gC.